Role of pH, calcium and vesicle trafficking in regulating hyphal tip growth of *Neurospora crassa*

Sabine Fischer-Parton

Ph.D.

University of Edinburgh

March 1999

This thesis is dedicated to my parents.

Declaration

This thesis has been composed by myself and the work of which it is a record has been carried out by myself. All sources of information have been specifically acknowledged by means of reference.

Sabine Fischer-Parton

March 1999

Acknowledgements

This work was supported by a Marie Curie Fellowship (ERBFMBICT 950455) from the European Community.

Most of all I thank my dear husband Richard M. Parton for all his help and emotional support.

Thanks to:
Dr N. D. Read for giving me the opportunity to pursue these interesting projects and reading the thesis.
Dr J. W. Deacon for helpful advice.

Tony J. Collins for invaluable help with computing matters (and the constant evolution of the lab computers ensured that we never missed a new development in that area).
Glyn Nelson for following into Tony's foot steps.

Rui Malhó for helpful discussions.

Amanda Collis, Jan Dijksterhuis, Patrick Hickey, John Love and Helen Page for their help and friendship.

Abstract

Tip growth is the predominant form of cell growth in fungi. The available evidence indicates that a gradient in cytosolic free calcium ($[Ca^{2+}]_c$) is present within growing hyphae. In contrast, evidence for the existence of pronounced cytoplasmic pH (pH_c) gradients has been contradictory. In this study confocal ratio imaging of the pH-sensitive fluorescent dye carboxy SNARF-1 (cSNARF-1) was applied to measure pH_c within growing hyphal apices of *Neurospora crassa*. The findings were that no pronounced pH gradient was detected over the apical 50 μm of growing hyphae with either AM loaded cSNARF-1 or injected 10 kDa dextran conjugate. Spatial resolution and precision over the range of pH 6.5-7.5 was estimated at 2.3 μm^2 and between ± 0.06 and ± 0.03 pH unit, respectively. Acidification of the cytoplasm in *Neurospora* hyphae using propionic acid at pH 7 and alkalinisation using trimethylamine at pH 8 slowed down but did not abolish growth. Manipulations of extracellular pH lead to small transient changes of pH_c and affected the growth pattern. Confocal imaging of $[Ca^{2+}]_c$ in tip-growing hyphae has proved less easy to achieve because of difficulties connected with loading of Ca^{2+}-sensitive dyes into hyphae. Introduction of the single wavelength dye Oregon green 488 BAPTA-1 by ester loading failed completely. Ionophoretic microinjection of the free acid and the 10 kDa dextran conjugate resulted in sequestration into the vacuolar system. Using pressure injection, this dextran conjugate was retained in the cytoplasm. Growing hyphal tips pressure injected with Oregon green 488 BAPTA-1 10 kDa dextran did not exhibit a tip focused gradient in $[Ca^{2+}]_c$. However, because calibration of single wavelength dyes is difficult, a ratiometric approach involving coinjection of 10 kDa dextran conjugates of Oregon green 488 BAPTA-1 and Rhodamine B was developed. Preliminary data indicate the absence of a pronounced tip focused gradient in $[Ca^{2+}]_c$ in *Neurospora*. Estimates of plasma membrane and wall assembly in the growing region of hyphal tips indicate the necessity for considerable membrane recycling during hyphal extension, which probably involves endocytosis. This was investigated with the amphiphilic styryl stain FM 4-64 which has been widely used as an endocytosis marker in living animal and yeast cells. Externally applied FM 4-64 stained up the plasma membrane

immediately. Subsequently dye was internalised within the hyphae, both in apical and subapical regions. The first visible intracellular fluorescent structures appeared about 1-2 minutes after applying dye and consisted of rounded organelles (<0.75 μm in diameter) which stained increasingly over the following 10 minutes and probably represent endosomes. After about 12 minutes the vacuolar membrane was visibly stained. It was discovered that FM 4-64 also stained the Spitzenkörper, an organelle complex predominated by vesicles and localised in the apex of a growing hypha and has been proposed to have a major role in driving hyphal growth. This allowed characterisation of Spitzenkörper dynamics. Spitzenkörper staining was visible as early as 90 seconds after application of the dye, which approximately coincided with the initial staining of the putative endosomes. Spitzenkörper staining increased to reach a maximum after about 20 minutes when it was significantly brighter than the surrounding cytoplasm. Spitzenkörper staining was also observed in a kinesin deficient *Neurospora* mutant, in *Rhizoctonia solani* and in *Trichoderma viride.* The results of this work indicate that pronounced longitudinal gradients in pH_c are not essential for the regulation of tip growth, although pH homeostasis is important for hyphal extension. The data for Ca^{2+} imaging was less convincing but suggested the absence of a tip focused $[Ca^{2+}]_c$ gradient associated with the growing apex. Further work will be necessary to clarify this. The results from the use of FM 4-64 provide evidence that there is rapid and extensive endocytosis and membrane recycling within hyphae of growing *Neurospora crassa*.

Abbreviations

Standard SI (International System of Units) were used throughout this thesis. Non-SI units are as follows:

AM	acetoxymethyl
ATP	adenosine triphosphate
BCECF	2',7'-bis-(2-carboxyethyl)-5-(and-6)-carboxyfluorescein
$[Ca^{2+}]_c$	cytosolic free Ca^{2+} concentration
CFDA	5-(and-6)-carboxy fluorescein diacetate
CG-1	Calcium green-1
CLSM	laser scanning confocal microscope
cSNARF-1	5-(and-6)-carboxy-seminapthorhodafluor-1
DASPMI	4-(4-(dimethylamino)styryl)-N-methylpyridinium iodide
dH_2O	deionised water
DMF	dimethylformamide
DMSO	dimethylsulphoxide
EtOH	ethanol
ER	endoplasmic reticulum
FITC	fluorescein isothiocyanate
FM 1-43	N-(3-triethylammoniumpropyl)-4-(4-(dibutylamino)styryl) pyridinium dibromide
FM 4-64	N-(3-triethylammoniumpropyl)-4-(6-(4-(diethylamino) phenyl)hexatrienyl)pyridinium dibromide
FRET	fluorescence resonance energy transfer
FWHM	full width half maximum
GFP	green fluorescent protein
h	hour/s
Ins1,4,5P_3	Inositol 1,4,5 triphosphate
kDa	kilodalton
LUT	look up table

M6P	mannose 6-phosphate
min	minute/s
MVB	multivesicular body
Na prop.	sodium propionate
NMR	nuclear magnetic resonance
OG-1	Oregon green 488 BAPTA-1
pH_c	cytoplasmic pH (cytosolic pH specified separately)
pH_{ext}	extracellular pH
PM	plasma membrane
PMT	photomultiplier
RB	Rhodamine B
ROI	region of interest
$R_{S/N}$	signal to noise ratio
s.d.	standard deviation
sec	second/s
s.e.m.	standard error of mean
TMA	trimethylamine
VM	Vogel's medium
VM_{110}	Vogel's medium with 10% higher concentration than standard
½VM	half strength Vogel's medium
VSC	vesicle supply centre
w/v	weight by volume

Table of Contents

1. Review of the literature

1.1 Tip growth in fungal hyphae

Tip growth is a highly polar form of cell extension which occurs commonly in eukaryotes. It is exhibited by fungal hyphae (Harold, 1997), pollen tubes (Steer and Steer, 1989), rhizoids of lower plants (Kropf, 1992), root hairs (Herrmann and Felle, 1995) and budding yeast (Chant, 1994). The characteristic feature of this growth form is that cell elongation is confined to the apex which involves localised secretion and cell wall synthesis (Gow, 1995). The polar processes of tip growth are reflected in a strictly polar cellular organisation (Grove, 1978). Tip growth is very complex involving the coordinated interplay of many cell functions such as localised secretion and cell wall deposition, the forward migration of cytoplasm and maintenance of the polarised distribution of organelles (Jackson and Heath, 1993a). It is not yet fully understood how this process is regulated on a cellular basis and, although all the above mentioned organisms display tip growth, it is by no means certain whether they employ the same basic mechanisms (Harold, 1997).

In the fungal kingdom, tip growth is a particularly important feature because, apart from a few exceptions, extension of fungal hyphae is restricted to the apex. Intercalary growth which is common in higher plants and filamentous algae, only occurs in a few cases (Gooday, 1995). The adaptive value of this type of growth is that it enables cells to exploit a vast area for nutrients and to penetrate solid substrates (Sietsma and Wessels, 1994).

The aim of the following section is to give an overview of important cellular aspects relevant to tip growth in filamentous fungi including: structural zonation of growing hyphae, role of Spitzenkörper, cytoskeleton, turgor and the cell wall. Some reference is also made to other cell types for comparison.

1.1.1 Structural and functional zonation of growing hyphae

The following terminology defined by López-Franco and Bracker (1996) to identify regions of a hyphal tip (Figure 1.1) is used throughout this thesis.

- The **apical pole** is the foremost part of the hyphal tip.
- The **apical dome** extends from the apical pole basipetally to a distance *d* which is defined by the hyphoid equation (Bartnicki-Garcia et al., 1989; see section 1.1.3 for further details).
- The **hyphal apex** extends from the apical pole basipetally to a distance 2*d*.
- The **subapical region** extends basipetally from the base of the hyphal apex at 2*d* to the first obvious vacuoles in the apical cell or to the first septum.
- The **hyphal tip** comprises all the above zones together and does not exceed the first septum.

The cytological organisation of growing hyphal tips is structurally and functionally different from that in the rest of the mycelium (Grove, 1978) and shows a distinctive zonation of organelles. The hyphal apex is mainly characterised by accumulations of a variety of vesicles and cytoskeletal structures, whereas the subapical region contains vesicles, mitochondria and other organelles (Figure 1.2). Mitochondria in the tip region differ from those further back and are filiform and orientated parallel to the long axis of the hypha (Grove, 1978). In *Neurospora crassa* the hyphal tip extends to about 50-100 μm from the apex. Behind this region mitochondria appear in the form of short rodlets or granules (Zalokar, 1959). Nuclei in *N. crassa* are numerous but absent at the very tip (first 5-10 μm) (Zalokar, 1959). Vacuoles in the subapical region occur as small and variously shaped structures probably belonging to the lysosomal system (Hoch and Howard, 1980). However, the degree of vacuolation increases distally and hyphal compartments more distant from the apex show a high degree of vacuolisation (Rees et al., 1994). Without any specific vacuolar staining only large spherical vacuoles can be distinguished in living hyphae of *N. crassa* imaged by light microscopy (Robertson and Rizvi, 1968). These vacuoles are usually absent from the apical hyphal compartment and from up to four sequent compartments. The appearance of cytoplasm in this region is therefore

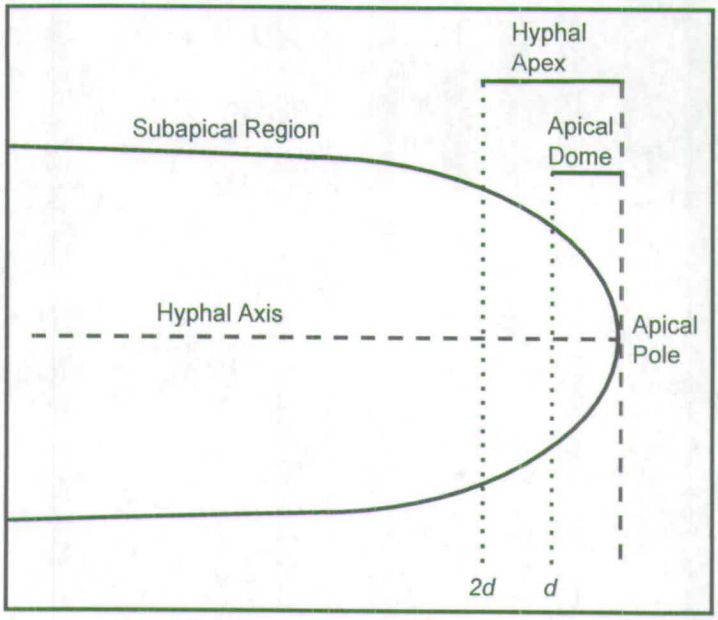

Figure 1.1. Definition of regions of a hyphal tip (based on López-Franco and Bracker (1996). The dashed line at *d* corresponds to the distance from the apical pole as defined in the hyphoid equation by Bartnicki-Garcia et al. (1989).

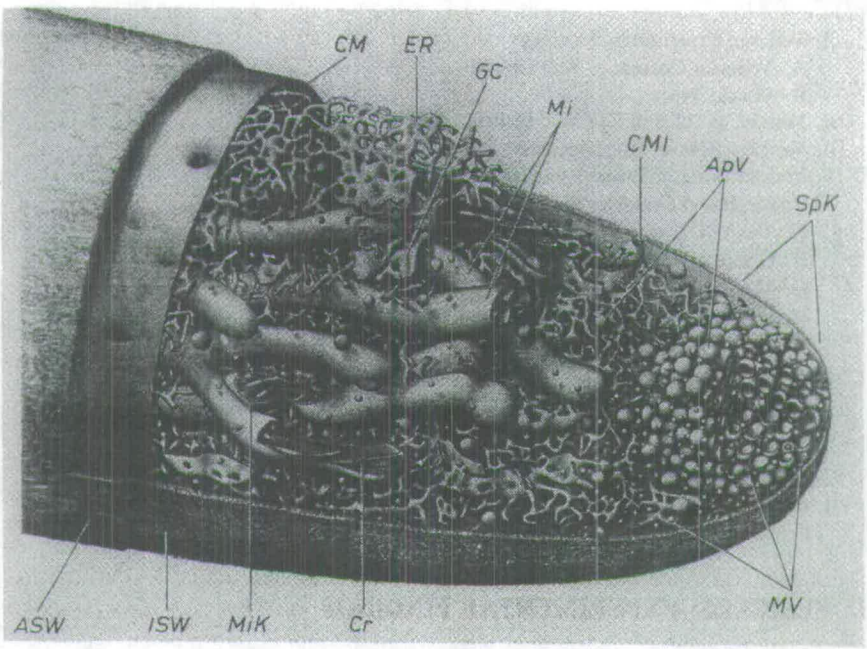

Figure 1.2. Reconstruction of the hyphal apex of *Polystictus versicolor* (from Girbardt, 1969) ApV = macrovesicles, ASW = outer mucilaginous wall layer, CM = plasma membrane, CMI = plasma membrane invagination, Cr = mitochondrial crista, ER = endoplasmic reticulum, GC = Golgi cisterna, ISW = inner fibrillar wall layer, Mi = mitochondrion, Mik = mitochondrial curvature, MV = microvesicles, SpK = Spitzenkörper.

homogenous. The following 10 to 20 compartments each possess one large spherical vacuole located adjacent to the septum. In more distal regions of hyphae the number of spherical vacuoles per compartment increases. Within the periphery of a mycelium the septal pores between hyphal compartments are normally unplugged, consequently each growing tip is supported by a certain length of hypha which can extend back a considerable distance (Zalokar, 1959; Bull and Trinci, 1973). Macromolecules, organelles and the cytoskeleton are produced all along the trunk (Harold, 1997) and transported tip-wards by rapid cytoplasmic streaming which slows down as it approaches the tip (Zalokar, 1959).

1.1.2 The Spitzenkörper

A phase-dark structure located at the hyphal apex, the Spitzenkörper (= apical body), is a common feature of growing hyphae of septate fungi (Ascomycetes, Basidiomycetes, and Deuteromycetes) (Girbardt 1955; 1957; McClure et al., 1968; Grove and Bracker, 1970; López-Franco and Bracker, 1996) with only a few exceptions. The Spitzenkörper in higher fungi is a highly dynamic and pleomorphic multicomponent complex lacking discrete boundaries and consisting of apical vesicles, microvesicles, a differentiated core region, microtubules, actin microfilaments and sometimes ribosomes. (Howard and Aist, 1979; Howard, 1981; Roberson and Fuller, 1988). The core contains actin and presumably serves as the organising structure for the vesicle cluster (Harold, 1997) The Spitzenkörper is required for growth, absent in non-growing tips, and the direction of growth is directly correlated with the orientation of the Spitzenkörper in the hyphal apex (Girbardt, 1957; 1973; Bracker et al., 1997). Although the precise function of the Spitzenkörper is unknown, it is thought to supply the growing apex with the secretory vesicles required for hyphal growth. These vesicles subsequently fuse with the cell membrane to release cell wall precursors into the matrix of the wall and deliver enzymes to the plasma membrane (Gooday and Gow, 1994). The vesicles themselves are most likely formed in subapical regions, in Golgi cisternae, and transported to advancing apices in a process which probably involves microtubules and actin microfilaments (Heath, 1994). Strong

evidence for the vectorial transport of vesicles to the apex was presented by the discovery of satellite Spitzenkörper which although smaller seem to be organised in a similar way to that of the main Spitzenkörper (López-Franco et al., 1995). Satellites were observed to appear beneath the plasma membrane within the hyphal apex, migrate towards and finally merge with the main Spitzenkörper (López-Franco et al., 1994).

A concentration of vesicles at the site of growth seems to be a general feature of apical extension. However, the way in which these vesicles are organised differs between organisms (Harold, 1997). Even within higher fungi there is considerable variation and several morphological patterns (Figure 1.3) have been described with respect to Spitzenkörper organisation (López-Franco and Bracker, 1996). No Spitzenkörper has ever been found in yeasts or aseptate ("lower") fungi, with exception of the Chytridiomycete *Allomyces macrogynus* which contains an apical structure resembling a Spitzenkörper. There is evidence that this structure functions as a microtubule-organising centre (Vargas et al., 1993; McDaniel and Roberson, 1998). Oomycetes, a group of organisms traditionally regarded as 'lower fungi' due to their similarity in life style and morphology, are phylogenetically more closely related to algae. These organisms are devoid of a discrete Spitzenkörper but accumulate a large number of vesicles in the apical cytoplasm (Groove,1978; Kaminsky and Heath, 1996). The same applies to other tip growing cells like pollen tubes, fucoid rhizoids and root hairs which generally possess an accumulation of apical vesicles but no distinct Spitzenkörper-like formation (Steer and Steer, 1989; Kropf, 1992; Ridge, 1995). Only in the tips of fast-growing rhizoids of the green alga *Chara fragilis* a Spitzenkörper-like structure consisting of a spherical, endoplasmic reticulum (ER) rich, clear zone surrounded by the apical Golgi-vesicle accumulation has been found (Bartnik and Sievers, 1988).

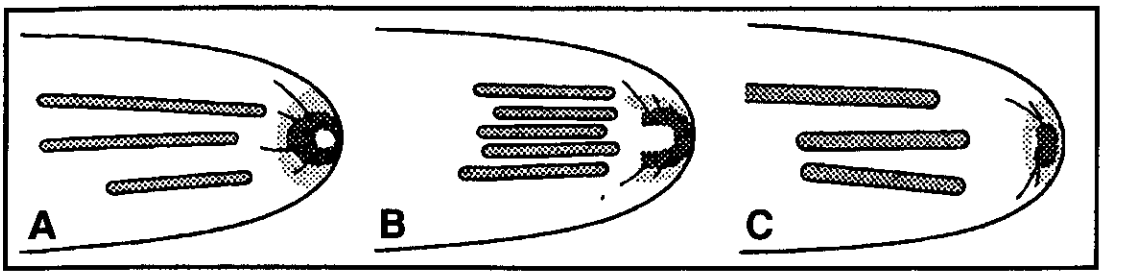

Figure 1.3. Diagrammatic representation of Spitzenkörper patterns (based on López-Franco and Bracker (1996). Presented are three of the nine patterns defined by López-Franco and Bracker (1996): (**A**) Pattern 3 represents a dark vesicle cluster with an eccentric light core usually oriented towards the apical pole and is found, for example, in *Trichoderma viride*. (**B**) Pattern 6 represents a cup-shaped dark vesicle cluster surrounding a large phase-light core and is observed, for example, in *Rhizoctonia solani*. (**C**) Pattern 8 represents a highly pleomorphic Spitzenkörper, often appearing as a thick dark band within a vesicle cloud, with a small light core behind the apical cluster. A notable example of this pattern is exhibited by *Neurospora crassa*. Rods = mitochondria; lightly shaded area = vesicle cloud; darkly shaded area = vesicle cluster; whiskers = cytoplasmic filaments; open circle = phase light core.

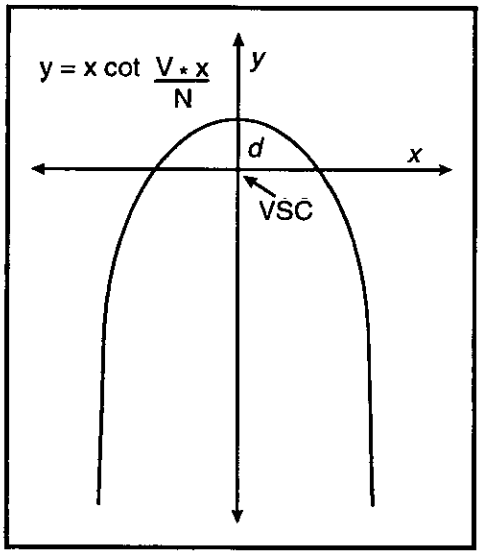

Figure 1.4. Hyphoid curve, plotted on an arbitrary scale (based on Bartnicki-Garcia et al., 1989). See text for details.

1.1.3 The vesicle supply centre and the hyphoid model

A mathematical model to explain how the release of vesicles from a vesicle organising centre and their subsequent fusion with the plasma membrane can create a hypha with a tubular shape and a tapered apex was proposed by Bartnicki-Garcia et al. (1989). This 'hyphoid model' is based on a hypothetical vesicle supply centre (VSC), the location of which appears to coincide with the Spitzenkörper. In the model it is proposed that the VSC releases wall-destined vesicles to the surface in random directions. Consequently its position and movement determines morphogenesis in the sense that a stationary VSC causes spherical growth and a sustained linear displacement of the VSC results in the typical cylindrical shape. The model yields the equation: $y = x \cot (x * V/N)$ which defines the overall shape of a hypha in longitudinal, median cross-section (Figure 1.4). In this equation, V represents the rate of linear displacement of the VSC and N the number of vesicles released per unit time. The ratio $N/V = d$ defines the distance between the VSC and the apical wall and can be calculated by measuring the diameter of a hypha at any given point (x) and distance of this point from the hyphal apex (y) using the equation $y = x \cot (x/d)$. The model accurately generates the outline of hyphal shapes including irregularities of the hyphal growth habit (Bartnicki-Garcia et al., 1995a; 1995b) and can simulate apical branching (Reynaga-Peña et al., 1997). However, the model was formulated for two dimensions and it describes the expansion of an area rather than the enlargement of a shell. According to Harold (1997) it presents an oversimplification of tip dynamics and will require elaboration to overcome certain limitations.

1.1.4 Cell wall formation during tip growth

In tip-growing hyphae new cell wall formation is confined to the apex. Vesicles originating from the ER and Golgi system provide wall building components like membrane bound enzymes and matrix polymers (Gooday, 1995). The vesicles fuse with the plasma membrane at the apex releasing their contents into the apoplastic space and inserting new plasma membrane which contains trans membrane proteins such as chitin synthase and glucan synthase. These enzymes synthesise the structural

wall polymers β-glucans and chitin, respectively, by accepting their substrate at the cytoplasmic side while the polymer is extruded to the outside. The vesicles involved in the transport of inactive chitin synthase to the plasma membrane in the growing region where activation of the enzyme occurs have been identified as microvesicles and named chitosomes. (reviewed by Sentandreu et al., 1994).

The newly forming cell wall at the apex remains plastic, allowing extension by stretching and insertion of new material. However, as the primary wall is displaced further from the tip it matures. The nascent chitin chains gradually become arranged into microfibrils by hydrogen bonding and are covalently cross-linked with cell wall glucans as they are displaced away from the tip by new material. This description of the series of events during hyphal tip growth was formulated into the "Steady-State Growth Theory" because of the maintenance of a steady-state amount of plastic wall at the growing apex (Wessels, 1993; Sietsma and Wessels, 1994). Early evidence for the occurrence of secondary changes during maturation of the cell wall was obtained by Robertson (1958) who concluded that the formation of apical branches after temporarily arresting growth resulted from the need to generate new exit points because in the meantime the whole apex had undergone secondary changes in the primary wall. Indeed, organisation of chitin chains into microfibrils and formation of covalent bonds between chitin and β-glucans are responsible for the rigidity and mechanical stability of the mature wall allowing it to withstand considerable turgor pressure. Matrix polymers (mainly mannoproteins) provide the embedding material for the structural fibres (Sentandreu et al., 1994). However, maturation of the cell wall does not prevent new branch formation. Wall lytic enzymes (chitinases and glucanases) have been found in growing fungi and it is generally accepted that they are involved in wall softening to allow branching to occur (Gooday, 1995). The Steady-State Growth Theory does not exclude the action of hydrolytic enzymes in the wall at the apical extension zone, either for wall loosening or modifying the wall polymers (Wessels, 1993).

1.1.5 The role of turgor during tip growth

It is generally believed that turgor supplies the driving force for expansion in walled cells through an interplay between turgor pressure and the controlled extensibility of the cell wall (Kropf et al., 1998). However, with respect to tip growing cells, there are general indications for a weak or non-existent correlation between turgor, growth rates, and cellular morphology (Heath, 1995a) and it has been concluded that although turgor may be necessary for growth in most cells, it does not play any fundamental role for growth rate or pattern of morphogenesis (Money, 1997). Notable examples for a nonessential function of turgor during tip growth are to be found in the Oomycetes *Achlya bisexualis* and *Saprolegnia ferax*. Unlike most walled organisms, they do not regulate their turgor under hyper-osmotic stress. Nonetheless, normal apical growth is sustained by circumventing the usual requirement of turgor for wall extension by softening of the apical cell wall (Money and Harold, 1992; 1993). Additionally, there is evidence that the actin cytoskeleton may be involved in generating protrusive forces for wall expansion (Money, 1997). Further investigation by Harold et al. (1996) showed that hyper-osmotic stress in *S. ferax* progressively constrained hyphae to grow on the surface of the solid medium by severely reducing the production of aerial hyphae and the ability to penetrate into solid agar medium. This indicates that turgor pressure is required to overcome mechanical resistance. In this context turgor acts as a hydroskeleton generating an erectile force within the cell rather than promoting cell extension (Harold et al., 1996). Further evidence against turgor as a major driving force in tip growth has been obtained from diatom algae where extension of setae (spine-like appendages) relies on tip growth. Setae of *Chaetoceros decipiens* can reach lengths of more than 120 μm at a diameter of 0.5-0.8 μm (Pickett-Heaps and Klein, 1998). According to the laws of physics the internal hydrostatic pressure necessary to extend such a narrow tube at the apex will be very large. However, many cells producing setae were partly plasmolysed within their walls which rules turgor out as the expansive force. The occurrence of a supportive "sleeve" in the tip region which presumably contains actin suggests that the cytoskeleton drives expansion of these setae (Pickett-Heaps and Klein; 1998).

1.1.6 The role of the cytoskeleton in tip growth

The cytoskeleton has several important functions in tip growth including vesicle transport, forward migration of the cytoplasm, providing structural support to the apical dome and probably generating force for apical extension (Heath, 1995a; Kaminsky and Heath, 1996). Major components of the fungal cytoskeleton are microtubules and microfilaments. Microtubules are 20-24 nm wide cylinders of laterally connected protofilaments which are a polymerisation product of α and β tubulins. Microfilaments (or F-actin) are about 7 nm in diameter and consist of two helically entwined linear chains of polymerised G-actin monomers. (Heath, 1995b).

There is evidence that both microtubules and actin microfilaments in fungal hyphae play an important role in long-distance intracellular transport of vesicles containing cell wall precursors (Heath, 1994). Microtubules are generally oriented parallel with the long axis of the hyphal tip and also occur within the Spitzenkörper region. (Howard and Aist, 1980, Bourett et al., 1998). Disruption of the microtubule system in *Fusarium acuminatum* severely affected polarised vesicle transport to the apex and caused vesicle distribution to become uniform over the whole tip concomitant with vesicle depletion in the Spitzenkörper and a drastic reduction in growth rate (Howard and Aist, 1980). There is also considerable evidence suggesting that actin is involved in vesicle transport in filamentous fungi (Heath, 1994). For example in subapical regions of *Sclerotium rolfsii* actin filaments are arranged as longitudinal fibres (Roberson, 1992) and inhibition of actin polymerisation in *Aspergillus nidulans* changed the growth pattern and inhibited enzyme secretion possibly by blocking vesicle transport to the tip (Torralba et al., 1998).

Organelle movement, including the transport of vesicles, is generally based on the interaction of actin microfilaments and microtubules with mechanochemical enzymes such as myosin, kinesin and dynein (Yamashita and May, 1998). Kinesins and dyneins move along microtubules and are involved in organelle transport in eukaryotic cells.

Kinesins have been identified in fungi and seem to be involved in the fast delivery of vesicles to the apex (Steinberg, 1998). In kinesin-deficient mutants of *N. crassa* (Seiler et al., 1997) and *Nectria haematococca* (Wu et al, 1998) the efficient transport of secretory vesicles to the growing apex is impaired causing several defects including a reduction in the size of the Spitzenkörper and colonial growth. However, tip growth is not abolished indicating that a redundant transport system for example involving an actin-myosin based mechanism might be active (Wu et al., 1998). In yeast cells, unlike most other fungi, vesicle motility and organelle transport relies mainly on myosins which move along actin filaments (Steinberg, 1998).

Although fungal hyphae have considerable turgor pressures the plastic cell wall at the apex does not burst under normal conditions. This is probably the result of a cytoskeletal scaffold on which the wall is built (Heath, 1994). It is believed that F-actin reinforces the plasma membrane at the apex. In the oomycete *Saprolegnia ferax* an F-actin cap of filaments associated with the apex has been found whereas the distal actin is mainly organised in the form of actin cables and patches (Jackson and Heath, 1993b). Such an actin cap has not been found in true fungi, although some fungi show numerous actin plaques at their tips near the plasma membrane (Roberson, 1992; Heath, 1994).

The cytoskeleton is also thought to be important for cell wall expansion, a function which becomes increasingly more important under low turgor conditions (Section 1.1.5). A possible mechanism to generate expansive force assumes the interplay of several activities of the actin cytoskeleton: actin polymerisation, myosin-generated sliding of microfilaments and gel pressure through hydration of an actin network (Money, 1997). In animal cells there is evidence that the actin cytoskeleton provides the force for extension. Formation of pseudopodia in amoeboid cells, for example, is based on rearrangements in the cytoplasmic F-actin system (Heath, 1995a). The expansion of very long setae in certain diatom algae cannot be explained by relying on turgor as driving force and is probably controlled by a fibrous sleeve of limited length in the tip region. This sleeve which presumably contains actin keeps the same position

relative to the apex, possibly by continuously assembling at its distal (tip) end and disassembling at its proximal end, employing a process known as actin cycling (Prickett-Heaps and Klein, 1998).

The dependence of tip growth upon cytoskeletal functions indicates that regulation of the cytoskeleton is crucial for proper coordination of the tip growth process. Ca^{2+} and pH have been found to influence cytoskeletal properties and may well be involved in regulation of the cytoskeleton (Madshuis, 1988; Edmonds et al., 1995; Heath, 1995b).

1.2 The role of Ca^{2+} and pH in tip growth of fungal hyphae

Current evidence suggests that localised ion movements and distributions, especially of Ca^{2+} and protons, are fundamental to cell polarity and tip growth (Heath, 1990). For Ca^{2+} there has been found a correlation between tip growth, extracellular Ca^{2+} currents and distribution of $[Ca^{2+}]_c$ at the apex in several tip growing systems (Schiefelbein et al., 1992; Felle and Hepler, 1997; Holdaway-Clarke et al., 1997; Messerli and Robinson, 1997), whereas for protons the findings are more controversial (Gibbon and Kropf, 1994; Robson et al, 1996; Fricker et al., 1997, Parton et al., 1997; Bibikova et al., 1998; Messerli and Robinson, 1998). Ca^{2+} and pH have many functions in a cell. An overview of their physiological significance is therefore necessary before their possible involvement in tip growth can be considered.

1.2.1 Cytosolic calcium and signal transduction

It is generally accepted that calcium ions act as universal intracellular signal or second messengers in eukaryotic cells. The cytosolic free calcium concentration ($[Ca^{2+}]_c$) is actively kept at a very low level of approximately 10-100 nM in spite of very steep gradients across the plasma membrane and intracellular membranes (Berridge and Bootman,1996). It is believed that the low level of $[Ca^{2+}]_c$, which is sustained by energised transport at both the plasma membrane and membrane-bounded

compartments, prevents Ca^{2+} binding to phosphate groups and consequently avoids potential toxicity (Gadd, 1995). The basic processes involved in maintaining intracellular calcium homeostasis in fungi are presented in Figure 1.5. Ca^{2+} efflux through the plasma membrane in *Neurospora* is proposed via a H^+/Ca^{2+}-ATPase which uses the electrochemical proton gradient generated by the plasma membrane H^+-ATPase (Miller et al., 1990). The vacuole is believed to function as the main Ca^{2+} storage organelle taking up Ca^{2+} via a Ca^{2+}/nH^+ antiport system driven by the proton motive force generated by the vacuolar membrane H^+-ATPase. There is little evidence for mitochondria being involved in Ca^{2+} regulation in fungi, whereas the ER most likely plays a role (Cunningham and Fink, 1994; Gadd, 1995). Transient elevation from 10^{-7} M to 10^{-5} M $[Ca^{2+}]_c$ for second messenger functions in eukaryotic cells does not alter the overall cellular ionic composition but can trigger Ca^{2+}-sensitive intracellular events like exocytosis, gene expression and cell-cycle progression. Little is known about Ca^{2+}-triggered processes in filamentous fungi, but there is evidence that in yeast Ca^{2+} may regulate similar processes (Cunningham and Fink, 1994; Gadd, 1995). To achieve transient elevation of $[Ca^{2+}]_c$, Ca^{2+} influx from the external medium into the cytoplasm through stretch-, receptor- or voltage-gated channels in the plasma membrane occurs. Animal cells may also use Ca^{2+} sequestered within the ER. Ca^{2+} release from the ER is mediated through channels operated by intracellular messengers such as Ca^{2+} itself and inositol 1,4,5 triphosphate (Ins1,4,5P_3) (Berridge and Bootman, 1996). In plant and fungal cells it is predominantly the vacuole that can release Ca^{2+} into the cytoplasm and there is evidence for a voltage-mediated and for an Ins1,4,5P_3-mediated Ca^{2+}-channel in the vacuolar membrane (Gadd, 1995).

Other components of the Ca^{2+} signal transduction systems already known in animal and plant cells have been found in filamentous fungi. These include calmodulin, G-protein-linked receptors and calcineurin. Calmodulin is a ubiquitous Ca^{2+}-binding protein in eukaryotes and a Ca^{2+}-induced conformational change is the prerequisite

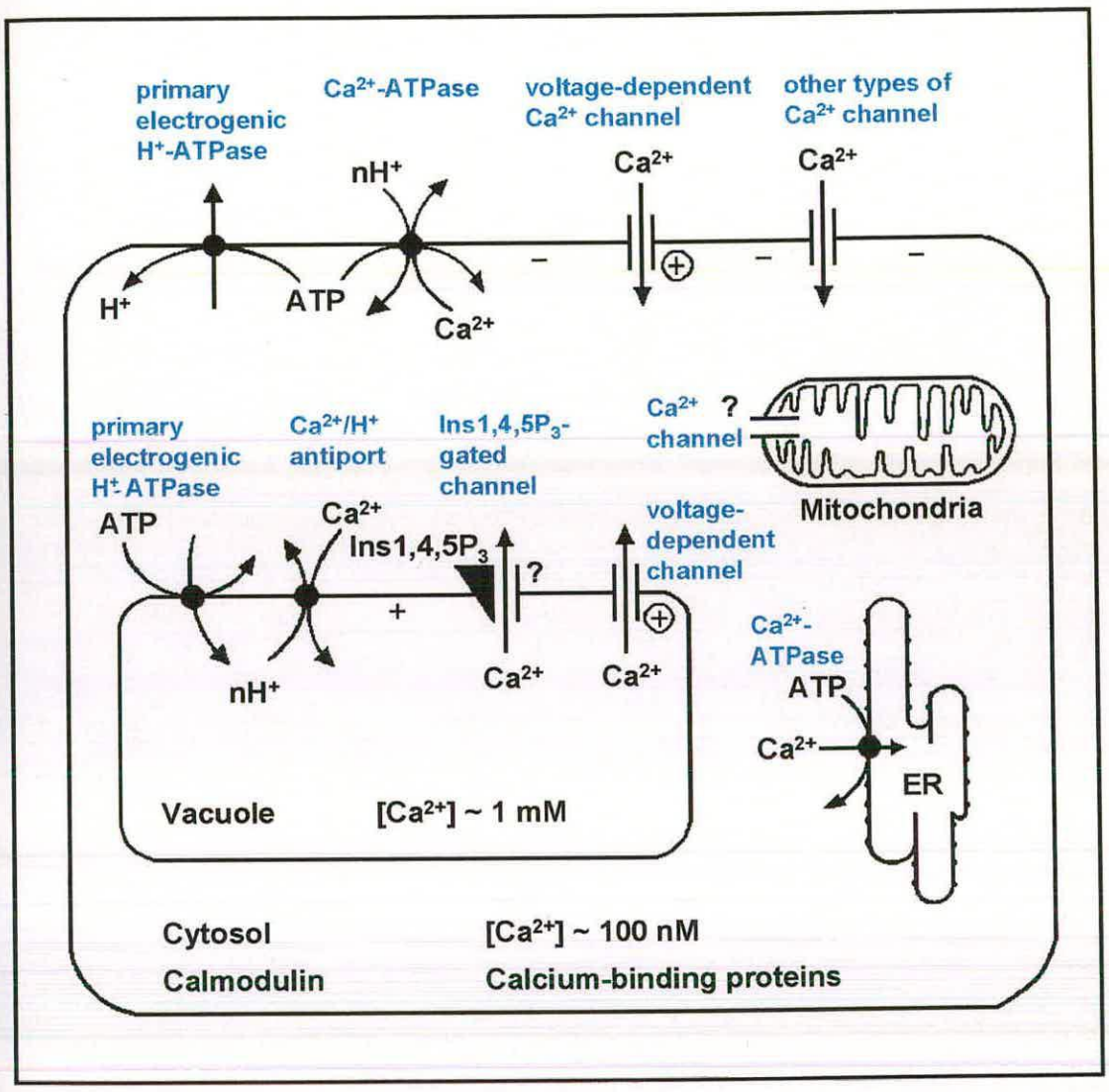

Figure 1.5. Simplified diagram of the identity and location of Ca^{2+} homeostatic systems in fungi (based on Gadd, 1995). The diagram shows transport systems on the plasma membrane and on the vacuolar membrane. A Ca^{2+} channel is shown in the outer mitochondria membrane as well as a Ca^{2+}-ATPase on the endoplasmic reticulum.

for interaction with several different target proteins, mainly a variety of protein kinases (Berridge and Bootman, 1996). Calmodulins have been identified in many filamentous fungi and yeasts and have been shown to be involved in several important cell functions including cell proliferation, cell cycle control and nuclear division (Anraku, 1991). Further components of the intracellular signalling system detected in fungi are G-protein-linked receptors and the phosphoinositol signalling system. Ins1,4,5P_3, as mentioned previously, links the receptors on the plasma membrane with intracellular Ca^{2+}-stores (Gadd, 1995). Calcineurin, a Ca^{2+}/calmodulin-dependent phosphoprotein phosphatase important for the activation of lymphocytes in animals (Berridge and Bootman, 1996) has been suggested to function in the control of Ca^{2+} homeostasis in yeast by repressing Ca^{2+} flux into a non-vacuolar compartment (Tanida et al., 1996). In *Neurospora* calcineurin was shown to be essential for growth and it appears to be involved in the regulation of tip growth (Prokisch et al., 1997).

1.2.2 Cytosolic pH

The cytosolic proton concentration influences important cellular processes such as enzyme activity and membrane transport and, therefore, controls the metabolic activity of a cell (Busa and Nuccitelli, 1984). Cytosolic pH has also an effect on the assembly and contractile activity of the cytoskeleton with low pH reducing the contractibility of actin and myosin and alkaline pH promoting microtubule disassembly (Madshuis, 1988). Consequently, regulation of cytosolic pH is very important for cells and there is substantial evidence that it is maintained within relatively narrow limits. Sudden changes in extracellular pH (pH_{ext}) have only relatively slight and transient effects. Direct manipulation of intracellular pH can be accomplished by applying membrane permeant weak acids and bases (Guern et al., 1991). These treatments have been employed to estimate intracellular pH and buffer capacity (Sanders and Slayman, 1982; Fröhlich and Wallert, 1995) and to assess the influence of pH on cell functions like tip growth (Hermann and Felle, 1995; Kropf et al., 1995; Parton et al., 1997).

The mechanisms to regulate cytosolic pH are primarily through metabolic processes which produce or consume protons and by net flux across membranes (Guern et al., 1991). In *N. crassa*, the primary pump in the plasma membrane is an outwardly directed electrogenic H^+-pump. However, this pump is ATP dependent and can, therefore, only have a limited regulatory function on cytosolic pH. Metabolic activity, which is able to produce or consume large amounts of protons, has been shown to be capable of controlling cytosolic pH in *Neurospora*, even when the proton pump is inhibited (Sanders and Slayman, 1982). The main function of the ATP fuelled H^+-pump is to create an electrochemical gradient of protons across the cell membrane enabling active nutrient uptake (Garrill, 1995).

There is evidence that cytosolic pH may act as a second messenger in that transient changes in intracellular pH have been found to procede certain cellular events (e. g. mitosis) (Busa and Nuccitelli, 1984). An example of a pH mediated process in fungi is zoosporogenesis in *Phytophthora cinnamomi* which requires a rise in intracellular pH (Suzaki et al., 1996). Additionally, most metabolic transitions involving pH are connected with altered Ca^{2+} fluxes (Busa and Nuccitelli, 1984). Addition of extracellular Ca^{2+} to submerged cultures of *Penicillium cyclopium* was shown to induce cytosolic alkalinisation (Roncal et al., 1993). In cells of organisms as different as *Zea mays* and *Riccia fluitans* a direct relationship between cytosolic pH and $[Ca^{2+}]_c$ was found indicating that regulation of both ions is interrelated (Felle, 1988).

1.2.3 Transcellular electrical currents

Polarised cells and organisms commonly drive electric currents through themselves (Harold, 1994) and such transcellular currents have been found in many tip-growing cells including pollen tubes (Fejó et al., 1995) and fungi (Gow, 1984). This led to the question whether these currents are important in the establishment and/or maintenance of cell polarity. In the majority of the cases positive current enters the tip region and is expelled subapically implying an asymmetric distribution of ion pumps and ion channels (Gow, 1995). For *Neurospora*, it has been shown that the current is carried

mainly by protons. Due to an asymmetric distribution of H^+-ATPase, protons are expelled distally from the tip and enter across the plasma membrane along the outermost 100-200 μm which corresponds to the length of the apical cell (McGillivray and Gow, 1987; Takeuchi et al, 1988). The uptake of protons is accompanied by nutrient uptake due to amino acid-proton cotransport (Gow, 1995). However, many exceptions to the above have been found, including normally extending *Neurospora* hyphae with reversed currents and non-growing hyphae exhibiting a distinct current (McGillivray and Gow, 1987; Takeuchi et al, 1988). Also, Chytridiomycetes like *Allomyces macrogynus* and *Blastocladiella emersonii* hyphae have a constitutive outward current from the tip with the current entering at the rhizoids which function in nutrient uptake (De Silva et al., 1992). The lack of any consistent relationship between extension and the intensity or polarity of the current has lead to the conclusion that the electric current cannot play an obligatory role in tip-growth but indicates the locus and polarity of nutrient transport (Harold, 1994). However, it also has to be considered that the currents measured represent the net flow of all ions that pass across the cell membrane. In fungi Ca^{2+} ions are normally a small fraction of the total ionic traffic and have not been investigated in detail (Gow, 1995). It cannot be excluded that part of the ionic current which is too small to be detected among the proton flux might be linked with tip growth. Indeed, in other tip-growing systems a connection between apical extension and influx of Ca^{2+} has been found. For pollen tubes it was demonstrated that there is a strict correlation between growth pulses, Ca^{2+} influx at the tip and tip localised $[Ca^{2+}]_c$ (Holdaway-Clarke et al., 1997). Growing root hairs generate an inwardly directed net current which is congruent with the zone of elevated $[Ca^{2+}]_c$ in the cell (Schiefelbein et al., 1992; Herrman and Felle, 1995; Felle and Hepler, 1997).

1.2.4 The role of ion gradients in tip growth

The discovery of extracellular ion fluxes led to the question whether these ion movements might be reflected by an equally polarised, intracellular distribution in ion concentration, most likely in the form of a gradient. Ca^{2+} ions are able to generate

sharp concentration gradients because their diffusion is restricted by association with cytosolic proteins and membrane-bound vesicles. The situation for protons is similar, while K^+, Na^+, Cl^- and Mg^{2+} are freely mobile (Harold, 1994).

1.2.4.1 Ca^{2+} gradients

Gradients in intracellular Ca^{2+} distribution have been discovered in a range of tip growing cells including fungi (reviewed by Jackson and Heath, 1993a) and it is now well established that there is a tip high gradient in $[Ca^{2+}]_c$ in growing pollen tubes (Malhó et al., 1994; 1995; Pierson et al.,1994; 1996) and growing root hairs (Felle and Hepler, 1997; Bibikova et al, 1997). Gradients in $[Ca^{2+}]_c$ are probably generated by localised Ca^{2+}-influx through the plasma membrane at the apex (Garrill et al., 1993; Pierson et al., 1996; Felle and Hepler, 1997). Subapically $[Ca^{2+}]_c$ is down regulated to resting levels via transport across the cell membrane and sequestration into organelles, including ER and mitochondria (Jackson and Heath, 1993a; Harold, 1994).

The possible function of $[Ca^{2+}]_c$ gradients in controlling tip extension is supported by the finding that Ca^{2+} regulates many of the processes which are connected with tip growth such as localised exocytosis, cell wall formation and the organisation of the cytoskeleton (Jackson and Heath, 1993b). The polymerisation of G-actin to F-actin is a Ca^{2+}-dependent process which probably determines the site where secretory vesicles are transported to the cell membrane (Garrill et al., 1993). In animal cells the fusion of microvesicles with the cell membrane is dependent on localised high $[Ca^{2+}]_c$ (Muallem and Lee, 1997). This concept of Ca^{2+} playing a key role in tip growth is further supported by findings that the orientation of the tip-focused gradient in $[Ca^{2+}]_c$ within the apical dome controls the growth-orientation of pollen tubes (Malhó and Trewavas, 1996). Also, pollen tubes have been shown to exhibit pulsed growth (like fungal hyphae) and oscillations in magnitude of both the tip-high $[Ca^{2+}]_c$ and the influx of extracellular Ca^{2+} into the apex (Pierson et al., 1996; Messerli and Robinson, 1997). The intracellular gradient was found to oscillate in phase with growth whereas the influx of intracellular $[Ca^{2+}]_c$ into the apex showed a phase delay, which is presumably related to the need to store Ca^{2+} between growth pulses (Holdaway-

Clarke et al., 1997). However, in root hairs Ca^{2+} apparently is not the only determinant of growth orientation and there is evidence for an endogenous polarity determining growth direction away from the root surface (Bibikova et al, 1997; Wymer, Bibikova and Gilroy, 1997). Altogether the evidence indicates that a tip high gradient in $[Ca^{2+}]_c$ may act as an important and ubiquitous factor in localising tip growth although it may not be the only determinant (Malhó, 1998).

1.2.4.2 pH gradients

In agreement with the transcellular ion current, growing *Neurospora* hyphae have been found to create a longitudinal pH_{ext} gradient in the surrounding medium (Takeuchi et al, 1988) which has led to the conclusion that proton influx at the tip could lead to a tip-acidic gradient in cytosolic pH. Although tip-acidic gradients in tip growing cells have been reported in the past (Turian, 1979; McGillivray and Gow, 1987; Roncal et al., 1993; Gibbon and Kropf, 1994), more recently the evidence for the involvement of intracellular pH gradients in regulating tip growth has been questioned. Herrmann and Felle (1995) and Bibikova et al. (1998) found no cytosolic pH gradient in tip growing root hairs and Fricker et al. (1997) and Parton et al. (1997) reported the lack of such a gradient in pollen tubes. Robson et al. (1996) described the occurrence of a tip-focused alkaline gradient in *Neurospora crassa* hyphae which is in contrast to Parton et al. (1997) who reported the lack of a pH gradient in this organism. In *Gigaspora margarita*, an arbuscular mycorrhizal fungus, Jolicoeur et al. (1998) found a rather complex pH pattern consisting of an acidification at the apex followed by immediate alkalinisation, then a slow decline to a basal pH level. Messerli and Robinson (1998) reported the lack of a standing pH gradient in tips of lily pollen tubes but detected a pulsation of the tip-localised pH resulting in a temporary drop for up to one pH unit from average cytosolic value. Taken all together, the results are very conflicting and more work is required to clarify the situation.

1.3 Role of endocytosis in membrane recycling during tip growth

Estimates of plasma membrane and wall assembly in the extending region of a tip-growing *Neurospora* hypha indicate the necessity for considerable membrane recycling during tip growth (Read, Fischer, López-Franco, Rentel and Bracker, unpublished results). Similar conclusions have been drawn for pollen tubes (Picton and Steer, 1983). In both cases it appears that the membrane incorporated from vesicle fusion for cell wall building is considerably more than necessary for the increase in cell surface area during growth. The mechanism which can account for membrane recycling in connection with secretion is endocytosis (Steer, 1988). This process is exclusively found in eukaryotic cells and involves invaginations of the plasma membrane which pinch off to form membrane-bounded vesicles containing some of the extracellular fluid as well as molecules adsorbed on the cell surface (Marty, 1997).

1.3.1. Endocytosis in animal cells

Endocytosis in animal cells has been researched extensively and is well documented in textbooks and review articles (e.g. Watts and Marsh, 1992; Gruenberg and Maxfield, 1995; Mellman, 1996; Geli and Riezman, 1998; Lodish et al., 1996). In the following sections (Sections 1.3.1.1 to 1.3.1.3) our understanding of endocytosis in animal cells, and how it integrates with the biosynthetic pathway, is reviewed.

1.3.1.1 Clathrin-dependent endocytosis

Conventionally, endocytosis is classified into phagocytosis (internalisation of large particles > 0.5 μm diameter mediated via F-actin) and pinocytosis (formation of vesicles < 0.2 μm usually mediated via the protein clathrin). Clathrin-dependent endocytosis constitutes the main endocytic route in many animal cells and is constitutive (Figure 1.6). Clathrin is a highly conserved fibrous protein that can form a basket-like structure composed of a network of hexagons and pentagons. It

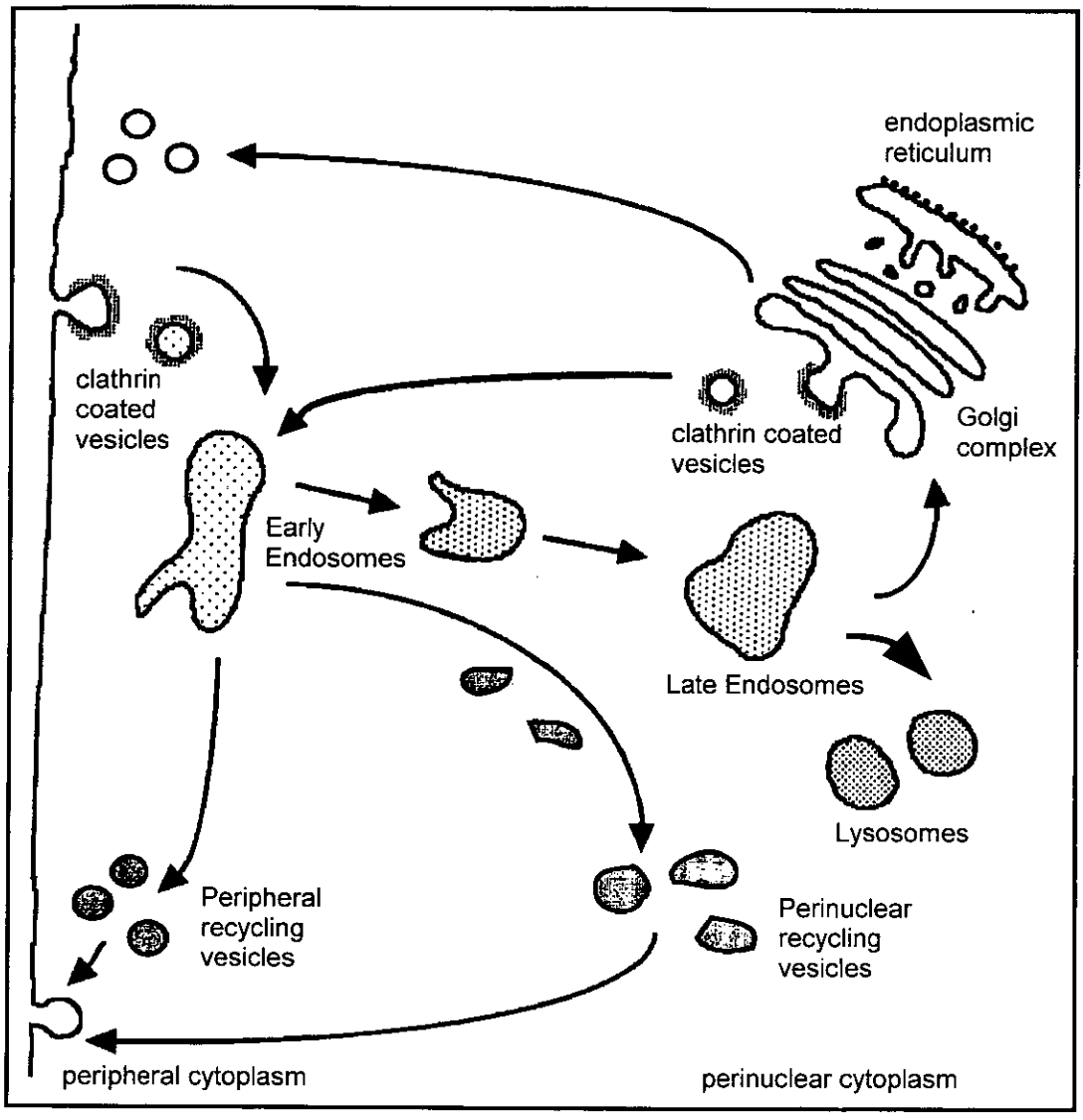

Figure 1.6. Organisation of the endocytic pathway in animals (based on Mellman, 1996). Endocytosis starts with the formation of clathrin-coated vesicles at the plasma membrane which fuse with early endosomes in the peripheral cytoplasm. Here, receptor-ligand complexes dissociate, which enables free receptors to return to the plasma membrane in recycling vesicles, some of which appear to first migrate to the perinuclear cytoplasm before reaching the plasma membrane. Dissociated ligands and other soluble macromolecules are transferred from early to late endosomes and lysosomes for digestion. Clathrin-coated vesicles are also thought to be responsible for the delivery of certain compounds from the Golgi complex to early endosomes.

assembles at the plasma membrane to form a planar coat which invaginates through conformational rearrangements resulting in a coated pit and finally a coated vesicle. The latter pinches off into the cytoplasm. This process accounts for the main uptake of extracellular fluid (*fluid-phase endocytosis*) and of specific macromolecules bound to plasma membrane receptors (*receptor-mediated endocytosis*). Due to specific sequence information in their cytoplasmic domain, most receptor-ligand complexes accumulate at clathrin-coated pits where the internalisation occurs. Additionally, a heterotetrameric adapter complex is required for attachment of clathrin to membranes and for recruiting membrane receptor proteins into the pit. Plasma membrane proteins lacking endocytosis signals can be non-selectively included in coated pits and are internalised by bulk membrane flow. Invagination of coated pits is promoted by the GTPase dynamin. After pinching off, the clathrin-coated vesicles lose their coat and fuse with early endosomes, organelles which consist of vacuolar areas and tubular extensions. The slightly acidic pH in early endosomes causes the dissociation of many ligand-receptor complexes which allows receptors and ligands to be separated. Free receptors accumulate in the tubular extensions from where they are transported back to the plasma membrane via recycling vesicles, and dissociated ligands collect in vacuolar areas. Thus, early endosomes primarily function as sorting organelles allowing rapid and efficient recycling of membrane components and they probably are involved in direct cycling of certain membrane proteins between the trans Golgi network and the plasma membrane. Another function of early endosomes in certain cell types is the production of specialised, endosome-derived storage compartments that allow the rapid delivery of proteins to the cell surface in response to external stimuli. In the course of further processing of early endosomes along the endocytic pathway, vacuolar elements containing ligands, receptors and other macromolecules destined for breakdown separate and function as carrier vesicles to late endosomes. Carrier vesicles often contain internal vesicles formed through invaginations of the endosomal membrane, hence the term multivesicular bodies (MVBs). They migrate to the perinuclear cytoplasm where fusion with late endosomes occurs. The low pH and the high concentration of lysosomal enzymes in these organelles starts the degradation process which is continued after fusion with lysosomes.

1.3.1.2 Communication with the secretory pathway

The endocytic pathway integrates with the secretory pathway indicating that the compartments and their membranes are all in constant communication with each other. Secretory proteins are synthesised at the cytoplasmic face of the ER and sequestered into this organelle where they are subjected to a range of modifications. Subsequently they are transferred to the cis Golgi reticulum via vesicular transport. Also via vesicles the proteins move through the Golgi apparatus for further processing. Finally they are sorted at the trans Golgi network and sent either to the endosomal/lysosomal system or to the cell surface. Late endosomes communicate with the biosynthetic pathway to accumulate lysosomal enzymes. For lysosomal hydrolases, sorting is achieved by the possession of mannose 6-phosphate (M6P) groups which are recognised by M6P receptor proteins, trans membrane proteins present in the trans Golgi network. Binding of the hydrolases to the M6P receptors is favoured in the Golgi cisternae due to their luminal pH of about 7, whereas release from the receptor is promoted in the more acidic environment (pH 6) of late endosomes. Recycling of M6P receptor proteins is mediated through vesicular transport from late endosomes back to the Golgi apparatus. Membrane recycling also occurs between the Golgi system and the ER, in the form of a retrograde pathway that can send escaped ER processing proteins and membrane back through the Golgi stacks to the ER.

1.3.1.3 Clathrin independent endocytosis

Uptake via clathrin-coated vesicles is the predominant endocytic pathway. However, the occurrence of clathrin-independent endocytosis was indicated through various treatments which, although inhibiting the assembly of plasma membrane clathrin coats, could not completely abolish endocytic uptake. Another way plasma membrane pits can be formed is by an accumulation of the integral membrane protein caveolin. The resulting invaginations are then called caveolae. There is evidence that these structures are involved in endocytosis. Another example of a clathrin-independent

endocytic event is macropinocytosis, a form of specialised fluid phase endocytosis probably dependent on the actin cytoskeleton. It occurs in some cell types after certain treatments and leads to uptake of considerable amounts of extracellular liquid by forming large vesicles of 1-5 μm diameter.

1.3.2 Endocytosis in yeast

The overall organisation of the endocytic pathway inside yeast cells resembles that of mammalian cells and there is evidence for the occurrence of both, clathrin-dependent and clathrin-independent endocytosis (Geli and Riezman, 1998). A major difference to animal cells is the general requirement of actin and several actin-associated proteins for endocytic internalisation in yeast. This may reflect the mechanism necessary to generate force for deforming the plasma membrane against surface tension and osmotic pressure (Geli and Riezman, 1998). An example of these actin-dependent proteins involved in endocytosis are members of the type I myosins which constitute a family of ATP-dependent molecular motors. They are thought to drive actin-dependent membrane motility and are required for the uptake step of receptor-mediated endocytosis in yeast performing the function of dynamin in animal cells (Geli and Riezman, 1996). Calmodulin has a key regulatory function in this process by directly interacting with type I myosin (Geli et al., 1998). The morphology of the yeast endocytic pathway has been revealed at the ultrastructural level: small vesicles of 30-50 nm diameter represent primary endocytic vesicles; peripheral, vesicular/tubular compartments are equivalent to early endosomes; multivesicular bodies near the vacuole correspond to late endosomes; and the vacuole functions as lysosomal compartment (Prescianotto-Baschong and Riezman, 1998). Receptor-mediated endocytosis in yeast can be monitored by following the internalisation and degradation of the mating pheromone factor and its plasma membrane receptor Ste2p. Ste2p is the best characterised of a large number of membrane proteins which are known to be internalised in a constitutive way. The receptor transiently appears in endosomes before it is degraded in the vacuole (Wendland et al, 1998). Internalisation of Ste2p is stimulated considerably after binding pheromone factor due to subsequent

phosphorylation of the receptor followed by ubiquitination which functions as the signal for internalisation of many yeast plasma membrane proteins (Hicke et al., 1998). Other molecules internalised by endocytosis, such as two of the three yeast chitin synthases, are not degraded but recycled directly back to the plasma membrane after passing through early endosomes (Ziman et al., 1996; 1998).

1.3.3 Endocytosis in plant cells

It is now generally believed that endocytosis occurs in plants (Hawes et al., 1995; Marty, 1997). This is indicated by the high turn over rate of plasma membrane as a consequence of secretion (Steer, 1988). Evidence is also provided by the identification of structures morphologically and functionally homologous to counterparts in animal cells that were found to be involved in endocytosis (e.g. the occurrence of plasma membrane derived clathrin-coated vesicles, of multivesicular bodies and evidence for the existence of adapter complex proteins, Marty, 1997). Also, the uptake of markers which bind non-specifically to the plasma membrane has been followed via coated pits and the vesicular pathway, with the marker finally delivered to the vacuole and the Golgi complex (Hawes et al., 1995). However, the uptake of physiologically significant macromolecules via coated vesicles, and involving receptor-mediated endocytosis, has not yet been demonstrated although plant cells have the cellular machinery necessary for this to occur (Hawes et al., 1995). It has also been difficult to establish whether fluid-phase endocytosis in plant cells occurs due to the lack of reliable tracers for this process. Lucifer Yellow-CH, a membrane impermeant, low-molecular weight, fluid phase endocytosis marker in animal cells, was shown to be taken up by probenecid-sensitive organic anion transporters located in both the plasma membrane and tonoplast of plant cells which invalidates this compound as an endocytic marker in these cell types (Oparka and Hawes, 1992; Wright and Oparka, 1994). Uptake experiments using fluorescent tracers conjugated to high molecular dextrans have to take into account the pore size of cell walls (Carpita et al., 1979; Money, 1990) which limits the molecular weight range of the dextrans that can be used. Furthermore, problems can result from the

contamination of dextran conjugates with free dye molecules and the possibility of enzymatic cleavage of the dextran conjugate within the cell wall (Cole et al., 1990). Nonetheless, in growing pollen tubes, 4 kDa dextran conjugate labelled with fluorescein isothiocyanate (FITC) was internalised in the tip region and accumulated in the vacuolar system. Thin layer chromatography of the dye extracted from the cell showed the same behaviour as the FITC coupled 4 kDa dextran on its own (O'Driscoll et al, 1993). The involvement of endocytosis in tip growth of plant cells has also been concluded from the distribution and number of coated pits in root hairs and pollen tubes. Obviously more membrane turnover takes place in growing root hairs than in full-grown ones and exocytosis and endocytosis apparently can occur near each other in the tip (Miller et al., 1997).

1.3.4 Endocytosis in filamentous fungi

Little is known about endocytosis in filamentous fungi and so far there are no reports showing endocytic uptake of biologically significant macromolecules. A first indication that endocytosis probably occurs in filamentous fungi was the morphological identification of coated vesicles in *Neurospora crassa* and *Uromyces phaseoli* which superficially resembled clathrin-coated vesicles (Caesar-Ton That et al., 1987). A study using membrane-impermeant fluorescent probes for tracing fluid phase endocytosis in the basidiomycete *Pisolithus tinctorius* on the other hand showed no indication for the occurrence of fluid phase endocytosis, because the dyes were not internalised (Cole et al., 1997). However, the authors presented evidence that the tubular vacuolar system is probably analogous to the animal endosomal/lysosomal system and to plant vacuoles. Recently, evidence for the occurrence of endocytosis and membrane turnover in the germ tube of *Uromyces fabae* was presented by Hoffmann and Mendgen, (1998) using the fluorescent dye FM4-64 as a tracer for bulk membrane internalisation. Evidence for FM4-64 internalisation by endocytosis has also been shown in hyphae of *N. crassa* and *Trichoderma viride* (Read et al., 1998). Further evidence for the occurrence of endocytosis in filamentous fungi results from the identification of molecular motors

known to be involved in endocytosis. As mentioned earlier (Section 1.3.2) type I myosins have been shown to function in receptor-mediated endocytosis in *Saccharomyces cerevisiae* (Geli and Riezman, 1996). A type I myosin has also been identified in *Aspergillus nidulans* and it was shown to function in actin dependent endocytosis as demonstrated by the internalisation of FM4-64 (Yamashita and May, 1998).

1.4 Ion concentration measurement in living cells

To investigate the role of cytosolic pH and $[Ca^{2+}]_c$ in cell functions like tip growth, intracellular differences in [ion] have to be monitored on the single cell level *in vivo*. There are several methods available to measure ion concentration in living cells, each with certain advantages and disadvantages (Sections 1.4.1-1.4.6). Ideally the method of measurement should satisfy the following criteria (Parton and Read, 1999): have a high selectivity for the ion of interest; provide an accurate quantification of ion concentration; provide high spatial and temporal resolution; and cause as little as possible interference with normal cell activities. Whereas some methods are restricted to either pH or Ca^{2+} measurements, others can be used for either ion by choosing the appropriate sensor.

1.4.1 Accumulation of radio-labelled or fluorescent weak acids and weak bases to determine intracellular pH

Weak acids and weak bases have been used to estimate cytoplasmic pH (pH_c) and vacuolar pH, respectively (Busa and Nuccitelli, 1984; Kurkdjian and Guern, 1989; Guern et al., 1991). The uncharged form of a conjugate acid-base pair can permeate membranes by passive diffusion which leads to accumulation of the probe. Weak acids predominately accumulate in the cytoplasm and weak bases predominately in the more acidic vacuole. When the equilibrium is reached the intracellular and extracellular total concentrations of the probe are measured. The accumulation ratio is a function of the pK (dissociation constant), intracellular and extracellular pH. Unfortunately, the

technique is rather inaccurate, has a low resolution (0.2-1 pH unit) and relatively long response times do not permit measurements of rapid pH changes. Moreover, the method is not normally applicable to single cells and detection of pH heterogeneity in the cytoplasm is not possible. To avoid pH clamping only low concentrations can be used. However, this sensitivity of intracellular pH to high probe concentrations allows the use of weak acids and bases to actively change intracellular pH (Parton et al., 1997).

1.4.2 Intracellular pH measurement by in vivo 31^P-nuclear magnetic resonance (NMR)

This technique relies on the fact that, when irradiated with an alternating electromagnetic field, the resonance frequency of the phosphorus nucleus of inorganic phosphate and other phosphorylated compounds depends strongly on pH (Busa and Nuccitelli, 1984; Kurkdjian and Guern, 1989; Guern et al., 1991). The method determines the pH-dependent chemical shift in the resonance of the phosphorus nuclei in comparison to a standard compound. The chemical shifts of glucose 6-phosphate and cytoplasmic inorganic phosphate enable the determination of pH_c, whereas the chemical shift of vacuolar inorganic phosphate allows an estimate of vacuolar pH values. Therefore, simultaneous measurement of the cytoplasmic and vacuolar pH is possible. The technique can be applied between pH 5.0 and 7.7, has a resolution 0.1-0.15 pH unit and provides additional information about the concentration of inorganic phosphate, hexose phosphates and nucleotides. Disadvantages are the large amount of biological material needed and the low time resolution (several min). The method does not permit measurement of localised pH_c domains at the single cell level.

1.4.3 Ion-sensitive microelectrodes

A typical ion selective microelectrode is a glass micropipette filled at the very tip with a hydrophobic sensor resin followed by the reference buffer (Felle, 1989; Guern et al., 1991). After impalement the electrode reports the electrochemical potential of the

relevant ion across the plasma membrane. The electrochemical potential is the sum of the chemical potential (caused by the ion gradient across the ion-selective microelectrode tip) and the membrane potential. A reference electrode has therefore to be employed to simultaneously record the membrane potential which has to be subtracted from the total potential reported by the ion-sensitive electrode. pH-sensitive microelectrodes are suitable for measuring pH in the range of pH 2.0 to 12.0 depending on the sensor used. Ca^{2+}-sensitive microelectrodes exhibit detection limits close to pCa 8. Although resin filled ion selective microelectrodes have a relatively fast response time (in the range of sec), they are much slower than voltage electrodes and artefactual ion transients can arise from fast changes of membrane potential. A main disadvantage is that microelectrodes always yield point measurements and do not allow ion concentration to be measured across the whole compartment. Also, measurements in tip-growing cells have to be subapical because insertion of a micropipette at the extending apex would rupture the cell.

1.4.4 Aequorin

Aequorin is a photoprotein consisting of the aequorin apoprotein, the cofactor coelenterazine and bound oxygen. Upon binding Ca^{2+}, aequorin emits blue light (475 nm) resulting from the oxidation of colenterazine. The gene encoding the apoprotein can be transformed into the genome of organisms and it is possible to target the protein to specific subcellular compartments. When transformed cells or organisms are incubated with coelenterazine, active aequorin forms and Ca^{2+} can be measured upon emission of blue light (Gilroy, 1997). The gene for apoaequorin has been successfully transformed into filamentous fungi such as *Neurospora crassa* (Collis, 1996) and *Aspergillus niger* and *A. awamori* (Nelson, 1999). However, aequorin is difficult to calibrate, generally has a low quantum efficiency and signal levels are usually too low to allow subcellular imaging (Gilroy, 1997).

1.4.5 pH- and Ca^{2+}-sensitive indicators based on green fluorescent protein

A new development are pH-sensitive mutants of green fluorescent protein (GFP) which can be introduced into cells or organelles by genetic manipulation (Llopis et al., 1998; Miesenböck et al., 1998). The range of pH-sensitive GFP mutants includes molecules which increase in fluorescence with increasing pH as well as ratiometric molecules. The latter are based on the observation that the excitation spectrum of wild type GFP shows a main peak at 395 nm and a smaller peak at 475 nm. The molecule was structurally altered to achieve a reversible excitation ratio change which is dependent on pH. At higher pH values excitation at 395 nm is more efficient whereas at lower pH values the excitation maximum at 475 nm increases. The method appears to be very promising, but is still being developed and has not yet been applied to fungi.

Genetically encoded fluorescent indicators for Ca^{2+}-measurement which do not depend upon cofactors have been developed and named camaeleons (Miyawaki et al., 1997). They are targetable to specific intracellular locations and consist of tandem fusions of a blue- or cyan-emitting GFP mutant, calmodulin, the calmodulin-binding peptide M13 and a green- or yellow-emitting GFP. The technique is based on fluorescence resonance energy transfer (FRET) between the two GFP molecules, which requires the emission spectrum of the GFP emitting at blue or cyan (donor) to overlap with the excitation spectrum of the GFP emitting at green or yellow (acceptor). FRET is only possible if donor and acceptor are sufficiently close. Binding of Ca^{2+} makes calmodulin wrap around the M13 domain, decreasing the distance between the two flanking GFPs and allowing FRET to occur upon excitation of the donor GFP. The ratio of the emission intensities of both GFPs is dependent on $[Ca^{2+}]_c$. Measurement of $[Ca^{2+}]$ in the range of 10^{-8} to 10^{-2} is possible with appropriate calmodulin mutations. However, the method is still in its infancy and will need further improvement in the GFP mutants to reduce leakage of the donor emission into the acceptor emission band and to increase the extent of maximal ratio changes.

1.4.6 Fluorescent dyes for Ca^{2+} and pH measurement

This method has been used extensively for the determination of Ca^{2+} and pH at the single cell level and abundant information about this technique is available. A great advantage of this approach is the high spatial resolution achievable. Therefore, it currently is the method of choice for investigating the occurrence of intracellular ion gradients. When used appropriately, the method satisfies the criteria listed under Section 1.4.

1.4.6.1 Characteristics of ion-sensitive fluorescent dyes

Fluorescent probes with high selecticity for certain ions (e.g. Ca^{2+} or protons) can be used to visualise these ions in single cell preparations (Czarnik, 1995; Haugland, 1996). The dyes exhibit spectral properties that vary with the concentration of the ion of interest. Ca^{2+}-sensitive dyes such as Fluo-3, Calcium green and Oregon green 488 BAPTA-1 and pH-sensitive dyes such as carboxy fluorescein show an increase in their fluorescence intensity which is proportional across the whole emission spectrum with increasing ion concentration (Figure 1.7A). These so called single-wavelength dyes are difficult to calibrate because the dye distribution within a cell is normally not homogeneous and consequently the amount of dye measured can vary. Dual wavelength (or ratio) dyes overcome this problem by exhibiting a shift in either their excitation or emission spectrum after binding to the ion (Bright et al., 1987; Read et al., 1992; Haugland, 1996; Parton and Read, 1999). The ratio of the fluorescence intensity at the two excitation or emission wavelengths is independent of the amount of dye measured but proportional to ion concentration. Ratio dyes for pH excited with visible light include the dual excitation dye BCECF and the dual emission dye cSNARF-1 (Figure 1.7B) (Haugland, 1996). Ratio dyes for Ca^{2+} are exclusively excited in the UV range and include Fura-2 (dual excitation) and Indo-1 (dual emission). To overcome the requirement for UV excitation for Ca^{2+} ratio imaging, a ratiometric approach using a mixture of dyes can be employed (Opas, 1997). Both dyes are excited at wavelengths in the visible range. It is usually a combination of a

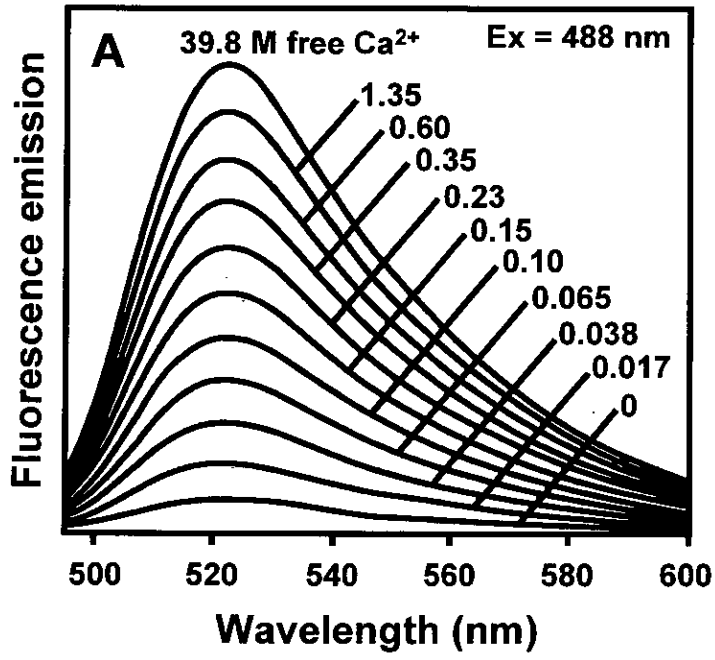

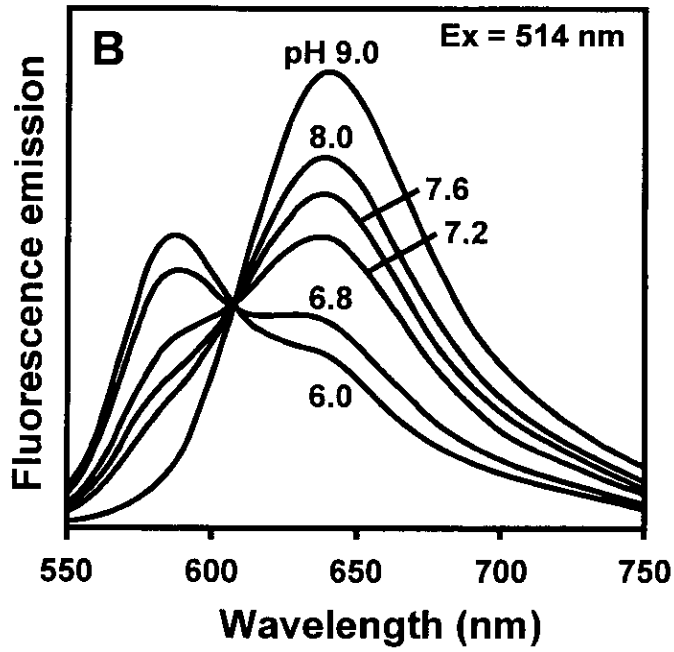

Figure 1.7. Fluorescence emission spectra of dyes used for intracellular ion concentration measurement (based on Haugland, 1996). (**A**) The emission intensity of the calcium sensitive single wavelength dye Oregon green 488 BAPTA-1 is directly proportional to the free calcium ion concentration. (**B**) The dual emission ratio dye carboxy SNARF-1 which is pH sensitive shows two emission peaks, one for the protonated and one for the deprotonated form of the dye. A ratio of the fluorescent peaks of the two forms is proportional to pH but independent of dye concentration.

Ca^{2+}-sensitive single wavelength dye such as Fluo-3 or Calcium green with either a Ca^{2+}-insensitive volume marker such as Rhodamine B (Bibikova et al., 1997) or with Fura Red which decreases its fluorescence intensity upon Ca^{2+}-binding (Lipp and Niggli, 1993). Care has to be taken to ensure that both dyes colocalise, that emission spectra can be separated sufficiently by the optical filters available and that adequate correction of bleed through is performed (Morris, 1993).

1.4.6.1 Loading of fluorescent dyes into cells

There are several procedures for introducing fluorescent dyes into walled cells (Callaham and Hepler, 1991; Read et al., 1992; Oparka and Read, 1994; Parton and Read, 1999). For ester-loading uncharged, lipophilic acetoxy methyl-ester (AM-ester) derivatives of dye molecules are used. These AM-esters are usually non-fluorescent and able to cross the plasma membrane. Inside the cell the AM-groups are cleaved off by non-specific esterases and the now charged, hydrophilic dye molecule, which is fluorescent, cannot readily cross the cell membrane again. Ester-loading also applies to Carboxy fluorescein diacetate (CFDA) which is the acetate-ester of Carboxy fluorescein. Another loading method is acid loading. This procedure is based on sufficient acidification of the culture medium to keep the dye molecule in its protonated uncharged form allowing it to cross the plasma membrane. The method requires prolonged incubations under conditions which can be far different from the experimental conditions and often results in poor loading (Callaham and Hepler, 1991, Read et al., 1992; Parton, 1996). Microinjection involves impaling a cell with a fine glass pipette filled with dye and subsequently discharging dye into the cell (Callaham and Hepler, 1991; Correa and Hoch, 1993; Jackson, 1995). The dye is driven into the cell either by an electric current (ionophoresis) which works for small charged molecules or by pressure (pressure microinjection) which is necessary to introduce larger and uncharged molecules. Ionophoresis is considered to be the less disruptive form of microinjection because it involves no pressure or volume changes. Additionally, a micropipette with a smaller tip diameter can be used allowing one to minimise wounding when the cell is impaled. In contrast, pressure microinjection is much more difficult to perform and more invasive because it alters the cell's volume

and turgor pressure. However, there are reports describing the successful pressure injection of fungal cells (Correa and Hoch, 1993; Jackson, 1995; Parton et al., 1997).

In fungal hyphae and in plant cells fluorescent indicator dyes have a tendency to be sequestered into organelles and to leak out (Read et al., 1992; Knight et al., 1993; Slayman et al., 1994; Brauer et al., 1996; Parton et al., 1997). An approach to avoid this problem is the use of high molecular weight dextran conjugates of the dyes which have to be loaded by pressure microinjection (Parton et al., 1997).

1.4.6.2 Ion imaging

The two main microscope technologies used for ion imaging are conventional fluorescence microscopy and confocal laser scanning microscopy (CLSM). With the appropriate equipment conventional imaging can be used with all the ratio dyes available (Read et al., 1992). However, it has the disadvantage that for objects which are not infinitely thin, the apparent depth of field is very much greater than the actual axial resolution. The out-of-focus light is collected as well and reduces the contrast of the signal from the region in focus. CLSM, on the other hand, eliminates the unwanted light ("out-of-focus blur") and only objects which lie within the depth of field given by the axial resolution of the microscope are visible (Pawley, 1995). With CLSM a laser is used for irradiation and there are only a limited number of laser lines available which restricts the number of dyes that can be used with this system. A considerable disadvantage of CLSM is the slow rate of imaging due to the low numbers of photons which may be collected in a given time. In conventional fluorescence imaging on the contrary, light from the whole imaged field is detected simultaneously allowing rapid image capture (Parton and Read, 1999).

Ion imaging can easily lead to artefacts (Moore et al., 1990; Bolsover and Silver, 1991; Silver et al., 1992; Read et al., 1992; Fricker et al., 1994; Slayman et al., 1994; Parton and Read, 1999). The most obvious problems are sequestration of ester-loaded dyes into organelles and leakage of the dyes from cells. The prevention of dye sequestration by applying organic anion transport inhibitors proved to be unsuccessful

for fungal hyphae (Knight et al., 1993). Opitz et al. (1994) observed an intracellular redistribution of the protonated indicator form of cSNARF-1 between cytosol and lipophilic compartments which lead to intracellular pK shifts of the indicator. These problems create the need for careful assessment of dye distribution. However, the only way to avoid them is probably the use of dye-dextran conjugates (Pierson et al., 1996; Parton et al., 1997). Other factors influencing dye fluorescence are the viscosity of the medium, the presence of other ions and the potential binding of dyes to proteins (Moore et al., 1990). A high intracellular concentration of dye may have cytotoxic effects and also buffer the ion of interest. The combination of dye loading and irradiation can be very detrimental to cell health caused by various effects of dye-light interactions (Pawley, 1995). Additionally, irradiation can lead to dye bleaching and the appearance of fluorescent but ion-insensitive dye-derivatives. This may result in low fluorescence signal and changed dye properties. In general it is good practice to reduce dye concentration and illumination as far as possible and to do appropriate controls to assess cell health (Callaham and Hepler, 1991; Read et al., 1992). Calibration - even of ratioable dyes - is difficult. As already pointed out, intracellular dye behaviour can change dye properties which is difficult to take into account with *in vitro* calibrations. *In vivo* calibrations create non-physiological conditions in cells making the results difficult to interprete (Fricker et al., 1994). The best approach is probably to combine imaging techniques with other methods such as microelectrode measurements (Kropf et al., 1995). Optimal set-up of the imaging system is needed to allow good performance and avoidance of artefacts created by, for example, chromatic aberration or by over- or under-sampling (Fricker et al., 1994; Pawley, 1995). In spite of all the technical pitfalls mentioned so far, when done carefully, ion imaging is a very important and powerful technique for the measurement of Ca^{2+} and pH. Main advantages are the high spatial resolution achievable and the versatility of the technique (Callaham and Hepler, 1991; Morris, 1993; Parton and Read, 1999).

1.5 Imaging of endocytosis and membrane trafficking

A main feature of tip growth is the accumulation of secretory vesicles at the apex and their subsequent fusion with the plasma membrane which leads to secretion of cell wall precursors and insertion of new cell membrane. It has been estimated that the new cell membrane generated is surplus to requirements for extension necessitating membrane recycling via endocytic vesicles (Section 1.3). There are several techniques available to measure exocytosis, endocytosis and membrane trafficking in living cells. Electrophysiological methods rely on patch-clamp measurements to determine increase (during exocytosis) or decrease (during endocytosis) of membrane surface area measured as changes in membrane capacitance (Angleson and Betz, 1997). Patch clamp measurements are not applicable to study processes in growing fungal hyphae because the necessity to remove the cell wall disrupts tip growth (Roberts et al., 1997). Electrochemical methods for measuring released secretory contents are limited to monitoring exocytosis (Angleson and Betz, 1997) and are not applicable to growing hyphae, either. Most promising for investigating membrane trafficking in growing fungal hyphae are optical methods for imaging membranes of compartments of the vesicle trafficking network that are stained with fluorescent dyes (Hoffmann and Mendgen, 1998; Read et al., 1998). Although exhibiting lower time resolution than electrochemical and electrophysiological methods these techniques can provide the necessary spatial information. Amphiphilic fluorescent styryl dyes like FM4-64 and FM1-43 (Fig. 1.8) have been designed for studying activity-dependent endosomal trafficking in living cells. They are believed to insert into the outer leaflet of surface membranes and to be unable to penetrate through membranes. The fluorescence is quenched in water and the quantum yield increases enormously when the dyes are dissolved in membranes (Betz et al., 1996). A recent report showed FM4-64 to be a reliable endocytosis marker in yeast using conventional fluorescence microscopy (Vida and Emr, 1995).

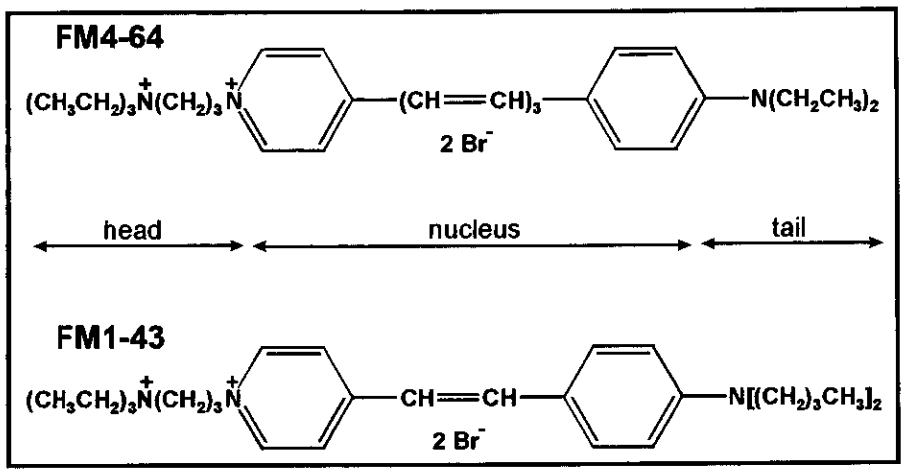

Figure 1.8 Molecular structures of FM 4-64 and FM 1-43 (Betz et al., 1996). The molecules are composed of three elements: a hydrophobic tail (partitions into membranes), a dicationic head (prevents membrane permeation) and a body or nucleus (determines spectral properties due to aromatic rings and double bonds).

1.6 Outline of the thesis

Fungal hyphae extend by the localised deposition of new plasma membrane and cell wall at the apex. This rather complex process is not yet fully understood (Section 1.1 and 1.2) and deserves further investigation.

The ascomycete *Neurospora crassa* is used as a research organism in many laboratories due to many advantageous features (Perkins, 1992): the fungus is haploid, nutritional requirements are simple, stocks can be preserved in suspended animation, growth is fast and generation time short. Over the decades a wealth of information has accumulated concerning genetics, biochemistry and morphology of this fungus. Additionally, many morphological mutant strains including strains with alteration in growth polarity are available. The hyphae are of sufficient size (diameter typically 8-20 μm) to allow microscopical observation and micromanipulation. For these reasons *Neurospora* was chosen as the experimental system to investigate novel aspects of the regulation of hyphal tip growth.

There is evidence that gradients in ion concentration, notably protons and Ca^{2+}, are involved in tip growth regulation. However, reports investigating the role of a

gradient in cytosolic pH in tip growth differ considerably in their findings and remain contradictory (Section 1.2.4.2). The first aim of this Ph.D.-project was to investigate whether there is a tip focused gradient of pH in tip growing cells of *Neurospora* and if such a gradient is required for tip growth. Using the dual emission dye cSNARF-1 and CLSM, the role of intracellular pH in tip growth was investigated with careful assessment of imaging parameters and taking into account limitations of the imaging technique. Using fluorescent dyes it is difficult to distinguish cytosolic pH from pH_c and in the context of this study pH_c will be used. The results indicated the absence of a significant gradient in pH_c (pH difference of > 0.1 unit) in growing hyphae within the first 50 μm behind the apical pole. However, tip growth was sensitive to any alteration in the normally maintained pH_c indicating that the tight regulation of pH_c is crucial for proper cell functioning.

The second aim of the research was to investigate the involvement of gradients of $[Ca^{2+}]_c$ in tip growth employing and extending the techniques established for imaging pH_c. Although Levina et al. (1995) show a Ca^{2+}-gradient in *Neurospora* using confocal microscopy of a Ca^{2+}-sensitive ratiometric dye combination, their data is not convincing and there is still the need to determine whether a tip high gradient of $[Ca^{2+}]_c$ does indeed exist in growing *Neurospora* hyphae. Therefore, a confocal ratiometric method using dextran conjugated derivatives of fluorescent dyes was developed in order to obtain reliable measurements of $[Ca^{2+}]_c$ in *Neurospora* hyphae.

Two new dyes (FM4-64 and FM1-43) have been used by others to image endocytosis and exocytosis in living animal and yeast cells (Haugland, 1996). In the present study living hyphae loaded with these dyes have been imaged by confocal microscopy for the first time. Evidence for endocytosis, and the integration of the endocytic and exocytotic pathways in *Neurospora* has been obtained. FM4-64 was found to stain the Spitzenkörper and this study provides the first confocal images of stained Spitzenkörper in living hyphae.

2. Materials and Methods

2.1. Chemicals

If not stated otherwise, chemicals were either purchased from BDH Ltd. (Poole, Dorset, UK), Aldrich Chemical Co (Gillingham, Dorset, UK) or Sigma Chemical Co (Poole, Dorset, UK).

2.2 Fungal material

Experiments were mainly performed on *Neurospora crassa* Shear and Dodge, wild type (74A, FGSC 262 from Fungal Genetics Stock Centre, Arcata, CA). Other fungi used were: the kinesin deficient mutant of *Neurospora crassa* NK01 (kind gift of M. Schliwa; Seiler et al., 1997); *Trichoderma viride* Pers.: Fr. (No. 2011 from J. F. Tuite, Purdue University); and *Rhizoctonia solani* Kuhn (No. 283 from E. E. Butler, University of California, Davis).

2.3 Media

2.3.1 Vogel's Medium

The standard culture medium employed was Vogel's Medium N (Vogel, 1956) plus 2% (w/v) sucrose, pH 5.8 (abbreviated as VM). It proved highly suitable for culturing *N. crassa* wild type, *N. crassa* NK01 mutant, *T. viride* and *R. solani*. Potato dextrose medium, which was used by López-Franco et al. (1994; 1995) for *N. crassa*, *T. viride* and *R. solani*, was not used here because, unlike VM, it exhibited considerable autofluorescence during fluorescence microscopy.

The composition of VM is listed in Table 2.1. A x50 stock solution was prepared and could be stored at room temperature for up to 18 months. The final medium was obtained after adding dH_2O and 2% (w/v) sucrose and subsequently autoclaving for

15 min at 121°C. For pouring plates or agar slants in test tubes the medium was solidified by the addition of 2% (w/v) of agar (Oxoid Agar No 3; Unipath Ltd., Basingstoke, Hampshire, UK).

Table 2.1. Composition of Vogel's medium

Component	molecular weight	X50 stock contains per litre dH_2O	final concentration in standard culture
Na_3 Citrate·2(H_2O)	294.1	126.7 g	8.62 mM
KH_2PO_4	136.1	250.0 g	36.74 mM
NH_4NO_3	80.04	100.0 g	24.98 mM
$MgSO_4$·7(H_2O)	246.5	10.0 g	0.81 mM
$CaCl_2$·2(H_2O)	147.0	5 g	0.68 mM
*Trace elements solution	-	5 ml stock	-
**Biotin solution	-	5 ml stock	-
Chloroform	-	2-3 ml	-

*Trace elements solution stock contains per 100 ml dH_2O	
Citric acid·1(H_2O)	5 g
$ZnSO_4$·7(H_2O)	5 g
$Fe(NH_4)_2$ (SO_4)$_2$·7(H_2O)	1 g
$CuSO_4$·5(H_2O)	0.25 g
$MnSO_4$·1(H_2O)	0.05 g
H_3BO_4	0.05 g
Na_2MoO_4·2(H_2O)	0.05 g

**Biotin solution stock contains per 100 ml 50% EtOH	
d-Biotin	5 g

2.3.2 Modifications of Vogel's Medium

In cases where a higher osmolarity of the medium was necessary to prevent bursting of hyphal tips (Section 2.5.2) the concentration of VM was increased by 10% (VM_{110}). For pH treatments, VM was diluted with sterile dH_2O to obtain half strength Vogel's medium (½VM), pH 5.95. Extracellular pH treatment was performed with ½VM, which was adjusted to pH 7.0 or 8.0 with 1.7 M KOH. Manipulation of intracellular pH was achieved with cell permeant weak acid and weak base solutions: ½VM containing 50 mM sodium propionate was adjusted with KOH to pH 6.15, 6.5 and 7.0 and ½VM containing 50 mM trimethylamine (TMA) was adjusted with KOH to pH 7.5 and 8.0. With all media the K^+ concentration was titrated to a final value of 38 mM with 1.7 M KCl to avoid affecting the membrane potential (Slayman and Slayman, 1962) and the H^+/K^+ symport mechanism (Rodriguez-Navarro et al., 1986). This value was determined by the amount of KOH necessary to adjust ½VM plus TMA, the strongest buffered medium, to pH 8.0.

2.4 Storage of fungal material

In order to provide spores for inoculation purposes, the *Neurospora* wild type and the mutant strain were cultured on agar slants (15 cm test tubes containing VM agar slants set at a steep angle and plugged with non-absorbent cotton wool). Incubation was at 25°C for 5-7 days until abundant spore production was evident (Davis and de Serres, 1970). Subsequently, test tubes were kept at 4°C for up to 4 weeks and spores from them were used to inoculate agar plates.

For long term storage, *Neurospora* spores were preserved on silica gel (Davis and de Serres, 1970; Smith and Onions, 1983). Silica gel (1-3 mm particle size) was sterilised at 180°C for 1.5 h and, after cooling, filled into sterile 20 ml glass vials with screw caps until half full (about 10 g silica gel per vial). The vials were temporarily closed and put on ice. The combined spores produced on one or two agar slants were suspended in 2 ml, autoclaved, 7% (w/v) non-fat dry milk (Marvel, obtained through Sainsburies, UK) in dH_2O. About 500 µl of this spore suspension was added drop-

wise to the silica gel in a vial which was held horizontally with the gel distributed along its length. The vial was subsequently tightly shut, vigorously shaken until the spores appeared to be evenly distributed, and finally put back on ice to dissipate the heat released by wetting the silica gel with the spore suspension. Vials were stored at 4°C in a sealed plastic box with a desiccant.

T. viride and *R. solani* were grown on VM agar slants plugged with cotton wool for two weeks at 25°C and subsequently stored at 4°C. The fungi were transferred to fresh agar slants every six months.

2.5 Culture methods

2.5.1 Culture on agar plates

Fungal inoculum was placed on 5 cm diameter plastic Petri dishes (Fisher Scientific UK, Loughborough, Leicestershire, UK) containing solid VM overlaid with sterile cellophane (gauge 525, uncoated Rayophane from A. A. Packaging, Walmer Bridge, Lancs., UK). *N. crassa* hyphae for pH treatments with media based on ½VM were grown on ½VM medium which was solidified with 2% (w/v) agar and overlaid with cellophane. Cultures were incubated at 25°C in the dark until the mycelial disk was 3-4 cm in diameter. About 7x7 mm sized pieces of cellophane containing the leading edge of the colony were excised and transferred to slide cultures (Section 2.5.2) or to race tubes (Section 2.9.1).

2.5.2 Slide cultures

2.5.2.1 Sandwich culture

For "sandwich cultures", a mounting method similar to the one described in Knight et al. (1993) was used: 1-2 mm wide strips of lithographer's tape (No. 616 Scotch Brand Lithographers tape, 3M) were placed on either long side of a glass coverslip (No. 1½, 22 x 50 mm, Chance Proper Ltd., obtained through Fisher Scientific UK) to

support an overlying coverslip (No. 1½, 18 x 18 mm, Chance Proper Ltd.). A 35 µl drop of medium was placed onto the lower coverslip and subsequently the piece of cellophane containing mycelium (Section 2.5.1) was carefully placed into the liquid. The mycelium usually floated off as soon as it contacted the liquid and the cellophane could easily be removed. The top coverslip was mounted carefully on the supporting strips of tape and held in place by small amounts of silicon grease (BDH Ltd.) on the edges. As a result of these procedures hyphae stopped growth and showed tip swelling but growth usually resumed within 2-10 min in the form of one or more new narrower tips (Figure 2.1). According to Robertson (1958), apical branching of hyphae is typical after treatments which temporarily arrest growth. Exchange of medium under the coverslip was performed by gently sucking through fresh medium using wicks cut from filter paper (Whatman No. 1, Fisher Scientific UK). To assess the physical effect of medium exchange on growing tips in sandwich culture, medium (VM) was exchanged with medium of the same composition. During this procedure, hyphae did not undergo tip swelling, tip growth did not stop and only a slight indentation in the lateral cell wall marked the point of treatment with an occasional slight reduction in diameter (Figure 2.1 arrow). The coverslip on top most likely restricts the oxygen supply to the mycelium. However, even though *Neurospora* is an obligate aerobe it still grows normally at low oxygen tensions (Slayman, 1965).

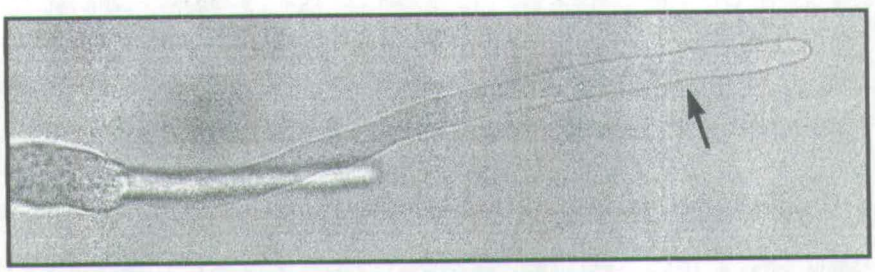

Figure 2.1. *N. crassa* hyphae in sandwich culture. After recovery two new tips of smaller diameter than the original hyphal tip emerged from the apex. The shorter apical branch is outside the focal plane. The arrow indicates the point when medium was exchanged against identical solution.

2.5.2.2 Open culture

"Open cultures" consisted of a thin layer of VM solidified with 2% (w/v) agarose (15 Electran, BDH Ltd.) evenly spread on a glass coverslip (No. 1½, 22 x 55 or 22 x 64 mm, Chance Proper Ltd.). For this procedure, 5 ml aliquots of VM with 2% agarose were autoclaved and stored for up to 8 weeks at 4°C. Immediately before use the medium was heated until completely liquid in a microwave oven and kept molten in a 70°C water bath. Coverslips were washed in 70% EtOH and then in sterile dH_2O. The dry coverslip was held at a steep angle and coated thinly and evenly with about 50 µl or 60 µl medium (depending on the size of the coverslip) starting from the top and working down. The medium rapidly solidified forming a thin layer. Two coated slides were put into an 8.5 cm diameter Petri dish (Disposables Media, Philip Harris Ltd., Clydebank, UK) with a disk of wet filter paper (Whatman No. 1) on the bottom to form a humid chamber. These chambers were sealed with Parafilm (PM 992, American National Can Co., obtained through Sigma) and stored at 4°C for a maximum of two days before use.

Slides were inoculated by placing a piece of cellophane containing mycelium on one end of the medium layer with the hyphal tips facing towards the other end. Subsequent incubation in the humid chamber at 25°C allowed the mycelium to extend between 0.5 and 1 cm over the agarose surface. Shortly before use the slides were covered with 150 µl of liquid VM_{110}. Frequently, bursting of hyphal tips was observed upon addition of VM. This was probably due to a mismatch in osmolarity between the VM agarose layer and liquid VM as a result of evaporation from the VM agarose during slide preparation. Robertson and Rizvi (1968) observed that hyphal tips of *Neurospora crassa* burst in contact with hypotonic solutions. Increasing the concentration of the medium used for covering by 10% (VM_{110}) greatly reduced the problem. After covering with VM_{110} hyphal tips swelled and resumed tip-growth within 2-5 min usually in form of one or two new tips (Figure 2.2). This behaviour corresponds with the one described by Robertson and Rizvi (1968) who state that any flooding treatment causes a cessation of growth in *N. crassa* and that hyphae frequently react with tip swelling, narrowing of the hyphal apex and branching when

growth resumes. The open cultures could be used for up to an hour after covering with medium. Cytoplasmic streaming throughout the mycelium was evident about 15 min after covering with liquid medium. Additions to the culture medium were added drop-wise on top of the liquid medium. If exchange of medium was necessary, the slide was held at a steep angle and rinsed gently in growth direction with 1 ml of fresh medium. Open culture was employed when free access to the hyphae was important and when oxygen deprivation had to be avoided.

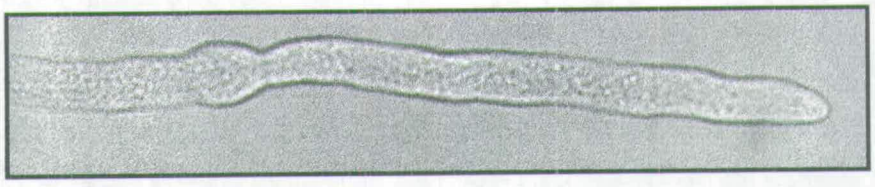

Figure 2.2. *N. crassa* hyphae in open culture. After recovery a new tip with a diameter similar to the original hyphal tip is formed.

2.6 Dye loading

Table 2.2 gives an overview of the fluorescent dyes used and the dye loading conditions. Pluronic F-127 and dyes were purchased from Molecular Probes Inc. (Eugene, Oregon, USA) except CFDA which was obtained from Sigma.

Generally the free acids and dextran conjugates of ion-sensitive dyes are cell impermeant and have to be introduced into the cell by a more invasive technique such as microinjection (Section 2.6.2). An alternative to the dye free acids are their cell permeant esters. Once inside the cell they are cleaved to yield the dye free acid. Other dyes are readily taken up by the cell and can be loaded directly (Oparka and Read, 1994).

The low pH loading method for introducing the free acids of ion sensitive dyes into hyphae was not attempted here because it is described as yielding unsatisfactorily low loading levels (Knight et al. 1993; Parton, 1996).

Table 2.2. Fluorescent dyes and loading conditions

Dye	Application	Loading method	stock solution	sub stock	final conc.	References
BCECF-AM ester	pH	Ester-loading	10 mM in DMSO	250 μM in 0.04% aqueous Pluronic	5-10 μM in medium	Robson et al., 1996; Fricker et al., 1997
cSNARF-1-free acid	pH	pressure MI	1 mM in dH_2O	---	1 mM in pipette tip	Opitz et al., 1994
cSNARF-1-AM ester	pH	Ester-loading	20 mM in DMSO	200 μM in 0.04% aqueous Pluronic	2-5 μM in medium	Slayman et al., 1994
cSNARF-1 10 kDa dextran	pH	pressure MI	1 mM in dH_2O	---	1 mM in pipette tip	Thiebaut, 1990; Gibbon and Kropf, 1994
CG-1 10 kDa dextran	Ca^{2+}	pressure MI	1 mM in dH_2O	---	1 mM in pipette tip	Messerli and Robinson,1997
OG-1 free acid	Ca^{2+}	ionophoretic MI; pressure MI	1 mM in dH_2O	---	1 mM in pipette tip	Brain and Bennett, 1997
OG-1 AM ester	Ca^{2+}	Ester-loading	10 mM in DMSO	200 μM in 0.04% aqueous Pluronic	20 μM in medium	Tertyshnikova and Fein, 1998
OG-1 10 kDa dextran	Ca^{2+}	ionophoretic MI; pressure MI	1 mM in dH_2O	---	1 mM in pipette tip	Brain and Bennett, 1997
RB 10 kDa dextran	volume marker for coinjection	pressure MI	1 mM in dH_2O	---	1 mM in pipette tip	Meng, 1994; Stricker, 1995; Bibikova et al., 1997

Table continued on following page

Table 2.2. (continued) Fluorescent dyes and loading conditions

Dye	Application	Loading method	stock solution	sub stock	final conc.	References
CFDA	fungal vacuoles	Ester-loading	5 mM in EtOH	---	20 µM in medium	Rees et al., 1994
DASPMI	mitochondria	can pass PM	27 mM in DMF	2.7 mM in dH_2O	27 µM in medium	Miyakawa,1984; Vida and Emr, 1995
FM 4-64	membranes	endocytic uptake	16 mM in DMSO	320 µM in dH_2O	3.2 - 12.8 µM in medium	Heuser et al., 1993; Vida and Emr, 1995
FM 1-43	membranes	endocytic uptake	16 mM in DMSO	320 µM in dH_2O	6.4 µM in medium	Smith and Betz, 1996

CG-1 = Calcium Green-1, conc. = concentration, MI = Microinjection, OG-1 = Oregon Green 488 BAPTA-1, PM = Plasma membrane, RB = Rhodamine B.

Stock solutions of AM-ester were generally stored at -70°C; all other dye stock solutions were kept at -20°C.
Sub stocks of AM-ester were kept at -20°C and used within 2 weeks. All other sub stocks could be stored at 4°C for several months.

2.6.1 Loading of cell permeant dyes

These dyes have only limited solubility in aqueous solutions and have to be dissolved in organic solvents before they can be diluted into the medium. In all cases the concentration of solvents (DMF, DMSO and EtOH) was kept below 0.2% (v/v) in the final loading medium. Pluronic F-127, a surfactant of low toxicity, helps to disperse AM-ester and so assists dye uptake (Haugland, 1996; Oparka and Read, 1994).

Two loading procedures were used: a) dye was loaded for 10-15 min and then washed out and b) continuous loading. The latter was employed when washing out was impractical, or lead to critical reduction in signal intensity as in the case of cSNARF-1 AM-ester. With the dyes used here, continuous loading was not found to lead to an increase in the fluorescence of the extracellular medium.

2.6.2 Microinjection

2.6.2.1 Equipment and general procedure

Microinjection was carried out on a Nikon Diaphot TMD inverted microscope (Nikon UK Ltd., Kingston, Surrey, UK) set up for fluorescence microscopy and fitted with Narishige (N-88) micromanipulators (supplied by Nikon UK Ltd.). The microscope was placed on a vibration free table (Newport Vibration isolated workstations - VW series, Newport Corporation, Irvine, California, USA).

For experiments involving coinjection of OG-1 and RB, the Narishige (N-88) micromanipulators were moved to a Leica DM IRBE microscope equipped with epifluorescence (Leica Microsystems Heidelberg GmbH, Germany).

Micropipettes for microinjection of dyes were pulled from borosilicate glass capillaries with filament (GC-100F, Clark Electromedical Instruments, Pangbourne, Reading, UK) on a Campden micropipette puller 773-082 (Campden Instruments Ltd., Sileby, Loughborough, UK) using a three stage programmed pull. Settings had to be

regularly adjusted to account for day-to-day variability. Dye was filtered (200 nm exclusion filter, Millipore Ltd., Watford, Hertfordshire, UK) to remove precipitates before back-filling needles. Back-filling was achieved by placing a 1 µl droplet of dye solution at the blunt end of the needle. Due to the filament in the capillary, dye moved towards the fine tip to fill it completely. Subsequently, the rest of the needle was filled with 100 mM KCl for ionophoresis or low-viscosity silicone oil (Dow Corning 200 / 20 cs; BDH Ltd.) for pressure microinjection, using a modified plastic syringe as described by Callaham and Hepler (1991).

For microinjection, *N. crassa* wild type hyphae were grown in open culture. The optimum time for injection proved to be 4-6 h after inoculation. By then only a limited number of aerial hyphae had developed. Hyphae growing on the agarose surface were found to be firmly adherent to the medium (Wilson, 1961) which allowed easy access of the needle and stopped the hyphae from moving during the injection process. The micropipette was placed perpendicular to the cell wall at an angle of 30-45 degree to the agarose using a dry x40 plan apo objective. After covering with liquid medium, newly formed hyphal tips had a tendency to grow within the liquid layer and sometimes out-of-focus. For this reason apical compartments were injected within 15 min of being covered with medium to ensure that these cell compartment were still adherent to the medium. Injection into the apical compartment was carried out near the first septum and was considered to be successful if the fluorescent signal intensity was appropriate and the tip resumed growth. For subapical injection a compartment with cytoplasmic streaming was chosen. The injection was considered successful if the cytoplasmic streaming recovered after sufficient dye had been loaded. After microinjection the micropipette was withdrawn slowly over a period of several minutes.

2.6.2.2 Ionophoretic microinjection

The micropipette, backfilled with KCl, was inserted into a needle holder (EH-3MS 120W, Clark Electromedical Instruments) with a platinum filament and connected to the power supply as described in Knight et al. (1993). Electric current was applied for

3-5 sec for the dye-free acid and 8-10 seconds for the dextran conjugate because the latter entered the cell more slowly. Successfully injected cells lost little cytoplasm and recovered within 5 min.

2.6.2.3 Pressure microinjection

The micropipette was positioned against the cell wall then pressure was increased to about 0.2 MPa using the pressure probe system described by Oparka et al. (1991). This pressure increase moved the micropipette forward so that the tip depressed but did not puncture the cell wall. After penetration the pressure was raised (up to 0.5 MPa if necessary) until dye entry was observed. Due to variability in micropipettes it was not predictable which pressure rise would be sufficient for adequate loading. Increasing the pressure resulted in a slight forward movement of the needle which could easily lead to a wounding too severe for the cell to seal. During injection the degree of loading had to be judged visually by epifluorescence. The loss of cytoplasm after withdrawing of the micropipette was usually greater than with ionophoresis and cells took longer to recover (typically 10-30 min).

2.7 Confocal microscopy

After loading, cells were imaged using a CLSM. In confocal microscopy fluorescence images have significantly better resolution and contrast than those from a conventional light microscope. The CLSM uses an aperture (pinhole) in front of the light detector which rejects out-of-focus blur and allows thin optical sectioning (Czymmek et al., 1994).

2.7.1 Equipment

For confocal microscopy a Bio-Rad MRC 600 CLSM fitted with a 25 mW Argon ion laser (lines at 488 and 514 nm) and connected to a Nikon Diaphot TMD inverted microscope with epifluorescence equipment was employed (all supplied by Bio-Rad Microscience, Hemel Hempstead, Herts., UK). Image capture and processing were

performed with a Research Machines Nimbus 486sx personal computer, containing a Synapse framestore, and running COMOS, MPL and TCSM software (all version 7, supplied by Bio-Rad). The laser beam could be regulated via neutral density filters to 1, 3 or 10% of the full intensity. The MRC 600 was equipped with two photomultipliers, PMT 1 (channel 1) and PMT 2 (channel 2), for fluorescence imaging. Alternatively, channel 2 could be used to collect a brightfield image via an optical fibre which collects light behind the condensor and can be inserted in front of PMT 2. Table 2.3 gives an overview of the filter sets used (all supplied by Bio-Rad).

Table 2.3. Bio-Rad filter sets for the MRC 600

Filterset	Excitation filter	Dichroic mirror	Emission filter	Signal
Standard BHS	488 / 10 nm BF	510 nm LP	515 nm LP	channel 1
Standard GHS	514 / 10 nm BF	540 nm LP	550 nm LP	channel 1
Custom built	---	610 nm LP	580 / 30 nm BF	channel 2
SNARF-block*			640 / 40 nm BF	channel 1

*used in combination with GHS; BF = barrier filter, BHS = blue excitation filter set, GHS = green excitation filter set, LP = longpass filter,

Confocal fluorescence imaging was also performed using the Leica TCS NT Confocal Microscope (Leica Microsystems Heidelberg GmbH, Germany) equipped with 4 channels (PMT 1-4) for fluorescence imaging and 1 brightfield channel (PMT T). The CLSM was controlled by a PC workstation with Pentium Pro processor (200 MHz) running Win NT and the TCS NT software. A 100 mW Argon ion laser and a 25 mW Krypton laser served to generate the excitation light whilst acoustooptical tunable filters allowed continuous adjustment of the intensity of laser lines. Table 2.4 shows the filter combination used.

Table 2.4. Filter set used on the Leica TCS NT

Excitation filter	Dichroic mirror	Emission filter	Signal
488/568 nm DD	580 nm RSP	530 / 30 nm BF	channel 1
		590 nm LP	channel 2

BF = barrier filter, DD = double dichroic mirror, RSP = reflection short pass filter, LP = longpass filter,

For imaging on the Bio-Rad MRC 600 the x40 dry (NA = 0.95) and the x60 oil (NA = 1.4) Nikon plan apo objectives were used. On the Leica TCS NT the x40 dry (NA = 0.75) Leica plan apo objective was employed. The resolution of the objectives under standard imaging conditions (Table 2.5) was estimated in terms of the FWHM (full width half maximum; Cogswell and Larkin, 1995) using green fluorescent microspheres with 63 nm diameter (Bangs Laboratories Inc., Carmel, IN, USA) as described in Technical reference 57 issued by Bangs Laboratory Inc. For this procedure coverslips (No. 1½ , 22 x 50 mm) were washed in 1 M HCl, rinsed with plenty of water, soaked in 0.01% polylysine solution (Sigma) for 10 min and rinsed again with dH_2O. On the coverslip a square was marked out with silicone grease, in which 100 µl of 1:2000 diluted microsphere solution was placed and allowed to settle for about 15 min. Excess liquid was washed off and a second coverslip (18 x 18 mm) placed on top. A series of scans (about 100 nm steps in z orientation) was collected under high zoom settings (zoom 10) through the centre of a microsphere using the 514 nm line on the Bio-Rad MRC 600 and the 568 nm line on the Leica TCS NT. After background subtraction the distance between the fluorescence values of half the maximum fluorescence intensity (FWHM) was measured in the x and z orientation.

Table 2.5. Estimated resolution of Objectives

FWHM	x40 dry plan apo (Nikon)	x60 oil plan apo (Nikon)	x40 dry plan apo (Leica)
lateral (xy)	0.6 µm	0.4 µm	0.5 µm
axial (xz)	1.6 µm	0.8 µm	1.4 µm
wavelength	514 nm	514 nm	568 nm

For data storage, a Panasonic 940 MB WORM optical disc drive (Phoenix computers Ltd., Brackmills, Northants, UK), an EZ 135 Syquest drive (Syquest Technology, Inc., Fremont, CA, USA) and a CD writer (Pilips Electronics NV, Amsterdam, NL) were used.

For producing hard copies, images were assembled on a PC using Confocal assistant (version 3.1, Bio-Rad), Paintshop Pro (version 4.12, JASC Inc., distributed by Digital Workshop, UK) and Powerpoint (version 7.0, Microsoft Corp., USA) and subsequently printed on a HP Deskjet 850 C (Hewlett Packard Company, Palo Alto, CA, USA).

2.7.2 CLSM settings for fluorescence imaging

Settings for CLSM are a compromise between image quality and the need to minimise stress to cells (Pawley, 1995; Parton and Read, 1999). Table 2.6 lists the conditions employed throughout the study. Cell health was assessed in terms of growth, cytoplasmic streaming and appearance under the microscope. Averaging over subsequent frames was not employed routinely because the temporal resolution of the confocal was too low in relation to the fast growth and cytoplasmic streaming of *N. crassa* hyphae. The Bio-Rad MRC 600 offered the possibility of improving the temporal resolution by reducing the box size in vertical orientation. This leads to a decrease in the number of lines necessary to scan one frame. The hyphae was orientated horizontally relative to the frame width and could be imaged in 1/3 of the time used for scanning the full frame, this made averaging of consecutive frames more feasible. The Leica TCS NT does not offer this option and the resolution was kept to 512 scan lines per frame (at a display frame size of 512 x 512 pixel); frame averaging was not employed.

Table 2.6. Settings for CLSM

Variable	Settings	
	Bio-Rad MRC 600	**Leica TCS NT**
Laser power	1 - 3% 25 mW Argon ion laser	~0.5-1% 100 mW Argon ion laser ~25% 25 mW Krypton laser
Scan Speed	F1 = 3 sec per 512 lines F2 = 1 sec per 512 lines	slow = 2.3 sec per 512 lines medium = 1.1 sec per 512 lines
Low Signal Enhance	employed (signal integrated over full pixel dwell time)	no option
PMT gain settings	40 - 70%	40 - 70%
PMT black level settings	to yield dark signal intensity of about 10	to yield dark signal intensity of about 10
Frame averaging	up to 2 scans Kalman filtering	not employed
Objectives	x40 dry (NA 0.95) or x60 oil (NA 1.4)	x40 dry (NA 0.75)
Confocal apertures	4-5 = ca. 30% open, (Lemasters et al., 1993)	1 Airy disk (ca. 25% open) or fully open
Electronic zoom	2-4	2-4

2.7.3 Single channel imaging

The Bio-Rad MRC 600 system was employed for single channel fluorescence imaging to obtain images of intracellular dye distribution and organellar stainings. Excitation with 488 nm (BHS filterset) was employed for CFDA, BCECF, DASPMI, CG-1 and OG-1. The 514 line (GHS filterset) was used to excite cSNARF-1, FM 4-64 and FM 1-43. Fluorescence images were collected in Channel 1 whereas Channel 2 was routinely used to obtain corresponding bright field images. However, intracellular dye distribution of RB was imaged on the Leica TCS NT using the 568 nm line of the Krypton laser and collecting the fluorescence signal above 590 nm.

Processing of single channel images was confined to background adjustment and contrast stretching to use the full dynamic range of 256 grey levels.

In vitro assessment of bleaching of OG-1 on the Bio-Rad MRC 600 was performed by imaging a solution of 20 μM OG-1 10 kDa dextran in buffer with 39.8 μM free Ca^{2+} pH 7.2 (Calcium calibration buffer kit II, Molecular Probes). This test revealed that after 10 scans under standard imaging conditions only 2-3 % of signal loss occurred. Even higher photo stability was found with cSNARF-1 and RB. Signal loss after 10 or more consecutive scans was less than 1% in both cases. RB 10 kDa dextran was tested on the Leica TCS NT at excitation with 568 nm. cSNARF-1 was analysed in MES / HEPES buffer pH 7 on the Bio-Rad MRC 600 using excitation at 514 nm.

2.8 Simultaneous dual-emission ratio imaging

Simultaneous dual-emission ratio imaging involves the collection of two fluorescence images at different wavelengths simultaneously with two photomultipliers. To obtain the ratio, the fluorescence intensity at one peak wavelength has to be divided by the fluorescence intensity at the other peak wavelength (Read et al., 1992). The pH-sensitive dye cSNARF-1 is a dual emission dye with two pH dependent fluorescence emission peaks (Haugland, 1996). The Ca^{2+} sensitive dye OG-1 does not shift its emission peak when binding the ion. However, a ratiometric approach using this dye in combination with an ion-insensitive volume marker can be employed (Bibikova et al., 1997).

2.8.1 pH imaging and calibration

cSNARF-1 ratio imaging was performed with the Bio-Rad MRC 600 in dual channel mode using the 514 nm laser line for dye excitation (GHS filter set) and the custom built SNARF filter block allowing optimal detection of the alkaline and acidic forms of cSNARF-1 by channel 1 and channel 2, respectively (Haugland, 1996).

For converting ratio values obtained from cSNARF-1 loaded cells into pH values a calibration had to be performed. An *in vivo*, or better *in situ*, calibration was not

considered because it has been shown to be very problematic with little reproducibility (Parton, 1996). The pH response of cSNARF-1 free acid and cSNARF-1 dextran conjugate was tested *in vitro* in simple 20 mM MES/HEPES buffer and in "pseudocytosol" medium designed to mimic the intracellular environment (Fricker et al., 1994). The composition of the pseudocytosol medium was: 100 mM KCl, 20 mM NaCl, 1 mM MgSO4, 10mM MES, 10 mM HEPES, 60% sucrose (to increase the viscosity) and 25% Ethanol (to increase the ionic strength). The calibrations were performed by imaging the fluorescence of the appropriate dye-buffer mixtures over the pH range 6.0 to 8.0 (the pH was adjusted with KOH). In all cases the pH response was approximately linear over the range pH 6.5-7.5 and between pH 6.0 and 8.0 it was strongly sigmoidal (Figure 2.3). The response of cSNARF-1 to different pH values was similar for both the simple buffer and pseudocytosol although the absolute fluorescence intensities recorded for the same concentration of dye at each pH were roughly three times higher in the pseudocytosol. Ethanol and sucrose were identified as the most important influences on cSNARF-1 (Parton, 1996). The pH response of cSNARF-1 10 kDa dextran in simple buffer and pseudocytosol showed similar behaviour. However, the ratio values obtained for the dextran-dye were generally lower than those obtained for the dye free acid. Because of the similarity of the pH responses in MES/HEPES and the pseudocytosol, and the difficulty to assess how well the pseudocytosol reflects the intracellular environment, all estimations for intracellular pH were done based on the MES/HEPES *in vitro* calibration. Although the *in vitro* calibration does not allow accurate determination of absolute pH values it does provide a basis for comparison of *in vivo* data. A three point MES/HEPES *in vitro* calibration was performed after each imaging session to take account of day-to-day variation in the imaging set-up.

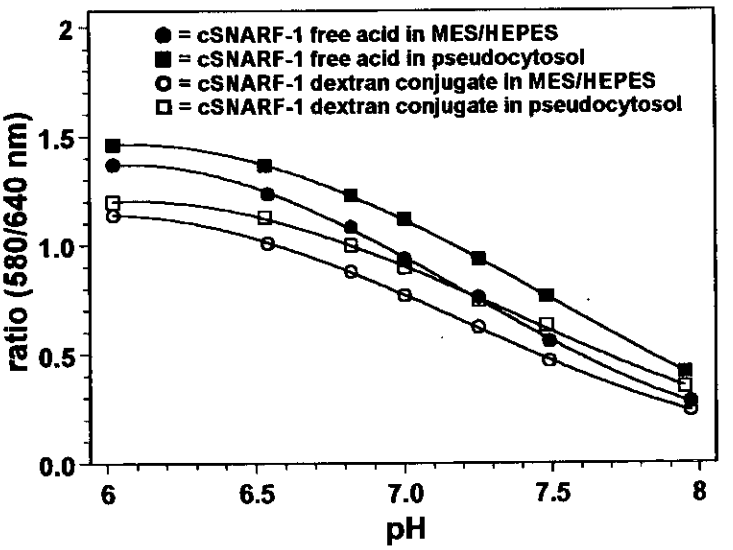

Figure 2.3. In vitro calibration for the pH response of cSNARF-1 imaged by CLSM.

2.8.2 Calcium imaging

For ratio imaging Ca^{2+} the Leica TCS NT had to be employed using dual excitation with 488 nm (OG-1 10 kDa dextran) and 568 nm (RB 10 kDa dextran). The OG-1 signal was detected in channel 1 and the RB signal in channel 2 using the filter combination described in Section 2.7.1. Control experiments showed that OG-1 was not excited by the 568 nm line, whereas RB showed a slight excitation by irradiation with 488 nm (ca. 3% of the signal obtained with 568 nm under the chosen conditions). The test for "bleed through" or "spill over" of dye fluorescence between the two channels involved imaging each dye on its own in a range of calcium standards (in μM: 0, 0.017, 0.038, 0.065, 0.1, 0.15, 0.225, 0.351, 0.602, 1.35, 39.8; Calcium calibration buffer kit II, Molecular Probes) and measuring the mean fluorescence intensity over the whole field-of-view. The spill over for RB fluorescence into channel 1 was less than 1% of the intensity in channel 2 and, therefore, RB spill over was not corrected for. OG-1 fluorescence showed consistently between 6-7% spill over into channel 2 when both channels were kept at the same gain settings (Figure 2.4). The intensity values obtained by imaging OG-1 with the calcium standards were fitted to equation I as described in Morris (1993). With equation I the spill over of OG-1 into channel 2 during simultaneous imaging of OG-1 and RB could

be calculated and subsequently subtracted from the signal measured in channel 2. Before manipulation all fluorescence images were corrected for the PMT dark signal.

	equation
$I(ch\ 2)_{sp} = A * I(ch\ 1) + B$	(I)
$I(ch\ 2)_{cor} = I(ch\ 2) - I(ch\ 2)_{sp}$	(II)

A = gradient; B = y intercept; I(ch 1) = intensity of OG-1 in channel 1; $I(ch\ 2)_{sp}$ = intensity of OG-1 spill over into channel 2; I(ch 2) = measured intensity in channel 2; $I(ch\ 2)_{cor}$ = Intensity in channel 2 after correction for spill over

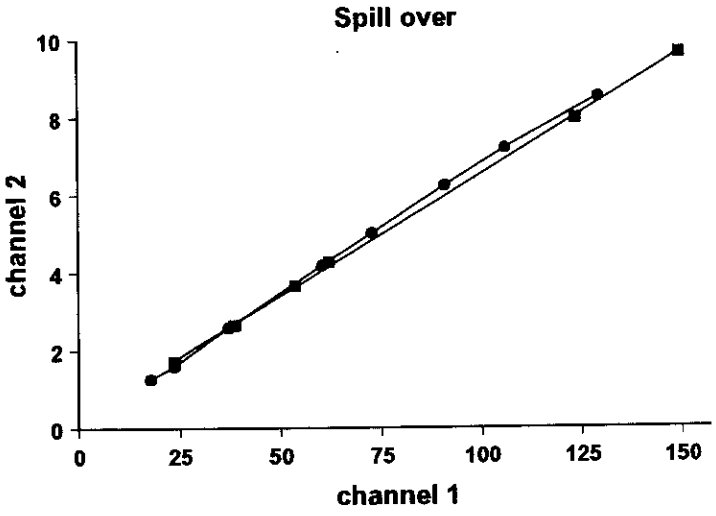

Figure 2.4. Measurement of spill over of OG-1 signal into channel 2 using 20 μM solutions of OG-1 in buffers of defined Ca^{2+} concentrations. ■ and ● indicate two independent measurements. Both axes indicate fluorescence pixel intensity.

For dual emission ratio imaging *in vitro*, OG-1 and RB were mixed 1:1. For estimation of the dynamic range an *in vitro* calibration was performed using the calcium standards from the calibration buffer kit II (Figure 2.5). The *in vitro* calibration indicated that the dynamic range of ratios between Ca^{2+} free buffer and buffer containing 39.8 μM free Ca^{2+} was nearly ten fold.

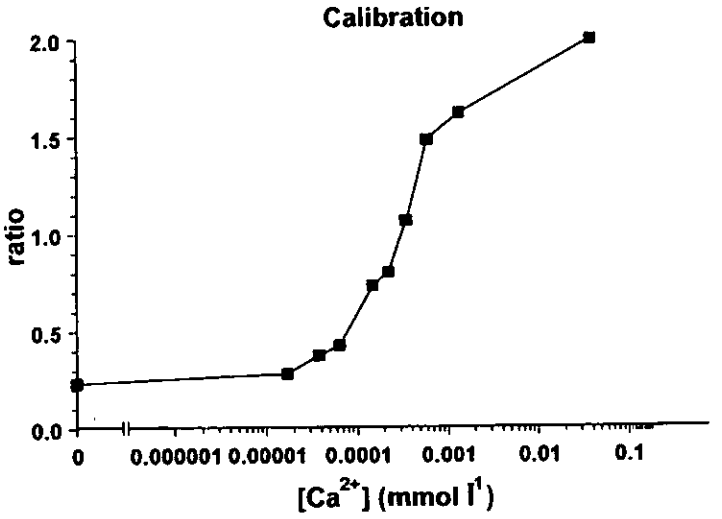

Figure 2.5. In vitro calibration on the Leica TCS NT using 25 μM of both, OG-1 and RB in solutions of defined Ca^{2+} concentrations.

For pressure microinjection the concentration ratio of the dextran conjugates OG-1 and RB had to be adjusted to 1:5 in the mixture in order to avoid too big an imbalance of signal intensity between the two channels after loading. Presumably due to apparent differences in viscosity of the two dye dextrans, more OG-1 seemed to be released from the micropipette than RB (Section 4.2.2.2).

2.8.3 Ratio processing for display purposes

Ratio processing of cSNARF-1 dual emission fluorescence images was carried out with the TCSM software. From each captured fluorescence image pair the photomultiplier dark signal was removed by a "dark image" subtraction. The ratio image was formed by a division of corresponding pixels in the image pair channel 2 / channel 1. Subsequently a 3x3 median filter was applied to reduce high frequency pixel variation. A pseudocoloured look up table (LUT) was applied in Confocal assistant.

For ratio processing of the data gathered on the Leica TCS NT, images were saved as TIFF files, subsequently reassembled in Paintshop Pro to fit the format required for a

Bio-Rad picture file and finally saved in Confocal assistant as Bio-Rad picture files. Processing which included background subtraction, correction of each pixel in channel 2 for spill over, ratioing of the two images and subsequently median filtering was performed using the MPL and the TCSM software on the Bio-Rad MRC 600.

2.8.4 Extraction of numerical data and statistical analysis

For statistical reasons data extraction can not be carried out on a ratio image. Instead, mean ratio values have to be calculated by dividing the mean fluorescence values of corresponding regions of interest (ROI) in the two fluorescent images (Parton et al., 1997).

After background subtraction data extraction for quantification was performed as follows: from a defined region of interest (ROI) in channel 1 and from the corresponding ROI in channel 2 the average pixel intensity was extracted using OPTIMAS version 5 (DataCell, Maidenhead, UK); where necessary spill over correction was performed; for cSNARF-1 the value from channel 2 was divided by the value from channel 1, for OG/RB the value from channel 1 by the value from channel 2.

For statistical analysis of the ROI data in both fluorescence images which was applied to the cSNARF-1 data, the intensity of each pixel had to be extracted, with corresponding pixels of the two images to be paired. This data was used to calculate the two means with their variances and the covariance of the paired data. These parameters were given to O. Papasouliotis and Prof. T. Leonard (Statistical Laboratory, University of Edinburgh) who had developed a procedure to calculate the 95% Bayesian confidence interval of the ratio value of the two means (Parton et al., 1997).

2.9 Growth rate measurement

Growth rate measurements represented the main criteria for assessing cell health and were carried out at 25°C under different conditions.

2.9.1 Growth in race tubes

Race tubes (ca. 40 cm long glass tubes with about 1 cm inner diameter and ends bent upwards) were placed horizontally and filled with medium plus 2% (w/v) agar until half full (Davis and de Serres, 1970). At one end of the tube the medium was inoculated with a piece of mycelium bearing the edge of a growing colony cut out from an agar plate overlaid with cellophane (Section 2.5.1). The tubes were incubated in the dark and the progression of the mycelial front was marked on the tube every 24 h.

2.9.2 Growth on agar plates

8.5 cm agar plates were inoculated in the centre with abundant spores and incubated in the dark. The diameter of the mycelium was marked on the bottom of the plate, first after 15 h and subsequently every 3 h.

2.9.3 Growth on slide cultures for microscopy

Growth rates under non-imaging conditions for the sandwich and the open slide culture were performed on a Nikon Diaphot TMD inverted microscope using a x20 dry plan apo objective. The side port of the microscope was connected to a Sony CCD camera (model XC-77CE) linked to a PC via a frame grabber (DT55, Data Translation Berkshire, UK). The hyphae were allowed to recover for 10 min after preparing the sample. A length measurement was made at two min intervals with OPTIMAS, version 4 (DataCell, Maidenhead, UK) over a 20-60 min period. Illumination was kept to a minimum using the 50 W microscope halogen bulb.

Growth rate measurements under laser irradiation were performed on the Bio-Rad MRC 600 applying the same conditions as for imaging (Section 2.7). One image was taken every min and length measurements were performed with the COMOS software, version 7 (Bio-Rad).

2.9.4 Growth in humid chambers for determination of dye cyto toxicity

Open cultures on 22x64 mm coverslips were prepared as described in Section 2.5.2.2 with the modification that the medium was supplied with defined concentrations of dye before spreading over the coverslip. After inoculation, slide cultures were incubated at 25°C in a humid chamber until the mycelium had grown about 5 mm. By that time hyphae were elongating at a constant linear rate and subsequent elongation of the mycelium was marked along the edge of the coverslip at defined time intervals.

2.10 Light Microscopy

Brightfield light microscopy was performed on the Nikon Diaphot using the x20 dry (NA = 0.7), x40 dry (NA = 0.9) and x60 oil (NA = 1.4) plan apo objectives; DIC microscopy was performed on the Reichert-Jung Polyvar (Leica UK Ltd., Milton Keynes, UK) equipped with DIC optics and x40 (NA = 1.0) and x100 (NA = 1.32) plan apo oil immersion objectives. Micrographs were recorded on Kodak TMAX 400 35 mm black and white film.

3. pH in tip growth of *Neurospora crassa* hyphae

3.1 Introduction

It is believed that intracellular ion gradients, notably of H^+ and Ca^{2+} are associated with tip growth in plant and fungal cells (Harold and Caldwell, 1990). Strong evidence supports the ubiquitous presence of a tip-based gradient of cytosolic free Ca^{2+} in tip growing cells (Berger and Brownlee, 1993; Jackson and Heath, 1993a; Malhó et al., 1994; 1995; Pierson et al., 1994; 1996; Bibikova et al., 1997; Felle and Hepler, 1997). However, evidence for the existence of cytosolic pH gradients and their involvement in regulating tip growth remain controversial. Whereas some systems such as algal rhizoids (Gibbon and Kropf, 1994) and certain mycorrhizal fungi (Jolicoeur et al., 1998) have been reported to exhibit a tip-acidic pH gradient, others such as root hairs (Herman and Felle, 1995; Bibikova et al., 1998) and pollen tubes (Fricker et al., 1997; Parton et al., 1997; Messerli and Robinson, 1998) do not appear to have a standing apical pH gradient. For *Neurospora crassa* there have been conflicting findings. Whereas Robson et al. (1996) detected a tip-alkaline gradient in growing *N. crassa* hyphae of up to 1.4 pH units in magnitude, Parton et al. (1997) did not find a pH gradient in this organism.

The aim of the work presented here was to investigate whether there is a tip-based gradient in pH_c or not in growing *N. crassa* hyphae. For pH measurement confocal ratio imaging was performed using the dual emission dye cSNARF-1. This dye had been used routinely before within the lab (Jelitto, 1995; Parton, 1996) and the necessary equipment was available. Another common dye for imaging pH is BCECF (Haugland, 1996). For ratio imaging this dye needs dual excitation at 440 nm and 490 nm which was not possible with the argon ion laser of the Bio-Rad MRC 600.

Suitable methods for loading cSNARF-1, both the free dye and the 10 kDa dextran conjugate, needed to be found, followed by careful assessment of intracellular dye distribution. Dye toxicity, especially in combination with laser irradiation, is a commonly encountered problem. Additionally, photobleaching, sample deterioration and other factors may also limit the time available for useful imaging (Parton and Read, 1999). It was therefore important to assess cell health and the useful imaging time under standard imaging conditions.

To determine whether a growing hypha exhibits a pronounced tip-focused pH gradient one has to be able to make meaningful comparisons between the pH values from different regions within the same cell. This requirement involved applying an appropriate statistical analysis (in collaboration with Statistical Laboratory, Edinburgh University) to ratio data in order to estimate the precision and spatial resolution of pH measurement. This work was carried out together with Richard M. Parton.

Since the manipulation of extracellular pH (pH_{ext}) by adding external buffers and of intracellular pH by adding weak bases or acids have clear effects on pH_c in compartments of non-growing *N. crassa* hyphae (Sanders and Slayman, 1982) the question arose how such pH changes would affect tip-growth and pH_c in actively growing hyphal tips of *N. crassa*.

3.2 Results

3.2.1 Loading of *Neurospora crassa* hyphae with cSNARF-1

For imaging pH, *N. crassa* hyphae had to be loaded with the pH sensitive, fluorescent dye cSNARF-1. The free dye could be introduced successfully by ester-loading (Section 2.6.1), although, continuous loading was necessary to maintain suitable fluorescence levels. Exchanging the dye containing medium with dye-free medium resulted in immediate signal loss from the hyphae indicating possible dye leakage from the cells (data not shown). Poor intracellular dye retention for free dye molecules has

been described previously (Callaham and Hepler, 1991). Fluorescence images of a subapical hyphal compartment and a growing hyphal tip after ester-loading with cSNARF-1 (Figures 3.1A and 3.1B, respectively) indicated that dye was excluded from spherical vacuoles. Bright fluorescent spots suggested that dye was sequestered within some unidentified spherical organelles. In the tip region (Figure 3.1B) dye partitioning within elongated tubular structures (probably mitochondria, compare Figure 5.10B) could be seen. The sequestration pattern appeared to be the same in both the 580 and 640 nm channels used for ratio imaging. Interestingly, the ratio showed no difference between areas of dye sequestration and areas of cytoplasmic dye (Figure 3.11A).

The 10 kDa dextran conjugate of cSNARF-1 had to be introduced by pressure microinjection (Section 2.6.2) which was much more difficult to achieve. cSNARF-1 and especially the cSNARF-1 dextran conjugate seemed to exhibit a greater viscosity than other dyes such as CG-1 and OG-1 and their dye-dextran conjugates because dye residues remained in pipette tips after aliquoting the dye and because injection micropipettes were poorly backfilled. This made microinjection very difficult and resulted in a low success rate. Fluorescence images of a subapical compartment and growing tip loaded with cSNARF-1 dextran by pressure microinjection (Figures 3.1C and 3.1D, respectively) showed that the dye fluorescence was even, with no obvious signs of dye sequestration within organelles. There was also no indication of a loss in fluorescence signal intensity in hyphal tips during growth. This was probably due to cytoplasmic streaming shifting dye loaded cytoplasm towards the extending tip (compare Section 4.2.1.2) and to the high photostability of cSNARF-1 (Section 2.7.3).

Pressure injection of free cSNARF-1 resulted in dye sequestration within small spherical bodies and the vacuolar system (Figure 3.2). Often, low intracellular dye retention was observed. Interestingly, there was no obvious dye sequestration into mitochondria in growing tips (Figure 3.2B). Altogether, this method did not seem to

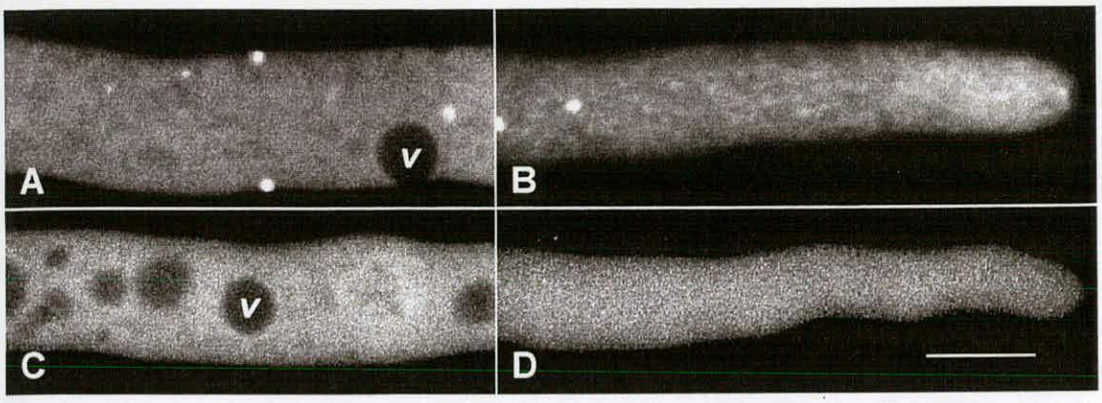

Figure 3.1. Confocal images showing the intracellular distribution of cSNARF-1 in *N. crassa* hyphae. (**A** and **B**) Subapical and apical regions, respectively, of an ester-loaded hypha. (**C** and **D**) Equivalent images of hyphae pressure microinjected with a 10 kDa dye-dextran conjugate. *V* = vacuoles. Bar = 10 μm.

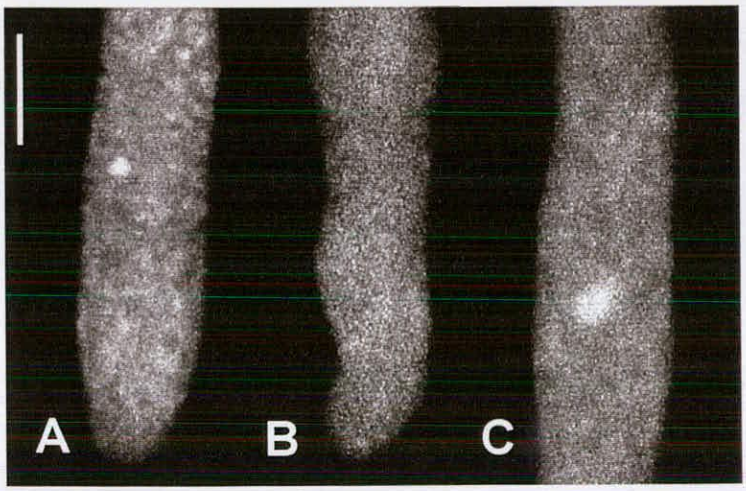

Figure 3.2. Confocal images showing the intracellular distribution of cSNARF-1 free acid in a *N. crassa* hypha after pressure microinjection. (**A**) Hyphal tip 9 min after injection and before resuming growth. (**B**) Same hypha as in (A) 28 min after injection with growing hyphal tip. (**C**) Subapical region of same hyphae as in (B) 31 min after injection. Bar = 10 μm.

result in improved intracellular dye behaviour in comparison to ester-loading, but proved much more difficult to perform and was abandoned.

3.2.2 Loading of *Neurospora crassa* hyphae with BCECF and CFDA

BCECF has been used for pH measurement in several other tip growing systems including *N. crassa* (e.g. Robson et al., 1996; Fricker et al., 1997). In order to assess intracellular dye distribution, the AM-ester of BCECF was loaded into *N. crassa* hyphae and excited at 488 nm. In subapical regions the dye was predominantly vacuolar whereas in tip regions it appeared to be partly cytoplasmic with clear signs of sequestration (Figure 3.3). In some hyphal tips a time dependent translocation of dye from the cytoplasm into the vacuole could be observed (Figure 3.4). BCECF was found to be cytotoxic upon laser irradiation causing hyphal growth to slow down after a few scans. In contrast to cSNARF-1, photo bleaching of BCECF was obvious after several scans.

The pH-sensitive fluorescent dye CFDA has been described as accumulating in the vacuolar system of fungi (Rees et al., 1994) and has been used to estimate vacuolar pH in fungal hyphae (Rost et al., 1995). Application of CFDA to *N. crassa* hyphae showed a very similar dye distribution to that found for BCECF (Figure 3.5). Subapical compartments appeared to exhibit complete dye sequestration into the vacuolar system. In apical compartments at least some of the dye appeared to be cytoplasmic (Figure 3.5C). CFDA was less bright and much less photostable than BCECF responding with rapid fading to laser irradiation.

3.2.3 Hyphal growth under imaging and non-imaging conditions

Confocal imaging can cause stress to cells mainly due to the combination of laser irradiation and dye-loading (Section 1.4.6.2) and, therefore, requires careful monitoring of cell health (Read et al., 1992). Assessment of cell health was

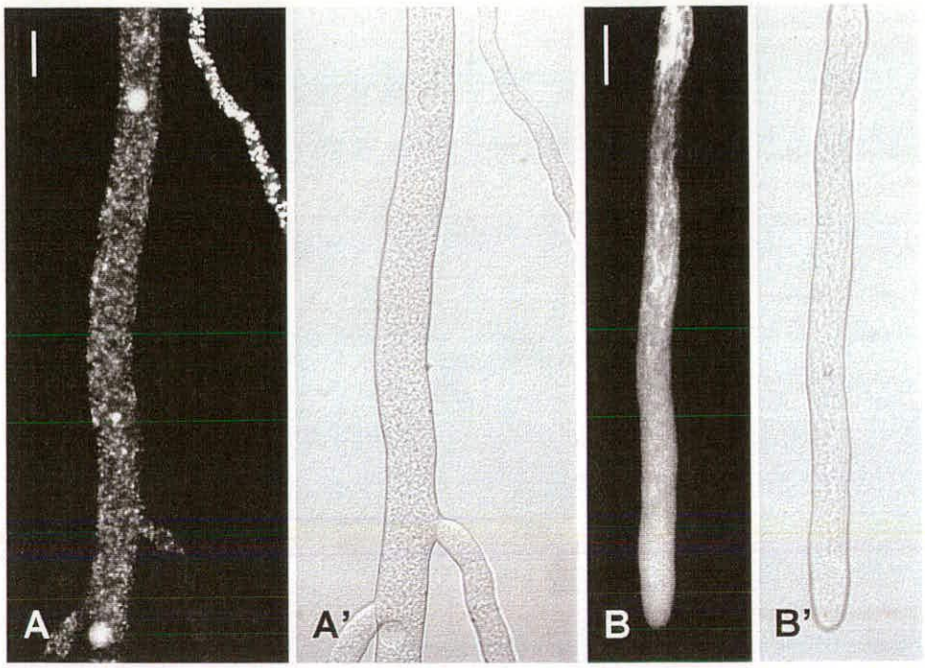

Figure 3.3. Confocal images showing the intracellular distribution of BCECF in *N. crassa* hyphae after ester-loading in sandwich culture. (**A**) Subapical compartments ca. 25 min after beginning of loading (the dye was washed out after 15 min) (**A'**) Corresponding bright field image. (**B**) Apical compartment ca. 30 min after beginning of loading). (**B'**) Corresponding bright field image. Bars = 20 μm.

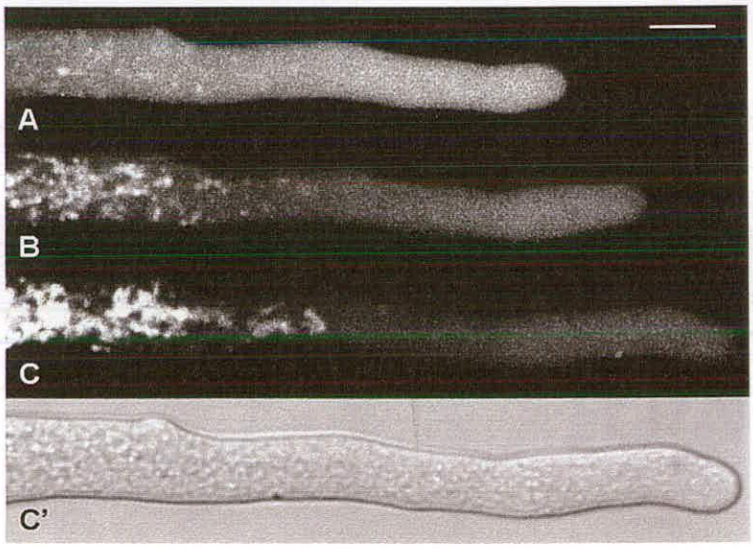

Figure 3.4. Confocal images showing the change in intracellular distribution of BCECF in a *N. crassa* hyphae with time after ester loading. (**A**, **B** and **C**) Hyphal tip ca. 40, 48 and 56 min after beginning of loading, respectively. (**C'**) Corresponding bright field image to (C). Bar = 10 μm. Images courtesy of Dr. Richard M. Parton.

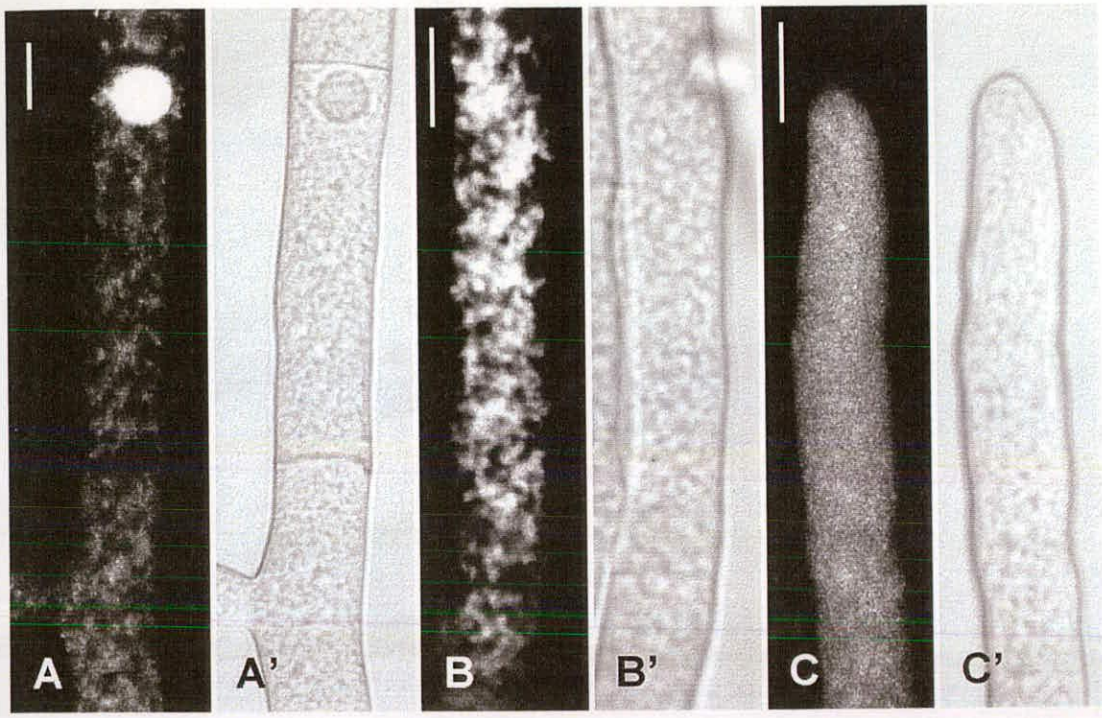

Figure 3.5. Confocal images showing the intracellular distribution of CFDA in *N. crassa* hyphae after ester-loading in sandwich culture. (**A** and **B**) Subapical compartments ca. 33 min after beginning of loading (the dye was washed out after 15 min) (**A'** and **B'**) Corresponding bright field images. (**C**) Apical compartment ca. 35 min after beginning of loading. (**C'**) Corresponding bright field image. Bars = 10 µm.

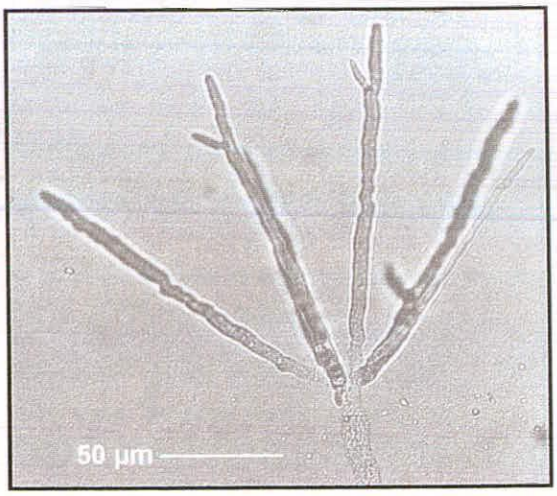

Figure 3.6. Effect of manipulation of external pH on tip growth and morphology of *N. crassa*. Hyphae react with undulating growth pattern and increased branching to a sudden change of the pH of the medium from 5.95 to 8.0.

based on hyphal extension rates and apical morphology which were monitored under different conditions relevant to the experiments employed (Table 3.1).

Table 3.1. Growth rates *of Neurospora crassa* measured under different conditions

medium	conditions	loaded	scanned	growth rate (µm/min ± s.d.)	No of replicates
VM	race tubes	-	-	61.46 ± 0.71	4
½VM	race tubes	-	-	61.77 ± 0.80	4
VM	agar plates	-	-	35.03 ± 1.70	6
½VM	agar plates	-	-	32.36 ± 2.49	7
VM	sandwich	-	-	17.17 ± 3.37	10
VM	sandwich	-	every min	17.52 ± 3.16[a]	10
VM	sandwich	ester	-	16.29 ± 3.24	9
VM	sandwich	ester	every min	15.15 ± 3.51[b]	9
½VM	sandwich	-	-	15.75 ± 2.79	11
½VM pH 7	sandwich	-	-	slowed down[c]	5
½VM pH 8	sandwich	-	-	slowed down[d]	5
VM	slide culture	-	-	31.70 ± 4.70	6
VM	slide culture	dextran	every min	9.70 ± 4.50[a]	6

[a] first ten data points taken for calculation because thereafter growth rate declined more than 10%
[b] first three to five data points taken for calculation because thereafter growth rate declined more than 10%
[c] irregular growth rate; after 30 min hyphae exhibited only 1/2 to 2/3 of original growth rate which was similar to control; there was a tendency for hyphae to exhibit an undulating growth pattern
[d] irregular growth rate; after 40 min growth rate < 4 µm/min; undulating hyphal growth pattern with multiple apical branches

For comparison, growth rates were measured on race tubes and agar plates (Table 3.1), where the extension of the whole mycelium in one direction from the point of inoculation was measured (plates were inoculated in the middle and race tubes at one end). In race tubes, mycelia showed the fastest growth with extension rates greater than 60 µm/min which is in good agreement with the value given by Perkins (1992). On agar plates this growth rate was halved, possibly due to the fact that the mycelium was spreading as a circular disk, unlike tubes where extension was confined to one

direction. There was no significant difference between VM and ½VM apart from the observation that sporulation on VM was stronger than on ½ VM.

The extension of single hyphae was monitored on slide cultures and with the sandwich system. For the sandwich system, under non-imaging conditions, linear growth could be observed up to 50 min after covering the mycelium with a second cover slip. This was probably because growing hyphae advanced into relatively fresh medium and avoided oxygen deprivation. Nevertheless, the average growth rate reached only one quarter of that under optimal conditions in race tubes. Under non-imaging conditions there was no significant difference in growth rate between hyphae in VM, ½VM or cSNARF-1 ester-loaded hyphae. However, as soon as laser irradiation was applied the growth rate decreased. Unloaded hyphae showed a decrease in growth rate of more than 10% after only 10 scans, whereas loaded hyphae started to decrease their growth rate after the first three to five scans. There was considerable individual variation which in part seemed to depend on the degree of loading (shown as brightness) of individual hyphae. Hyphae loaded with the most dye proved to be the most susceptible to laser irradiation.

Changes in external pH influenced growth rate and growth pattern. Transferring hyphae from ½VM, pH 5.95, to ½VM at pH 7.00 resulted in a continuous decrease in growth rate. Hyphae also tended to have a more undulated growth pattern. Transferring hyphae from ½VM to ½VM pH 8.00 resulted in even more drastic effects. The extension rate of the hyphae slowed down within a few minutes and tips started to form multiple apical branches with marked undulated growth (Figure 3.6).

The less stressful conditions in slide culture were reflected in the growth rate of the unloaded, non-irradiated hyphae, which was twice as high as in the sandwich system. The significant difference in growth rate in slide cultures between control hyphae under non-imaging conditions and dextran-loaded hyphae which were imaged is most likely due to the injection procedure rather than irradiation.

To maintain suitable fluorescence levels using the dye-ester, continuous loading was necessary. To rule out that this treatment had negative effects on growth and ratio values a time course was performed (Figure 3.7A). Ten min after preparing the sample, a *N. crassa* hypha was imaged once every min. The pH_c was estimated according to an *in vitro* calibration using MES/HEPES buffer solutions (Section 2.8.1). Forty min after sample preparation, which is equal to 30 min of imaging, the growth rate gradually decreased concomitantly with increasing cytoplasmic acidification. Additionally, a decrease in fluorescence occurred (Figure 3.7B). Consequently, the period available for useful imaging comprised the first 30 min after loading for all hyphae treated in this way. During the whole course of the experiment no increase in background fluorescence was detectable.

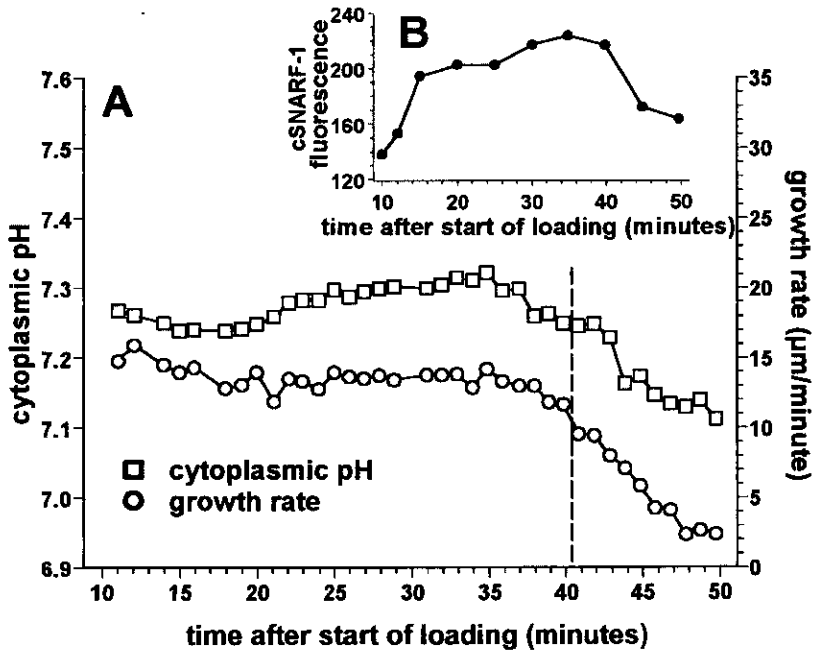

Figure 3.7. Assessment of useful imaging time in a *N. crassa* hypha during continuous ester-loading with cSNARF-1 in sandwich culture. **(A)** Hyphal growth rate and estimated pH_c plotted against time after the start of continuous dye loading for a typical hypha. The dashed line indicates the maximum useful imaging time (40 min). After this time, the growth rate gradually decreased concomitantly with increasing cytoplasmic acidification indicating cell stress. **(B)** Change in overall intracellular dye fluorescence intensity (dye fluorescence detected by channel 1 and channel 2 have been combined) over time. Note the decrease in fluorescence intensity after 40 min.

3.2.4 Statistical analysis and estimation of spatial resolution and precision of pH measurement

The results presented in this section were obtained in collaboration with Richard M. Parton.

To investigate the occurrence of an ion gradient within a cell, one has to be able to make meaningful comparisons between different regions of the same image. Therefore, statistical analysis is required in order to estimate precision of measurement and spatial resolution (Parton and Read, 1999). Precision of measurement means the smallest differences or changes in ion concentration which can be reliably detected. It is predominately limited by the noise of the fluorescence signal which leads to random variation in individual fluorescence pixel values and limits the signal to noise ratio ($R_{S/N}$) of images. The $R_{S/N}$ is defined as the ratio of the fluorescence signal and the variation in that signal. The $R_{S/N}$ and at the same time the precision can be improved by averaging several frames or the pixels within a region of interest (ROI). This comes at a cost because averaging frames over time will reduce the temporal resolution and averaging pixels within a ROI will decrease the spatial resolution. Therefore, resolution and precision are directly linked to each other. In order to provide estimates of the precision of quantitative data for particular sample sizes (defining the spatial resolution) and confidence limits to allow meaningful comparison between different ROIs of the same image, a method to quantify the magnitude of the variation between pixel values is needed. This necessitates rigorous statistical analysis.

When dealing with fluorescence images mean fluorescence values from ROIs and their pixel value variation (which may be determined as a standard deviation) can be extracted directly from the fluorescence image. In the case of ratio imaging, however, the extraction of data and the statistical analysis may not be carried out on the final ratio image produced by the pixel by pixel division of corresponding pairs of pixels in the fluorescence images. The reason for this is that the average ratio value of a ROI in the final ratio image is not equal to the ratio of the average fluorescence intensity

values of that ROI collected in channel 1 and channel 2 (Figure 3.8). The extent of this difference is dependent on the degree of variation in the fluorescence images. Images or ROIs of low signal intensity suffer under a lower $R_{S/N}$ and are characterised by a pronounced skewing of the ratio pixel value distribution (Figure 3.8B'). In terms of a cell showing differences in dye signal caused by variations in pathlength, especially at the cell periphery, noise induced differences in the ratio image can occur which might not reflect real pH differences. Therefore, it is necessary to sample mean fluorescence values from corresponding areas in both channels and then divide one mean by the other to obtain a ratio value, instead of extracting values by sampling ROIs directly from the ratio image. The size of the sampled ROI for a certain image is dependent on the requirements for spatial resolution and precision of pH. This implies that an image of low $R_{S/N}$ the sampled area size will have to be larger (which means decreased spatial resolution) to obtain a comparable precision of pH to an image of higher $R_{S/N}$.

The confidence limits for the mean ratio value must be calculated by taking into account the variation in the pixel values of both fluorescence images. The Bayesian theory of inference (Kappenman et al., 1970) had to be employed (in collaboration with T. Leonard and O. Papasouliotis, Statistical Laboratory, Edinburgh University) because standard statistical methods are not suitable for ratio data. A requirement for this type of analysis was that the fluorescence pixel distribution was approximately normal and not skewed (Figures 3.8A and B). Experimental analysis of the spatial resolution and precision of pH measurement within individual images was done *in vitro* by ratio imaging cSNARF-1 free acid in MES/HEPES buffer over the range pH 6.5-7.5. The 95% Bayesian intervals for variation in ratio values between sample areas of different sizes were calculated by the Statistical Laboratory and from this the optimum precision of pH measurement and spatial resolution *in vitro* were determined (Figure 3.9; Table 3.2). For a more detailed explanation see Parton *et al.* (1997) and Parton and Read (1999).

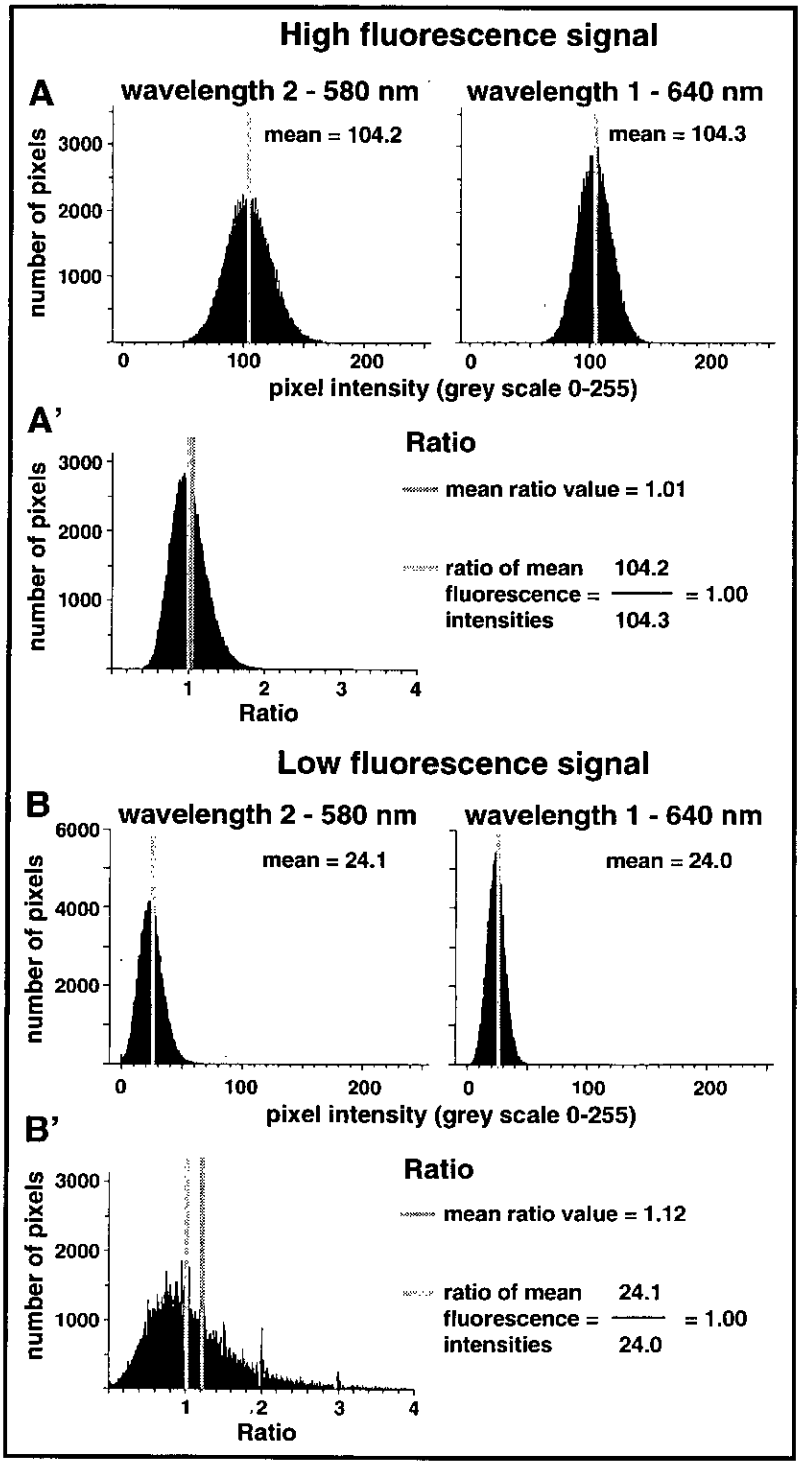

Figure 3.8. Pixel value frequency plots. (**A** and **B**) Pixel intensity frequency plots of simultaneous dual emission confocal fluorescence images of cSNARF-1 free acid (pH 7) at 580 and 640 nm. (A) Fluorescence image pair of high average fluorescence intensity; (B) Fluorescence image pair of low average fluorescence intensity. (**A'** and **B'**) Ratio value frequency plot for the ratio image produced by the pixel-by-pixel division of the fluorescence images examined in (A and B), respectively. In all cases the area sampled contained 256 x 384 pixels.

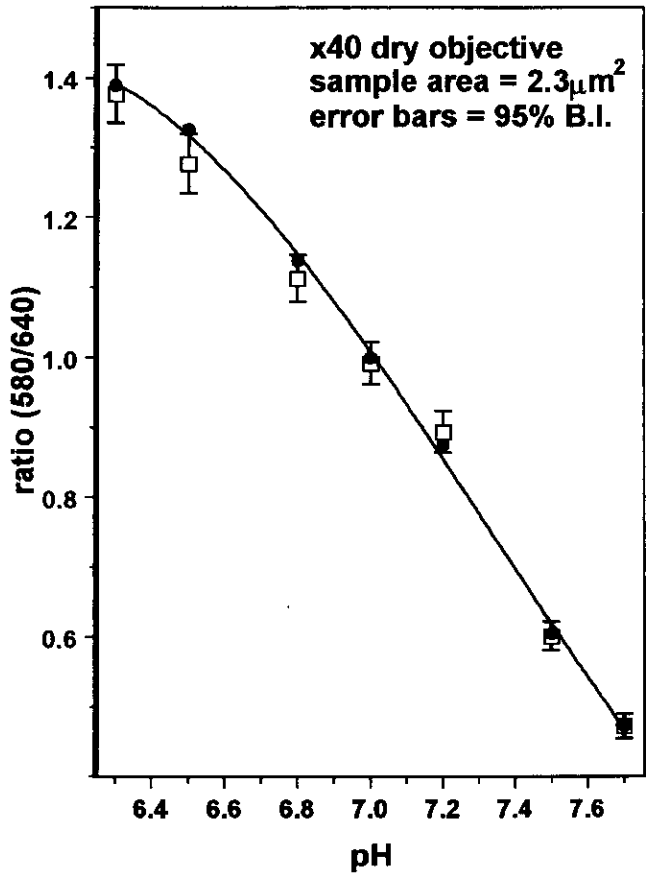

Figure 3.9. *In vitro* calibration for the pH response of cSNARF-1. □ represent ratio values derived from small sample areas (14 x 14 pixels); error bars are the 95% Bayesian interval based on the pixel variation within small sample areas. ● represent ratio values derived from 256 x 384 pixel areas.

Table 3.2. Precision of pH estimation in relation to spatial resolution for cSNARF-1 ratio imaging

Sample area (pixels)	spatial resolution (μm^2)	Precision of pH measurement
20 x 20	4.8	±0.04 to ±0.02
14 x 14	2.3	±0.06 to ±0.03
10 x 10	1.2	±0.08 to ±0.04

The values given are the best and worst estimated precision over the pH range tested (pH 6.5-7.5)

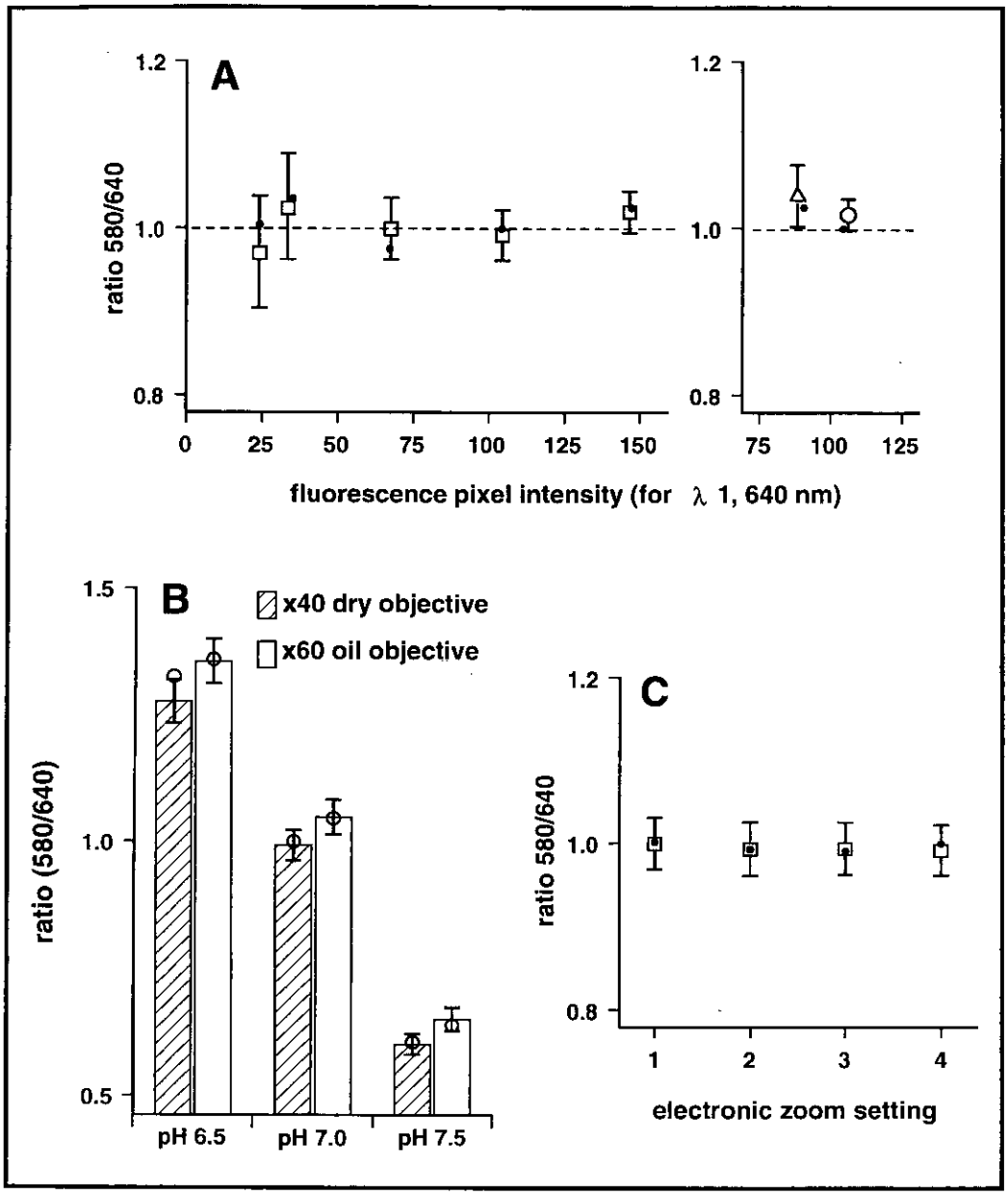

Figure 3.10. The effect of different fluorescence imaging parameters on the variation in ratio values for confocal imaging of cSNARF-1 *in vitro*. All imaging was performed with the x40 dry objective at zoom 4, unless otherwise stated. (**A**) The effect of fluorescence pixel intensity (with single scan imaging), □; accumulation of low signal, Δ; and Kalman filtering, O. Open symbols are the average ratio value of 14 x 14 pixel sample areas. ● represent ratio values derived from 256 x 384 pixel areas The dashed line is the expected ratio value for pH 7.0. (**B**) A comparison of the influence of using a x40 dry and x60 oil objectives. Average ratio value for 14 x 14 pixel sample areas are shown as bars (error bars = 95% B.I.) O = average ratio value of 256 x 384 sample areas. (**C**) The effects of using different electronic zoom settings during fluorescence image capture (symbol conventions are as in (A).

Average signal strength in fluorescence images and the use of Kalman and Accumulative filters all influenced the precision of pH measurement (Figure 3.10A). Increasing average fluorescence brightness values from 25 to 150 (on a scale of 0-255) gave an improvement in precision of > 150%. Accordingly, images with high average fluorescence brightness (typically > 100) were used where possible. Kalman filtering (n=3) gave an improvement of ~40% over direct image collection. Accumulative filtering (n=3) to increase signal strength also improved precision but was inferior to the direct capture of images at a signal strength equivalent to the accumulated image. There was no apparent difference in precision between the x40 dry and the x60 oil objective (Figure 10B) when the imaging conditions and the number of pixels sampled were kept the same. However, due to the higher magnification of the x60 oil objective this implies an improved spatial resolution (14 x 14 pixel correspond to 2.3 μm^2 for the x40 and to 1 μm^2 for the x60 objective). The electronic zoom between 1 and 4 had no apparent effect on precision of pH measurement when the number of pixels sampled was kept the same (Figure 10C). The higher the zoom the smaller the pixel size, therefore, at zoom 4 which was used routinely the spatial resolution is higher than at lower zoom.

3.2.5 Cytoplasmic pH

In the case of confocal ratio imaging of cSNARF-1 in both, ester-loaded (Figure 3.11A and A') and dextran-injected (Figure 3.11B and B') hyphae of *N. crassa*, no pronounced pH_c gradient was detectable within the limits of the precision of measurement (0.1 pH units) over the first 50 µm of growing hyphae with a spatial resolution of 2.3 μm^2. pH_c-values were estimated on the basis of a MES/HEPES buffer *in vitro* calibration (Figure 2.3) under different conditions (Table 3.3). Independent of the method of sample preparation (which influenced the amount of oxygen available to the cells) growing, ester-loaded hyphae generally showed a pH_c of about 7.2. The ionic strength of the medium had no significant effect on this value although VM and ½VM slightly differed in their pH (5.80 versus 5.95, respectively). With the x60 oil objective, even with its better optical sectioning properties and

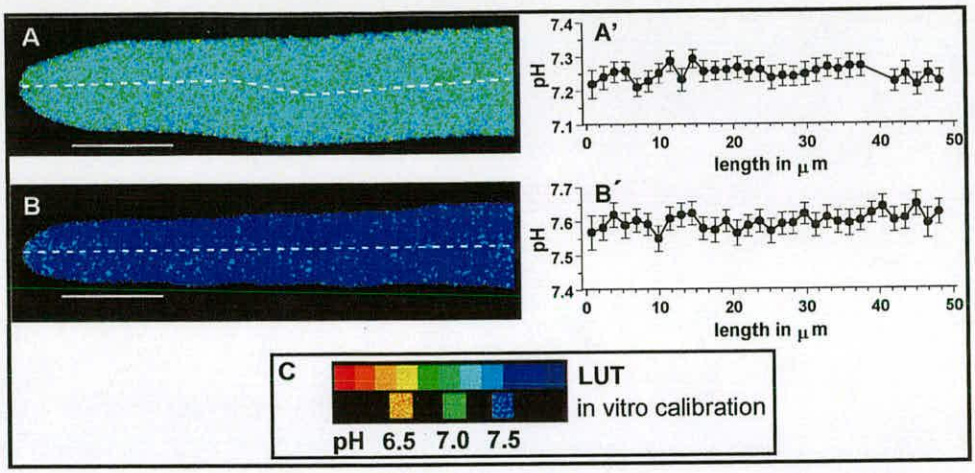

Figure 3.11. Cytoplasmic pH in the apical regions of growing *N. crassa* hyphae examined by confocal ratio imaging of cSNARF-1. (**A** and **B**) Ratio images of hyphae which were ester-loaded with cSNARF-1 and pressure-injected with 10 kDa cSNARF-1 dextran, respectively. (**A′** and **B′**) Graphs of pH_c sampled over 2.3 μm^2 areas along the lines indicated. Error bars = 95% Bayesian intervals. (**C**) Pseudocolour scale with corresponding pH values from *in vitro* calibration. Bars = 10 μm.

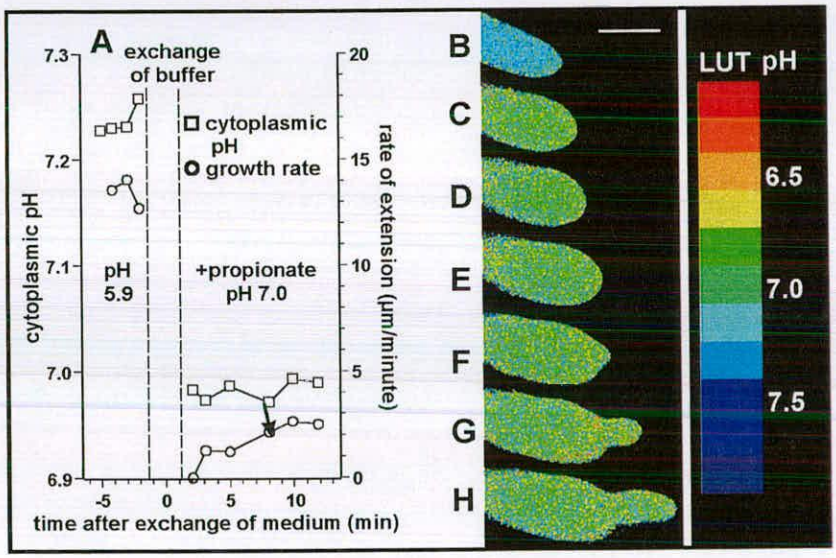

Figure 3.12. Effects of acidifying the pH_c of a *N. crassa* hypha by adding 50 mM sodium propionate at pH 7.0. The hypha was continuously ester-loaded with cSNARF-1. (**A**) Plot of pH_c and growth rate against time before and after exchange from ½VM pH 5.95 to medium containing sodium propionate. The arrowhead shows the point at which a new tip is generated. (**B-H**) Ratio images of the same hypha analysed in (A) showing pH_c and tip morphology two min before treatment (B), and two (C), three (D), five (E), eight (F), ten (G) and twelve (H) min after treatment. Bar = 10 μm.

higher resolution, similar values as with the x40 dry objective were obtained. The difference in pH_c between dextran-injected and ester-loaded hyphae was nearly 0.4 pH units. It could be ruled out that this was due to oxygen deprivation in the sandwich method because ester-loaded hyphae on slide cultures showed similar pH values. It is possible that partitioning of the ester-loaded cSNARF-1 into membranes shifts the spectral properties resulting in an increase in the overall pH reading relative to the dextran result. Evidence for this phenomenon has been obtained by Opitz et al. (1994). No correlation was found between the growth rates and average pH_c values of individual *N. crassa* hyphae which varied from pH 7.02 to 7.29 in ester-loaded cells and from pH 7.51 to 7.59 in dextran-dye loaded cells (data not shown).

Table 3.3. Measured pH values

medium	conditions	loaded	objective	mean pH_c	number of cells	cell growth
½VM	sandwich	ester	x40 dry	7.23 ± 0.05	31	+
½VM	sandwich	ester	x60 oil	7.20 ± 0.03	8	+
VM	sandwich	ester	x40 dry	7.17 ± 0.05	22	+
VM	slide culture	ester	x40 dry	7.25 ± 0.07	6	+
VM	slide culture	dextran	x40 dry	7.57 ± 0.05	6	+

3.2.6 Manipulation of intracellular pH and the effect on apical growth

Weak acids and bases, of which common examples are propionic acid and ammonia, perturb the pH_c upon entering the cell (Fröhlich and Wallert, 1995). Therefore, weak acids and bases were applied to cSNARF-1 loaded *N. crassa* hyphae in order to change their pH_c (Table 3.4).

Table 3.4. Effect of 50 mM weak acid and week base treatments on hyphae loaded with cSNARF-1

pH treatment[a]	loaded	shift in pH units	growth rate (μm/min)	recovery time[b]	number of cells
Na prop. pH 6	ester	-0.7	no tip growth	no recovery	5
Na prop. pH 6	dextran	-0.9	no tip growth	no recovery	2
Na prop. pH 6.5	ester	-0.5	no tip growth	no recovery	7
Na prop. pH 6.5	dextran	-0.7	no tip growth	no recovery	2
Na prop. pH 7	ester	-0.2-0.3 (not stable)	< 3	5-10 min	5
TMA pH 7.5	ester	+0.4 (not stable)	< 3	5-10 min	3
TMA pH 8	ester	+0.7 (not stable)	< 3	5-10 min	5

Na prop. = sodium propionate, TMA = trimethylamine.
[a] all treatments were reversible if buffers were washed out after 15 min and cells eventually resumed growth
[b] recovery took place in the form of emergence of new smaller growing tips in presence of TMA or Na propionate.

Ratio imaging revealed that the application of a cell permeant weak acid (50 mM propionic acid) at pH 7.0 resulted in the cytoplasm of ester-loaded *N. crassa* hyphae being evenly acidified (Figures 3.12B-H). Immediately after this treatment, the hyphal tip became swollen which resulted in a gradual increase in hyphal length (Figures 3.12B-E). Five to ten minutes after treatment, there was the obvious regeneration of a new tip (Figures 3.12F-H), narrower than that of the parent hypha and with a growth rate which was slower (ca. 2-3 μm min^{-1}) than it's parent hypha (14-15 μm min^{-1}, Figure 3.12A). Similar treatments with propionic acid at pH 6.0 or 6.5 resulted in even greater acidification of intracellular pH, an initial slight hyphal swelling but subsequent tip regeneration was completely inhibited (Figures 3.13 and 3.14). Cells loaded with cSNARF-1 dextran conjugate responded in a similar way to ester-loaded cells and showed a clear acidification in propionic acid at pH 6.0 or 6.5 and did not resume growth (Figure 3.14). The weak base ammonia proved to be very cytotoxic to *N. crassa* cells resulting in extensive vacuolation, disruption of the

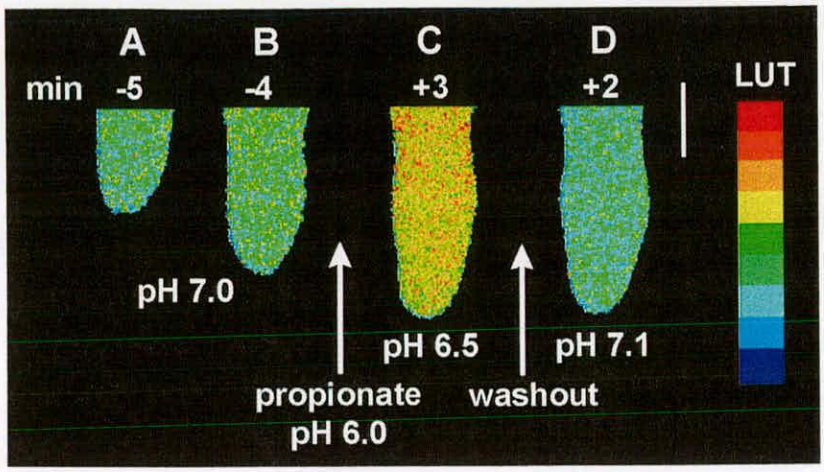

Figure 3.13. Confocal ratio images of a *N. crassa* hypha ester-loaded with cSNARF-1. (**A** and **B**) Hypha before and (**C**) after treatment with 50 mM sodium propionate. (**D**) Hypha after washout of the propionate. Min indicate the time before (negative) and after (positive) adding the weak acid or washing out. Bar = 10 μm.

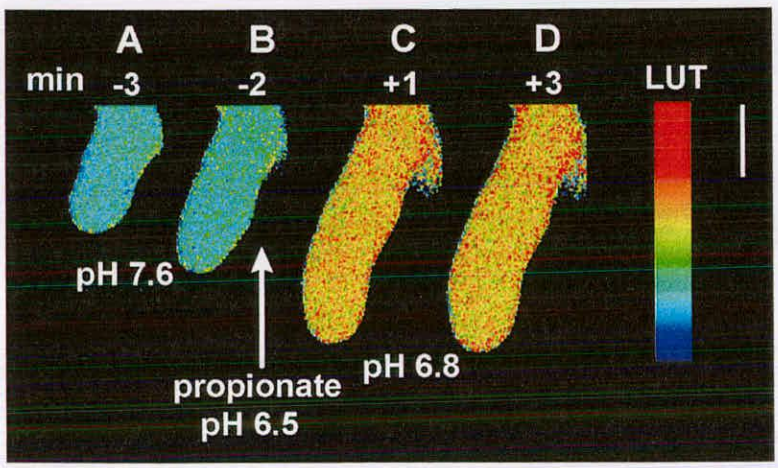

Figure 3.14. Confocal ratio images of a *N. crassa* hypha loaded with cSNARF-1 10 kDa dextran conjugate. (**A** and **B**) Hypha before and (**C** and **D**) after treatment with 50 mM sodium propionate. Min indicate time before (negative) and after (positive) adding the weak acid. Bar = 10 μm.

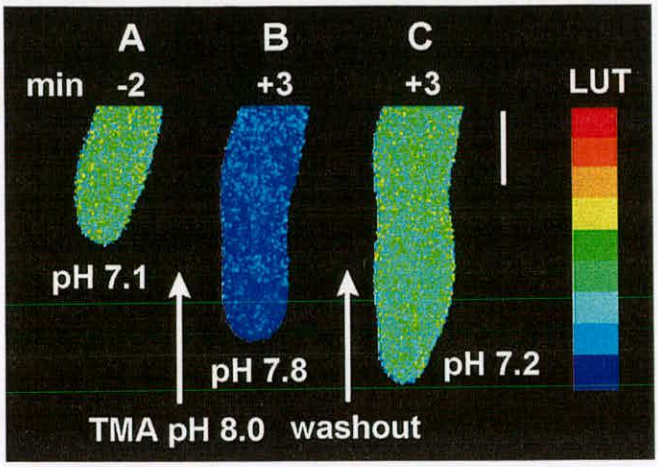

Figure 3.15. Confocal ratio images of a *N. crassa* hypha ester-loaded with cSNARF-1. (**A**) Hypha before and (**B**) after treatment with 50 mM TMA. (**C**) Hypha after washout of TMA. Min indicate the time before (negative) and after (positive) adding the weak base or washing out. Bar = 10 μm.

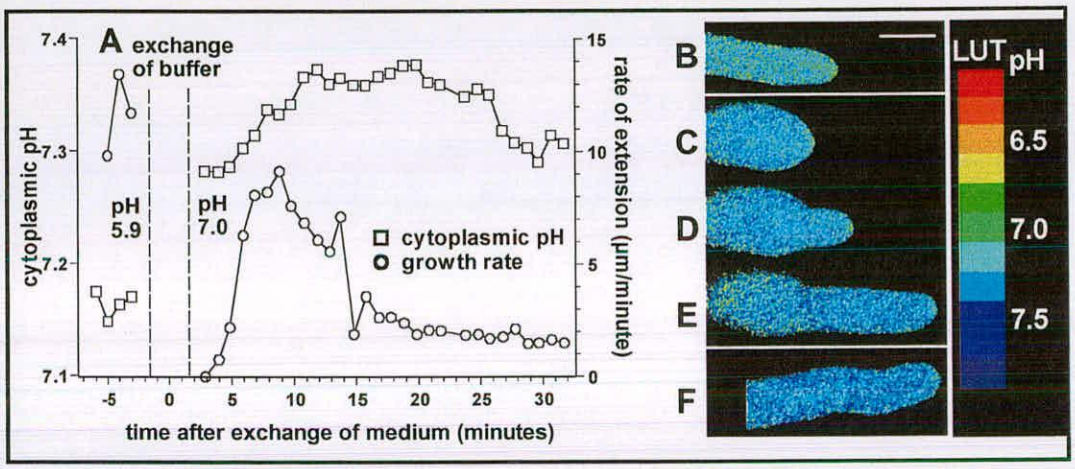

Figure 3.16. Effects of manipulation of the external pH on tip morphogenesis and growth rate of a *N. crassa* hypha ester-loaded with cSNARF-1. (**A**) Plot of pH_c and growth rate against time after changing the external pH from pH 5.95 to 7.00. A period of physical stress due to medium exchange is indicated between the dashed lines. (**B-F**) Ratio images of the same hypha as shown in (A) three min before changing the external pH (B), and five (C), six (D), eight (E) and 20 (F) min after changing the external pH. Note that there is an initial swelling of the hyphal tip (C) followed by the regeneration of a new tip (C-F). Bar = 10 μm.

cytoplasm and loss of fluorescence signal (data not shown) and was therefore found to be unsuitable. Instead the cell permeant weak base trimethylamine (TMA) was used to increase pH_c (Taggart et al., 1994). Addition of 50 mM TMA at pH 7.5 and pH 8.0 to ester-loaded hyphae caused increased alkalinisation of the hyphal cytoplasm and a similar pattern of hyphal swelling and tip regeneration as observed after weak acid treatment at pH 7.0 (Figure 3.15). Tip swelling occurring after medium exchange may primarily be caused by differences in medium composition rather than by mechanical stress (Section 2.5.2.1). The shifts in internal pH due to weak acid or base treatment between pH 7 and 8 were only stable for approximately 10-15 min. Thereafter, the cytoplasm slowly reverted back to its original pH_c value. All treatments were reversible when washing out of the weak acid or base was performed within 15 min after application. In ester-loaded, but not in dextran containing hyphae, addition of weak acid or base promoted dye sequestration into the vacuolar system.

3.2.7 Manipulation of extracellular pH and the effect on apical growth

Extracellular pH (pH_{ext}) treatments were also found to change the pH_c (Table 3.5) and growth rate (Table 3.1) of *N. crassa* hyphae. An increase in pH_{ext} from 5.95 (½VM) to 7.00 resulted in an elevation in pH_c by 0.2-0.3 pH units which reached a plateau after about 10-15 min, and was later often followed by a slight reduction in pH_c. This treatment also caused a constant reduction in growth rate (Figure 3.16A-F, n=5). Increasing the pH_{ext} to 8.00 led to an increase in pH_c by 0.5-0.6 pH units but this reverted to values nearer to the original pH_c within 20-40 min (data not shown). At pH 8.0, hyphal growth rate was reduced to < 4 μm min^{-1} (n=5), and tips tended to have an undulating growth pattern and typically exhibited increased apical branching (Figure 3.6).

Table 3.5. Effect of pH_{ext} on pH_c in hyphae ester-loaded with cSNARF-1

pH treatment	shift in pH	recovery time	observations
1/2 VM pH 7	+0.2-0.3	3-5 min	pH shift maximum reached after ca. 10 min and was stable for 10-15 min; subsequently the pH_c decreased
1/2 VM pH 8	+0.5-0.6	3-5 min	pH shift after exchanging of buffer; pH_c subsequently decreased slowly but steadily

3.3 Discussion

3.3.1 pH_c gradients are not a common feature of tip-growing cells

The existence of pronounced pH_c gradients in tip-growing cells has been a controversial topic. In particular, evidence for pronounced pH_c gradients based on older investigations (e.g. Turian, 1979; McGillviray and Gow, 1987) is unconvincing because the methodologies used in these studies have since been found to be inadequate. The pH indicator dyes used were not vital stains and whether cells resumed growth was not assessed.

More recent reports employing vital dyes suggested the occurrence of pH_c gradients in fungal hyphae. Using fluorescence ratiometric imaging of *N. crassa* hyphae loaded with BCECF, Robson et al. (1996) detected a tip-alkaline pH gradient with a magnitude of up to 1.4 pH units extending over a distance of up to 80 μm. The magnitude and the extent of the pH gradient was found to be positively correlated with growth rate. The imaging method was non confocal allowing no rejection of out of focus blur which made dye distribution difficult to assess. Therefore, the authors performed confocal microscopy to check for sequestration and found that older regions exhibited dye partitioning within vacuoles which agrees with observations presented here (Figure 3.3.A). According to Robson et al. (1996) dye distribution within the apical compartment appeared to be predominately cytoplasmic, although

they detected staining of small spherical vacuoles and of a filamentous network which they assumed to be mitochondria. Interestingly, the data presented by Robson et al. (1996) did not show filamentous staining in the subapical region directly behind the hyphal apex, where filiform mitochondria are most abundant (Section 1.1.1), but approximately several tens of micrometers (the precise distance cannot be determined because scale bars were not included in the publication) behind the apex. There was no correlative staining with a mitochondrion-specific stain shown which would have clarified this issue. Based on the evidence presented here (Figures 3.3 and 3.4) it is more likely that these filamentous structures are part of the vacuolar system. The conclusion of Robson et al. (1996) that within the growing margin of the colony BCECF was mainly cytosolic is consistent with data shown in Figures 3.3B and 3.4A, However, it is also evident that there was a time dependent tendency to sequestrate BCECF within the vacuolar system (Figure 3.4.) The vacuolar system, although not very prominent and difficult to detect, is still present in subapical regions (Figures 4.1A and 4.2A; Section 1.1.1). Sequestrated dye would certainly influence the pH reading and the deviation of the reading from the actual pH_c towards lower pH values would be dependent on the extent of vacuolation. The subapical region in a growing hypha contains most of the cytoplasm whereas more distal regions become increasingly more vacuolated until a certain level of vacuolation is achieved (Section 1.1.1). It is conceivable that there may be a gradient in vacuolation along the growing hypha. Possibly the tip alkaline gradient Robson et al. (1996) detected was rather a gradient in the extent of vacuolation than in cytoplasmic pH. A feature of the pH gradient reported in this paper was that its magnitude and its length were dependent on growth rate and non-growing hyphae did not exhibit a gradient but the same pH as the base of the gradient in growing hyphae. It can be speculated that growth rate might be correlated with the amount of cytoplasm accumulated in the subapical region: the more cytoplasm, the higher the growth rate, the less vacuole, the higher the pH reading. In non-growing hyphae there is generally no need for a polar organisation of the apical compartment which could cause the disappearance of the gradient in vacuolation in favour of a more extended vacuolation throughout the tip explaining why non-growing hyphae exhibited the same pH as that found at the base

of the gradient. Based on the arguments presented above, it can be concluded that the study by Robson et al. (1996) did not convincingly solve the question whether or not there is a pronounced pH gradient in growing *N. crassa* hyphae.

Another recent study employing fluorescence ratio imaging (including photometric analysis) of BCECF loaded fungal hyphae (Jolicoeur et al., 1998) indicated the existence of an acidic pH over the first 2 μm behind the apical pole followed by a sharp rise to more alkaline pH values and then a subsequent continuous decrease over several hundred micrometers to a more acidic basal level. Taking into account that the authors did not do a rigorous analysis of intracellular dye distribution it might be the case that this investigation suffered from the same problems as proposed here for the data shown by Robson et al. (1996). BCECF is structurally closely related to CFDA (Haugland, 1996) which has been used to characterise the tubular vacuolar system in many fungi covering representatives of all known fungal groups (Rees et al., 1994). It seems likely that as CFDA accumulates in the vacuoles of so many fungi then BCECF may do as well. At least for *N. crassa* the pattern of dye sequestration looks strikingly similar for both dyes (Figures 3.3 and 3.5). Jolicoeur et al. (1998) stated that the fluorescence intensity at the hyphal apex was lower than in the rest of the hypha due to the tapering and the accumulation of vesicles in this region. They therefore performed a test to assess the $R_{S/N}$ necessary for reliable measurements simply by increasing the background fluorescence and obtained a minimum value of 0.55. It can only be guessed whether this $R_{S/N}$ value might represent the ratio of intracellular fluorescence against background fluorescence? If this is the case, Jolicoeur et al. (1998) obviously confused background fluorescence with noise. It is also not clear from which part(s) of the hypha the signal was measured to obtain this value (apical or subapical regions?). According to Pawley (1995) there are several sources for noise associated with microscopical measurements (such as statistical noise resulting from counting photons, noise from detector dark-current and noise from background fluorescence). Quantities such as background fluorescence, cellular autofluorescence and detector dark-current should be subtracted from the genuine dye signal. They should not be considered as noise themselves, but due to variability they will

contribute to the overall noise of the signal (Parton and Read, 1999). Considering the arguments above it is difficult to understand how simply increasing background fluorescence can be employed to assess the reliability of measurements of low signal at the apex. Another critical point is that Jolicoeur et al. (1998) apparently extracted their ratio data from final ratio images and therefore their results might suffer from the noise-induced artefact described in Section 3.2.4 which could explain the more acidic value found within the first 2 μm behind the apical pole.

The most convincing data showing a pH_c gradient associated with tip growth has come from the analysis of rhizoids in the brown alga *Pelvetia* using confocal ratio imaging of cSNARF-1 dextran and ion-selective microelectrodes (Gibbon and Kropf, 1994). Growing rhizoid cells were found to generate a longitudinal pH_c gradient in which the apical region was 0.3 to 0.5 units more acidic than the region at the base of the cell.

On the other hand there are several investigations which have provided evidence that pH_c gradients are not a general feature of tip-growing cells, Herrmann and Felle (1995) failed to detect a gradient (>0.1 pH unit) in growing root hairs by using ion-selective microelectrodes. Bibikova et al. (1998) also reported the absence of a detectable tip-based pH_c gradient in growing root hairs employing confocal microscopy of BCECF 10 kDa dextran. Interestingly, before the onset of tip growth, the pH_c was found to be temporarily elevated at the root hair initiation site concomitant with localised cell wall acidification indicating that root hair initiation and root hair tip growth differ in their pH requirements. Performing confocal ratio imaging of BCECF it has been demonstrated that pronounced pH_c gradients are not associated with growing *Lilium* pollen tubes (Fricker et al., 1997). Messerli and Robinson (1998) confirmed the absence of standing pH_c gradients in *Lilium* pollen tubes, but found tip-localised pulses of pH_c that occur during pulsatile growth using confocal ratio imaging of cSNARF-1 10 kDa dextran. Parton et al. (1997) showed the absence of pH_c gradients in *Agapanthus* pollen tubes, *Dryopteris* fern rhizoids and *Neurospora* hyphae. The findings by Parton et al. (1997) concerning *N. crassa* are

based on the work presented here. This work has shown that pronounced longitudinal pH_c gradients (ΔpH >0.1 pH unit) are not present within the apical 50 µm of actively growing *N. crassa* hyphae (Section 3.2.5).

3.3.2 Confocal ratio imaging of cSNARF-1 loaded *Neurospora crassa* hyphae

Simultaneous, dual channel confocal ratio imaging is the most suitable method for visualising pronounced pH_c gradients in tip growing cells (Section 1.4.6). However, this procedure is potentially fraught with artefacts and thus requires rigorous controls. In order to validate the conclusion that pronounced pH_c gradients were absent in *N. crassa*, emphasis was laid on careful assessment of the specific problems of cell perturbation during imaging, dye partitioning within organelles (Opitz et al, 1994), $R_{S/N}$ and "edge" artefacts in ratio images (Bright et al., 1987; Pawley, 1995), and calibration of cSNARF-1 (Fricker et al., 1994). A pronounced longitudinal pH_c gradient was defined in this study as having a ΔpH of >0.1 pH unit over a distance >2 µm for two reasons. First, these were the limits of the precision of pH measurement and spatial resolution which could be routinely achieved by confocal ratio imaging of cSNARF-1 within healthy cells (Section 3.2.4). Second, ΔpH of >0.1 pH unit are within the range considered to be of physiological significance (Busa and Nuccitelli, 1984; Guern et al., 1991). The results presented here do not discount the possible presence of highly localised pH gradients which might be associated with the plasma membrane (Roos, 1992). Previously reported pH_c values for plant and fungal cells usually lie between pH 6.8 and 7.9 (e.g. see Sanders and Slayman, 1982; Guern et al. 1991). According to data shown here, the estimated values of mean pH_c with ester-loaded dye were around 7.2 for *N. crassa*. With hyphae loaded with the dextran dye by pressure injection, however, the estimated mean pH_c was nearly pH 7.6. It is generally believed that the results obtained with dextran dyes provide a better estimate of pH_c because of their superior localisation and retention within the cytosol (Haugland, 1996; Miller et al., 1992). It is significant that, although the pH_c values estimated with ester-loaded free dye and pressure-injected dextran dye in *Neurospora*

differed, no significant pH_c gradient was detected with either. The estimated pH_c was very reproducible between individual cells and variation in average pH_c between individual cells was within the limits of precision of measurement for the imaging technique. This is in agreement with the general finding that pH_c is tightly regulated within growing cells (Guern et al., 1991). For the work reported here, cSNARF-1 proved to be the most appropriate dye. Another ratio dye widely used to measure pH_c is BCECF (Haugland, 1996), but this has a number of disadvantages compared with cSNARF-1. First, in *Neurospora* it exhibits more pronounced sequestration within vacuoles and has more detrimental effects on growth when laser irradiated (Section 3.2.2; Slayman et al., 1994). Second, BCECF is a dual excitation dye requiring sequential excitation at two wavelengths. Improved temporal resolution can be achieved with cSNARF-1 which is excited at one wavelength and detected simultaneously at two wavelengths.

3.3.3 Role pH_c and pH_{ext} in regulating tip growth

The lack of pronounced pH_c gradients in several cell types during active tip growth (Herrmann and Felle, 1995; Fricker et al., 1997; Parton et al., 1997; Bibikova et al., 1998) argues strongly against a fundamental role for gradients of this type regulating the polar organisation and active processes of tip growth. This conclusion is further supported by the finding that *Neurospora* hyphae continued to grow in the presence of relatively high concentrations of cell permeant propionic acid (pKa 4.87) which would be expected to collapse any pH_c gradient. Gibbon and Kropf (1994) found that 10 mM propionic acid (at pH 7.0) dissipated the pH_c gradients and drastically reduced growth of *Pelvetia* rhizoids. They suggested that these observations provided evidence for a pH_c gradient regulating tip growth in these cells. The validity of this interpretation is open to question. Both, Herrmann and Felle (1995) and Bibikova et al. (1998), performed similar weak acid treatments on root hairs and recorded similar inhibitory effects on growth. However, in the absence of a detectable pH_c gradient within growing root hairs, they concluded that the inhibitory effects of the weak acids on growth may be due to a disruption of the normally maintained pH_c rather than

effects on a standing pH gradient at the tip. Treatment of cells with membrane permeant weak acids may have a number of non-specific effects relevant to tip growth, including: (1) Both, organellar pH and cytosol pH will be affected and changes in organellar pH may be important for certain processes involved in tip growth (e.g. the exocytotic pathway). (2) Acidifying cells can increase the cytosolic calcium concentration (Felle, 1988; Guern et al., 1991). Artificially induced increases in cytosolic free calcium have been shown to inhibit tip growth in pollen tubes (Franklin-Tong et al., 1993; Malhó et al., 1994). (3) The membrane potential will be changed by cytoplasmic acidification which will affect ion transport across membranes. Such non-specific effects may explain the inhibition of tip growth, although the probable existence of highly localised unseen pH_c gradients (e.g. adjacent to membranes) cannot be ignored.

The weak acid and base treatments also make clear that intracellular cSNARF-1, both the ester-loaded dye and the dextran conjugate, was responsive to intracellular pH changes (Section 3.2.6). Therefore, a pH gradient of over 1 pH unit as indicated by Robson et al. (1996) or pulses in $[H^+]$ as demonstrated by Messerli and Robinson (1998) for pollen tubes should have been detected if they were features of growing *N. crassa* hyphae.

It can be concluded from the results shown here that both pH_c and pH_{ext} have a significant influence on the growth of *N. crassa* hyphae. Tip growth was sensitive to any alteration in the normally maintained pH_c. Changing pH_{ext} influenced the rate of tip growth, the width of hyphal tips, and the formation of new tips (branch formation). Altering pH_{ext} was commonly accompanied by a transient change in pH_c. However, it is unlikely that the effects of altering pH_{ext} were due to this transient influence on pH_c alone - (e.g. consider increased branching in *N. crassa* which continues throughout the period of culture at increased pH_{ext}). Changes in membrane potential and transport activities may also be important.

pH_c regulation is undoubtedly an important aspect of cellular physiology. It has been proposed as a mechanism by which cells co-ordinate the regulation of various processes that lack any other common factors and also may provide a regulatory link between metabolic state and physiological responses, such as those involved in tip growth (Busa and Nuccitelli, 1984; Felle, 1996). However, the pervasive nature of H^+ throughout all cellular processes makes it difficult to determine strict cause and effect relationships and to assign specific second messenger functions.

4. Calcium in tip growth of *Neurospora crassa* hyphae

4.1 Introduction

Tip high gradients in cytosolic free Ca^{2+} ($[Ca^{2+}]_c$) are thought to be involved in the regulation of tip growth and have been shown to occur in several different tip growing systems using fluorescence microscopy of high molecular weight dextran conjugates of Ca^{2+} sensitive dyes: root hairs (Felle and Hepler, 1997; Bibikova et al, 1997); pollen tubes (Pierson et al.,1994; 1996); and rhizoids of algae (Berger and Brownlee, 1993). In the case of fungi, considerable circumstantial evidence is available supporting the existence of a tip high gradient in $[Ca^{2+}]_c$ in growing hyphae (reviewed by Jackson and Heath, 1993a). However, a direct measurement of such a gradient has proven difficult. Knight et al. (1993) demonstrated the problems with ester-loading and ionophoresis of Calcium Green-1 (CG-1) in a range of fungi. For *N. crassa* (Knight et al., 1993) it has been shown that AM-esters of Ca^{2+}-sensitive dyes are not taken up. Ionophoresis of CG-1 free acid and CG-1 10 kDa dextran conjugate resulted in dye sequestration (Knight et al., 1993). Subsequent studies by Levina et al. (1995) and Hyde and Heath (1997) used the acid loading technique (Section 1.4.6.1) to introduce a ratiometric dye-pair consisting of a Ca^{2+}-sensitive single wavelength dye (Fluo-3) and a Ca^{2+}-insensitive volume marker (carboxy SNARF-1) into *N. crassa* (Levina et al, 1995) and the oomycete *Saprolegnia ferax* (Hyde and Heath, 1997). Although this approach generally resulted in very low intracellular dye concentrations the authors were able to detect tip high gradients in $[Ca^{2+}]_c$ in growing hypha. The gradient in *N. crassa* hyphae was found to peak at 3 μm behind the tip (Levina et al, 1995), whereas in *S. ferax* hyphae it apparently peaked right at the tip (Hyde and Heath, 1997). However, these results were obtained using dye free acids which are more likely to sequestrate into organelles or leak out of cells than the more reliable high molecular dye dextran conjugates (Haugland, 1996).

The aim of the work presented here was to establish a confocal ratiometric imaging method to measure $[Ca^{2+}]_c$ in growing *N. crassa* hyphae using high molecular weight dextran conjugates of dyes.

The first step was to find a suitable Ca^{2+}-sensitive dye for measuring $[Ca^{2+}]_c$ using a confocal microscope. Loading of dye free acids and high molecular weight dextran conjugates was attempted by ionophoresis and pressure microinjection. Low pH loading as performed by Levina et al. (1995) and Hyde and Heath (1997) was not considered an option because it has been described as yielding unsatisfactorily low levels of loaded dye and it is unsuitable for loading high molecular dextran conjugates (Knight et al., 1993; Parton, 1996; Parton and Read, 1999). The second step was to develop and apply a ratiometric approach for imaging $[Ca^{2+}]_c$ in *N. crassa* hyphae. Initially only the Bio-Rad MRC 600 supplied with an argon ion laser (Section 2.7.1) was available. Therefore, UV-excited ratio dyes, such as Fura-2 and Indo-1 (Haugland, 1996), could not be used and dyes exitable by visible laser light had to be chosen in order to obtain a ratiometric dye combination (Gilroy, 1997; Opas, 1997).

4.2 Results

4.2.1 Loading of Ca^{2+} sensitive single wavelength dyes

4.2.1.1 Loading of OG-1 by ionophoresis and ester-loading

The Ca^{2+}-sensitive dye Oregon green 488 BAPTA-1 (OG-1) is structurally very similar to CG-1, but has a much better absorbance at 488 nm wavelength resulting in increased brightness at similar dye concentrations (Haugland, 1996). As a starting point, ester-loading and ionophoresis as described in Knight et al. (1993) were performed for OG-1. Ester-loading of OG-1 into *N. crassa* hyphae yielded no fluorescence above the cellular autofluorescence on high gain settings (data not shown). Ionophoresis of the free acid (Figure 4.1A and B) appeared to result in complete dye sequestration from the cytosol, probably within the vacuolar system.

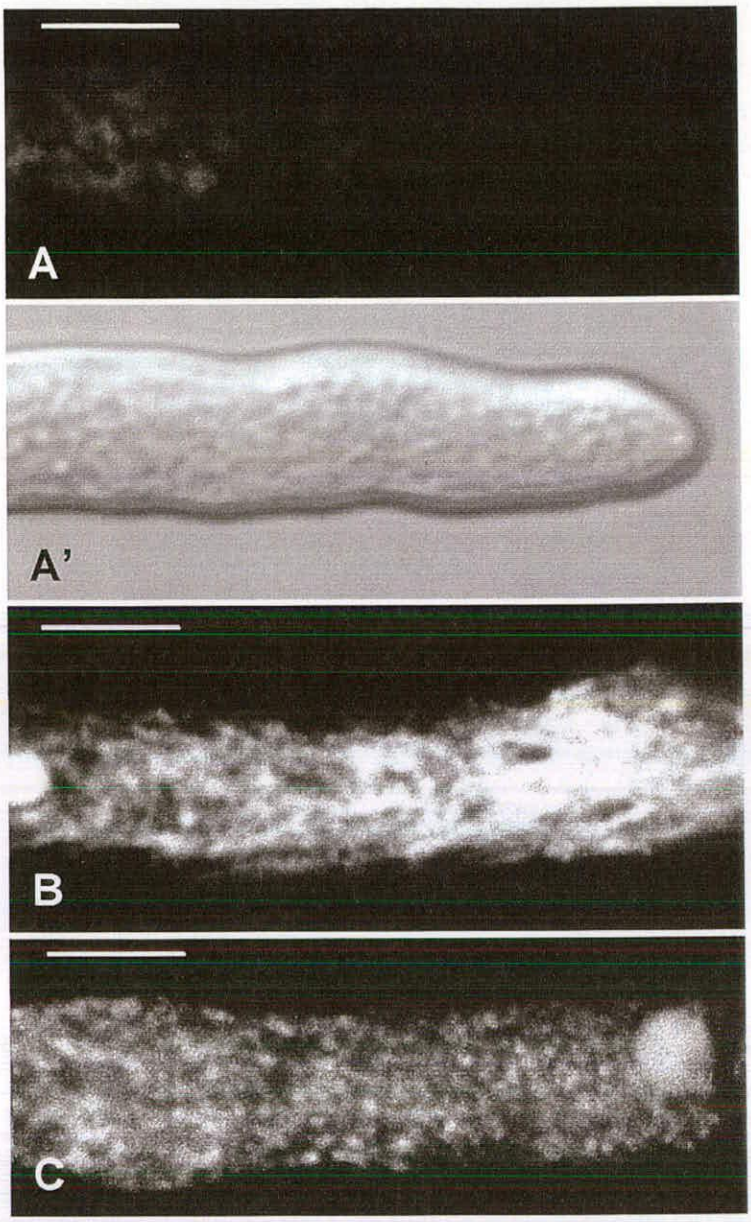

Figure 4.1. Confocal images of *N. crassa* hyphae loaded with OG-1 by ionophoresis. (**A**) Growing tip loaded with OG-1 free acid. The image was taken 5 min after restart of growth. Note the pronounced dye sequestration and the exclusion of dye from the first 20 μm. Growth rate = 18 μm min^{-1}. (**A'**) Corresponding bright field image. (**B**) Subapical region of the apical compartment of the same tip as in (A) 7 min after restart of growth. (**C**) Subapical compartment (more than 500 μm distant from the apex) of a hypha loaded with OG-1 10 kDa dextran by ionophoresis. Note the less intense signal than in (B). Bars = 10 μm.

Vacuolar localisation of OG-1 was confirmed by comparison of OG-1 loaded cells with those stained with the vacuolar marker 6-carboxyfluorescein diacetate (Section 3.2.2, Figure 3.5). The vacuolar system loaded with OG-1 was very pleomorphic. Vacuole sequestered dye was transported away from the injection site towards the tip. Interestingly, there was a very low fluorescence signal within the first 15-20 μm of the tip (Figure 4.1A) which was presumably due to a very reduced vacuolar system in this region (Section 1.1.1). Strikingly similar results were obtained by ionophoresis of the 10 kDa dextran conjugate (Figure 4.1C) which is consistent with the data presented by Knight et al. (1993). The dextran conjugate appeared to be predominantly vacuolar, the fluorescence was somewhat less intense than that obtained with the free dye.

4.2.1.2 Loading by pressure injection

Due to the shortcomings of ionophoresis, loading of *N. crassa* hyphae by pressure injection was performed. Introduction of OG-1 free acid by pressure injection resulted in pronounced sequestration (Figure 4.2) indistinguishable from that obtained by ionophoresis of this compound (i.e. mainly vacuolar dye retention with very little or no fluorescence signal at the first 15-20 μm of the tip region was observed).

With pressure microinjection of OG-1 10 kDa dextran much more promising results were obtained (Figure 4.3). Loading of a hypha several hundred micrometers behind the tip gave an even intracellular dye distribution with visible dye exclusion from large vacuoles (Figure 4.3A). In this part of the mycelium hyphae usually showed vigorous cytoplasmic streaming which recovered after successful pressure injection. The rapid intracellular streaming transported dye towards the tip region resulting in dilution and reduction of fluorescence intensity (Figure 4.3B). Occasionally, especially when the amount of dye injected was large, slight sequestration into large spherical vacuoles was observed (data not shown). After recovery of cytoplasmic streaming, which led to dilution of dye, sequestration did not occur in subsequent compartments suggesting that it was concentration dependent.

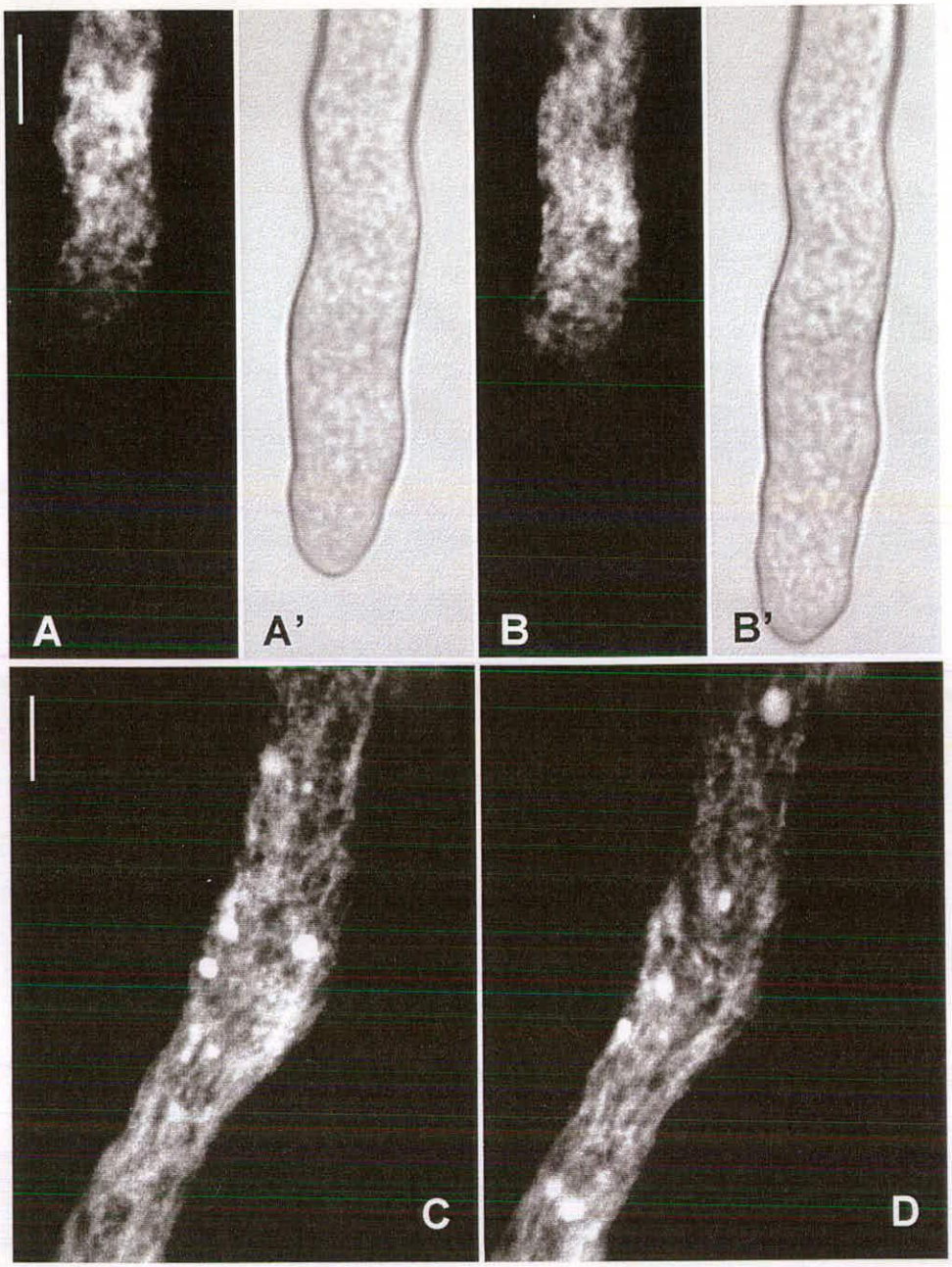

Figure 4.2. Confocal images of *N. crassa* hyphae pressure injected with OG-1 free acid. (**A** and **B**) Growing tip 9 min and 9 min 40 sec after restart of growth, respectively. Note the dye sequestration and the absence of loading within the first 20 μm. Growth rate = 14 μm min^{-1}. (**A'** and **B'**) corresponding bright field images. (**C** and **D**) Subapical region of the same tip as shown in (A and B) 5 min and 5 min 40 sec after restart of growth, respectively. Note the pronounced sequestration within the vacuolar network. The hypha exhibited rapid cytoplasmic streaming towards the apical region as indicated by translocation of the small spherical vacuoles. Bars = 10 μm.

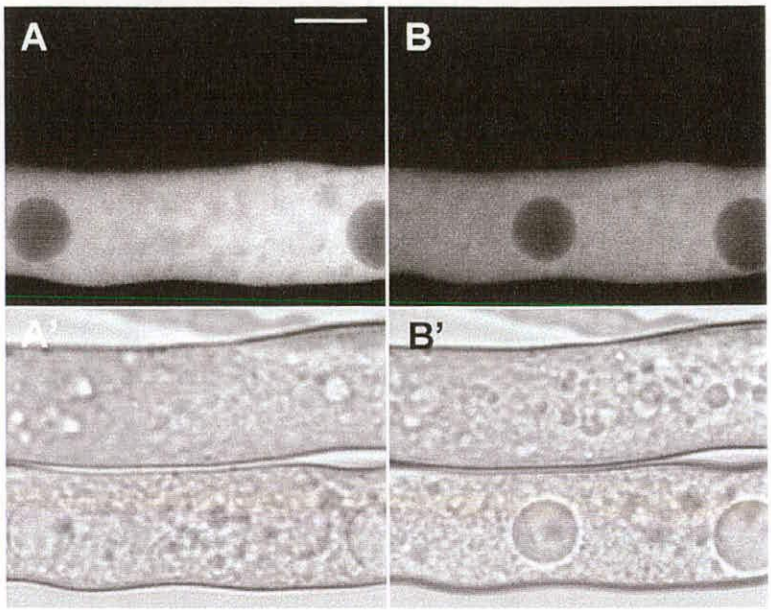

Figure 4.3. Confocal images of *N. crassa* subapical hyphal compartments pressure microinjected with OG-1 10 kDa dextran conjugate. (**A** and **B**) Compartment below injection site 2 min and 3 min after recovery of cytoplasmic streaming, respectively. (**A'** and **B'**) corresponding bright field images. Note the lack of fluorescence in the adjacent hypha which has not been injected. Rapid cytoplasmic streaming transports dye towards the tip. Bars = 10 μm.

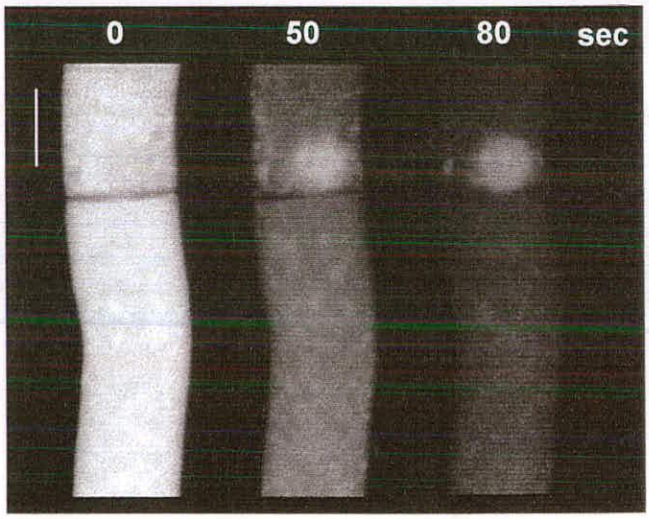

Figure 4.4. Confocal images of *N. crassa* subapical hyphal compartments pressure injected with CG-1 10 kDa dextran conjugate. A compartment below the injection site is displayed. The first image was taken about 5 min after withdrawing of the micropipette when the hypha had resumed vigorous cytoplasmic streaming which displaced the dye towards the tip region. Bar = 10 μm. Note the dye sequestration into the vacuole.

For comparison CG-1 10 kDa dextran conjugate was pressure injected into *N. crassa* hyphae. However, the dye distribution of CG-1 (Figure 4.4) was less favourable consistently showing sequestration into the vacuolar system.

Successful injection of the OG-1 10 kDa dextran conjugate into the apical compartment was followed by formation of new tips after recovery. Confocal median sections of loaded growing tips showed an even dye distribution (Figure 4.5A-C). However, small cytoplasmic domains of slightly increased fluorescence starting 15-20 μm behind the apex could be discerned. These areas, which may represent dye sequestration within nuclei via nuclear pores, were not observed at lower dye concentration (Figure 4.6A-C). However, it is possible that the poor dye signal from these cells may not have been great enough to detect small variations in the intracellular dye fluorescence as observed in Figure 4.5 A-C. There is evidence that the nucleoplasm affects the spectral properties of fluorescent dyes such as Fluo-3 leading to an increase in fluorescence intensity which is not related to the Ca^{2+} concentration (Perez-Terzic et al., 1997). Nonetheless, in both cases transects through the hyphae showed that there was no obvious tip high gradient in fluorescence (Figures 4.5A'-C' and 4.6A'-C'). Single wavelength dyes do not take account of uneven distribution of the cytosol and the data is therefore difficult to interpret (Read et al., 1992).

During imaging of growing tips loaded with OG-1 10 kDa dextran conjugate there was usually very little reduction in fluorescence intensity. The stability of the fluorescent signal was probably due to two factors: dye photostability under the imaging conditions used for the Bio-Rad MRC 600 (Section 2.7.3) and cytoplasmic streaming. The tip-ward orientation of the latter caused dye to remain within the apical compartment during hyphal elongation. Repeated scanning of loaded hyphae caused a decrease in growth rate and hyphal narrowing. Another problem limiting imaging time was the tendency for hyphae to grow out of focus.

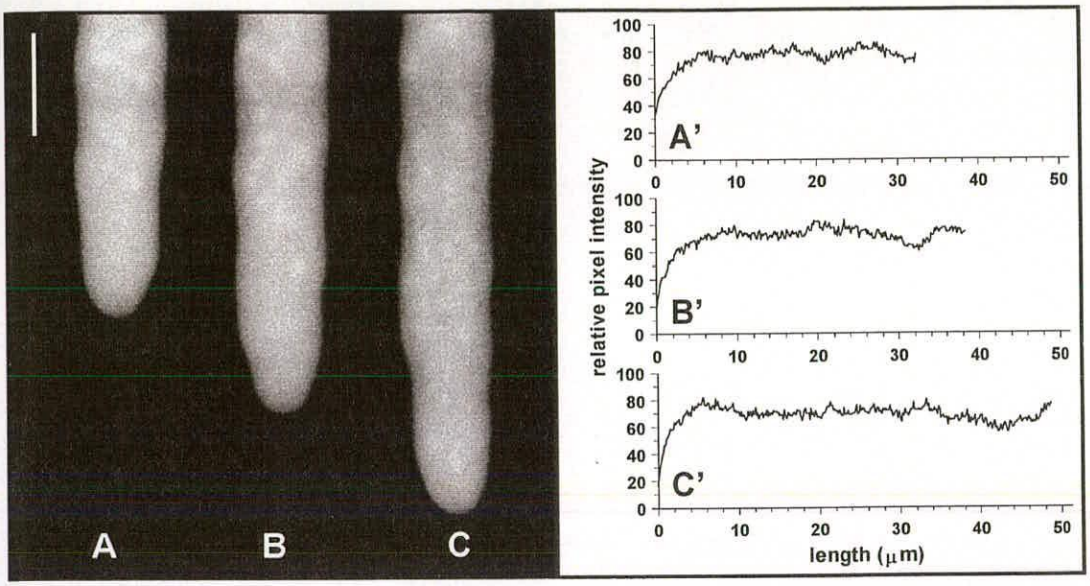

Figure 4.5. *N. crassa* hyphae loaded with OG-1 10 kDa dextran conjugate by pressure microinjection. (**A, B** and **C**) Confocal images of a hypha ca. 10, 11 and 12 min after restart of growth, respectively. Growth rate = 11 μm min^{-1}. (**A', B'** and **C'**) Pixel intensity along a 10 pixel wide transect through the long axis of the hypha at (A, B and C), respectively. Bars = 10 μm.

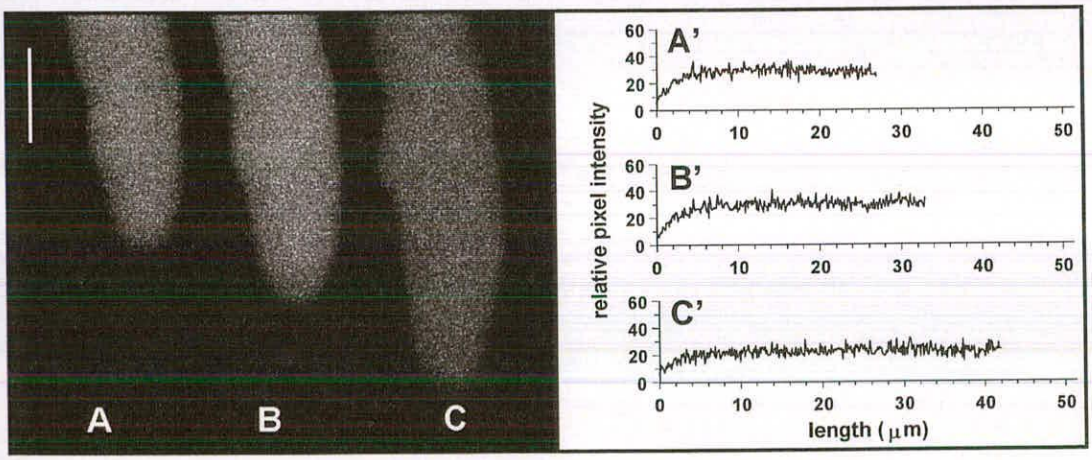

Figure 4.6. *N. crassa* hyphae loaded with OG-1 10 kDa dextran conjugate by pressure microinjection at considerable lower dye concentration than in Figure 4.5. (**A, B** and **C**) Confocal images taken ca. 13, 13.5 and 14 min after restart of growth, respectively. Growth rate = 12.5 μm min^{-1}. (**A', B'** and **C'**) Pixel intensity along a 10 pixel wide transect through the long axis of the hypha at (A, B and C), respectively. Bars = 10 μm.

An indication that dye is present in the cytosol is the ability to increase fluorescence by treatments which raise $[Ca^{2+}]_c$. Collis (1996) showed that exogenous $CaCl_2$ added to *N. crassa* spheroblasts transformed with the aequorin gene transiently increased $[Ca^{2+}]_c$. It was investigated whether this effect could be reproduced by externally adding Ca^{2+} to OG-1 10 kDa dextran loaded growing hyphal tips (Figure 4.7). Indeed, the fluorescence showed a transient increase and a subsequent decline which suggested that a considerable amount of dye was cytosolic. Incidentally, the series of images shown in Figure 4.7 also demonstrates how an oblique section through a cell can create the impression of a gradient when a single wavelength dye is used.

4.2.2 Ratio approach

4.2.2.1 Selection of a ratiometric dye combination

Currently available Ca^{2+}-sensitive ratio dyes are exclusively excited by UV light (Haugland, 1996). If UV light excitation is not an option because of restrictions imposed by the equipment (Levina et al., 1995; Hyde and Heath, 1997) or the experimental set up (Bibikova et al, 1997), Ca^{2+}-ratio imaging can be achieved by using a suitable combination of two dyes excitable by visible light (Opas, 1997). The dye combination used by Levina et al. (1995) and Hyde and Heath (1997), Fluo-3 and carboxy SNARF-1, both excitable with the 488 nm laser line, proved to be unsuitable mainly because Fluo-3 is not available as a high molecular dextran conjugate. As an alternative to Fluo-3, CG-1 and OG-1 were considered because of their very similar fluorescence spectra to Fluo-3. These dyes, of which dextran conjugates are available, also exhibit brighter fluorescence (Haugland, 1996). Berger and Brownlee (1993) used a combination of carboxy SNARF-1 and CG-1 10 kDa dextran conjugate for ratiometric Ca^{2+} imaging. However, the emission spectra of OG-1 or CG-1 overlapped considerably with the emission spectrum of carboxy SNARF-1 and could not be separated sufficiently with the available filter combinations. Another drawback was the enormous difficulty in introducing the carboxy SNARF-1 10 kDa dextran conjugate into *Neurospora* hyphae (Section 3.2.1). Using Fura-Red instead of carboxy SNARF-1 (Lipp and Niggli, 1993; Schild et al., 1994) was not attempted

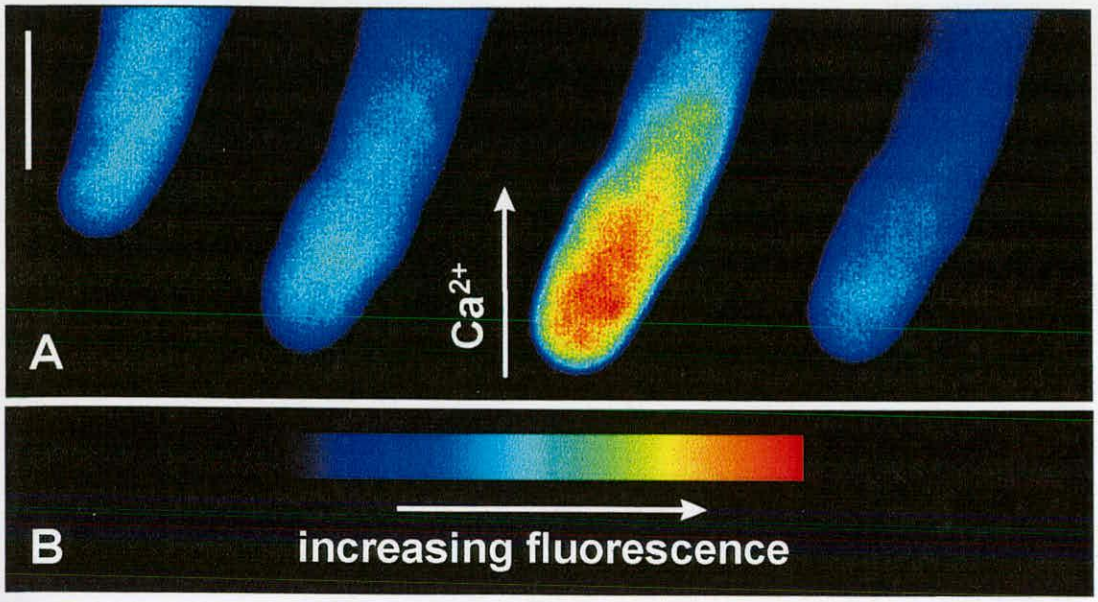

Figure 4.7. (**A**) Pseudo coloured confocal fluorescence images of a *N. crassa* tip cell pressure microinjected with OG-1 10 kDa dextran conjugate. The arrow indicates application of 75 mM Ca^{2+} to the external medium which leads to a rise in $[Ca^{2+}]_c$. Note that only part of the tip region is in focus which is responsible for the signal fall off towards the base of the hypha. Bar = 10 μm. (**B**) Look up table.

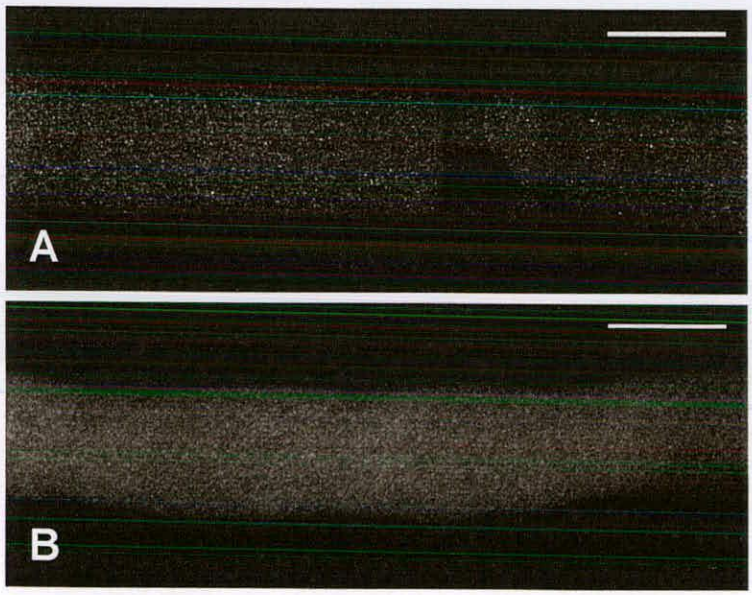

Figure 4.8. Confocal images of *N. crassa* subapical hyphal compartments pressure injected with RB 10 kDa dextran conjugate. (**A**) The injection resulted in lower intracellular dye concentration whereas in (**B**) a higher intracellular dye concentration could be achieved. Note the even dye distribution. Bars = 10 μm.

here because Fura-Red is described as poorly fluorescent making it necessary to load it at a high concentration (Haugland, 1996). Bibikova et al. (1997) used a combination of Calcium Green-2 10 kDa dextran (Ca^{2+}-sensitive dye) and Rhodamine B (RB) 10 kDa dextran (volume marker). Excitation of RB, a green excited dye, on the MRC 600 proved unsuccessful using the 514 nm laser line. Access to a new Leica TCS NT confocal microscope with more laser lines, including two UV lines, and more filter combinations, opened more possibilities. Nonetheless, it was decided to pursue the approach with a ratiometric dye combination because it might be useful for future experiments when UV light could not be used for excitation due to interference with certain treatments such as caged probes release (Bibikova et al., 1997). The Leica confocal microscope was equipped with a Krypton laser as well as an Argon ion laser. This opened the possibility of using RB in combination with OG-1.

4.2.2.2 Loading of the ratiometric dye combination into *Neurospora crassa* hyphae

To assess intracellular dye distribution of RB 10 kDa dextran conjugate, the dye was injected into *Neurospora* hyphae. An aqueous dye solution of RB dextran (1 mM) was more viscous than that of OG-1 or CG-1 dextran (as indicated by residues left in pipette tips after transferring aliquots of RB dextran solution), but it did not appear to be quite as viscous as carboxy SNARF-1 10 kDa dextran (Section 3.2.1) and injection was feasible although it was difficult to achieve a good loading. Injection of RB 10 kDa dextran on its own showed that there was no apparent sequestration and that it was retained within the cell (Figure 4.8). However, injection of a mixture of both OG-1 and RB dyes proved problematic. The OG-1 signal was usually much brighter then the RB signal. Furthermore, the relative fluorescence intensity of both channels in comparison to each other varied considerably between different cells. Also, it was difficult to achieve adequate loading mainly because the microscope was not placed on a vibration free table. This reduced the time over which dye could be injected before injury to the cell caused by vibration of the micropipette prevented sealing. Therefore, to increase the fluorescence signal detected it was necessary to

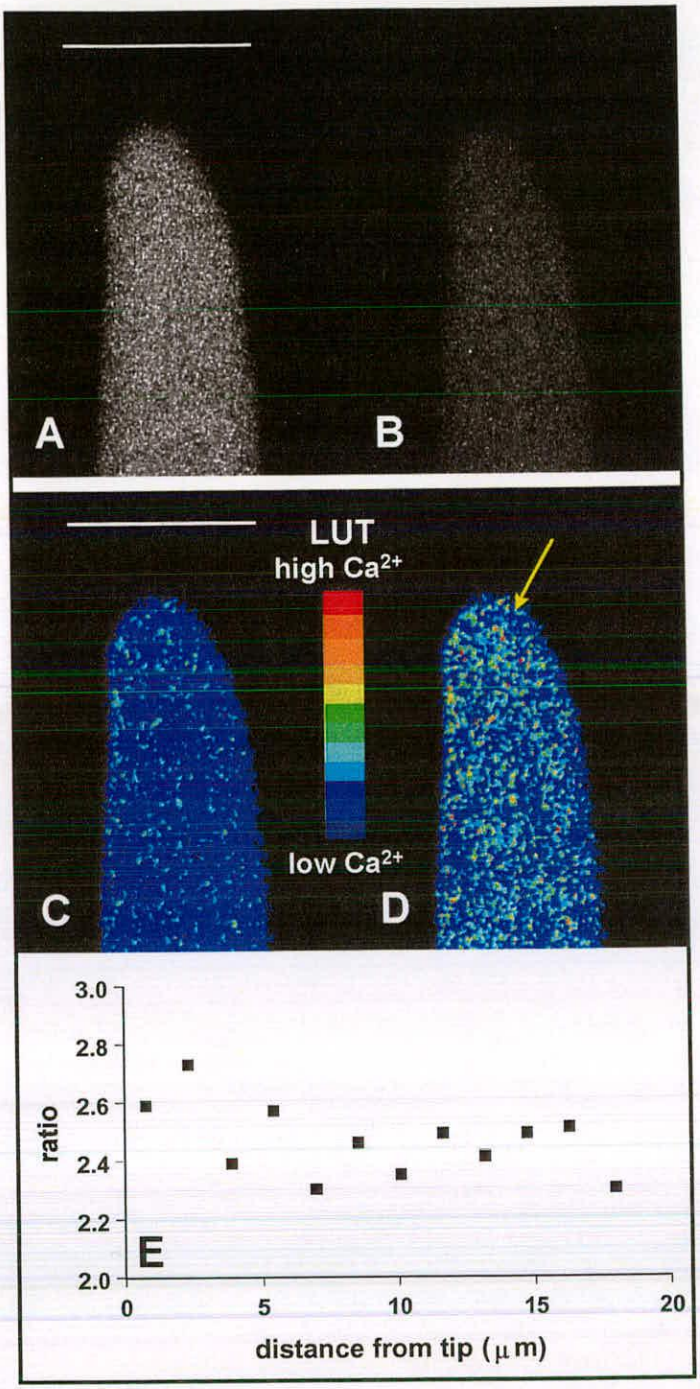

Figure 4.9. Ratio imaging of *N. crassa* hypha injected with OG-1 and RB, both in the form of 10 kDa dextran conjugates. (**A** and **B**) Fluorescence images of the OG-1 and the RB channel after dark signal subtraction, respectively. (**C** and **D**) Ratio images before and after spill over correction, respectively. (**E**) Display of ratio values along the hyphal axis. The ratios were obtained in the following way. Average fluorescence pixel intensities from 2.4 μm^2 boxes along the hyphal axis in both fluorescence images were extracted. After correction for spill over OG-1 values were divided by RB values to obtain ratios. Bars = 10 μm.

increase the gain voltage and open the pinhole completely. Frame averaging to improve the signal-to-noise ratio ($R_{S/N}$) was not feasible because of hyphal growth. Successful injection of apical compartments clearly resulted in an even dye distribution in both channels without any signs of dye sequestration (Figure 4.9A and B). Ratioing after dark signal subtraction and correction of spill over (Section 2.8.2) did not consistently reveal a tip-high gradient in $[Ca^{2+}]_c$ (data not shown). Three hyphae were analysed and only in one case a very shallow tip-focused gradient in $[Ca^{2+}]_c$ which extended over about the first 10 μm was revealed (Figure 4.9D). Calibration of the data was not performed because it was not possible to determine the relative amount of each dye loaded. The data was not statistically analysed because at the gain settings necessary for image capture (70%) the pixel distribution in fluorescence images obtained with the Leica TCS NT was skewed (Figure 4.10). For statistical analysis the pixel distribution has to be approximately Normal (Section 3.2.4).

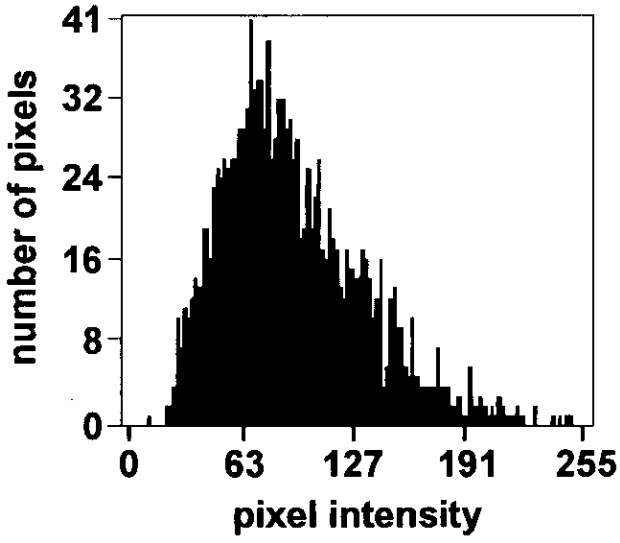

Figure 4.10. Histogram of an area containing 2500 pixels. The area was extracted from the OG-1 channel of an image of a cell loaded with OG-1 and RB.

4.3 Discussion

4.3.1 The need for further investigation into the existence of tip high $[Ca^{2+}]_c$ gradients in fungal hyphae

In fungi, gradients in $[Ca^{2+}]_c$ have been reported for *N. crassa* (Levina et al., 1995) and the oomycete *S. ferax* (Hyde and Heath, 1997) using a ratiometric dye-pair on a Bio-Rad MRC 600 confocal microscope. Both studies originated from the same laboratory and were based on the same technical approach. However, in both cases the results suffered from several technical problems originating mainly from the loading procedure used. The acid-loading technique results in a very low intracellular dye concentration (Parton and Read, 1999). Therefore, during imaging amplification of a weak fluorescence signal is required.

For measuring low fluorescence signals on the Bio-Rad MRC 600 confocal microscope the "Fast photon counting mode" is available. Whilst using this facility the PMT is operated in a pulse counting mode which eliminates the dark current and improves the signal-to-noise ratio ($R_{S/N}$) (Pawley, 1995; Bio-Rad MRC 600 Operating Manual). Photon counting is used in the accumulation mode and it is recommended to accumulate ten or more frames (Bio-Rad MRC 600 Operating Manual). Indeed, Levina et al. (1995) and Hyde and Heath (1997) admit the need for accumulation of frames to obtain an image of "sufficient brightness". Whereas Levina et al. (1995) do not give further details, Hyde and Heath (1997) stated that an accumulation of approximately 10 frames were required to collect one image. If the photon counting mode on the Bio-Rad MRC 600 is used with the F2 scan speed which takes 1 sec per frame, collecting one final image would take on average 10 sec. The *S. ferax* hyphae imaged by Hyde and Heath (1997) showed growth rates ranging from 0-8 $\mu m\ min^{-1}$ with a mean of 1.69 $\mu m\ min^{-1} \pm 2.57$ s.e.m. Accumulation of frames may have comparatively little effect when slow growing hyphae are imaged, whereas with faster growing hyphae it can lead to considerable image distortion. A hypha growing at 8 $\mu m\ min^{-1}$ will have grown 1.3 μm within 10 sec, therefore, likely to cause considerable blurring of the image. Hyde and Heath, (1997) reported a positive

correlation between growth rate and steepness of Ca^{2+} gradient slopes but did not state whether they considered the effect different growth rates could have had on the extent of image distortion. Furthermore, Levina et al. (1995) did not state either the number of frames averaged nor the growth rates exhibited by the *N. crassa* hyphae under imaging conditions.

The acid-loading technique required cultivation of hyphae under non-physiological conditions for prolonged time periods (Parton and Read, 1999). This might be one reason for the rather slow growth rates observed by Hyde and Heath (1997). These values which are quoted above, compare unfavourable with other studies using *S. ferax* for microscopic observation (Yuan and Heath, 1991a; 1991b).

Another approach to increase a weak signal is to use high laser intensity for excitation. This was apparently done by Levina et al. (1995) and Hyde and Heath (1997), who used the full laser intensity at 488 nm for excitation (15 mW Krypton / Argon laser). However, compensating for poor dye loading by high laser intensity is problematic and can lead to fluorescence saturation especially at low dye concentrations (Pawley, 1995). If a significant number of fluorescent molecules are constantly in the excited state they can no longer absorb light at the usual wavelength which reduces the effective dye concentration. The signal becomes dependent upon variables other than dye concentration and the rate of photobleaching is likely to increase (Pawley, 1995).

In spite of these criticisms it cannot be excluded that the principal finding of these two studies (existence of a tip-high Ca^{2+} gradient) from Heath's lab may be correct. It is in the authors' favour that their result corresponds with expectations based on general evidence linking tip growth to a tip-high gradient in $[Ca^{2+}]_c$ (Jackson and Heath, 1993a) However, the results are probably over interpreted and several possible artefacts were not considered by the authors. The evidence for the existence of tip high $[Ca^{2+}]_c$ in growing hyphae based on dye measurements is still not compelling.

There is, therefore, the necessity to develop improved approaches for imaging $[Ca^{2+}]_c$ in hyphae.

4.3.2 Imaging Ca^{2+} in fungal hyphae using high molecular dextran conjugates of fluorescent dyes

Pressure microinjection of dye dextran conjugates showed that dye was retained within cells for long periods of time and sequestration was much reduced (Figures 3.1C, 3,1D, 4.3, 4.5, 4.6 and 4.8). However, the 10 kDa dextran conjugates of different dyes exhibited unforeseen differences in behaviour which made it necessary to test each dye for suitability for microinjection and to assess intracellular dye distribution. Although CG-1 and OG-1 are structurally very similar (Haugland, 1996), the CG-1 dextran conjugate showed a clear tendency to sequester into the vacuolar system. With OG-1 dextran there was very little, if any, sequestration noticeable (Figures 4.3). RB and cSNARF-1 dextrans showed no signs of sequestration at all (Figures 4.8, 3.1C and 3.1D). Interestingly, these two dyes were apparently more viscous than the CG-1 and OG-1 dextran. For cSNARF-1 increased viscosity was not only observed with the dextran conjugate but also with the dye free-acid. Viscosity problems with high molecular weight dextrans is well known (Guner, 1995). However, it appears that the dye molecule of the conjugate also influences viscosity and each dye has to be tested for its suitability for microinjection.

Sequestration of dextran conjugates was also promoted by ionophoretic microinjection (Figure 4.1C). Complete sequestration of CG-1 10 kDa dextran conjugate after ionophoretic injection has previously been reported by Knight et al. (1993). The reason for the difference in dye localisation between ionophoresis and pressure injection of the dextran conjugate is not yet understood. One speculation is that ionophoresis might promote electropermeabilisation of organelle (e.g. vacuole) membrane.

Research on pollen tubes (Pierson et al., 1994; 1996; Malhó and Trewavas, 1996) has shown that the tip-based Ca^{2+} gradient detected by ratio methods is not detected with single wavelength dyes. According to Hepler (1997) this is due to the fact that variations in path length at the apex are not compensated for. Indeed, after pressure injecting *N. crassa* hyphae with OG-1 10 kDa dextran, no tip-high gradient was detected (Figures 4.5). However, Ca^{2+} buffering caused by fluorescent dyes is a known effect (Moore et al., 1990), and it cannot be excluded that this reduced the magnitude of the gradient. Therefore, a cell with much reduced loading was imaged but still no gradient in fluorescence was discernible (Figure 4.6). This indicates that Ca^{2+} buffering is not responsible for the lack of a visible gradient when imaging a single wavelength dye loaded into a hyphal tip. It is remarkable that Hyde and Heath (1997) and Levina et al. (1995) both reported the presence of gradients in fluorescence in the Ca^{2+}-sensitive channel before ratioing.

Injection resulted in varying relative amounts of OG-1 and RB entering the cell. It can only be speculated that differences in viscosity influence the relative uptake of the two dyes during filling which is based on capillary forces due to the filament.

At this stage it is clear that the method is viable, however, so far there is not enough data available to draw conclusions about a $[Ca^{2+}]_c$ gradient in *N. crassa*. Further work will be necessary to clarify this question. It will be important to increase the dye loading to improve the $R_{S/N}$. In the near future microinjection on the Leica TCS NT should be easier when the vibration-free table has been installed, and all other technical problems have been sorted out. It was subsequently found that the PMT detecting the RB fluorescence was defective. It can be expected that after mending the PMT, the RB signal should improve in intensity and $R_{S/N}$. The results will have to be compared with those obtained from experiments with Indo-1 and excitation with UV light.

5. Evidence for endocytosis and membrane recycling during tip growth of *Neurospora crassa*

5.1 Introduction

Tip-growing cells like fungal hyphae extend by localised secretion of cell wall precursors and localised cell wall synthesis at the very apex (Gow, 1995). Estimates of plasma membrane insertion at the hyphal tip after vesicle fusion for secretion of cell wall material indicate the necessity for considerable endocytic membrane recycling during extension. (Read, Fischer, López-Franco, Rentel and Bracker, unpublished results). So far, however, evidence for the occurrence of endocytosis in tip-growing filamentous fungi is contradictory (Caesar-Ton That et al., 1987; Cole et al., 1997; 1998; Hoffmann and Mendgen, 1998; Read et al., 1998).

Amphiphilic fluorescent styryl dyes like FM4-64 and FM1-43 (Figure 1.8) have been designed for studying activity-dependent endosomal trafficking in living cells (Haugland, 1996). A recent report by Vida and Emr (1995) demonstrated FM4-64 to be a reliable and specific fluorescent marker of the yeast vacuolar membrane after endocytic uptake of plasma membrane inserted dye. In the study presented here, FM4-64 was applied to *Neurospora crassa* hyphae with the intention of staining the membrane of the complex vacuolar network. However, the dye showed a rather complex staining pattern including staining of the Spitzenkörper which suggested an application in the study of hyphal tip growth (Read et al., 1998; Read, Fischer, López-Franco, Rentel and Bracker, unpublished results).

The first aim of the following study was to test the suitability of confocal microscopy for imaging filamentous fungi stained with FM4-64 in terms of dye cytotoxicity, dye stability and phototoxicity after irradiation.

Previously, the uptake and intracellular distribution of FM4-64 into yeast cells has been shown to be based on an endocytic mechanism (Vida and Emr, 1995). Therefore, the second aim of the work presented was to gather evidence whether or not the dye was taken up into *N. crassa* hyphae by endocytosis by monitoring the kinetics of dye uptake under different conditions. Furthermore, the structurally related molecule FM1-43 which has been used in many studies to investigate neuronal membrane recycling (Haugland, 1996) was to be tested for comparisons.

The third aim was to investigate whether the staining of hyphae with FM4-64 allows the observation of Spitzenkörper dynamics using confocal microscopy. Apart from *N. crassa* two other filamentous fungi (*Trichoderma viride* and *Rhizoctonia solani*) were employed to survey the higher fungi (i.e. *Ascomycetes*, *Deuteromycetes* and *Basidiomycetes*). Additionally, a kinesin deficient *N. crassa* mutant, NK01, which has been reported to lack a discrete Spitzenkörper (Seiler et al., 1997) was stained with FM4-64. Main questions were:

- How does the structure of the Spitzenkörper revealed by positive staining with FM4-64 compare with its structure in unstained hyphae imaged by phase contrast microscopy (Girbardt, 1955; 1957; López-Franco and Bracker, 1996)?
- Can the data gathered from stained hyphae contribute to information about formation and maintenance of the Spitzenkörper and how it integrates into the dynamics of membrane trafficking?

5.2 Results

5.2.1 Imaging living hyphae stained with FM4-64 and FM1-43 by CLSM

The dye concentrations of 20-40 µM FM4-64 used by Vida and Emr (1995) proved to be severely cytotoxic for hyphae of *N. crassa* (data not shown). However, to obtain suitable confocal images a dye concentration between 3.2 and 6.4 µM was found to be sufficient. This is in good agreement with the study on *Uromyces fabae*

where the dye was applied at a concentration of 4 μM (Hoffmann and Mendgen, 1998). A test was performed to assess whether this concentration affected cell health. Fungi were grown on medium supplemented with different concentrations of the dye in the agarose medium on slide cultures in humid chambers (Section 2.9.4). The results (Table 5.1) indicated that at dose concentrations of 3.2 and 6.4 μM growth rates exhibited no significant difference to the control loading dose (Student's t-test). The higher concentration of 12.8 μM only significantly affected the kinesin-deficient mutant NK01. Confocal microscopy of hyphae grown on slides with the dye-supplemented agarose medium up to 36 hours after inoculation revealed that the hyphae were still stained and thus the dye had not been degraded by that time (data not shown).

Table 5.1. Growth rate measurements on open cultures supplied with different concentrations of FM4-64. Means ± s.e.m. sig. dif. = significant difference. N = no significant difference, Y = significant difference at the 5% level. For *N. crassa* 8 replicates for each treatment, for all others 4 replicates for each treatment.

	Neurospora crassa		**NK01**	
concentration (μM)	growth rate (μm/min)	sig. dif. P = 0.05	growth rate (μm/min)	sig. dif. P = 0.05
0 (control)	29.2 ± 1.1	-	5.2 ± 0.3	-
3.2	28.7 ± 1.1	N	5.3 ± 0.1	N
6.4	26.5 ± 3.5	N	4.4 ± 0.3	N
12.8	29.2 ± 0.9	N	4.3 ± 0.1	Y

	***Trichoderma* viride**		***Rhizoctonia* solani**	
concentration (μM)	growth rate (μm/min)	sig. dif. P = 0.05	growth rate (μm/min)	sig. dif. P = 0.05
0 (control)	13.1 ± 0.4	-	12.7 ± 0.1	-
3.2	13.0 ± 0.3	N	13.1 ± 0.4	N
6.4	12.7 ± 0.4	N	13.3 ± 0.3	N
12.8	12.6 ± 0.2	N	13.0 ± 0.3	N

The filter settings for rhodamine imaging have been described as suitable for FM4-64, whereas the filter settings for fluorescein imaging have been described as suitable for FM1-43 (Betz et al.,1996). However, both dyes were excited well by both the 488 nm and the 514 nm line of the Argon ion laser. The 514 nm line was chosen due to the lack of detectable autofluorescence under the imaging conditions used. Neither dye exhibited any detectable fluorescence in solution, but both were found to bind to the surface of the cover glass used for sandwich chambers which increased the background fluorescence detectable in conventional fluorescence imaging. Washing out the dye-loading medium did not remove glass-bound dye, although, it reduced the plasma membrane staining which improved image contrast in the hyphal tip region. The signal from the glass surface usually did not interfere with confocal microscopy.

Frequent scanning (one frame every 10-15 sec) of hyphae loaded with 6.4 μM FM4-64 in sandwich culture was employed to assess the effect of irradiation on hyphal growth (Figure 5.1). After the first 5-10 min of frequent scanning hyphae usually became narrower and in some cases showed distortion in shape. Figure 5.1 A-C show the growth rates of hyphae scanned frequently under standard conditions (x40 plan apo dry objective, 3% laser intensity and scan speed F2 which takes 1 sec for the full frame of 512 lines) and indicate the variability in hyphal growth rate observed under imaging conditions. Reducing the laser power to 1% and compensating for the signal loss by choosing the slower scan speed F1, which takes 3 sec for the full frame, appeared to be more detrimental for cell health (Figure 5.1 D) and was, therefore, not chosen for routine imaging. Use of the x60 plan apo oil objective, with its higher numerical aperture, did not show much difference to the x40 plan apo dry objective (Figure 5.1 E). The growth rate of the kinesin deficient mutant NK01 (Figure 5.1 F) was little influenced by frequent scanning. Although frequent irradiation generally had little influence on the growth rate during the first 5-10 min in all cases, the image quality often suffered and features became slightly blurred after less then 10 frames. This may be due to photobleaching (Betz et al., 1996) and slight cytotoxic effects which are not readily reflected in the growth rate. The problem could be avoided by allowing longer intervals between collecting images. Generally, in order to minimise

detrimental effects which affected image quality, hyphae were scanned for only a maximum of 10 frames with short intervals of a few sec between frames, otherwise the intervals between images were kept at 1-2 min or more.

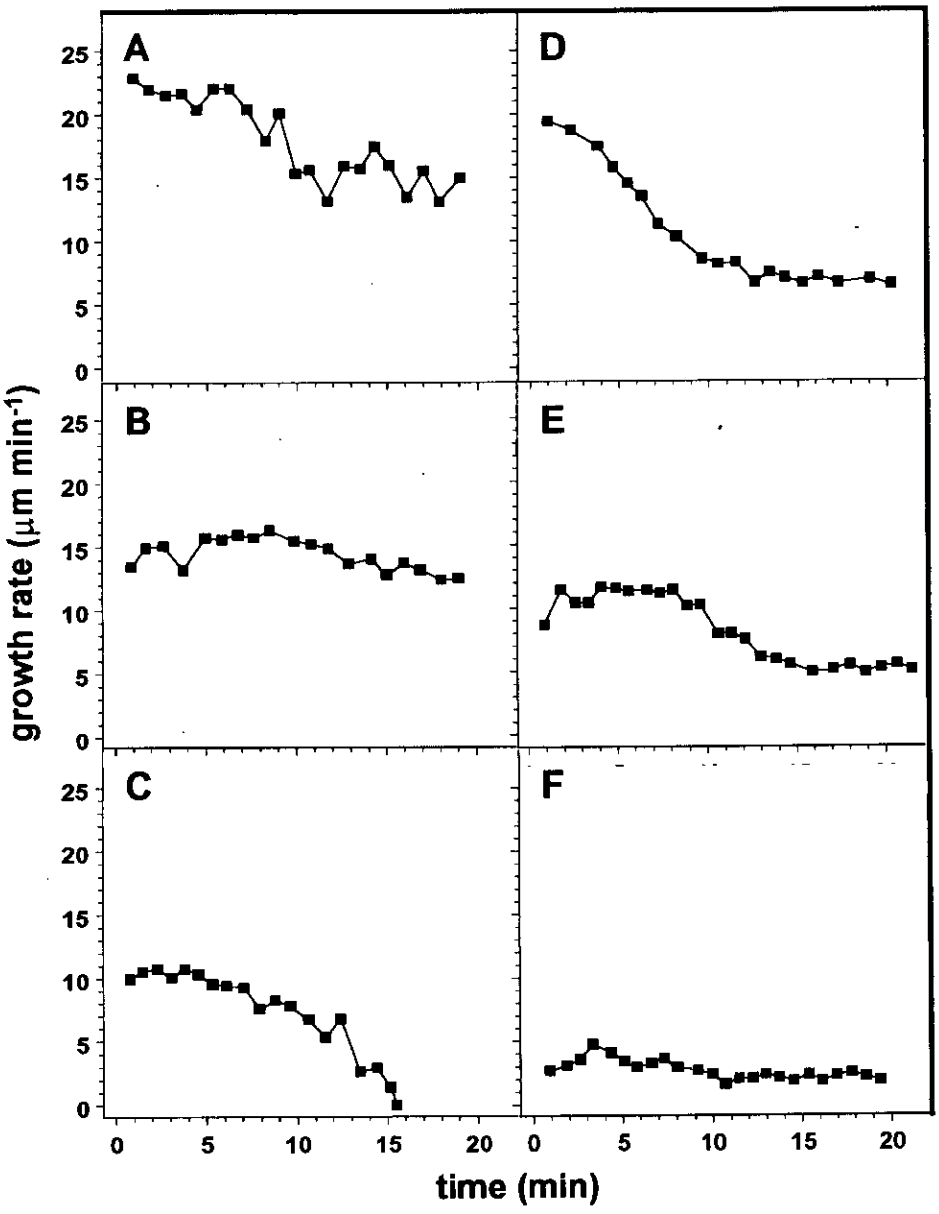

Figure 5.1. Growing hyphae of *N. crassa* loaded with 6.4 μM FM4-64 in sandwich culture. Hyphae were imaged every 10-15 sec. A measurement for growth rate was taken from every 5th image. (**A**, **B** and **C**) Wild type, 3% laser intensity, normal scan speed, x40 plan apo dry objective. (**D**) Wild type, 1% laser intensity, slow scan speed, x40 plan apo dry objective. (**E**) Wild type,3% laser intensity, normal scan speed, x60 oil immersion objective. (**F**) NK01 mutant, 3% laser intensity, normal scan speed, x40 plan apo dry objective.

FM1-43 proved to be much more sensitive to laser irradiation because after 2-3 scans features started to fade considerably and therefore imaging of a cell was confined to a short scanning period for focusing (at fast scan speed: 4 full frames/sec) followed by collection of a single frame (at standard scan speed: 1 full frame/sec).

5.2.2 Evidence for endocytic uptake of FM4-64 in hyphae of *Neurospora crassa*

Monitoring FM4-64 uptake was primarily performed by collecting time courses on the confocal microscope after covering hyphae grown on open cultures with dose loading medium. Sandwich cultures, which allow better optical resolution (no imaging through agarose), were used when the oxygen deprivation inflicted by this system was a desired effect or had no apparent influence on the process studied. Also, in the case of a filamentous fungus like *N. crassa* one has to distinguish between the tip region and compartments further behind because they are structurally different (Section 1.1.1). Therefore, some experiments involved an analysis of both regions. Subapical compartments proved to be more suitable for collecting time courses because, unlike extending tips, they do not grow out of focus or the field of view.

Immediately after its application the dye was found to bind to the cell exterior which became intensely fluorescent (Figure 5.2). To confirm that the dye was binding to the plasma membrane and not the cell wall, hyphae were plasmolysed by adding 1 M sucrose solution (Figure 5.3).

Dye uptake occurred in a time dependent manner as demonstrated by Figure 5.4, a time course for a subapical compartment. Between one and two min after dye application roughly spherical bodies of ca 0.75 μm diameter stained up faintly. These bodies became brighter together with an increasing diffuse background staining, until they were indistinguishable within the intracellular diffuse staining. The big round

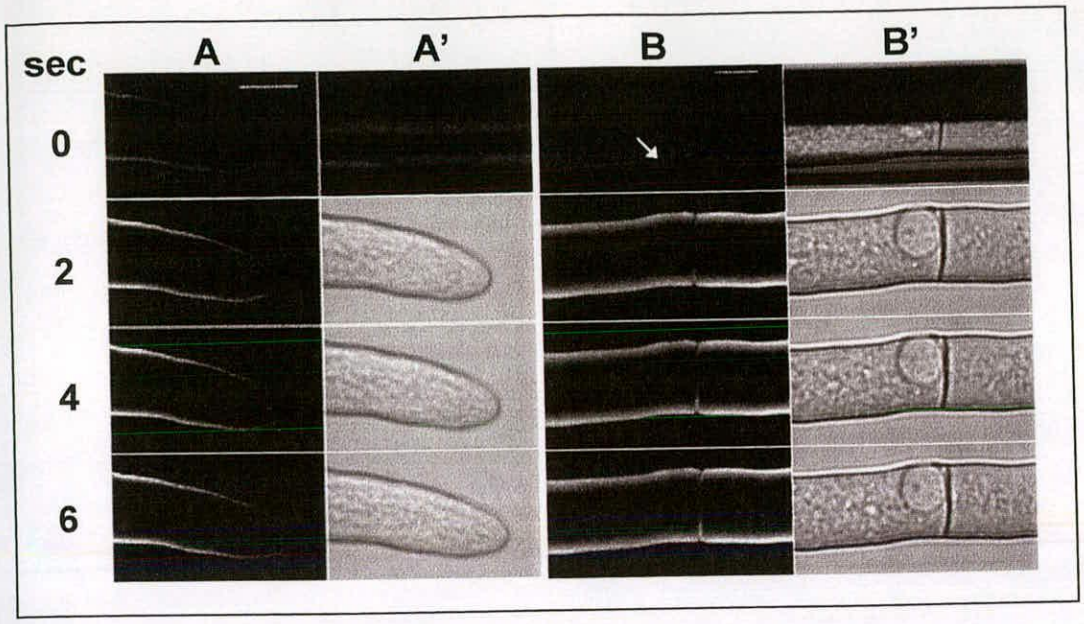

Figure 5.2. Confocal images of *Neurospora crassa* hyphae showing rapid staining of the plasma membrane by FM4-64. (**A** and **B**) Fluorescence images of growing tip and subapical hypha, respectively. (**A'** and **B'**) Corresponding brightfield images; the pipette used to apply dye partly obscures the brightfield images at 0 sec. Numbers indicate sec after dye application. Note that loading is initiated from the side closest to dye application (see arrow in (B) at 0 sec). Bars = 10 μm.

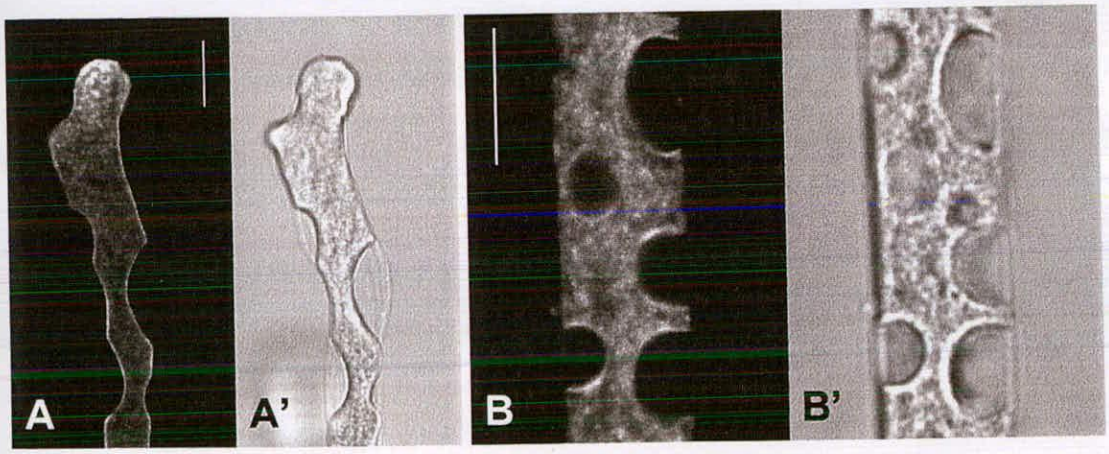

Figure 5.3. *Neurospora crassa* hyphae after plasmolysis showing that the plasma membrane but not the cell wall stains with FM4-64. (**A** and **B**) Confocal fluorescence images of an apical and a subapical cell compartment, respectively. (**A'** and **B'**) Corresponding brightfield images. Hyphae were loaded with FM4-64 before plasmolysis with 1 M sucrose solution. Bars = 10 μm.

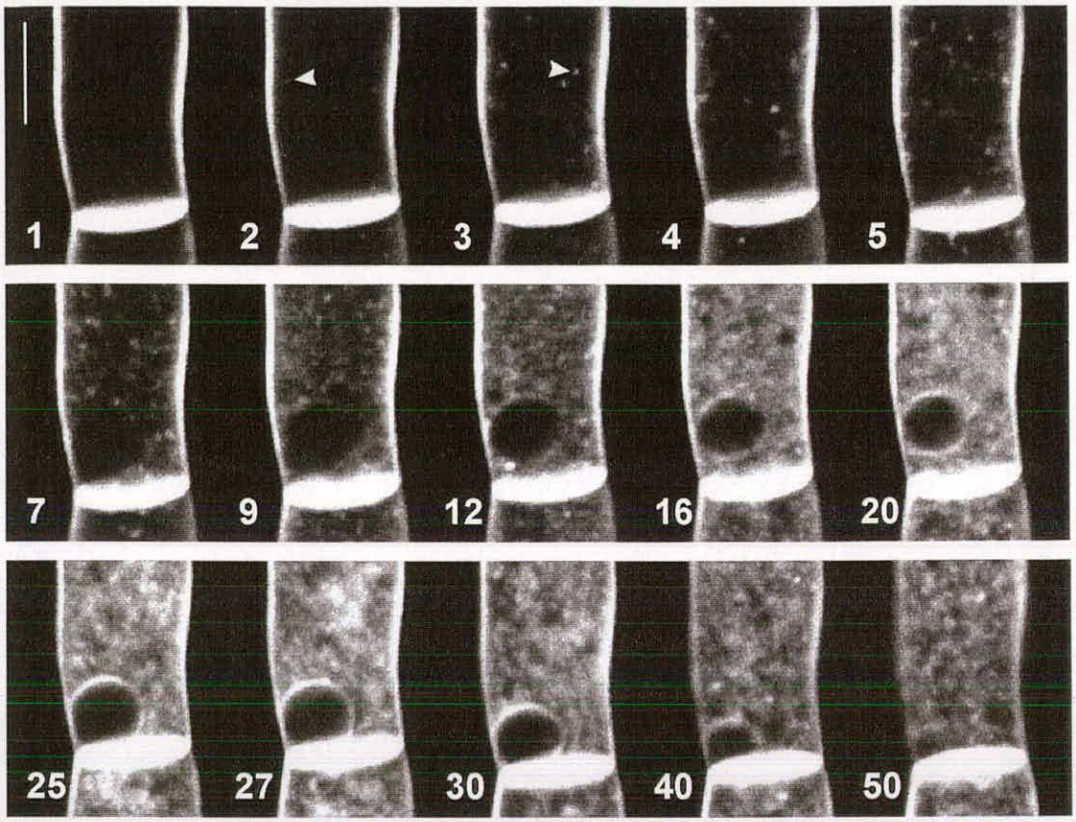

Figure 5.4. Confocal images of a *Neurospora crassa* subapical compartment. Time course showing uptake of FM4-64 in open culture under continuous loading. Numbers indicate min after dye application. Putative endosomes (arrows) are clearly visible after 2 min. Bar = 10 μm.

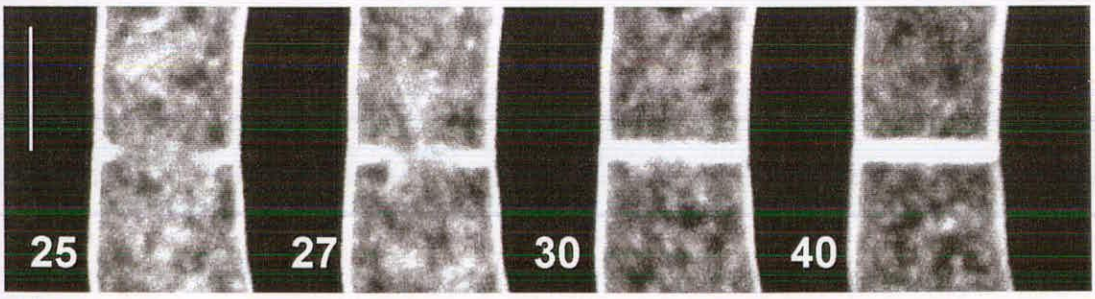

Figure 5.5. *Neurospora crassa* subapical compartment loaded with FM4-64 in open culture with no washout of loading buffer. The hypha was imaged by confocal microscopy during septum formation. Numbers indicate min after application of dye. Bar = 10 μm.

vacuole lying adjacent to the septum (Section 1.1.1) was originally visible as a zone of dye exclusion until at about 9 min the vacuolar membrane faintly stained up and was strongly stained at about 20 min. At that time the cell interior showed an irregular staining pattern which did not considerably change during the next half hour. The cell membrane hardly decreased its signal during the experiment which was most likely due to an abundance of dye in the extracellular medium. Strong staining of septa in this sample (Figure 5.4) is obvious and septum formation could be observed (Figure 5.5) due to pronounced staining of the septal region right from the start of septum formation.

Time course analysis was also performed to investigate temperature dependence of dye loading (Figure 5.6). Hyphae grown in open culture were cooled down to 5°C for 10 min and subsequently loaded at 5°C for 10 min. The loading buffer was washed out with cold medium and hyphae monitored immediately on the confocal microscope at room temperature. Kinetics of dye loading were drastically reduced, strongly suggesting that the dye is not internalised by diffusion. During imaging the sample warmed up which allowed dye uptake to proceed. Notable is the continuous reduction in staining of the plasma membrane during the recording period concomitant with increased staining of the cell interior. Thus, this pulse-chase experiment allowed internalisation of dye from the plasma membrane to be visualised.

Oxygen availability also influenced loading (Figure 5.7). With subapical cells loaded in sandwich culture, where free access of oxygen is limited, dye uptake was arrested at the stage of the small spherical bodies.

The tip region was much less affected by the oxygen deprivation in sandwich culture and loading did not stop at an intermediate stage of small spherical bodies (Figure 5.8). A reason could be that the tips which are growing at the margin of the colony are advancing into "fresh" medium. Staining of the Spitzenkörper in apical cells was evident after 1-2 min (Figures 5.8A and B). Spherical bodies also appeared in the

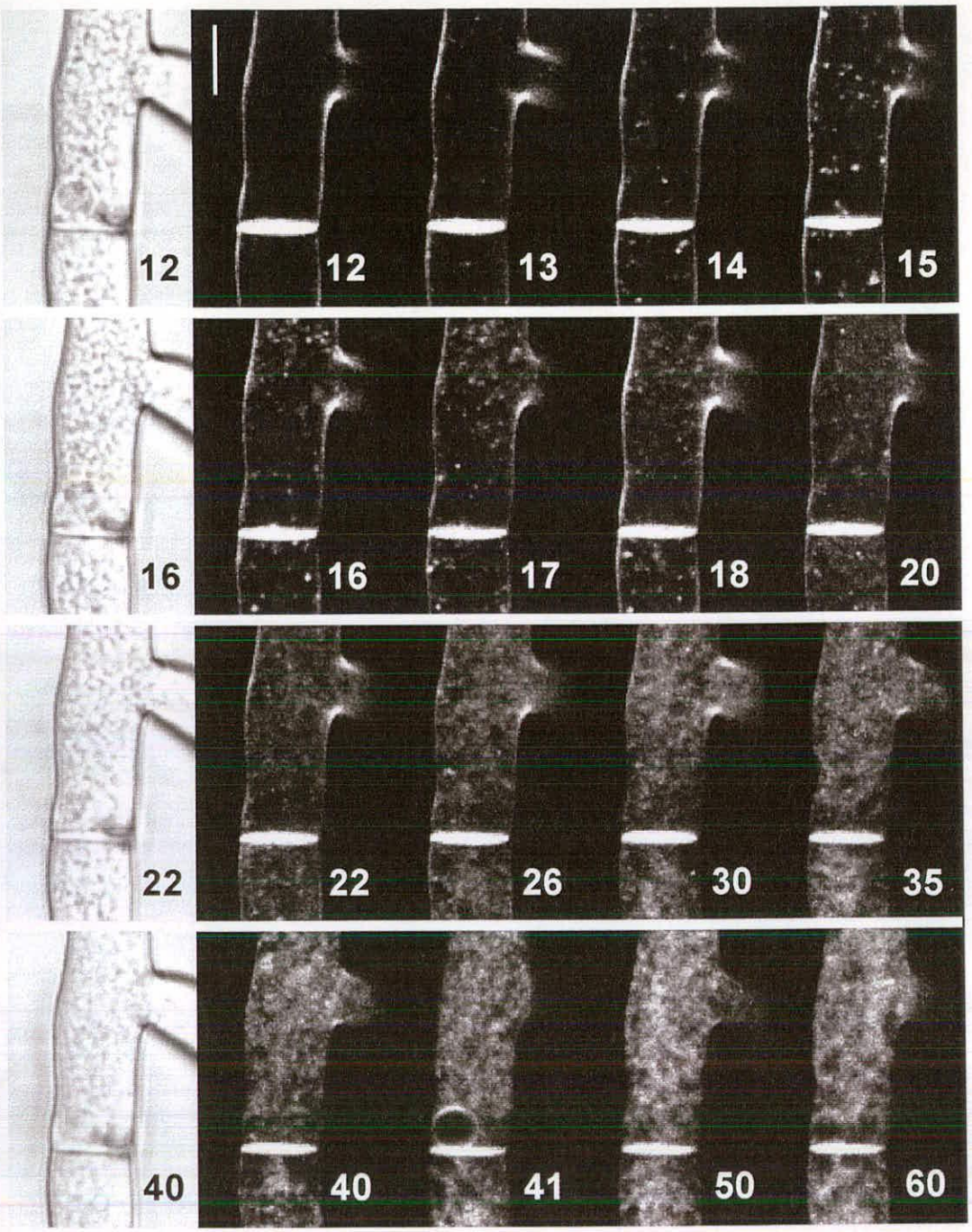

Figure 5.6. Confocal images of *N. crassa* subapical hyphal compartments in open culture after 10 min loading at 5°C with FM4-64 and then washing with dye free medium. Subsequently dye uptake was monitored at room temperature. Outer left row bright field images, all others fluorescent images. Numbers indicate min after dye application. The focal plane was chosen for maximum cell membrane signal except at 41 min where the focus was adjusted to show the vacuolar membrane. Bar = 10 μm.

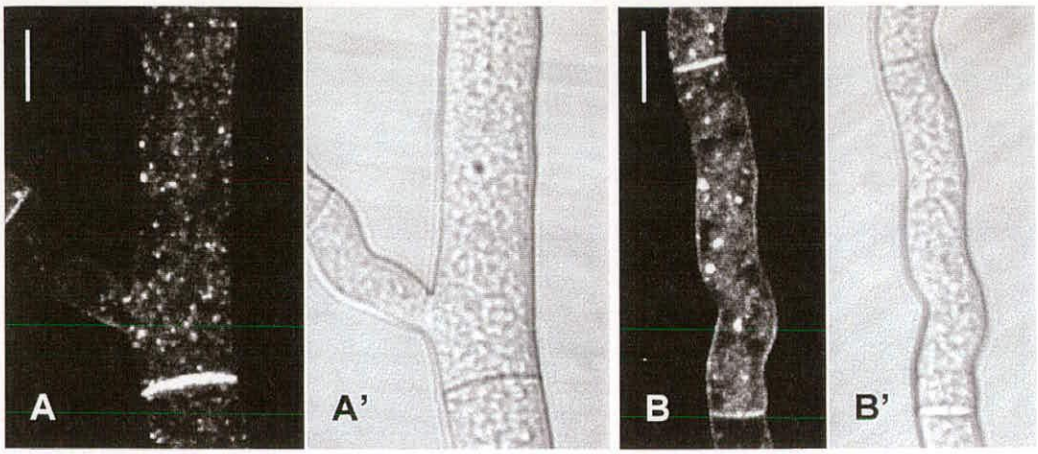

Figure 5.7. Subapical hyphal compartments of *N. crassa* loaded with FM4-64 in an oxygen-deprived sandwich culture for 60 min. (**A** and **B**) Confocal fluorescence images; (**A'** and **B'**) Corresponding brightfield images. Bars = 10 μm.

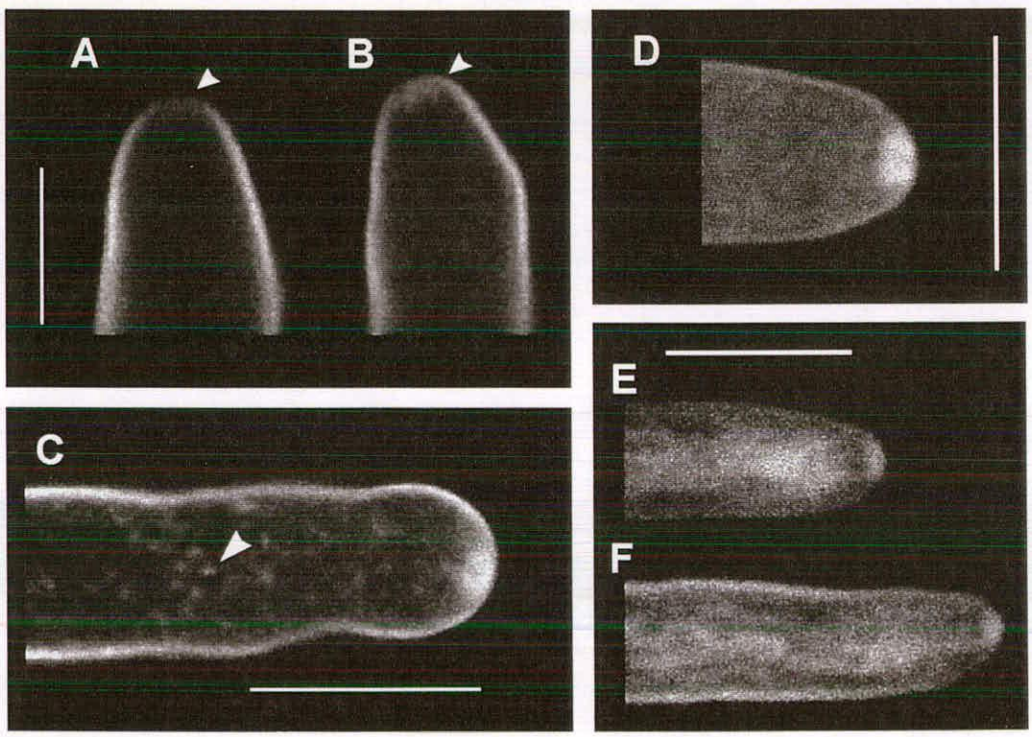

Figure 5.8. Confocal images of growing *N. crassa* hyphae stained with FM4-64 in sandwich culture. (**A** and **B**) Loading of the Spitzenkörper (arrows) 1.5 min and 2 min after dye application, respectively. (**C**) Hypha 8 min after adding FM4-64. The arrow points to fluorescent spherical bodies. (**D**) Growing hypha 10 min after washing out the dye which had been loaded for 10 min (growth rate 16 μm min^{-1}). Note the pronounced staining of the Spitzenkörper. (**E** and **F**) Hypha 60 min and 60 min 30 sec after FM 4-64 wash out, respectively (growth rate 15.8 μm min^{-1}). Note the staining of elongated structures resembling mitochondria. Bars = 10 μm.

apical cell compartment around this time, but they were less pronounced than in subapical compartments. Intensity of the spherical bodies increased (Figure 5.8C) before they disappeared in a more general intracellular staining (Figure 5.8D). Spitzenkörper staining increased to a maximum intensity after about 15-20 min (Figure 5.8D). With longer staining (about 60 min) elongated structures, possibly corresponding to mitochondria, appeared (Figures 5.8E and F; compare with Figure 5.10).

5.2.3 Staining of *Neurospora crassa* hyphae with FM1-43

The structurally related dye FM1-43 was applied to *N. crassa* hyphae which were subsequently imaged on the confocal microscope. Hyphae loaded in open culture (Figure 5.9A and B) exhibited dye uptake which led to staining of the cell interior and the vacuolar membrane similar to FM4-64 although, membrane staining appeared to be more pronounced. Under oxygen deprivation in sandwich culture staining was arrested at the stage of the small spherical bodies (Figure 5.9C) similar to that shown previously with FM4-64. However, FM1-43 did not stain septa as intensely as did FM4-64 in either open or in sandwich cultures. Examination of FM1-43 staining in the tip region (Figure 5.10A) revealed that the dye accumulated in the Spitzenkörper and later into the mitochondria, especially the latter became very distinctly stained as verified by comparison with hyphal tips stained with DASPMI (Figure 5.10B). FM1-43 proved less suitable than FM4-64 for observations on the Spitzenkörper because of a rapid loss of dye signal during scanning (section 5.2.1).

5.2.4 Monitoring of Spitzenkörper morphology and behaviour

5.2.4.1 The Spitzenkörper in *Neurospora crassa*

The Spitzenkörper in living, growing hyphae of higher fungi can be readily observed by phase contrast microscopy where it appears as a dark structure against a lighter background of apical cytoplasm (Girbardt, 1955; 1957; López-Franco and Bracker; 1996). Video-enhanced phase contrast microscopy revealed that the Spitzenkörper of

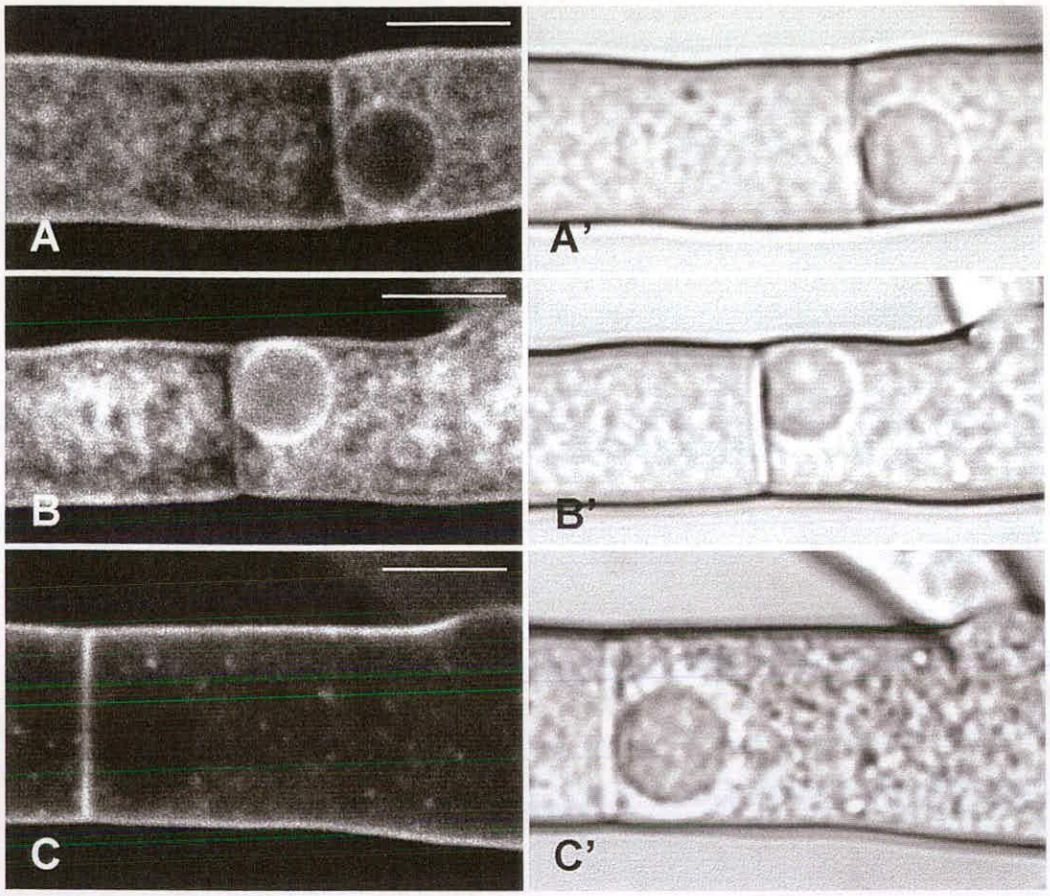

Figure 5.9. *N. crassa* subapical compartments loaded with FM1-43. (**A** and **B**) Confocal fluorescence images in open culture after loading for 30 and 60 min, respectively. The loading buffer was not washed out. (**A'** and **B'**) Corresponding bright field images. (**C**) Confocal fluorescence image after loading for 30 min in sandwich culture. (**C'**) Corresponding bright field image. Bars = 10 μm

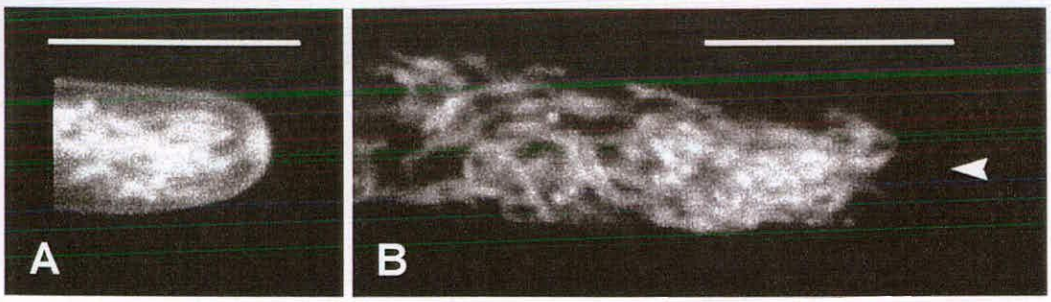

Figure 5.10. Confocal images of *N. crassa* hyphal tips in sandwich culture. (**A**) The hypha was loaded with FM1-43 for 10 min, then the medium was washed out and the hypha imaged 40 min later (growth rate 9.6 μm min^{-1}). (**B**) The hypha was loaded with DASPMI for mitochondria staining (growth rate 12 μm min^{-1}). The arrow head indicates the position of the apical pole. Bars = 10 μm.

N. crassa is highly variable in shape and size with a small phase light core sometimes visible (López-Franco and Bracker, 1996). Interestingly, the Spitzenkörper visualised by positive staining with FM4-64 and confocal imaging (Figures 5.8 and 5.11) resembled closely the structure seen with video-enhanced phase contrast microscopy. It showed the above mentioned variability in shape and size ranging from a more or less irregular spheroid cluster occasionally to a U-form shape or a flattened band. A zone of reduced fluorescent signal within the Spitzenkörper corresponded most likely to the core region (Figure 5.11 at 0 sec).

The intimate association of the Spitzenkörper with hyphal tip growth could be observed during subapical branch initiation (Figure 5.12). The mycelium was grown for 8 h in open culture with the agarose medium supplemented with FM4-64. Under these conditions Spitzenkörper staining was still obvious. The first structure indicating formation of a new tip was a diffuse fluorescent area which was brighter than the rest of the cell and located behind a very slight bulge on the lateral cell wall (Figure 5.12 at 0 sec). This rudimentary Spitzenkörper suggested the accumulation of a vesicle cluster preceding branch formation. It developed into a more defined band connected with a visible outgrowth of the lateral cell wall (Figure 5.12 at 30 sec) before it enlarged into a spheroid structure at the tip of the growing branch (Figure 5.12 at 90 sec to 180 sec).

The Spitzenkörper is a very sensitive structure and shows a tendency to disperse and disappear after environmental changes concomitant with cessation of apical growth (Girbardt, 1957; López-Franco and Bracker, 1996). Girbardt (1957) applied a temporary illumination shock to growing hyphae of *Polystictus versicolor* and followed Spitzenkörper behaviour using phase contrast microscopy. Shortly after 3 sec exposure to light from a 500 W Hg lamp growth stopped and subsequently the Spitzenkörper was found to retract and finally to disperse. A similar experiment was performed with *N. crassa* hyphae in sandwich culture stained with FM4-64 by applying light above 300 nm wavelength from the 100 W Hg lamp used for fluorescence microscopy for 10-15 sec. Confocal images were taken approximately

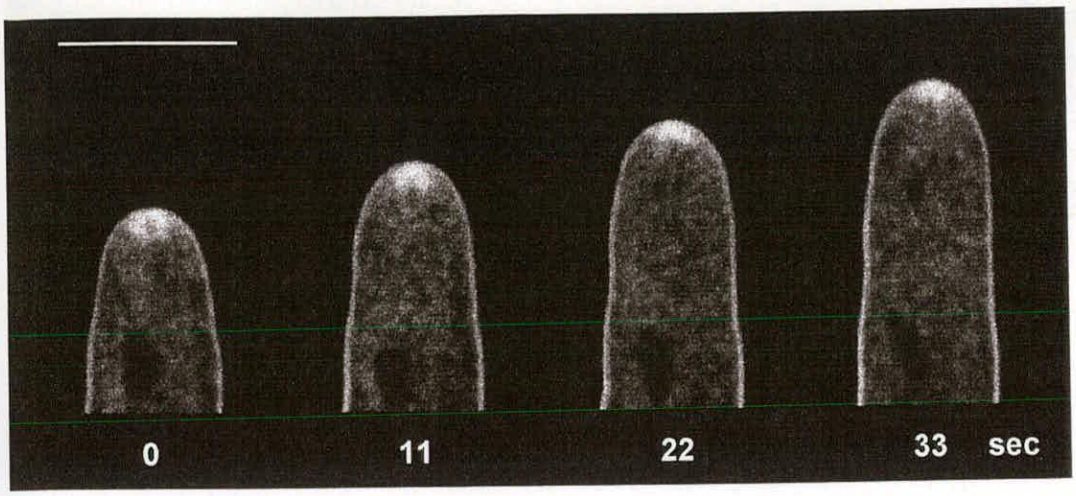

Figure 5.11. Confocal images of a *N. crassa* hypha (growth rate 12 μm min^{-1}) loaded with FM 4-64 for 25 min in sandwich culture. Images were taken at 11 sec intervals. Note the predominant staining of the Spitzenkörper which shows a less stained region corresponding to the core in the image at 0 sec. Bar = 10 μm.

Figure 5.12. Confocal images showing different stages of subapical branch formation in a *N. crassa* hypha. The mycelium was grown for 8 h in open culture in a humid chamber with the agarose medium containing FM4-64. The Spitzenkörper at the apex of the hypha at 0 and 30 sec is not visible because it is out of focus (growth rate 9.8 μm min^{-1}). The focal plane is centred on the Spitzenkörper in the branch (growth rate 8.8 μm min^{-1}). Bar = 10 μm.

10-15 sec before and after light exposure. Within 10 sec after irradiation the Spitzenkörper began to withdraw until it reached a position ca. 6 μm behind the apical pole about 50 sec later (Figure 5.13). Over the next 1-2 min it gradually disappeared. The experiment was repeated five times. In all cases hyphae reacted with cessation of growth, which was followed by gradual withdrawal of the Spitzenkörper over 1-3 min after exposure until it reached a position about 3-6 μm behind the apical pole. This was followed by a gradual dissipation within the next 3-5 min. In one case the Spitzenkörper withdrew, disappeared and reassembled which led to restart of growth 3 min after light treatment.

To image the Spitzenkörper preferentially a median section through this organelle is required. However, this section does not always correspond to the median section through the hypha, because the Spitzenkörper in *N. crassa* is highly variable and mobile (López-Franco and Bracker, 1996). The plasma membrane staining, however, is best visible in a median or near median section through a hypha. If the Spitzenkörper is located in an eccentric position it may occupy a focal plane more or less outside the median section through the cell. This is demonstrated by a series of optical sections through a growing hypha (Figure 5.14) which is located near the coverslip surface with the apex bent towards the coverslip. The Spitzenkörper is asymmetrically located within the apical dome and is closest to the coverslip surface. The prominence of the plasma membrane staining varies between and within individual optical sections because of changes in the orientation of the hyphal tip as it grows. Therefore the fluorescent signal from the plasma membrane needs to be interpreted with caution if not sectioned through the median of the cell.

5.2.4.2 The Spitzenkörper in *Trichoderma viride* and *Rhizoctonia solani*

Spitzenkörper staining with FM4-64 in other filamentous fungi was performed using the sandwich system and images were collected with the x60 oil objective (Figure 5.15). The Spitzenkörper in *Trichoderma viride* (Figure 5.15A) and *Rhizoctonia solani* (Figure 5.15B) proved to be distinctive and different from that in *N. crassa*. In *T. viride* it appeared as a positively stained spheroid structure often with a less

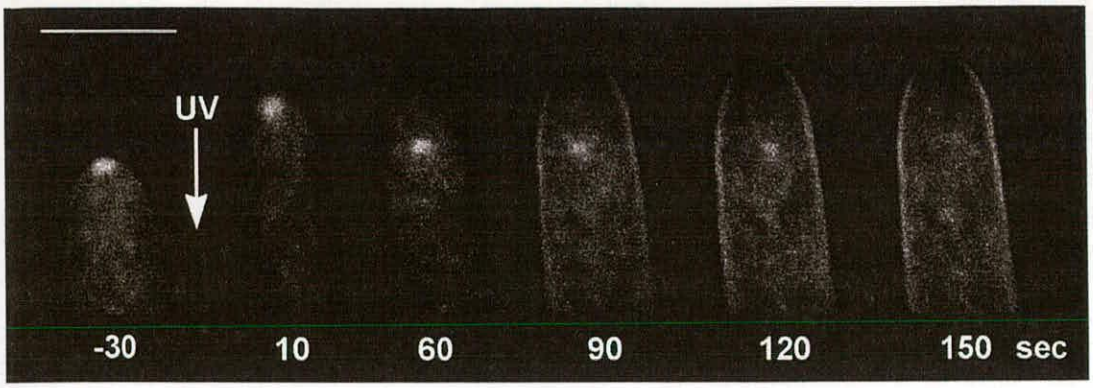

Figure 5.13. Confocal images of a *N. crassa* hyphal tip before and after exposure to light stress. The hypha was irradiated with light above 300 nm wavelength from a 100 W mercury lamp for 15 sec at the point marked by the arrow. The times indicated are the periods which have elapsed after applying the light treatment. The illumination leads to cessation of hyphal growth within 10 sec after exposure and subsequently to withdrawal of the Spitzenkörper from the apical pole within the next 50 sec. After 150 sec the Spitzenkörper has dissipated. Scale bar = 10 μm.

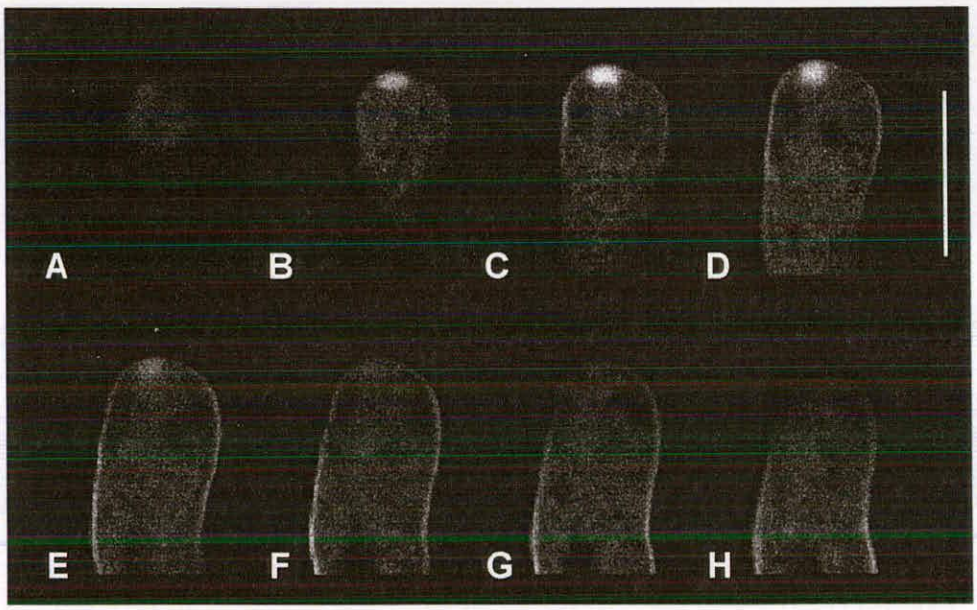

Figure 5.14. Series of successive confocal optical sections at increments of 1 μm through a growing hyphal tip of *N. crassa* (growth rate 9.6 μm min^{-1}). Note that, depending on the optical plane, the prominence of plasma membrane staining varies. (**A**) is the section closest to the coverslip surface. The tip is bent down towards the coverslip and the Spitzenkörper is asymmetrically located within the hyphal tip and closer towards the coverslip surface. The images were captured at 2 sec intervals. Bar = 10 μm.

stained region towards the apical pole, and in *R. solani* as a bright horseshoe surrounding a less fluorescent area. The shapes corresponded to the patterns described in López-Franco and Bracker (1996). According to this source the *T. viride* Spitzenkörper possessed a mostly spheroid phase dark vesicle cloud with an eccentric phase light core towards the apical pole, whereas *R. solani* exhibited a Spitzenkörper consisting of a cup-shaped phase dark vesicle cloud with a large phase light core. The correlation supports the conclusion that FM4-64 primarily stains the vesicle cluster of the Spitzenkörper but not the core in these fungi.

5.2.4.3 Satellite Spitzenkörper in *Trichoderma viride*

Satellite Spitzenkörper of *T. viride* which are known from electron microscopy to consist of small clusters of vesicles (López-Franco et al., 1995) showed positive staining with FM4-64 (Figure 5.16). This is another indication that FM4-64 stains the vesicle population in the Spitzenkörper. Images of *T. viride* had to be collected within 20 min after applying the dye because otherwise the Spitzenkörper and the satellites became difficult to discern because of increased intracellular fluorescence. This was independent of washing out the loading buffer. *T. viride* was more sensitive to the conditions of the sandwich chamber which caused narrowing in the tip region and slow recovery of tip growth. Open cultures provided better conditions for hyphal growth and detection of satellites. Satellite Spitzenkörper appeared as faint fluorescent plaques adjacent to the plasma membrane several micrometers behind the main Spitzenkörper, migrated towards and then merged with it. The whole event took less then 10 sec. Satellite Spitzenkörper in the other investigated species were not obvious and were not followed up further due to technical limitations. A laser scanning confocal microscope is a rather slow imaging instrument and is, therefore, not suitable to do routine investigations of satellite behaviour because they migrate too fast for the temporal resolution of such a device. First, the number of frames which can be obtained in a given time is limited. Second, the hyphae have a tendency to grow out of focus, which makes it difficult to do an automatic time course because frequent refocusing is usually necessary. Third, the imaging time, especially with short intervals, is restricted due to phototoxic and/or bleaching effects as explained

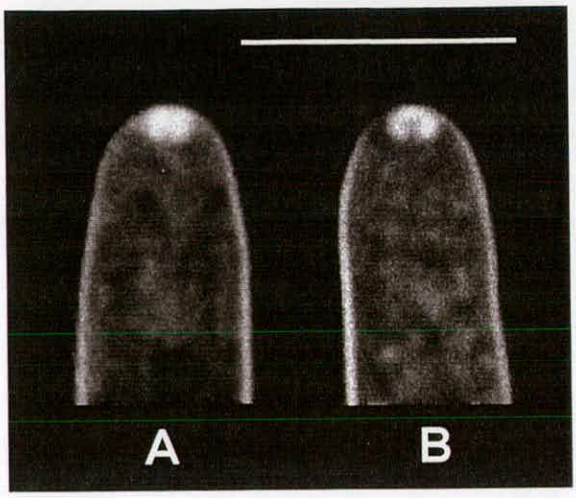

Figure 5.15. Confocal images of hyphae stained with FM4-64 in sandwich culture. (**A**) Growing hypha of *Trichoderma viride* (growth rate 6.2 μm min^{-1}). The dye was washed out 10 min after application and the hypha imaged another 10 min later. Note the slightly less stained region in the Spitzenkörper corresponding to the core. (**B**) Growing hypha of *Rhizoctonia solani* (growth rate 4.5 μm min^{-1}). The hyphae was imaged 35 min after dye removal which had followed a 10 min loading period. Note the horse shoe like shape of the Spitzenkörper. Bar = 10 μm.

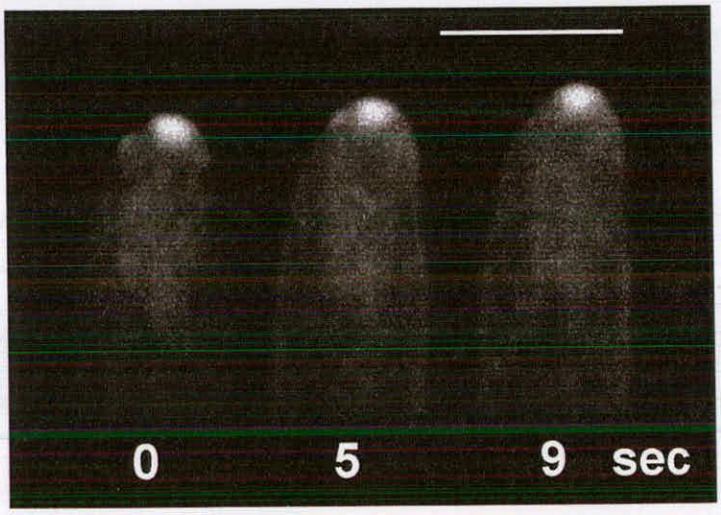

Figure 5.16. Confocal images of a growing hyphal tip of *Trichoderma viride* in open culture (growth rate 7.7 μm min^{-1}). After loading with FM4-64 for 10 min and washing with dye free medium, the image was taken 10 min later. Note the satellite Spitzenkörper migrating from a subapical position to the main Spitzenkörper and merging with the latter. Bar = 10 μm.

previously (section 5.2.1). This limits the screening for satellites and makes it difficult to capture a whole sequence of satellite development.

5.2.4.3 The Spitzenkörper in the kinesin-deficient mutant NK01

The kinesin-deficient mutant NK01 has previously been reported to lack a Spitzenkörper (Seiler et al., 1997). However, after staining with FM4-64 and confocal imaging Spitzenkörper were clearly visible in growing hyphae (Figure 5.17A). Interestingly, they were smaller and more labile than wild type Spitzenkörper and changed location, shape and size frequently. Mutant hyphae showed a considerably slower growth rate (2.8 ± 0.5 μm min^{-1} s.e.m. n=6) than wild type hyphae (16.7 ± 1.1 s.e.m. n=11) when loaded and imaged in sandwich culture. NK01 hyphae exhibited an irregular growth pattern, producing numerous lateral bulges, bends, and aborted branches (Figure 5.17B). Although mutant hyphae were much more sensitive to physical disturbances than wild type hyphae and needed about 30 min after sample preparation to resume growth (the wild type took between 2 and 5 min), growing hyphae of the mutant did not appear to be significantly more sensitive to laser irradiation than the wild type.

5.3 Discussion

5.3.1 Use of the styryl dyes FM4-64 and FM1-43

Styryl dyes, notably FM1-43, have been used widely for investigating endocytosis and exocytosis in animal cells, particularly in relation to the trafficking of recycled synaptic vesicles (Betz et al., 1996). In the yeast *Saccharomyces cerevisiae* FM4-64 was used as a tool for studying vacuolar organelle morphology and dynamics and the endocytic pathway (Vida and Emr, 1995; Rieder et al., 1996). Also, FM4-64 was included in an assay for identifying yeast endocytosis mutants by screening for internalisation defects (Wendland et al., 1996). Vida and Emr (1995) demonstrated that FM4-64 can be used as a fluorescent marker for bulk internalisation of plasma membrane into yeast. Dye uptake was temperature, energy and time dependent. The plasma

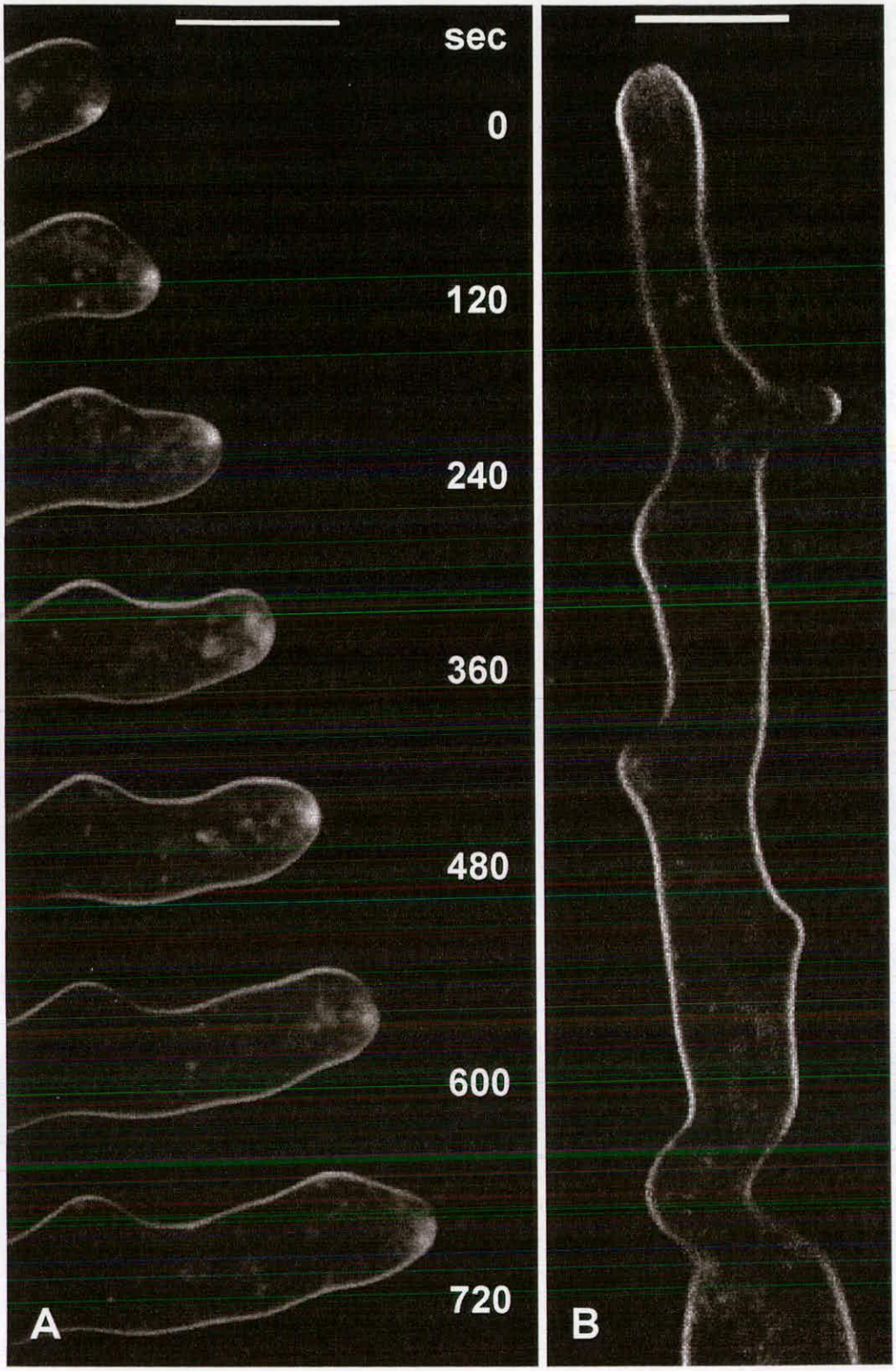

Figure 5.17. Confocal images of a *Neurospora crassa* NK01 hyphal tip (growth rate 1.7 μm min^{-1}). (**A**) The hypha was stained for 10 min with FM4-64 followed by washing the dye from the external medium and imaging 30 min later. Note that the Spitzenkörper is smaller and more labile than that of the wild type. (**B**) Same hypha as that shown in (A) but recorded 20 min after the image at 720 sec. Bars = 10 μm.

membrane was the first structure to stain up, then small punctate fluorescent objects (presumed to be endosomes) appeared. Subsequently plasma membrane and punctate staining of the cytoplasm decreased with a concomitant staining of the vacuolar membrane.

Recently, application of these stains to filamentous fungi has been explored. Vesicle trafficking in germ tubes of the rust fungus *Uromyces fabae* was visualised by staining with FM4-64 (Hoffmann and Mendgen, 1998). After binding to the plasma membrane dye was taken up in a time dependent manner. No uptake occurred at 4°C or in presence of NaN_3. Within 5 min, dye was internalised in the area 5-20 µm behind the apical pole and subsequently accumulated in what were interpreted as endosomal compartments. The authors found the first evidence of fluorescence in the apex only about 10 min after dye application and after 15 min the apical vesicle cloud was visibly stained. This apical vesicle cloud is interpreted as being equivalent to the Spitzenkörper (López-Franco and Bracker, 1996)

In contrast Cole et al. (1998) observed little or no uptake of FM4-64 into hyphae of *Pisolithus tinctorious*. Based on this result and earlier findings (Cole et al., 1997) which demonstrated the lack of internalisation of fluid phase endocytosis markers the occurrence of endocytosis in filamentous fungi was doubted by Cole et al. (1998). Although the authors pointed out that good labelling of both, plasma and vacuolar membrane, in *P. tinctorious* could only be achieved in dead or damaged hyphae, they did not consider that the low or non-existent dye uptake into healthy hyphae might be caused in the first place by poor dye-binding to the plasma membrane rather than the absence of endocytosis. The kinetics of dye binding to membranes are poorly understood (Betz et al., 1996) and it cannot be excluded that dye-plasma membrane interactions vary between species.

Dye uptake into hyphae of *Neurospora crassa* and *Trichoderma viride* leading to staining of the Spitzenkörper and satellite Spitzenkörper was reported by Read et al. (1998). In the study presented here these preliminary findings have been extended to

investigate whether FM4-64 is taken up by endocytosis and whether imaging of FM4-64 stained hyphae can be used to image Spitzenkörper behaviour and vesicle trafficking in the filamentous fungus *N. crassa*.

5.3.2 Dye uptake and staining pattern in *Neurospora crassa* hyphae

For *N. crassa* it was investigated whether FM4-64 uptake followed a similar pattern as in yeast (Vida and Emr, 1995). Dye loading was shown to be dependent on temperature, time and oxygen availability (Section 5.2.2). These characteristics exclude the possibility that dye internalisation occurs by diffusion. The fact that dye molecules possess two positive charges under physiological conditions (Figure 1.8) should make the styryl dyes relatively membrane impermeant (Betz et al., 1996).

The plasma membrane of *N. crassa* hyphae exhibited intense staining after addition of FM4-64 (Figure 5.2) indicating dye partitioning into the membrane. Subsequent dye uptake was evident through staining of roughly spherical structures with a diameter of <75 μm which corresponded most likely to endosomes as endocytic intermediates similar to the structures described in yeast by Vida and Emr (1995). Based on the endocytic pathway occurring in animal cells (Figure 1.6) and evidence presented by Caesar-Ton That (1987) who found clathrin-like coated vesicles in *N. crassa*, it seems reasonable to assume that membrane transport between the plasma membrane and endocytic intermediates in *N. crassa* occurs by vesicle transport. Endocytic vesicles probably pinch off from the plasma membrane and subsequently fuse with endosomes. However, due to the small size of endocytic vesicles (< 0.2 μm) one would not expect to visualise them by confocal microscopy unless they were extremely well loaded with dye and far enough separated from each other to fall within the resolution of the imaging set up used (Section 2.7.1). This is very unlikely. For a cell it has to be taken into account that the resolution is also affected by aberrations induced by imaging through cytoplasm (White et al., 1996). The loss in resolution is even greater when cells are not completely adjacent to the coverslip or imaged through agarose in open culture (Hell et al., 1993).

Subsequent to the staining of the putative endosomes in *N. crassa* the vacuolar membrane of large spherical vacuoles exhibited fluorescence, which was again similar to the situation in yeast (Vida and Emr, 1995). However, in contrast to the situation in yeast cells the intracellular staining pattern was much more diffuse and apparently more complex. It has to be considered that the vacuolar system in *N. crassa* (Section 1.1.1) consists of an extensive tubular and reticulate network which creates an abundance of intracellular vacuolar membrane functioning as target for FM4-64 staining. Also, mitochondria were stained in *N. crassa* after prolonged incubation in dose (Figures 5.8E and F) which should also contribute to the intracellular fluorescence. Mitochondria labelling appeared later than endosomal or vacuolar staining, indicating that the dye went through a longer pathway before it reached the mitochondria. A continuity between the ER and the outer membrane of mitochondria has been shown in several organisms including fungi (Bracker and Grove, 1971; Franke and Kartenbeck, 1971). Due to the physical connection between the secretory and the endocytic pathway and the occurrence of retrograde vesicle transport (Section 1.4.1.2), membrane stained with FM4-64 could reach the ER. This implies that prolonged incubation after adding dye should also lead to ER staining, and therefore it is quite likely that, given enough time, the whole endomembrane system should exhibit staining in *N. crassa*. In yeast the dye has been reported not to stain mitochondria (Vida and Emr, 1995). The authors performed double staining experiments using the mitochondrion sensitive dye DASPMI in combination with FM4-64 and demonstrated that the fluorescent spherical bodies visible 10 min after chasing with fresh medium were not mitochondria but presumably endocytic intermediates. It is clear from the data presented by Vida and Emr (1995) that after 10 min the dye uptake in yeast had only reached the endosomes and not the vacuolar membrane. Therefore, the conclusion by these authors that FM4-64 does not stain yeast mitochondria has to be adjusted to FM4-64 does not stain mitochondria at that early stage of loading. However, the data does not necessarily rule out mitochondria staining at a longer time after dye application which was not investigated.

The data presented here suggests that dye internalisation in *N. crassa* hyphae is most likely via an endocytic pathway. Evidence for the endocytic internalisation in both apical and subapical compartments indicates the occurrence of a general turnover of plasma membrane within hyphae, This membrane turnover is thus not just restricted to the growing region of the hypha where presumably membrane recycling is necessary (Read, Fischer, López-Franco, Rentel and Bracker, unpublished results).

5.3.3 Spitzenkörper staining

Comparison of published data obtained using phase contrast microscopy (López-Franco and Bracker, 1996) with confocal images of FM4-64 stained hyphae (Section 5.2.4) showed that the latter approach can be used for investigating the dynamic structure and function of the Spitzenkörper during tip growth. However, confocal microscopy has a much lower temporal resolution than video microscopy which will limit the application. Nonetheless, it can complement the data obtained by phase microscopy.

The results presented indicate that FM4-64 stains vesicles present within the Spitzenkörper which could help to localise where the vesicles are derived from. Given enough time endocytic internalisation of dye labelled membrane should lead to staining of the endomembrane system (Section 1.3.1). Therefore, Golgi derived vesicles destined for exocytosis at the apex would exhibit fluorescence and cause staining of the Spitzenkörper. However, this does not satisfactorily explain how the Spitzenkörper is stained within 1-2 min of dye application, shortly after the first indication of endosome staining, but well before labelling of other structures. Therefore, it is suggested that one pathway of the vesicle trafficking network may involve rapid recycling of membrane back to the Spitzenkörper (Figure 5.18). This idea is supported by findings indicating that yeast cells recycle chitin synthase I (CSI) and chitin synthase III (CSIII) which are not degraded but remain metabolically stable (Ziman et al., 1996; 1998). In yeast CSI and CSIII exist in the plasma membrane and in intracellular endocytic compartments called chitosomes which may serve as a cell

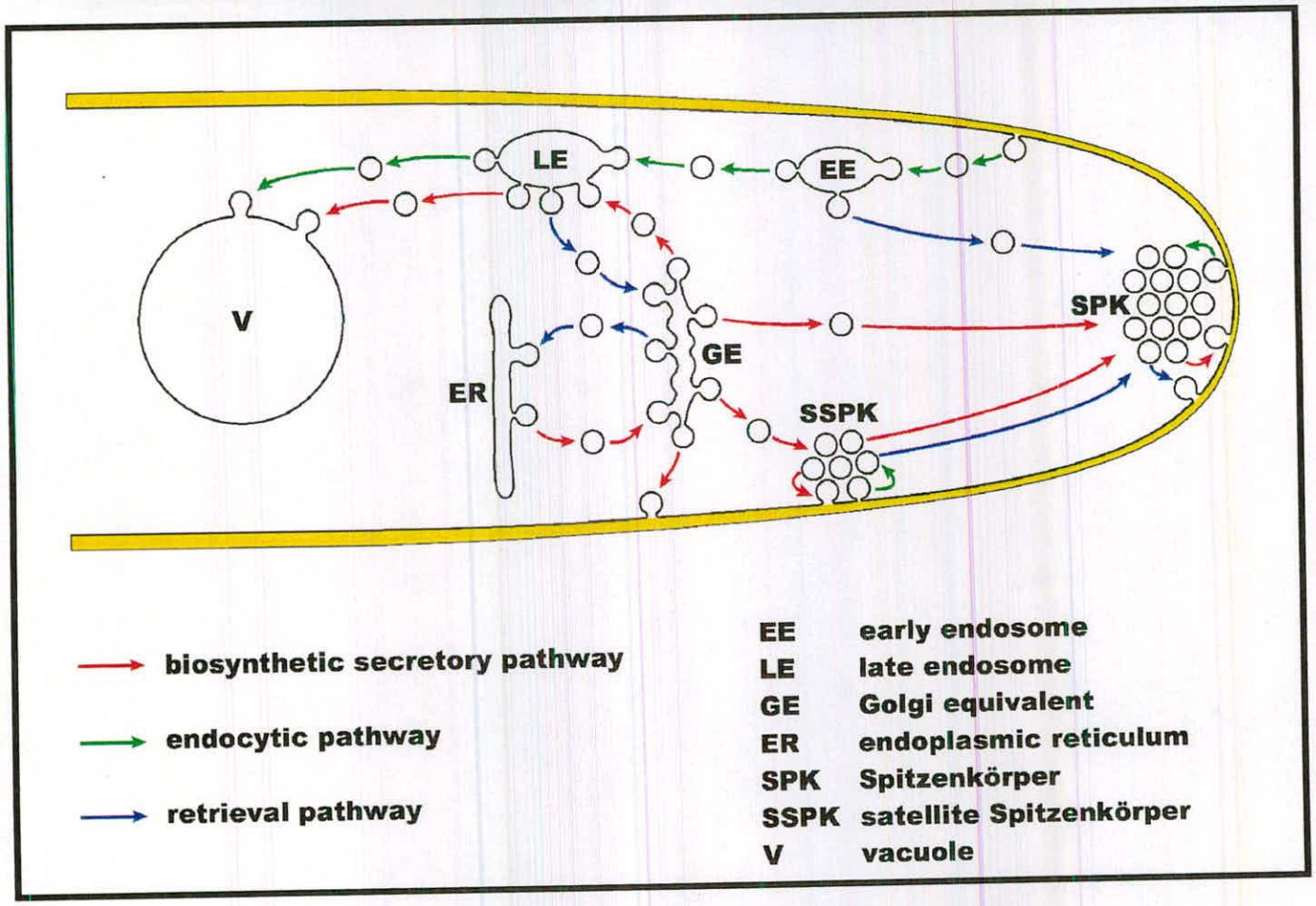

Figure 5.18 Hypothetical vesicle trafficking pathways in fungal cells. The scheme is based on the current knowledge about endocytosis summarised in Section 1.3 and on the results presented in Chapter 5. (Figure drawn by Patrick Hickey.)

cycle-regulated enzyme reservoir that can be mobilised directly to the site of action (Ziman et al., 1996; 1998). It is conceivable that in *N. crassa* integral membrane proteins involved in tip growth could be recycled in a similar way after they have been displaced from the growth zone at the apex by insertion of new membrane. After endocytic uptake into an endosome-like compartment these membrane proteins could be transported back to the plasma membrane at the site of active growth via the Spitzenkörper.

Satellite Spitzenkörper in *T. viride*, which consist predominantly of vesicles (Lopez-Franco et al., 1995), stain up with FM4-64 indicating that their membrane source is already stained. A source for stained vesicles could be the Golgi apparatus. For satellite staining hyphae were imaged about 20 min after dye application when intracellular loading was already quite strong which might be enough time for the stain to reach the Golgi apparatus. An alternative source for stained vesicles could be the plasma membrane. A hypothetical recycling mechanism for integral membrane proteins, similar to the one found in yeast for recycling CHSI and CHSIII activity (Ziman et al., 1996; 1998) could generate vesicles and directly channel them into satellite Spitzenkörper. Future work examining how long after dye application satellite Spitzenkörper exhibit staining should help to solve this question.

Intracellular movement of organelles and vesicles relies on the microtubule and actin cytoskeletal systems and is mediated by molecular motors which are fuelled by ATP hydrolysis (Yamashita and May, 1998). A study on the function of microtubules for tip growth in filamentous fungi using an inhibitor of fungal microtubule assembly (Howard and Aist, 1980) showed that microtubules play an important role in long-distance intracellular transport of vesicles containing cell wall precursors. Kinesins represent motor molecules which associate with membrane-bounded organelles and move along microtubules (Yamashita and May, 1998). Recently, kinesins have been found in several fungal species including *Nectria haematococca* (Wu et al., 1998) and *N. crassa* (Seiler et al., 1997). Deletion of the kinesin genes in these organisms was not lethal but had profound effects on hyphal morphology and tip growth: the growth

rate was considerably reduced; hyphae were gnarled and contorted; and the mycelium was highly branched (colonial phenotype). The Spitzenkörper in these mutant hyphae was severely affected: Wu et al. (1998) reported a reduction in size and aberrant behaviour in *N. haematococca* whereas Seiler et al. (1997) were not able to detect a discrete Spitzenkörper in the kinesin deficient *N. crassa* mutant NK01, apart from an occasional diffuse structure. These findings indicate that fungal kinesin is essential for efficient transport of secretory vesicles to the growing apex and is involved in Spitzenkörper organisation and behaviour (Seiler et al., 1997; Wu et al., 1998). However, in spite of a complete loss of kinesin tip growth still proceeded. Possible reasons are that either other microtubule motors with overlapping functions or transport systems not based on microtubules are used for vesicle movement (Yamashita and May, 1998). In contrast to the reported absence of Spitzenkörper in *N. crassa* NK01 (Seiler et al., 1997) it is now clear from the results reported here that this mutant possesses Spitzenkörper within growing hyphal tips, as revealed by staining with FM4-64 (Section 5.2.4.3). However, the mutant Spitzenkörper were quite sensitive to environmental disturbances and after handling for microscopic observation hyphae took a relatively long time to recover and to restart growth. In comparison with the wild type, the FM4-64 stained Spitzenkörper of *N. crassa* NK01 were smaller, more labile and showed increased tendency to move around within the apical dome. The increased motion of the Spitzenkörper was reflected in the irregular growth pattern. Interestingly, Wu et al. (1998) described a very similar behaviour for the kinesin deficient mutant of *N. haematococca* and related the erratic growth pattern to a very mobile Spitzenkörper.

5.3.4 Differences between FM4-64 and FM1-43

This study was mainly based on application of FM4-64, with use of the structurally related dye FM1-43 for comparison (Section 5.2.3). It seems likely that the basic uptake mechanism should be the same for both compounds. The fluorescent staining with FM1-43 was first evident in the plasma membrane. It subsequently occurred in endocytic intermediates, and then it appeared in the membranes of the large spherical

vacuoles which was concomitant with increasing general intracellular staining. Finally, in the subapical region of growing tips, the mitochondria became extremely well stained. FM1-43 seemed to stain membranes more distinctly than FM4-64 and staining was generally less hazy. Both compounds are structurally very similar and represent amphiphilic molecules with cationic "heads" and lipophilic "tails" (Figure 1.8). The double positive charge in the head region prevents the dye from crossing the membrane. The lipophilic tail comprises two aliphatic hydrocarbon chains and is responsible for insertion in the outer leaflet of membranes (Betz et al., 1996) with the effect that molecules with short tails are less lipophilic, bind less strongly to membranes and thus stain less brightly. FM4-64 contains two carbon atoms in each alkyl chain of the tail, whereas in FM1-43 contains four carbon atoms in each chain. Therefore, FM1-43 is expected to bind more strongly and less reversibly to membranes. This could explain why the membrane staining with FM1-43 (Figures 5.9 and 5.10A) is more pronounced than with FM4-64.

Another obvious difference between the two dyes concerns staining of the septa. The strong FM4-64 signal around septa (Figures 5.4, 5.5, 5.6 and 5.7) could be due to optical reasons. Firstly, septa contain two membranes which are only separated by the septal wall. Secondly, in relation to the optical section in the septal plate there is a higher density of membrane, whereas a curved membrane at the cell margins provides a lower density of membrane which consequently leads to a less intense signal. Thirdly, if the septum lies at an angle other than 90° to the optical plane, this will create the impression of a bright structure. Fourthly, differences in membrane composition at septa may cause a different affinity for dye binding and thus leading to a stronger fluorescent signal. However, in contrast to FM4-64, for unknown reasons FM1-43 did not stain up the septal region more strongly. Interestingly, Hoffman and Mendgen (1998) observed a clear difference in plasma membrane fluorescence along the germ tube in *U. fabae*. The authors attribute the much reduced signal behind the two nuclei to either reduced endocytic activities or reduced cell wall permeability in this region. Another possible reason, not considered by the authors, could be differences in the composition of the plasma membrane. For animal cells it is known

that different regions of the same plasma membrane can be specialised for different functions which is reflected in structural differences (Lodish et al., 1996).

6. Future work

The results described in this thesis have clearly shown that a pronounced tip-based pH_c gradient is not required for tip growth. With respect to gradients in $[Ca^{2+}]_c$, the results are not conclusive yet and future work should focus on establishing without doubt whether or not a tip high gradient in $[Ca^{2+}]_c$ is important in regulating tip growth in *Neurospora* and other filamentous fungi. Findings from using both, a ratiometric dye combination and the UV excited ratio dye Indo-1 should be compared. If the results are in favour of a gradient an investigation into the characteristics of that gradient should be conducted. Some interesting questions will then include:

- Does a localised rise of $[Ca^{2+}]_c$ precede branch formation?
- Does the magnitude of the gradient relate to growth rate?
- Does the $[Ca^{2+}]_c$ gradient oscillate during pulsatile hyphal growth?
- Does $[Ca^{2+}]_c$ regulate Spitzenkörper behaviour?

Contrary to reports questioning the occurrence of endocytosis in fungal hyphae (Cole et al., 1997) the results shown here indicate that endocytosis is a feature of fungal hyphae and involved in tip growth. Future work should concentrate on consolidating these findings. Aspects which need to be analysed further include:

- Quantifying the kinetics of dye movement from the plasma membrane into the cytoplasm and organelles to determine the rate of endocytosis and the rate of recycling of stained membrane to the Spitzenkörper.
- Localisation of FM4-64 at the ultrastructural level to determine which organelles are stained by this dye and the time course of staining (Henkel et at., 1996).
- Analysis of vesicle trafficking in FM4-64 stained hyphae of mutants compromised in different aspects of cell polarity regulation, secretion, endocytosis and cytoskeletal functioning.

7. References

Angleson, J.K. and Betz, W.J. (1997) Monitoring secretion in real time: capacitance, amperometry and fluorescence compared. *Trends in Neurosciences* **20:** 281-287.

Anraku, Y., Ohya, Y., and Iida, H. (1991) Cell cycle control by calcium and calmodulin in *Saccharomyces cerevisiae. Biochimica et Biophysica Acta* **1093:** 169-177.

Bartnicki-Garcia, S., Bartnicki, D.D., and Gierz, G. (1995) Determinants of fungal cell wall morphology: the vesicle supply center. *Canadian Journal of Botany-Revue Canadienne de Botanique* **73:** S 372-S 378.

Bartnicki-Garcia, S., Bartnicki, D.D., Gierz, G., López-Franco, R., and Bracker, C.E. (1995) Evidence that Spitzenkörper behavior determines the shape of a fungal hypha - a test of the hyphoid model. *Experimental Mycology* **19:** 153-159.

Bartnicki-Garcia, S., Hergert, F., and Gierz, G. (1989) Computer simulation of fungal morphogenesis and the mathematical basis for hyphal (tip) growth. *Protoplasma* **153:** 46-57.

Bartnik, E. and Sievers, A. (1988) *In vivo* observations of a spherical aggregate of endoplasmic reticulum and of golgi vesicles in the tip of fast growing *Chara* rhizoids. *Planta* **176:** 1-9.

Berger, F. and Brownlee, C. (1993) Ratio confocal imaging of free cytosolic calcium gradients in polarising and polarised *Fucus* zygotes. *Zygote* **1:** 9-15.

Berridge, M.J. and Bootman, M.D. (1996) Calcium signalling. In: *Signal Transduction* (Heldin, C.H. and Purton, M. Eds.) 205-221. Chapman & Hall, London.

Betz, W.J., Mao, F., and Smith, C.B. (1996) Imaging exocytosis and endocytosis. *Current Opinion in Neurobiology* **6:** 365-371.

Bibikova, T.N. and Gilroy, S. (1997) The role of cytoplasmic calcium in directing root hair formation and growth in *Arabidopsis thaliana. Plant Physiology* **114:** 72

Bibikova, T.N., Jacob, T., Dahse, I., and Gilroy, S. (1998) Localized changes in apoplastic and cytoplasmic pH are associated with root hair development in *Arabidopsis thaliana*. *Development* **125:** 2925-2934.

Bolsover, S.R. and Silver, R.A. (1991) Artifacts in calcium measurement: recognition and remedies. *Trends in Cell Biology* **1**: 71-74.

Bourett, T.M., Czymmek, K.J., and Howard, R.J. (1998) An improved method for affinity probe localization in whole cells of filamentous fungi. *Fungal Genetics and Biology* **24:** 3-13.

Bracker, C.E. and Grove, S.N. (1971) Continuity between cytoplasmic endomembranes and outer mitochondrial membranes in fungi. *Protoplasma* **73:** 15-34.

Bracker, C.E., Murphy, D.J., and López-Franco, R. (1997) Laser microbeam manipulation of cell morphogenesis in growing fungal hyphae. *The International Society for Optical Engineering* **2983:** 67-80.

Brain, K.L. and Bennett, M.R. (1997) Calcium in sympathetic varicosities of mouse vas deferens during facilitation, augmentation and autoinhibition. *Journal of Physiology-London* **502:** 521-536.

Brauer, D., Uknalis, J., Triana, R., and Tu, S.I. (1996) Subcellular compartmentation of different lipophilic fluorescein derivatives in maize root epidermal-cells. *Protoplasma* **192:** 70-79.

Bright, G.R., Fisher, G.W., Rogowska, J., and Taylor, D.L. (1987) Fluorescence ratio imaging microscopy - temporal and spatial measurements of cytoplasmic pH. *Journal of Cell Biology* **104:** 1019-1033.

Bull, A.T. and Trinci, A.P.J. (1973) The physiology and metabolic control of fungal growth. In: *Advances in Microbial Physiology* (Rose, A.H. and Tempest, D.W. Eds.) Academic Press, London.

Busa, W.B. and Nuccitelli, R. (1984) Metabolic regulation via intracellular pH. *American Journal of Physiology* **246:** R409-R438.

Caesar-Ton That, T.C., Hoangvan, K., Turian, G., and Hoch, H.C. (1987) Isolation and characterization of coated vesicles from filamentous fungi. *European Journal of Cell Biology* **43:** 189-194.

Callaham, D.A. and Hepler, P.K. (1991) Measurement of free calcium in plant cells. In: *Cellular calcium: a practical approach* (McCormack, J.G. and Cobbold, P.H. Eds.) 383-412. IRL Press, Oxford.

Carpita, N.C., Sabularse, D., Montezinos, D., and Delmer, D.P. (1979) Determination of the pore size of cell walls of living plant cells. *Science* **205:** 1144-1147.

Chant, J. (1994) Cell polarity in yeast. *Trends in Genetics* **10:** 328-333.

Cogswell, C.J. and Larkin, K.G. (1995) The specimen illumination path and its effect on image quality. In: *Handbook of Biological Confocal Microscopy* (Pawley, J.B. Ed) 27-37. Plenum Press, New York.

Cole, L., Coleman, J., Evans, D., and Hawes, C. (1990) Internalization of fluorescein isothiocyanate and fluorescein isothiocyanate-dextran by suspension-cultured plant-cells. *Journal of Cell Science* **96:** 721-730.

Cole, L., Hyde, G.J., and Ashford, A.E. (1997) Uptake and compartmentalisation of fluorescent probes by *Pisolithus Tinctorius* hyphae: evidence for an anion transport mechanism at the tonoplast but not for fluid-phase endocytosis. *Protoplasma* **199:** 18-29.

Cole, L., Orlovich, D.A., and Ashford, A.E. (1998) Structure, function, and, motility of vacuoles in filamentous fungi. *Fungal Genetics and Biology* **24:** 86-100.

Collis, A.J. (1996) The development of transgenic aequorin as an indicator for cytosolic free calcium in *Neurospora crassa. Ph.D. thesis.* University of Edinburgh.

Correa, A. and Hoch, H.C. (1993) Microinjection of urediospore germlings of *Uromyces appendiculatus. Experimental Mycology* **17:** 253-273.

Cunningham, K.W. and Fink, G.R. (1994) Ca^{2+} transport in *Saccharomyces cerevisiae. Journal of Experimental Biology* **196:** 157-166.

Czarnik, A.W. (1995) Desperately seeking sensors. *Chemistry & Biology* **2:** 631

Czymmek, K.J., Whallon, J.H., and Klomparens, K.L. (1994) Confocal microscopy in mycological research. *Experimental Mycology* **18:** 275-293.

Davis, R.H. and de Serres, F.J. (1970) Genetic and microbiological research techniques for *Neurospora crassa.* In: *Methods in Enzymology Vol. 17 -*

Metabolism of amino acids and amines (Tabor, H. and White Tabor, C. Eds.) 79-143. Academic Press, New York and London.

Desilva, L.R., Youatt, J., Gooday, G.W., and Gow, N.A.R. (1992) Inwardly directed ionic currents of *Allomyces macrogynus* and other water molds indicate sites of proton-driven nutrient transport but are incidental to tip growth. *Mycological Research* **96:** 925-931.

Edmonds, B.T., Murray, J. and Condeelis, J. (1995) pH regulation of the F-actin binding-properties of *Dictyostelium* elongation-factor 1-alpha. *Journal of Biological Chemistry* **270**: 15222-15230.

Feijo, J.A., Malhó, R., and Obermeyer, G. (1995) Ion dynamics and its possible role during in vitro pollen germination and tube growth. *Protoplasma* **187:** 155-167.

Felle, H. (1988) Cytoplasmic free calcium in *Riccia fluitans* and *Zea mays*: interaction of Ca^{2+} and pH. *Planta* **176:** 248-255.

Felle, H. (1989) Ca^{2+}-selective microelectrodes and their application to plant cells and tissues. *Plant Physiology* **91:** 1239-1242.

Felle, H.H. (1996) Control of cytoplasmic pH under anoxic conditions and its implication for plasma membrane proton transport in *Medicago sativa* root hairs. *Journal of Experimental Botany* **47:** 967-973.

Felle, H.H. and Hepler, P.K. (1997) The cytosolic Ca^{2+} concentration gradient of *Sinapis alba* root hairs as revealed by Ca^{2+}-selective microelectrode tests and fura-dextran ratio imaging. *Plant Physiology* **114:** 39-45.

Franke, W.W. and Kartenbeck, J. (1971) Outer mitochondrial membrane continuous with endoplasmic reticulum. *Protoplasma* **73:** 35-41.

Franklin-Tong, V.E., Ride, J.P., Read, N.D., Trewavas, A.J., and Franklin, F.C.H. (1993) The self-incompatibility response in *Papaver rhoeas* is mediated by cytosolic-free calcium. *Plant Journal* **4:** 163-177.

Fricker, M.D., Tlalka, M., Ermantraut, J., Obermeyer, G., Dewey, M., Gurr, S., Patrick, J., and White, N.S. (1994) Confocal fluorescence ratio imaging of ion activities in plant cells. *Scanning Microscopy* **Supplement 8:** 391-405.

Fricker, M.D., White, N.S., and Obermeyer, G. (1997) pH gradients are not associated with tip growth in pollen tubes of *Lilium longiflorum*. *Journal of Cell Science* **110:** 1729-1740.

Fröhlich, O. and Wallert, M.A. (1995) Methods of measuring intracellular pH in the heart. *Cardiovascular Research* **29:** 194-202.

Gadd, G.M. (1995) Signal transduction in fungi. In: *The Growing Fungus* (Gow, N.A.R. and Gadd, G.M. Eds.) 183-210. Chapman and Hall, London, Glasgow, Weinheim, New York, Tokyo, Melbourne, Madras.

Garrill, A. (1995) Transport. In: *The Growing Fungus* (Gow, N.A.R. and Gadd, G.M. Eds.) 183-210. Chapman and Hall, London, Glasgow, Weinheim, New York, Tokyo, Melbourne, Madras.

Garrill, A., Jackson, S.L., Lew, R.R., and Heath, I.B. (1993) Ion channel activity and tip growth - tip-localized stretch-activated channels generate an essential Ca^{2+} gradient in the oomycete *Saprolegnia ferax*. *European Journal of Cell Biology* **60:** 358-365.

Geli, M.I. and Riezman, H. (1996) Role of type-I myosins in receptor-mediated endocytosis in yeast. *Science* **272:** 533-535.

Geli, M.I. and Riezman, H. (1998) Endocytic internalization in yeast and animal cells: similar and different. *Journal of Cell Science* **111:** 1031-1037.

Geli, M.I., Wesp, A., and Riezman, H. (1998) Distinct functions of calmodulin are required for the uptake step of receptor-mediated endocytosis in yeast: the type I myosin Myo5p is one of the calmodulin targets. *Embo Journal* **17:** 635-647.

Gibbon, B.C. and Kropf, D.L. (1994) Cytosolic pH gradients associated with tip growth. *Science* **263:** 1419-1421.

Gilroy, S. (1997) Fluorescence microscopy of living plant cells. *Annual Review of Plant Physiology and Plant Molecular Biology* **48:** 165-190.

Girbardt, M. (1955) Lebendbeobachtungen an *Polystictus versicolor* (L.). *Flora* **142:** 540-563.

Girbardt, M. (1957) Der Spitzenkörper von *Polystictus versicolor* (L.). *Planta* **50:** 47-59.

Girbardt, M. (1969) Die Ultrastruktur der Apikalregion von Pilzhyphen. *Protoplasma* **67:** 441-441.

Girbardt, M. (1973) Die Pilzzelle. In: *Grundlagen der Cytologie* (Hirsch, G.C., Ruska, H., and Sitte, P. Eds.) 441-460. Gustav Fischer Verlag, Stuttgart.

Gooday, G.W. and Gow, N.A.R. (1994) Shape determination and polarity in fungal cells. In: *Shape and Form in Plants and Fungi* (Ingram, D.S. and Hudson, A. Eds.) 329-344. Academic Press, London.

Gooday, G.W. (1995) The dynamics of hyphal growth. *Mycological Research* **99:** 385-394.

Gow, N.A.R. (1984) Transhyphal electrical currents in fungi. *Journal of General Microbiology* **130:** 3313-3318.

Gow, N.A.R. (1995) Tip growth and polarity. In: *The Growing Fungus* (Gow, N.A.R. and Gadd, G.M. Eds.) 277-299. Chapman and Hall, London, Glasgow, Weinheim, New York, Tokyo, Melbourne, Madras.

Grove, S.N. and Bracker, C.E. (1970) Protoplasmic organization of hyphal tips among fungi: Vesicles and Spitzenkörper. *Journal of Bacteriology* **104:** 989-1009.

Grove, S.N. (1978) The cytology of hyphal tip growth. In: *The Filamentous Fungi* (Smith, J.E. and Berry, D.R. Eds.) 28-50. Edward Arnold.

Gruenberg, J. and Maxfield, F.R. (1995) Membrane transport in the endocytic pathway. *Current Opinion in Cell Biology* **7:** 552-563.

Guern, J., Felle, H., Mathieu, Y., and Kurkdjian, A. (1991) Regulation of intracellular pH in plant-cells. *International Review of Cytology-A Survey Of Cell Biology* **127:** 111-173.

Guner, A. (1995) Association of dextran aqueous solutions. *Journal of Applied Polymer Science* **56:** 1561-1565.

Harold, F.M and Caldwell, (1990) Tips and currents: electrobiology of apical growth. In: *Tip growth in plant and fungal cells* (Heath, I.B. Ed.) 59-90. Academic Press, San Diego.

Harold, F.M. (1994) Ionic and electrical dimensions of hyphal growth. In: *Growth, Differentiation and Sexuality* (Wessels, J.G.H. and Meinhardt, F. Eds.) 89-109. Springer-Verlag, Berlin Heidelberg.

Harold, F.M. (1997) How hyphae grow: morphogenesis explained? *Protoplasma* **197:** 137-147.

Harold, R.L., Money, N.P., and Harold, F.M. (1996) Growth and morphogenesis in *Saprolegnia ferax* - is turgor required. *Protoplasma* **191:** 105-114.

Haugland (1996) Handbook of fluorescent probes and research chemicals. Molecular Probes, Inc., Eugene, Oregon.

Hawes, C., Crooks, K., Coleman, J., and Satiat-Jeunemaitre, B. (1995) Endocytosis in plants: fact or artifact? *Plant, Cell and Environment* **18:** 1245-1252.

Heath, I.B. (1994) The cytoskeleton in hyphal growth, organelle movements, and mitosis. In: *Growth, Differentiation and Sexuality* (Wessels, J.G.H. and Meinhardt, F. Eds.) 43-65. Springer-Verlag, Berlin Heidelberg.

Heath, I.B. (1995a) Integration and regulation of hyphal tip growth. *Canadian Journal of Botany-Revue Canadienne de Botanique* **73:** S131-S139.

Heath, I.B. (1995b) The cytoskeleton. In: *The Growing Fungus* (Gow, N.A.R. and Gadd, G.M. Eds.) 99-134. Chapman and Hall, London, Glasgow, Weinheim, New York, Tokyo, Melbourne, Madras.

Hell, S., Reiner, G., Cremer, C., and Stelzer, E.H.K. (1993) Aberrations in confocal fluorescence microscopy induced by mismatches in refractive-index. *Journal of Microscopy-Oxford* **169:** 391-405.

Henkel, A.W., Lubke, J., and Betz, W.J. (1996) FM1-43 dye ultrastructural localisation in and release from frog motor nerve terminals. *Proceedings of the National Academy of Sciences of the United States of America* **93:** 1918-1923.

Hepler, P.K. (1997) Tip growth in pollen tubes: calcium leads the way. *Trends in Plant Science* **2:** 79-80.

Herrmann, A. and Felle, H.H. (1995) Tip growth in root hair-cells of *Sinapis alba*: significance of internal and external Ca^{2+} and pH. *New Phytologist* **129:** 523-533.

Heuser, J., Zhu, Q.L., and Clarke, M. (1993) Proton pumps populate the contractile vacuoles of *Dictyostelium* amoebae. *Journal of Cell Biology* **121:** 1311-1327.

Hicke, L., Zanolari, B., and Riezman, H. (1998) Cytoplasmic tail phosphorylation of the alpha-factor receptor is required for its ubiquitination and internalization. *Journal of Cell Biology* **141:** 349-358.

Hoch, H.C. and Howard, R.J. (1980) Ultrastructure of freeze-substituted hyphae of the basidiomycete *Laetisaria arvalis*. *Protoplasma* **103:** 281-297.

Hoffmann, J. and Mendgen, K. (1998) Endocytosis and membrane turnover in the germ tube of *Uromyces fabae*. *Fungal Genetics and Biology* **24:** 77-85.

Holdaway-Clarke, T.L., Feijo, J.A., Hackett, G.R., Kunkel, J.G., and Hepler, P.K. (1997) Pollen tube growth and the intracellular cytosolic calcium gradient oscillate in phase while extracellular calcium influx is delayed. *Plant Cell* **9:** 1999-2010.

Howard, R.J. (1981) Ultrastructural analysis of hyphal tip cell growth in fungi: Spitzenkörper, cytoskeleton and endomembranes after freeze-substitution. *Journal of Cell Science* **48:** 89-103.

Howard, R.J. and Aist, J.R. (1979) Hyphal tip cell ultrastructure of the fungus *Fusarium*: Improved preservation by freeze-substitution. *Journal of Ultrastructure Research* **66:** 224-234.

Howard, R.J. and Aist, J.R. (1980) Cytoplasmic microtubules and fungal morphogenesis: Ultrastructural effects of methyl benzimidazole-2-ylcarbamate determined by freeze-substitution of hyphal tip cells. *The Journal of Cell Biology* **87:** 55-64.

Hyde, G.J. and Heath, I.B. (1997) Ca^{2+} gradients in hyphae and branches of *Saprolegnia ferax*. *Fungal Genetics and Biology* **21:** 238-251.

Jackson, S.L. (1995) Microinjection of fungal cells - a powerful experimental-technique. *Canadian Journal of Botany-Revue Canadienne de Botanique* **73:** S 435-S 443.

Jackson, S.L. and Heath, I.B. (1993a) Roles of calcium ions in hyphal tip growth. *Microbiological Reviews* **57:** 367-382.

Jackson, S.L. and Heath, I.B. (1993b) The dynamic behavior of cytoplasmic F-actin in growing hyphae. *Protoplasma* **173:** 23-34.

Jelitto, T.C. (1995) Role of external signals in regulating the pre-penetration phase of infection by the rice blast fungus *Magnaporthe grisea*. *Ph.D. Thesis*, University of Edinburgh.

Jolicoeur, M., Germette, S., Gaudette, M., Perrier, M., and Becard, G. (1998) Intracellular pH in arbuscular mycorrhizal fungi - a symbiotic physiological marker. *Plant Physiology* **116:** 1279-1288.

Kaminsky, S.G.W. and Heath, I.B. (1996) Studies on *Saprolegnia ferax* suggest the general importance of the cytoplasm in determining hyphal morphology. *Mycologia* **88:** 20-37.

Kappenmann, R.F., Geisser, S. and Antle, C.E. (1970) Bayesian and Fiducial solutions for the Fieller-Creasy problem. *Sankhya, Indian Journal of Statistics* **32:** 331-340.

Knight, H., Trewavas, A.J., and Read, N.D. (1993) Confocal microscopy of living fungal hyphae microinjected with Ca^{2+}-sensitive fluorescent dyes. *Mycological Research* **97:** 1505-1515.

Kropf, D.L. (1992) Establishment and expression of cellular polarity in fucoid zygotes. *Microbiological Reviews* **56:** 316-339.

Kropf, D.L., Bisgrove, S.R., and Hable, W.E. (1998) Cytoskeletal control of polar growth in plant cells. *Current Opinion in Cell Biology* **10:** 117-122.

Kropf, D.L., Henry, C.A., and Gibbon, B.C. (1995) Measurement and manipulation of cytosolic pH polarizing zygotes. *European Journal of Cell Biology* **68:** 297-305.

Kurkdjian, A. and Guern, J. (1989) Intracellular pH: measurement and importance in cell activity. *Annual Review of Plant Physiology and Plant Molecular Biology* **40:** 271-303.

Levina, N.N., Lew, R.R., Hyde, G.J., and Heath, I.B. (1995) The roles of Ca^{2+} and plasma-membrane ion channels in hyphal tip growth of *Neurospora crassa*. *Journal of Cell Science* **108:** 3405-3417.

Lipp, P. and Niggli, E. (1993) Ratiometric confocal Ca^{2+}-measurements with visible wavelength indicators in isolated cardiac myocytes. *Cell Calcium* **14:** 359-372.

Llopis, J., McCaffery, J.M., Miyawaki, A. Farquhar, M.G. and Tsien, R.Y. (1998) Measurement of cytosolic, mitochondrial, and Golgi pH in single living cells with green fluorescent proteins. *Proceedings of the National Academy of Sciences of the United States of America* **95:** 6803-6808.

Lodish, H., Berk, A., Matsudaira, P., Baltimore, D., Zipursky, L. and Darnell, J. (1996) Molecular Cell Biology. H.W. Freeman and company, New York.

López-Franco, R. and Bracker, C.E. (1996) Diversity and dynamics of the Spitzenkörper in growing hyphal tips of higher fungi. *Protoplasma* **195:** 90-111.

López-Franco, R., Bartnicki-Garcia, S., and Bracker, C.E. (1994) Pulsed growth of fungal hyphal tips. *Proceedings of the National Academy of Sciences of the United States of America* **91:** 12228-12232.

López-Franco, R., Howard, R.J., and Bracker, C.E. (1995) Satellite Spitzenkörper in growing hyphal tips. *Protoplasma* **188:** 85-103.

Madshus, I.H. (1988) Regulation of intracellular pH in eukaryotic cells. *Biochemical Journal* **250:** 1-8.

Malhó, R. and Trewavas, A.J. (1996) Localized apical increases of cytosolic free calcium control pollen tube orientation. *Plant Cell* **8:** 1935-1949.

Malhó, R., Read, N.D., Pais, M.S., and Trewavas, A.J. (1994) Role of cytosolic-free calcium in the reorientation of pollen tube growth. *Plant Journal* **5:** 331-341.

Malhó, R., Read, N.D., Trewavas, A.J., and Pais, M.S. (1995) Calcium channel activity during pollen tube growth and reorientation. *Plant Cell* **7:** 1173-1184.

Marty, F. (1997) The biogenesis of vacuoles: insights from microscopy. *Advances In Botanical Research Incorporating Advances In Plant Pathology* **25:** 1-42.

McClure, W.K., Park, D., and Robinson, P.M. (1968) Apical organisation in the somatic hyphae of fungi. *Journal of General Microbiology* **50:** 177-182.

McDaniel, D.P. and Roberson, R.W. (1998) γ-Tubulin is a component of the Spitzenkörper and centrosomes in hyphal-tip cells of *Allomyces macrogynus*. *Protoplasma* **203:** 118-123.

McGillviray, A.M. and Gow, N.A.R. (1987) The transhyphal electrical current of *Neurospora crassa* in carried principally by protons. *Journal of General Microbiology* **133:** 2875-2881.

Mellman, I. (1996) Endocytosis and molecular sorting. *Annual Review of Cell and Developmental Biology* **12:** 575-625.

Meng, C.L. and Chang, D.C. (1994) Study of calcium signaling in cell cleavage using confocal microscopy. *Biological Bulletin* **187:** 234-235.

Messerli, M.A. and Robinson, K.R. (1997) Tip localized Ca^{2+} pulses are coincident with peak pulsatile growth rates in pollen tubes of lilium longiflorum. *Journal of Cell Science* **110:** 1269-1278.

Messerli, M.A. and Robinson, K.R. (1998) Cytoplasmic acidification and current influx follow growth pulses of *Lilium longiflorum* pollen tubes. *The Plant Journal* **16:** 87-91.

Miesenböck, G., De Angelis, D.A., and Rothman, J.E. (1998) Visualizing secretion and synaptic transmission with pH-sensitive green fluorescent proteins. *Nature* **394:** 192-195.

Miller, A.J., Vogg, G., and Sanders, D. (1990) Cytosolic calcium homeostasis in fungi: roles of plasma membrane transport and intracellular sequestration of calcium. *Proceedings of the National Academy of Sciences of the United States of America* **87:** 9348-9352.

Miller, D.D., Callaham, D.A., Gross, D.J., and Hepler, P.K. (1992) Free Ca^{2+} gradient in growing pollen tubes of lilium. *Journal of Cell Science* **101:** 7-12.

Miller, D.D., deRuijter, N.C.A., and Emons, A.M.C. (1997) From signal to form: aspects of the cytoskeleton-plasma membrane-cell wall continuum in root hair tips. *Journal of Experimental Botany* **48:** 1881-1896.

Miyakawa, I., Aoi, H., Sando, N., and Kuroiwa, T. (1984) Fluorescence microscopic studies of mitochondrial nucleoids during meiosis and sporulation in the yeast, *Saccharomyces cerevisiae*. *Journal of Cell Science* **66:** 21-38.

Miyawaki, A., Llopis, J., Heim, R., McCaffery, J.M., Adams, J.A., Ikura, M., and Tsien, R.Y. (1997) Fluorescent indicators for Ca^{2+} based on green fluorescent proteins and calmodulin. *Nature* **388:** 882-887.

Money, N.P. (1990) Measurement of pore size in the hyphal cell wall of *Achlya bisexualis*. *Experimental Mycology* **14:** 234-242,.

Money, N.P. (1997) Wishful thinking of turgor revisited: the mechanics of fungal growth. *Fungal Genetics and Biology* **21:** 173-187.

Money, N.P. and Harold, F.M. (1992) Extension growth of the water mold *Achlya*: Interplay of turgor and wall strength. *Proceedings of the National Academy of Sciences of the United States of America* **89:** 4245-4249.

Money, N.P. and Harold, F.M. (1993) 2 water molds can grow without measurable turgor pressure. *Planta* **190:** 426-430.

Moore, E.D.W., Becker, P.L., Fogarty, K.E., Williams, D.A., and Fay, F.S. (1990) Ca^{2+} imaging in single living cells: Theoretical and practical issues. *Cell Calcium* **11:** 157-179.

Morris, S.J. (1993) Simultaneous multiple detection of fluorescent molecules. In: *Optical Microscopy: Emerging Methods and Applications* (Herman, B. and Lemasters, J.J. Eds.) 177-212. Academic Press, London.

Muallem, S. and Lee, M.G. (1997) High $[Ca^{2+}]_{(i)}$ domains, secretory granules and exocytosis. *Cell Calcium* **22:** 1-4.

Nelson, G. (1999) Development of the recombinant aequorin method and its evaluation for calcium measurement in filamentous fungi. *Ph.D. Thesis*, Edinburgh University.

O'Driscoll, D., Hann, C., Read, S.M., and Steer, M.W. (1993) Endocytotic uptake of fluorescent dextrans by pollen tubes grown in vitro. *Protoplasma* **175:** 126-130.

Oparka, K.J. and Hawes, C. (1992) Vacuolar sequestration of fluorescent probes in plant cells: a review. *Journal of Microscopy* **166:** 15-27.

Oparka, K.J. and Read, N.D. (1994) The use of fluorescent probes for studies of living plant cells. In: *Plant Cell Biology. A Practical Approach* (Harris, N. and Oparka, K.J. Eds.) 27-50. IRL Press, Oxford.

Oparka, K.J., Murant, E.A., Wright, K.M., Prior, D.A.M., and Harris, N. (1991) The drug probenecid inhibits the vacuolar accumulation of fluorescent anions in onion epidermal-cells. *Journal of Cell Science* **99:** 557.

Opas, M. (1997) Measurement of intracellular pH and pCa with a confocal microscope. *Trends in Cell Biology* **7:** 75-80.

Opitz, N., Merten, E., and Acker, H. (1994) Evidence for redistribution-associated intracellular pK shifts of the pH-sensitive fluoroprobe carboxy-SNARF-1. *Pflügers Archiv-European Journal of Physiology* **427:** 332-342.

Parton (1996) Confocal microscopy analysis of the roles of intracellular pH in the regulation of polarised growth of *Dryopteris* protonemata. *Ph.D. Thesis*, Edinburgh University.

Parton, R.M., Fischer, S., Malhó, R., Papasouliotis, O., Jelitto, T.C., Leonard, T., and Read, N.D. (1997) Pronounced cytoplasmic pH gradients are not required for tip growth in plant and fungal cells. *Journal of Cell Science* **110:** 1187-1198.

Parton, R.M. and Read, N.D. (1999) Calcium and pH imaging in living cells. In: *Light Microscopy in Biology: A Practical Approach 2nd Edition* (Lacey, A.J. Ed.) Oxford University Press, Oxford (in press).

Pawley, J.B. (1995) Fundamental limits in confocal microscopy. In: *Handbook of Biological Confocal Microscopy* (Pawley, J.B. Ed.) 19-37. Plenum Press, New York.

Perez-Terzic, C., Stehno-Bittel, L., and Clapham, D.E. (1997) Nucleoplasmic and cytoplasmic differences in the fluorescence properties of the calcium indicator fluo-3. *Cell Calcium* **21:** 275-282.

Perkins, D.D. (1992) *Neurospora* - the organism behind the molecular revolution. *Genetics* **130:** 687-701.

Pickett-Heaps, J.D. and Klein, A.G. (1998) Tip growth in plant cells may be amoeboid and not generated by turgor pressure. *Proceedings of the Royal Society of London Series B-Biological Sciences* **265:** 1453-1459.

Picton, J.M. and Steer, M.W. (1983) Membrane recycling and the control of secretory activity in pollen tubes. *Journal of Cell Science* **63:** 303-310.

Pierson, E.S., Miller, D.D., Callaham, D.A., Shipley, A.M., Rivers, B.A., Cresti, M., and Hepler, P.K. (1994) Pollen-tube growth is coupled to the extracellular calcium-ion flux and the intracellular calcium gradient - effect of BAPTA-type buffers and hypertonic media. *Plant Cell* **6:** 1815-1828.

Pierson, E.S., Miller, D.D., Callaham, D.A., Vanaken, J., Hackett, G., and Hepler, P.K. (1996) Tip-localized calcium-entry fluctuates during pollen-tube growth. *Developmental Biology* **174:** 160-173.

Prescianotto-Baschong, C. and Riezman, H. (1998) Morphology of the yeast endocytic pathway. *Molecular Biology of the Cell* **9:** 173-189.

Prokisch, H., Yarden, O., Dieminger, M., Tropschug, M., and Barthelmess, I.B. (1997) Impairment of calcineurin function in *Neurospora crassa* reveals its essential role in hyphal growth, morphology and maintenance of the apical Ca^{2+} gradient. *Molecular & General Genetics* **256:** 104-114.

Read, N.D., Allan, W.T.G., Knight, H., Knight, M.R., Malhó, R., Russell, A., Shacklock, P.S., and Trewavas, A.J. (1992) Imaging and measurement of cytosolic free calcium in plant and fungal cells. *Journal of Microscopy* **166:** 57-86.

Read, N.D., Fischer, S., and Parton, R.M. (1998) Physicochemical and biophysical panel of the SCI pesticides group and the royal microscopical society meeting: microlocalisation of chemicals within biological systems - imaging Spitzenkörper, pH and calcium dynamics in growing fungal hyphae. *Pesticide Science* **54:** 179-181.

Rees, B., Shepherd, V.A., and Ashford, A.E. (1994) Presence of a motile tubular vacuole system in different phyla of fungi. *Mycological Research* **98:** 985-992.

Reynaga-Pena, C.G., Gierz, G., and Bartnicki-Garcia, S. (1997) Analysis of the role of the Spitzenkörper in fungal morphogenesis by computer simulation of apical branching in *Aspergillus niger*. *Proceedings of the National Academy of Sciences of the United States of America* **94:** 9096-9101.

Ridge, R.W. (1995) Recent developments in the cell and molecular biology of root hairs. *Journal of Plant Research* **108:** 399-405.

Rieder, S.E., Banta, L.M., Kohrer, K., McCaffery, J.M., and Emr, S.D. (1996) Multilamellar endosome-like compartment accumulates in the yeast vps28 vacuolar protein sorting mutant. *Molecular Biology of the Cell* **7:** 985-999.

Roberson, R.W. (1992) The actin cytoskeleton in hyphal cells of *Sclerotium rolfsii*. *Mycologia* **84:** 41-51.

Roberson, R.W. and Fuller, M.S. (1988) Ultrastructural aspects of the hyphal tip of *Sclerotium rolfsii* preserved by freeze substitution. *Protoplasma* **146:** 143-149.

Roberts, S.K., Dixon, G.K., Dunbar, S.J., and Sanders, D. (1997) Laser ablation of the cell wall and localized patch clamping of the plasma membrane in the filamentous fungus *Aspergillus*: characterization of an anion-selective efflux channel. *New Phytologist* **137:** 579-585.

Robertson, N.F. (1958) Experimental control of hyphal branching and branch form in hyphomycetous fungi. *Journal of the Linnean Society* **56:** 207-211.

Robertson, N.F. and Rizvi, S.R.H. (1968) Some observations on the water-relations of the hyphae of *Neurospora crassa*. *Annals of Botany* **32:** 279-291.

Robson, G.D., Prebble, E., Rickers, A., Hosking, S., Denning, D.W., Trinci, A.P.J., and Robertson, W. (1996) Polarized growth of fungal hyphae is defined by an alkaline pH gradient. *Fungal Genetics and Biology* **20:** 289-298.

Rodriguez-Navarro, A., Blatt, M.R., and Slayman, C.L. (1986) A potassium-proton symport in *Neurospora crassa* . *Journal of General Physiology* **87:** 649-674.

Roncal, T., Ugalde, U.O., and Irastorza, A. (1993) Calcium-induced conidiation in *Penicillium cyclopium* - calcium triggers cytosolic alkalinization at the hyphal tip. *Journal of Bacteriology* **175:** 879-886.

Roos, W. (1992) Confocal pH topography in plant-cells - acidic layers in the peripheral cytoplasm and the apoplast. *Botanica Acta* **105:** 253-259.

Rost, F.W.D., Shepherd, V.A., and Ashford, A.E. (1995) Estimation of vacuolar pH in actively growing hyphae of the fungus *Pisolithus tinctorius*. *Mycological Research* **99:** 549-553.

Sanders, D. and Slayman, C.L. (1982) Control of intracellular pH - Predominant role of oxidative metabolism, not proton transport, in the eukaryotic microorganism *Neurospora*. *Journal of General Physiology* **80:** 377-402.

Schiefelbein, J.W., Shipley, A., and Rowse, P. (1992) Calcium influx at the tip of growing root-hair cells of *Arabidopsis thaliana*. *Planta* **187:** 455-459.

Schild, D., Jung, A., and Schultens, H.A. (1994) Localization of calcium entry through calcium channels in olfactory receptor neurons using a laser scanning microscope and the calcium indicator dyes fluo-3 and fura-red. *Cell Calcium* **15:** 341-348.

Seiler, S., Nargang, F.E., Steinberg, G., and Schliwa, M. (1997) Kinesin is essential for cell morphogenesis and polarized secretion in *Neurospora crassa*. *Embo Journal* **16:** 3025-3034.

Sentandreu, R., Mormeneo, S., and Ruiz-Herrera, J. (1994) Biogenesis of the fungal cell wall. In: *Growth, Differentiation and Sexuality* (Wessels, J.G.H. and Meinhardt, F. Eds.) 111-124. Springer-Verlag, Berlin Heidelberg.

Sietsma, J.H. and Wessels, J.G.H. (1994) Apical wall biogenesis. In: *Growth, Differentiation and Sexuality* (Wessels, J.G.H. and Meinhardt, F. Eds.) 125-141. Springer-Verlag, Berlin Heidelberg.

Silver, R.A., Whitaker, M., and Bolsover, S.R. (1992) Intracellular ion imaging using fluorescent dyes - artifacts and limits to resolution. *Pflügers Archiv-European Journal of Physiology* **420:** 595-602.

Slayman, C.L. (1965) Electrical properties of *Neurospora crassa* - Respiration and the intracellular potential. *Journal of General Physiology* **49:** 93-116.

Slayman, C.L. and Slayman, C.W. (1962) Measurement of membrane potentials in *Neurospora*. *Science* **136:** 876-877.

Slayman, C.L., Moussatos, V.V., and Webb, W.W. (1994) Endosomal accumulation of pH indicator dyes delivered as acetoxymethyl esters. *Journal of Experimental Biology* **196:** 419-438.

Smith, C.B. and Betz, W.J. (1996) Simultaneous independent measurement of endocytosis and exocytosis. *Nature* **380:** 531-534.

Smith, D. and Onions, A.H.S. (1983) A comparison of some preservation techniques for fungi. *Transactions of the British Mycological Society* **81:** 535-540.

Steer, M.W. (1988) Plasma membrane turnover in plant cells. *Journal of Experimental Botany* **39:** 987-996.

Steer, M.W. and Steer, J.M. (1989) Tansley review no 16 pollen-tube tip growth. *New Phytologist* **111:** 323-358.

Steinberg, G. (1998) Organelle transport and molecular motors in fungi. *Fungal Genetics and Biology* **24:** 161-177.

Stricker, S.A. (1995) Time-lapse confocal imaging of calcium dynamics in starfish embryos. *Developmental Biology* **170:** 496-518.

Suzaki, E., Suzaki, T., Jackson, S.L., and Hardham, A.R. (1996) Changes in intracellular pH during zoosporogenesis in *Phytophthora cinnamomi*. *Protoplasma* **191:** 79-83.

Taggart, M., Austin, C., and Wray, S. (1994) A comparison of the effects of intracellular and extracellular pH on contraction in isolated rat portal vein. *Journal of Physiology-London* **475:** 285-292.

Takeuchi, Y., Schmid, J., Caldwell, J.H., and Harold, F.M. (1988) Transcellular ion currents and extension of *Neurospora crassa* hyphae. *Journal of Membrane Biology* **101:** 33-41.

Tanida, I., Takita, Y., Hasegawa, A., Ohya, Y., and Anraku, Y. (1996) Yeast Cls2p/Csg2p localized on the endoplasmic reticulum membrane regulates a non-exchangeable intracellular Ca^{2+} pool cooperatively with calcineurin. *FEBS Letters* **379:** 38-42.

Tertyshnikova, S. and Fein, A. (1998) Inhibition of inositol 1,4,5-trisphosphate induced Ca^{2+} release by cAMP dependent protein kinase in a living cell. *Proceedings of the National Academy of Sciences of the United States of America* **95:** 1613-1617.

Thiebaut, F., Currier, S.J., Whitaker, J., Haugland, R.P., Gottesman, M.M., Pastan, I., and Willingham, M.C. (1990) Activity of the multidrug transporter results in alkalinization of the cytosol -measurement of cytosolic pH by microinjection

of a pH-sensitive dye. *Journal of Histochemistry & Cytochemistry* **38:** 685-690.

Torralba, S., Raudaskoski, M., Pedregosa, A.M., and Laborda, F. (1998) Effect of cytochalasin a on apical growth, actin cytoskeleton organization and enzyme secretion in *Aspergillus nidulans*. *Microbiology* **144:** 45-53.

Turian, G. (1979) Cytochemical gradients and mitochondrial exclusion in the apices of vegetative hyphae. *Experientia* **35:** 1164-1166.

Vargas, M.M., Aronson, J.M., and Roberson, R.W. (1993) The cytoplasmic organization of hyphal tip cells in the fungus *Allomyces macrogynus*. *Protoplasma* **176:** 43-52.

Vida, T.A. and Emr, S.D. (1995) A new vital stain for visualizing vacuolar membrane dynamics and endocytosis in yeast. *Journal of Cell Biology* **128:** 779-792.

Vogel, H.J. (1956) A convenient growth medium for *Neurospora* (medium N). *Microbiol. Gen. Bull.* **13:** 42-43.

Watts, C. and Marsh, M. (1992) Endocytosis: what goes in and how? *Journal of Cell Science* **103:** 1-8.

Wendland, B., Emr, S.D., and Riezman, H. (1998) Protein traffic in the yeast endocytic and vacuolar protein sorting pathways. *Current Opinion in Cell Biology* **10:** 513-522.

Wendland, B., McCaffery, J.M., Xiao, Q., and Emr, S.D. (1996) A novel fluorescence-activated cell sorter-based screen for yeast endocytosis mutants identifies a yeast homologue of mammalian eps15. *Journal of Cell Biology* **135:** 1485-1500.

Wessels, J.G.H. (1993) Wall growth, protein excretion and morphogenesis in fungi. *New Phytologist* **123:** 397-413.

White, N.S., Errington, R.J., Fricker, M.D., and Wood, J.L. (1996) Aberration control in quantitative imaging of botanical specimens by multidimensional fluorescence microscopy. *Journal of Microscopy* **181:** 99-116.

Wilson, J.F. (1961) Micrurgical techniques for *Neurospora*. *American Journal of Botany* **48:** 46-51.

Wright, K.M. and Oparka, K.J. (1994) Physicochemical properties alone do not predict the movement and compartmentation of fluorescent xenobiotics. *Journal of Experimental Botany* **45:** 35-44.

Wu, Q.D., Sandrock, T.M., Turgeon, B.G., Yoder, O.C., Wirsel, S.G., and Aist, J.R. (1998) A fungal kinesin required for organelle motility, hyphal growth, and morphogenesis. *Molecular Biology of the Cell* **9:** 89-101.

Wymer, C.L., Bibikova, T.N., and Gilroy, S. (1997) Cytoplasmic free calcium distributions during the development of root hairs of *Arabidopsis thaliana*. *Plant Journal* **12:** 427-439.

Yamashita, R.A. and May, G.S. (1998) Motoring along the hyphae: molecular motors and the fungal cytoskeleton. *Current Opinion in Cell Biology* **10:** 74-79.

Yuan, S. and Heath, I.B. (1991) A comparison of fluorescent membrane probes in hyphal tips of *Saprolegnia ferax*. *Experimental Mycology* **15:** 103-115.

Yuan, S. and Heath, I.B. (1991) Chlortetracycline staining patterns of growing hyphal tips of the oomycete *Saprolegnia ferax*. *Experimental Mycology* **15:** 91-102.

Zalokar, M. (1959) Growth and differentiation of *Neurospora* hyphae. *American Journal of Botany* **46:** 602-610.

Ziman, M., Chuang, J.S., and Schekman, R.W. (1996) Chs1p and chs3p, two proteins involved in chitin synthesis, populate a compartment of the *Saccharomyces cerevisiae* endocytic pathway. *Molecular Biology of the Cell* **7:** 1909-1919.

Ziman, M., Chuang, J.S., Tsung, M., Hamamoto, S., and Schekman, R. (1998) Chs6p-dependent anterograde transport of Chs3p from the chitosome to the plasma membrane in *Saccharomyces cerevisiae*. *Molecular Biology of the Cell* **9:** 1565-1576.

8. Published papers

Part of the data has been published in:

- Parton, R. M., Fischer, S., Malhó, R., Papasouliotis, O., Jelitto, T., Leonard, T. and Read, N. D. (1997). Pronounced cytoplasmic pH gradients are not required for tip growth in plant and fungal cells. *Journal of Cell Science* **110**, 1187-1198.

- Read, N.D., Fischer, S., and Parton, R.M. Physicochemical and Biophysical Panel of the SCI Pesticides Group and the Royal Microscopical Society Meeting: Microlocalisation of chemicals within biological systems - imaging Spitzenkörper, pH and calcium dynamics in growing fungal hyphae. *Pesticide Science* 54, 179-181, 1998.

Pestic. Sci. 1998, **54**, 179–181

Extended Summary Physicochemical and Biophysical Panel of the SCI Pesticides Group and the Royal Microscopical Society Meeting: Microlocalisation of Chemicals within Biological Systems

The following extended summary is based on a paper presented at the above meeting organised by D. Bartlett and N. Read on behalf of the Physicochemical and Biophysical Panel of the SCI Pesticides Group and the Royal Microscopical Society, held on 10 September 1997 at Zeneca Agrochemicals, Jealott's Hill Research Station, Bracknell, UK. This is entirely the responsibility of the authors and does not necessarily reflect the views of the Editorial Board of Pesticide Science.

Imaging Spitzenkörper, pH and Calcium Dynamics in Growing Fungal Hyphae

Nick D. Read, Sabine Fischer & Richard M. Parton

Fungal Cell Biology Group, Institute of Cell and Molecular Biology, University of Edinburgh, Rutherford Building, Edinburgh EH9 3JH, UK

Plant diseases caused by filamentous fungi result in the loss of crops worth billions of pounds per year. Agrochemical companies are therefore continually trying to discover and develop new and effective antifungal compounds which prevent or inhibit the growth of fungal pathogens in order to improve crop quality and yield.[1] The mechanistic basis of the growth of filamentous fungi is currently the focus of much research. A major challenge in the future will be to discover novel antifungal targets within the multifactorial process of fungal growth.

Tip growth is the main way by which fungi grow, involving the polarized extension of a hypha by means of localized secretion and cell-wall synthesis at the hyphal apex.[2,3] In Edinburgh we are using confocal microscopy with a range of vital fluorescent probes to analyse hyphal tip growth and its regulation in living cells.[4,5] Three aspects being concentrated on are: (1) Spitzenkörper behaviour; (2) intracellular pH; and (3) intracellular Ca^{2+}.

Growing hyphal tips contain a multi-component organelle assemblage called the Spitzenkörper which is assumed to contain the secretory vesicles responsible for tip growth. Spitzenkörper behaviour is associated intimately with the dynamic growth pattern and morphogenesis of the hyphal tip.[5–11] We have developed a fluorescent staining procedure which allows the dynamic behaviour of the Spitzenkörper to be visualised (in growing hyphae) for the first time.[5]

The Spitzenkörper-selective dye we use is FM4-64. This styryl dye stains components of the endocytotic pathway and also, after membrane recycling, exocytotic vesicles. FM4-64 (and related dyes especially FM1-43) has been extensively used to image and analyse membrane trafficking during endocytosis and exocytosis in animal cells,[12] and more recently has been used to study endocytosis in yeast.[13,14] Using this dye we have stained the Spitzenkörper in growing hyphae of a wide range of filamentous fungi including *Aspergillus niger. v.* Teig, *Neurospora crassa* Shear & Dodge, *Puccinia graminis* Pers., *Rhizoctonia solani* Kuhn, *Sclerotium rolfsii* Sacc. and *Trichoderma viride* Pers. (Fischer, S., Rentel, M. C., Hickey, P., Dijksterhuis, J. & Read, N. D., unpubl.). At appropriate concentrations the dye is non-cytotoxic to hyphae and, compared with other dyes, relatively resistant to photobleaching.[5]

We found that the organization and behaviour of Spitzenkörper in stained hyphae of *N. crassa*, *R. solani* and *T. viride* visualized by confocal microscopy closely resembled that in unstained hyphae imaged by computer-enhanced, phase-contrast microscopy.[5] The dynamic shape of the stained Spitzenkörper and its close association with sites of localized cell expansion within the growing hyphal tip are clearly evident (Fig. 1). Hyphal branch formation can be readily monitored

 Pestic. Sci. 0031–613X/98/$17.50. Printed in Great Britain

Fig. 1. *Neurospora crassa.* Confocal images of a hyphal tip at three stages of growth showing staining of the Spitzenkörper with FM4-64. Bar, 5 μm.

and a differentiated core region within the Spitzenkörper is often seen. Satellite Spitzenkörper, which arise several micrometres behind the main Spitzenkörper and subsequently fuse with it, are frequently visible (Fig. 2). Staining also allows the effects of environmental stress (e.g. UV light) on Spitzenkörper behaviour and tip growth to be examined.[5] A kinesin-deficient mutant of *N. crassa*, recently reported to lack a Spitzenkörper,[15] has been found to contain one which was smaller and more labile than the Spitzenkörper of wild-type hyphae.[5] Overall, it is clear that the combination of confocal microscopy and FM4-64 staining will provide a new and powerful tool for analysing the role of the Spitzenkörper and vesicle trafficking during hyphal tip growth.[5]

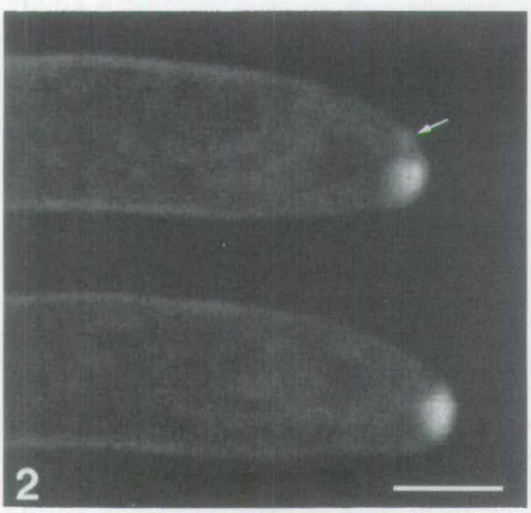

Fig. 2. *Trichoderma viride.* Confocal images of a hyphal tip at two stages of growth showing staining of the main Spitzenkörper and a satellite Spitzenkörper (arrow). Bar, 5 μm.

Gradients in cytosolic pH and Ca^{2+} have both been implicated as playing important roles in regulating tip growth in the hyphae of higher fungi, and a number of studies involving dye imaging have reported the existence of these gradients.[16–19] Unfortunately, none of this published work has provided convincing evidence supporting the existence of cytosolic pH or Ca^{2+} gradients in higher fungal hyphae because insufficient controls were performed to eliminate the potential problems of imaging artefacts. These artefacts include those resulting from dye partitioning from the cytosol into organelles, altered behaviour of the dye within the cellular microenvironment, and poor dye loading into cells.[4,20–22] Over the last few years we have developed improved methods for the imaging and measurement of cytosolic pH and Ca^{2+} in hyphae using ion-sensitive fluorescent dyes and confocal microscopy.

To analyse cytosolic pH in *N. crassa* we performed confocal ratio imaging of hyphae loaded with the pH-sensitive fluorescent dye carboxy SNARF-1.[4] Using this approach, cytosolic pH could be measured with a precision of $\pm 0{\cdot}3$ to $\pm 0{\cdot}06$ pH unit and a spatial resolution of equal to or better than 2·3 μm^2. Based on in-vitro calibrations, estimated values of the mean cytosolic pH were 7·20–7·25 in hyphae loaded with dye-ester and 7·57 in hyphae loaded with dextran-conjugated dye. Dextran-dyes are believed to provide better estimates of cytosolic pH because of their superior localization and retention within the cytosol, although pressure injection of dextran-conjugated dyes is much more difficult to perform than other dye loading techniques. Pronounced longitudinal cytosolic pH gradients (Δ 0.1 pH unit) were absent from the apical 50 μm of growing *N. crassa* hyphae loaded with either dye-ester or dextran-dye. Further evidence against pronounced cytosolic pH gradients being essential for tip growth was obtained when hyphae continued growing after their cytoplasm had been either acidified or alkalinized with a cell-permeant weak acid or base. These treatments would be expected to collapse pronounced cytosolic pH gradients. Nevertheless, cytosolic pH is normally tightly regulated because changes in external pH resulted in only small transient changes in cytosolic pH. External pH can regulate the initiation of cell polarity because elevating the external pH from 5·7 to 8·0 induced increased branch formation.[4]

Imaging cytosolic free Ca^{2+} has proved considerably more difficult than imaging cytosolic pH in the hyphae of higher fungi. Ester-loading Ca^{2+}-sensitive dyes was mostly unsuccessful and ionophoretic injection of free

Journal of Cell Science 110,1187-1198 (1997)
Printed in Great Britain © The Company of Biologists Limited 1997
JCS4385

Pronounced cytoplasmic pH gradients are not required for tip growth in plant and fungal cells

R. M. Parton[1], S. Fischer[1], R. Malhó[2], O. Papasouliotis[3], T. C. Jelitto[1,*], T. Leonard[3] and N. D. Read[1,†]

[1]Molecular Signalling Group, Institute of Cell and Molecular Biology, University of Edinburgh, Rutherford Building, Edinburgh EH9 3JH, UK
[2]Departamento de Biologia Vegetal, Faculdade de Ciências de Lisboa, R. Ernesto de Vasconcelos, Bloco C2, 1780 Lisboa, Portugal
[3]Statistical Laboratory, Department of Mathematics and Statistics, University of Edinburgh, James Clerk Maxwell Building, Edinburgh EH9 3JZ, UK

*Present address: The Plant Laboratory, University of York, York YO1 5YW, UK
†Author for correspondence

SUMMARY

The existence of pronounced cytoplasmic pH gradients within the apices of tip-growing cells, and the role of cytoplasmic pH in regulating tip growth, were investigated in three different cell types: vegetative hyphae of *Neurospora crassa*; pollen tubes of *Agapanthus umbellatus*; and rhizoids of *Dryopteris affinis* gametophytes. Examination of cytoplasmic pH in growing cells was performed by simultaneous, dual emission confocal ratio imaging of the pH-sensitive probe carboxy SNARF-1. Considerable attention was paid to the fine tuning of dye loading and imaging parameters to minimise cellular perturbation and assess the extent of dye partitioning into organelles. With optimal conditions, cytoplasmic pH was measured routinely with a precision of between ±0.03 and ±0.06 of a pH unit and a spatial resolution of 2.3 μm^2. Based on in vitro calibration, estimated values of mean cytoplasmic pH for cells loaded with dye-ester were between 7.15 and 7.25 for the three cell types. After pressure injecting *Neurospora* hyphae with dextran-conjugated dye, however, the mean cytoplasmic pH was estimated to be 7.57. Dextran dyes are believed to give a better estimate of cytoplasmic pH because of their superior localisation and retention within the cytosol. No significant cytoplasmic pH gradient (ΔpH of >0.1 unit) was observed within the apical 50 μm in growing cells of any of the three cell types. Acidification or alkalinisation of the cytoplasm in *Neurospora* hyphae, using a cell permeant weak acid (propionic acid at pH 7.0) or weak base (trimethylamine at pH 8.0), slowed down but did not abolish growth. However, similar manipulation of the cytoplasmic pH of *Agapanthus* pollen tubes and *Dryopteris* rhizoids completely inhibited growth. Modification of external pH affected the growth pattern of all cell types. In hyphae and pollen tubes, changes in external pH were found to have a small transient effect on cytoplasmic pH but the cells rapidly readjusted towards their original pH. Our results suggest that pronounced longitudinal gradients in cytoplasmic pH are not essential for the regulation of tip growth.

Key words: SNARF, Confocal ratio imaging, Tip growth, Cytoplasmic pH, *Neurospora*, *Agapanthus*, *Dryopteris*, Hypha, Pollen tube, Rhizoid

INTRODUCTION

Tip growth is the predominant method of cell growth in fungi, and is also exhibited by a number of specialised plant cell types such as pollen tubes, rhizoids and root hairs. Tip growth involves the polarised extension of a walled cell in which the increase in cell length is restricted to a narrow region of a few micrometers at the cell apex (Heath, 1990). Much recent research has focused on how this important mode of growth is regulated.

It is now accepted widely that both intracellular and extracellular ion gradients, notably of H^+ and Ca^{2+}, are associated with polarised growth in plant and fungal cells (Harold and Caldwell, 1990; Jackson and Heath, 1993). Extracellular pH (pH_{ext}) gradients are commonly associated with the apices of tip-growing cells (Harold and Caldwell, 1990; Gibbon and Kropf, 1991) and cytoplasmic pH (pH_{cyt}) gradients have also been reported (Turian, 1979; Roncal et al., 1993; Gibbon and Kropf, 1994). While a primary regulatory role for pH_{ext} gradients has largely been discounted (Harold and Caldwell, 1990; Gibbon and Kropf, 1991), evidence for the existence of pH_{cyt} gradients and their involvement in regulating tip growth remain controversial (Herrman and Felle, 1995). This is in contrast to the situation with Ca^{2+} where strong evidence supports the ubiquitous presence of a tip-focused gradient of cytosolic free Ca^{2+} in growing pollen tubes (e.g. Pierson et al., 1994; Malhó et al., 1995), and further evidence suggests similar gradients probably exist in other tip-growing cell types (Jackson and Heath, 1993; Berger and Brownlee, 1993; Herrmann and Felle, 1995).

A number of cellular processes central to tip growth, such as cytoskeletal organisation, vesicle fusion and enzyme activity are

sensitive to pH and might be regulated at the cell apex by local differences in pH_{cyt} (Guern et al., 1991; Roos, 1992; Grabski et al., 1994). There is, however, a problem in identifying specific roles for pH_{cyt} in the regulation of tip growth because of the involvement of pH_{cyt} in basic cellular processes which have an indirect effect on, or are consequential or incidental to tip growth (Felle, 1996). Localised uptake of nutrients, localised metabolic activity and maintenance of polarised membrane potential are polarised activities in which protons probably do not have a direct regulatory role in tip growth (Harold and Caldwell, 1990).

With respect to a possible fundamental regulatory role of pH_{cyt} in tip growth, two key questions need to be addressed. First, are pH_{cyt} gradients a general feature of tip-growing cells? Second, how dependent is tip growth on pH_{cyt} and pH_{ext}? In the current study we have performed a rigorous quantitative, spatial analysis of pH_{cyt} in three taxonomically diverse types of tip-growing cells (fungal hyphae, higher plant pollen tubes and fern rhizoids; Fig. 1) which exhibit contrasting lifestyles. This analysis has involved simultaneous dual channel confocal ratio imaging of the pH-sensitive probe cSNARF-1 (5-(and-6)-carboxy-seminapthorhodafluor-1). Our data demonstrate that pronounced, longitudinal pH_{cyt} gradients ($\Delta pH > 0.1$ pH unit) are absent from the apical 50 μm of the three cell types during active tip growth. We have also shown how experimentally induced changes in pH_{cyt} or pH_{ext} influence tip growth. Our results suggest that pronounced, longitudinal pH_{cyt} gradients are not fundamental to the regulation of tip growth but that changes in pH_{cyt} and pH_{ext} can significantly influence the growth rate and morphogenesis of tip-growing cells.

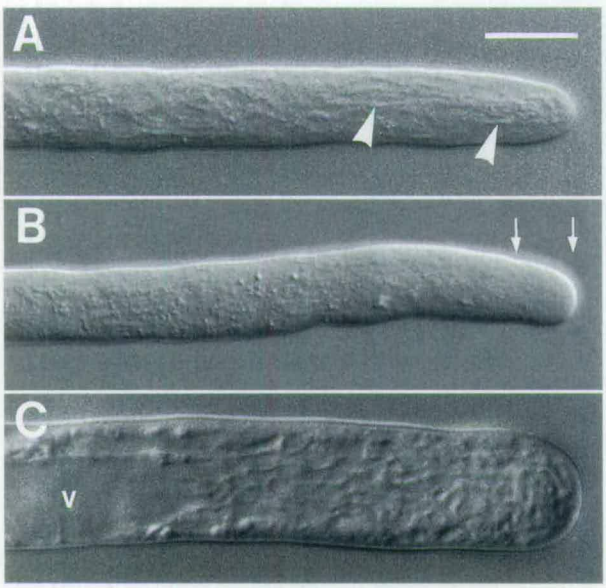

Fig. 1. Differential interference contrast micrographs showing the apical cytology of the three cell types examined. (A) Vegetative hypha of *Neurospora*. Elongated mitochondria can be discerned as long structures (arrow heads) throughout the apical 30 μm. (B) Pollen tube of *Agapanthus*. The apical 30-50 μm is predominantly free of large vacuoles. However, a vesicle packed region, 'the apical clear zone' from which other organelles are excluded, is found in the apical 5-10 μm (arrows). (C) Gametophyte rhizoid of *Dryopteris*. The cytoplasm is predominantly distributed as a thin peripheral layer thickening to 2-4 μm at the apex. Behind the apical region lies a large subapical vacuole (v). Within the apical 10-30 μm there exists a complex arrangement of tubules and vesicles, possibly part of the vacuolar system. Bar, 10 μm.

MATERIALS AND METHODS

Chemicals

Chemicals for cell culture and experimental manipulations were obtained from Sigma Chemical Co. (Poole, Dorset, UK). pH-sensitive fluorescent dyes (free acid, AM-ester and 10 kDa dextran-conjugate of cSNARF-1), fluorescent beads (200 nm nile red FluoSpheres) and Pluronic F-127 were obtained from Molecular Probes Inc. (Eugene, Oregon, USA). For ester-loading, cSNARF-1 AM (20 mM stock in dimethylsulphoxide) was diluted to 200 μM with aqueous Pluronic F-127 (0.04% v/v) detergent solution.

Cell culture and handling

Typical examples of the experimental material used are shown in Fig. 1 and a summary of the methods of dye loading are given in Table 1.

Neurospora crassa (wild type [74A], Fungal Genetics Culture Collection, strain 262) was cultured and prepared for loading with dye as described previously (Knight et al., 1993). For cSNARF-1 AM ester-loading, hyphae were cultured in half strength liquid Vogel's medium (Vogel, 1956) and sandwiched between two glass coverslips using the mounting method described by Knight et al. (1993). For pressure microinjection of the cSNARF-1 dextran conjugate, hyphae were excised from the leading edge of a colony cultured on agar medium overlaid with cellophane (gauge 525, uncoated Rayophane from A. A. Packaging, Walmer Bridge, Lancs., UK) and subsequently transferred to slide culture on a thin, even layer of Vogel's medium (containing 2% w/v agarose) spread over a glass coverslip. Slides were incubated at 25°C in a humid chamber for 5-8 hours. Five to ten minutes prior to microinjection, hyphae were covered with liquid medium.

Pollen tubes of *Agapanthus umbellatus* were cultured from stored pollen grains as described by Malhó et al. (1994). Briefly, pollen was evenly scattered onto 200 μl agar medium, which had been spread thinly and evenly over glass coverslips, and incubated under humid conditions at 25°C for 1-2 hours to produce 200-2,000 μm long tubes. Growing pollen tubes were loaded with dye, either by the ester method or by ionophoretic injection of cSNARF-1 free acid.

Spores of *Dryopteris affinis*, morphotype *affinis/borreri* (Newman) Fraser-Jenkins, collected in the grounds of Edinburgh University, were cultured under conditions modified from those described by Dyer and Cran (1976). After initial rhizoid emergence (typically 5 days after sowing), spores were transferred to modified liquid medium containing 6.1 mM $Ca(NO_3)_2$, 1.2 mM KNO_3 and 2.0 mM $MgSO_4$. They were then cultured for a further 24-36 hours under white light (~100 $\mu Em^{-2}s^{1}$) at 19-21°C to allow rhizoids to grow to 150-300 μm in length. Cells were only loaded with cSNARF-1 by the ester method.

Microinjection

Microinjection was carried out on a Nikon Diaphot TMD inverted microscope set up for fluorescence microscopy and fitted with Narishige N-88 micromanipulators. Ionophoretic microinjection involved the use of the equipment described by Knight et al. (1993). Pressure microinjection was performed with the pressure probe system described by Oparka et al. (1991).

Needles for ionophoretic microinjection were pulled on a Narishige PB-7 electrode puller (single stage pull) from GC-150F borosilicate glass (Clark Electromedical Instruments, Pangbourne, Reading, UK); needles for pressure injection were pulled with a Campden 773 micropipette puller (three stage programmed pull) from GC-100F glass.

pH treatments

Manipulation of pH_{cyt} was performed with modified culture media

Table 1. Parameters used for loading cSNARF-1 into cells

Loading method	cSNARF-1	Cell type	Dye concn	Loading conditions	Imaging time (minutes)*	Growth rates (μm/minute ± s.d.)†	
						Control	Loaded
Ester-loading	AM ester	*Agapanthus*	2-5 μM in medium‡	Continuous loading	~30	22.2±0.3	21.6±0.3
		Neurospora	2-5 μM in medium‡	Continuous loading	~30	15.8±2.8§	15.2±3.5§
		Dryopteris	2-5 μM in medium‡	~15 minutes loading	20-30	0.23±0.02	0.25±0.04
Pressure injection	10 kDa dextran	*Neurospora*	10 mg/ml in needle	0.4 MPa for ~30 seconds	<60	(31.7±4.7)¶	9.7±4.5¶
Ionophoresis	Free acid	*Agapanthus*	100 μM in needle	Single pulse 0.5-2.0 nA for 5 seconds	<30	22.2±0.3	19.5±0.4

*Imaging time refers to the period, after dye loading, over which images could be obtained of sufficient quality to produce reliable ratios. Dye sequestration within organelles, dye leakage from the cell and phototoxic dye effects all limited the useful imaging period.

†Growth was examined on the CLSM under typical imaging conditions. 'Control' rates are for unloaded cells; 'loaded' rates are for dye-loaded cells.

‡Medium refers to the standard culture medium (see Materials and Methods).

§Growth rate relates to leading hyphae (7-11 μm wide) in liquid medium under a coverslip which probably results in anoxia.

¶Growth rates relate to leading hyphae in slide culture without an overlying coverslip before ('control') and after ('loaded') pressure injection. Hyphae which had been pressure-injected with dye were narrower (8.5-9.5 μm wide) than hyphae from which they regenerated (12-16 μm wide). In general, unloaded hyphae with wider diameters grow faster thus making direct comparisons between the growth rates of unloaded and loaded hyphae invalid.

containing a cell permeant weak acid or base buffer: pH 6.0-7.0 (15, 30 or 50 mM sodium propionate added) and pH 7.0-8.0 (30 mM ammonium chloride or 50 mM trimethylamine added). The pH_{ext} was shifted by exchanging the standard medium with similar media of different pH adjusted with KOH or HCl. Images were usually collected between 3 and 10 minutes after buffer application.

Confocal microscopy and imaging

Confocal laser scanning microscopy (CLSM) was performed with the Bio-Rad MRC-600 system (described by Read et al., 1992) running COMOS, MPL and TCSM software (all version 7.0) supplied by Bio-Rad (Hemel Hempstead, UK).

Intracellular distribution of cSNARF-1 was determined by CLSM imaging in single channel mode with excitation at 514 nm and detection of total dye fluorescence emission (>550 nm). cSNARF-1 ratio imaging was performed with the CLSM in dual channel mode using 514 nm excitation and a custom built SNARF emission filter block (supplied by Bio-Rad). The filter block contained a 610 nm dichroic mirror and 640/40 and 580/30 nm filters. CLSM settings used for confocal ratio imaging of cSNARF-1 are summarised in Table 2.

Table 2. Optimised imaging parameters for confocal ratio imaging of cSNARF-1 loaded cells

Variable	Settings*	Significance
Laser power	1%-3% (25 mW argon ion laser)	
Scan speed	1-3 seconds per frame (512 lines)	Optimisation of signal detection
Low signal enhance†	Signal integrated over full pixel dwell-time	
Photomultiplier -gains	Ch1:Ch2 gains set (over the range 55-75%) to give a fluorescence intensity ratio of 1 at pH 7.0	
Black-level setting	Dark signal pixel intensity of ~10	
Accumulate filter	Up to 3 (addition of subsequent scans)	Improvement in the signal to noise ratio
Kalman filter	Up to 3 (cumulative averaging of subsequent scans)	
Objectives	×40 dry (NA 0.95) or ×60 oil (NA 1.4)	Determines optical resolution and pixel size
Confocal apertures	Pinhole ~30% open for both channels	
Electronic zoom	3-4	

*Settings refer to the Bio-Rad MRC-600 confocal microscope (see Pawley, 1995, for a more detailed explanation).

†Only available in slow scan mode (slow scan speed and low signal enhance were used routinely for imaging).

A ×40 (0.95 NA) dry objective and ×60 (1.4 NA) oil immersion objective were used. Whilst the oil immersion objective was superior to the lower NA dry objective in terms of optical resolution and efficiency of light collection, the latter still gave useful resolution and was more amenable to the examination of fast growing cells.

Axial and lateral resolution for the different objectives and confocal aperture settings used were estimated in terms of the FWHM (full width half maximum) value obtained from images of 200 nm nile red FluoSpheres (Cogswell and Larkin, 1995). With a confocal aperture of 30% (Table 2), the ×40 dry objective gave an estimated axial resolution of 1.3 μm and lateral resolution of 0.6 μm; the corresponding values for the ×60 oil immersion objective were 0.8 μm and 0.4 μm, respectively. Confocal apertures were opened to ~30%, slightly greater than the value reported to give maximum axial and lateral resolution (Lemasters et al., 1993), because of the need to maximise the collection of emitted photons for a given dye loading to improve the signal to noise ratio ($R_{S/N}$). In addition, the slow scan mode (integrating over the full pixel dwell time) was used and images were averaged or accumulated over several scans where possible (Table 2).

Procedures for ratio processing

Ratio images were produced using the TCSM software. From each fluorescence image pair the photomultiplier dark signal was removed by a 'dark image' subtraction. Dark images were collected by blocking the laser illumination path. Thresholding, usually at brightness values of 10-15 (grey scale from 0-255), was used to remove background noise from outside the fluorescent specimen. The ratio image was formed by division of corresponding pixels in the image pair Ch-2/Ch-1. Ratio images were scaled such that the pixel range 0-255 corresponded to ratio values between 0 and 4 depending upon the pH range covered. Finally a 3×3 median filter was applied to improve image appearance and images were displayed with a pseudo-coloured look up table (LUT).

Ratio values were calculated by dividing average pixel intensity values extracted from defined areas at corresponding positions in the 580 and 640 nm fluorescence images, using COMOS and MPL commands (Length, Histogram and Stats). Numerical data were

displayed graphically through Fig P (version 2.7) from Biosoft (Cambridge, UK).

Calibration of cSNARF-1 pH response

In vitro calibration of cSNARF-1 ratio values was performed by imaging the fluorescence of the appropriate dye-buffer mixtures over the pH range 6.0 to 8.0. Image collection and processing were as described above. The buffer media compared were a simple 20 mM MES/Hepes buffer and a 'pseudocytosol' medium designed to mimic the intracellular environment (Fricker et al., 1994). The dye concentration used in each of the different buffers was adjusted to give fluorescence image intensities of about 100 (on a scale of 0-255) in both channels at pH 7.0.

Estimation of the average pH_{cyt} in cell populations

Average pH_{cyt} of cell populations was determined from the average pH_{cyt} measured over large sample areas (>5,000 pixels) within individual cells. Pixel variation within individual images was not considered and variation in pH_{cyt} within the population was assumed to be normally distributed and reported as ± s.e.m values.

Statistical analysis and estimation of spatial resolution and precision of pH measurement

Whilst autofluorescence was negligible and photomultiplier dark signal was subtracted during ratioing, the degree of intrinsic noise in the number of detected photons (Pawley, 1995) could not be controlled. Intrinsic noise, leading to random variation in individual pixel values, arises from several sources during the process of digital imaging (Sheppard et al., 1995). One of the principal sources of such random variation between pixel values is the Poisson distributed variation in photons detected from the specimen, known as 'shot' noise (Pawley, 1995), which imposes a fundamental limit upon the $R_{S/N}$ of images with respect to the number of photons detected at each pixel. The variation between individual pixel values within an image becomes increasingly important when extracting quantitative data from small image areas (of the order of hundreds of pixels), and when making comparisons between the values from different regions within the same image. Therefore, a means of quantifying the magnitude of the variation between pixel values is required to provide: (a) estimates of the precision of quantitative data for particular sample sizes (and thus the spatial resolution) and (b) confidence limits to allow meaningful comparison between different regions of the same image. Hence the need for rigorous statistical analysis.

In the case of ratio imaging the inherent noise in the individual fluorescence images is propagated during the ratio processing steps. Furthermore, the analysis of noise in ratio imaging may not be carried out on the final ratio image produced by the pixel by pixel division of corresponding pairs of pixels in the fluorescence images. This is because the average ratio value of the final ratio images is not equal to the ratio of the average fluorescence intensity values at wavelengths 1 (λ_1) and 2 (λ_1). Thus, for an image of n pixels:

$$\text{mean fluorescence } \lambda_2/\text{mean fluorescence } \lambda_1 \neq \Sigma\,(P1\lambda_2/P1\lambda_1, \ldots\ldots\ldots, Pn\lambda_2/Pn\lambda_1)/n$$

(where $P1\lambda_2$ is the value of the first pixel in the wavelength 2 fluorescence image and $Pn\lambda_2$ is the value of the nth pixel)

The extent to which the two mean ratio values differ is itself dependent upon the degree of noise in the fluorescence images; the more noisy the greater the difference.

Mean ratio values must, therefore, be calculated by dividing the mean fluorescence values from corresponding sample areas in the λ_2 and λ_1 images. The confidence limits for the mean ratio value must be calculated by taking into account the variation in the pixel values of both fluorescence images. Unfortunately this variation could not be analysed effectively by conventional statistical methods and thus a Bayesian approach had to be adopted (see Appendix).

Experimental analysis of the spatial resolution and precision of pH measurement within individual images was initially done in vitro by ratio imaging cSNARF-1 free acid buffered (MES/Hepes) at pH values (accurate to ±0.005 units) over the range pH 6.5-7.5 (Fig. 2). Imaging parameters used were as defined in Table 2.

In in vitro test samples, the average ratio determined from all pixels in a fluorescence image pair was considered as the 'true mean' ratio value. However, variation in ratio values at the level of individual fluorescence pixel pairs influenced how well a small sample of pixels estimated the true mean. This uncertainty, which represented the precision with which pH could be estimated for a particular sample area size, was assessed according to the Bayesian theory of inference (Kappenman et al., 1970). An algorithm for determining the posterior density function of sample mean ratio values (see Appendix) was written in S-plus from MathSoft (StatSci Europe, Oxford, UK). The 95% Bayesian intervals for variation in ratio values of sample areas of different sizes were determined and from this the optimum precision of pH measurement and spatial resolution in vitro were determined (Fig. 2 and Table 3).

Average signal strength in fluorescence images and the use of Kalman and Accumulative filters all influenced the precision of pH measurement. Increasing average fluorescence brightness values from 25 to 150 (on a 0-255 scale) gave an improvement in precision of >150%. Accordingly, images with high average fluorescence brightness (typically >100) were used where possible. Kalman filtering (n=3) gave an improvement of ~40% over direct image collection. Accumulative filtering (n=3) to increase signal strength also improved precision but was inferior to the direct capture of images at a signal strength equivalent to the accumulated image. Standardised image capture (Table 2) made data more amenable to the application of systematic statistical analysis.

Light microscopy

Living cells were examined with a Reichert-Jung Polyvar light microscope using differential interference contrast (DIC) optics and a ×40

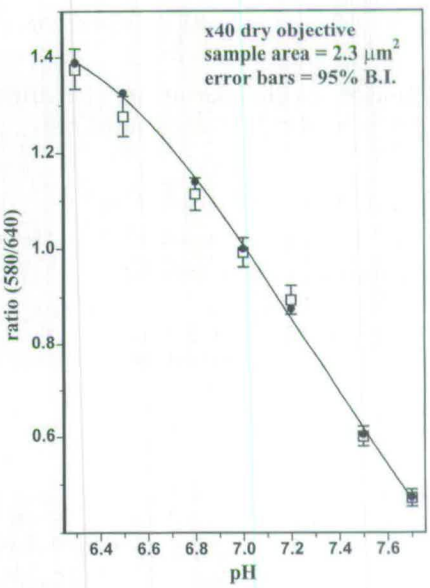

Fig. 2. Analysis of the precision of pH measurement achieved with the CLSM. Estimation of precision was based on plots of the pH response of cSNARF-1 in vitro over the pH range 6.5-7.5. The limit to the precision of measurement for sampling within small areas of images (□), which is imposed by shot noise in fluorescence data, was estimated according to the Bayesian theory of inference and shown here as error bars representing the 95% Bayesian interval (BI). Average values for all pixels in each calibration image are also shown (●). Spatial resolution was determined by the number of pixels used as the sampling area size (in this case 14×14 pixels).

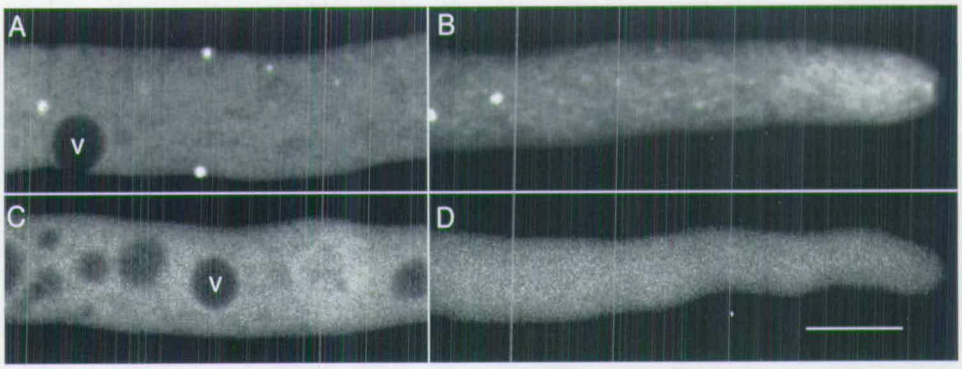

Fig. 3. Confocal images showing the intracellular distribution of cSNARF-1 in growing *Neurospora* hyphae. (A and B) Subapical and apical regions, respectively, of an ester-loaded hypha after 15 minutes continuous dye loading. (C and D) The equivalent images of hyphae pressure microinjected with a 10 kDa dye-dextran conjugate. The dark regions in A and C are large vacuoles (v) excluding dye. The bright spots in A and B are small, unidentified organelles which accumulated dye. Bar, 10 μm.

(1.0 NA) or ×100 plan apo (1.32 NA) oil immersion objective. Micrographs were recorded on Kodak TMAX 400 35 mm black and white film.

RESULTS

Health of cells during pH_{cyt} imaging

The health of cells during pH_{cyt} imaging was assessed on the basis of their apical morphology (Figs 1, 3, 4 and 5) and growth rates (Table 1). Stressed cells exhibited increased apical vacuolation, altered apical morphology, and reduced growth rates. The phototoxic effects of laser-irradiating intracellular dye was found to be the most significant threat to cell health. However, the dye-loading and low dosages of laser irradiation employed (Tables 1 and 2) did not generally cause stress responses in cells over the usual period of 20-30 minutes during which images were obtained. Adverse affects on tip growth (e.g. from dye toxicity and pH buffering) were also considered negligible as similar growth rates were obtained with loaded and unloaded cells. Based on a comparison with fluorescence images of dye/buffer mixtures in vitro the cytoplasmic concentration of loaded dye was estimated to be <100 μM.

Intracellular distribution of cSNARF-1

Intracellular dye distribution was found to depend upon the dye-loading method, cell type and time after the start of loading (Figs 3, 4 and 5). cSNARF-1 was successfully introduced into all cell types as its AM-ester. However, dye sequestered from the cytosol into organelles. In *Neurospora* hyphae and *Agapanthus* pollen tubes, continuous loading was necessary to maintain suitable fluorescence levels, and even then after 20-40 minutes the fluorescence intensity began to decrease (Figs 4A,B and 6). *Dryopteris* rhizoids could not be continuously loaded due to extensive vacuolar accumulation of dye so loading was halted once suitable cytoplasmic fluorescence levels were reached (Fig. 5A and B).

Ester-loaded hyphae of *Neurospora* exhibited bright dye fluorescence throughout the cytosol (Fig. 3A and B). Dark areas in subapical hyphal compartments corresponded to exclusion of dye from large vacuoles. Bright fluorescent spots, ~0.5 μm in diameter, were evident throughout ester-loaded hyphae. These spots represented dye sequestered within unidentified, roughly spherical organelles. Within the apical 50 μm of hyphae, dye fluorescence was uneven and elongated tubular structures could be discerned. These structures correlated with the morphology and distribution of mitochondria (Fig. 1).

Ester-loading of *Agapanthus* pollen tubes initially resulted in

Table 3. Precision of pH estimation in relation to spatial resolution for cSNARF-1 ratio imaging

Sample area (pixels)	Spatial resolution (μm†)	Precision of pH measurement
20×20	4.8	±0.04 to ±0.02
14×14	2.3	±0.06 to ±0.03
10×10	1.2	±0.08 to ±0.04
10×10*	0.5	±0.05 to ±0.02*

Precision of pH measurement determined as described in Materials and Methods and Fig. 2. The values given are the best and worst estimated precision over the pH range tested (pH 6.5-7.5) with the ×40 objective.

*As above for images collected with the ×60 objective and Kalman-filtered (n=3).

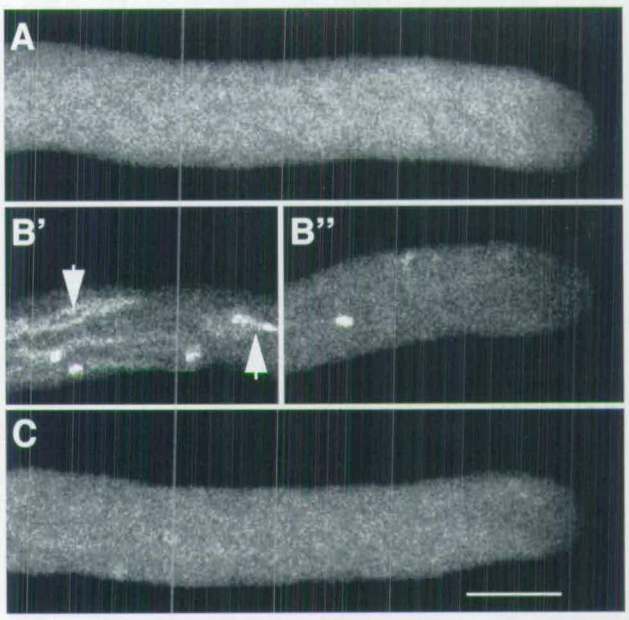

Fig. 4. Confocal images showing the intracellular distribution of cSNARF-1 in growing *Agapanthus* pollen tubes. The 'apical clear zone' (see Fig. 1) can be seen as a region (~6 μm long) of reduced fluorescence intensity at the tip of each pollen tube. (A) Pollen tube loaded for 10 minutes with AM-ester. (B′ and B″) Pollen tube after 30 minutes of continuous ester-loading. Subapical dye sequestration is indicated (arrows). B′ shows the region 60-90 μm behind the tip and B″ shows the tip itself. (C) A pollen tube immediately after ionophoretic microinjection with dye free-acid. Bar, 10 μm.

Fig. 5. Confocal images showing the intracellular distribution of cSNARF-1 in growing *Dryopteris* rhizoids. (A) A single rhizoid immediately after loading. Note the unloaded large subapical vacuole (v) and the strongly loaded nucleus (n). (B) A rhizoid at two stages of growth: The first image shows the rhizoid 15 minutes after ester-loading, immediately after dilution of the dye ester, whilst the second image shows the same rhizoid 9 minutes later. Vacuoles excluding dye appear dark. (C) The redistribution of dye 45 minutes after ester-loading. The vacuoles and cytoplasm are hard to distinguish from each other because dye is present in both. (D) Vacuolar accumulation of cSNARF-1 free acid in a rhizoid three hours after ester-loading. Bars, 15 μm.

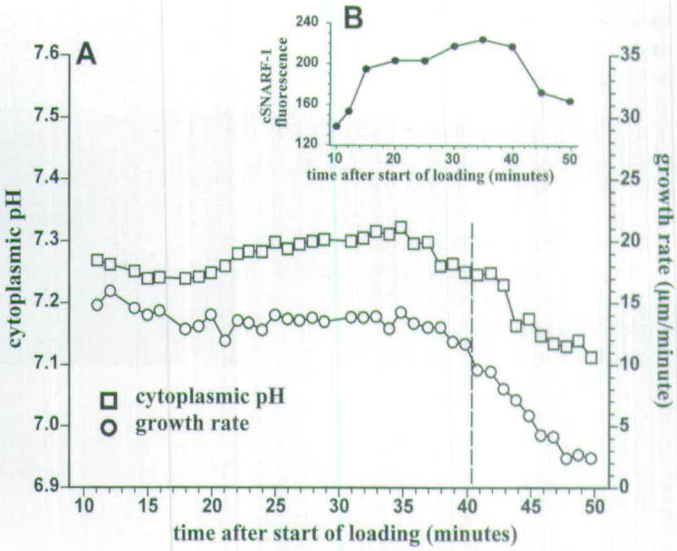

Fig. 6. Assessment of useful imaging time in a *Neurospora* hypha during continuous ester-loading with cSNARF-1. (A) Hyphal growth rate and estimated pH_{cyt} plotted against time after the start of continuous dye loading for a typical hypha. The dashed line indicates the maximum useful imaging time (40 minutes). After this time, the growth rate gradually decreased concomitantly with increasing cytoplasmic acidification indicating cell stress. (B) Change in overall intracellular dye fluorescence intensity (dye fluorescence detected by Ch-1 and Ch-2 have been combined) over time. Note the decrease in fluorescence intensity after 40 minutes.

a very uniform distribution of dye fluorescence except within the 5-10 μm apical region where the fluorescence was reduced (Fig. 4A). The latter corresponded to the apical 'clear zone' (Derksen et al., 1995; Fig. 1) in which the high concentration of vesicles probably excluded dye. Sequestration of dye was more obvious after 30 minutes (Fig. 4B′ and B″) when bright tubules, possibly part of the vacuolar system, became apparent.

Initially, *Dryopteris* rhizoids rapidly accumulated ester-loaded dye in the cytoplasm with the vacuolar system appearing non-fluorescent (Fig. 5A and B). Brighter patches of fluorescence within the cytoplasmic regions were visible very early during loading (Fig. 5B) and were probably mitochondria (Parton, 1996). Gradual redistribution of dye from the cytoplasm to the vacuolar system occurred from the start of loading but was only significant after >30 minutes (Fig. 5C and D).

The fluorescence distribution in *Neurospora* hyphae pressure-injected with the 10 kDa dextran conjugate of cSNARF-1 differed in several important ways from hyphae ester-loaded with dye (compare Fig. 3C with 3A and 3D with 3B). First, there was no indication of dextran-dye associated with putative mitochondria. Second, the dextran-dye was excluded from both the large subapical vacuoles and the small unidentified organelles which sequestered dye after ester-loading. Third, the fluorescence of dextran-dye within hyphae diminished much more slowly with time. Fortuitously, the dextran-dye tended to move forward from the subapical injection site towards the tip during growth.

Ionophoretic microinjection of *Agapanthus* pollen tubes with cSNARF-1 free acid resulted in a pattern of dye loading and sequestration within organelles similar to that obtained after ester-loading (cf. Fig. 4C and A).

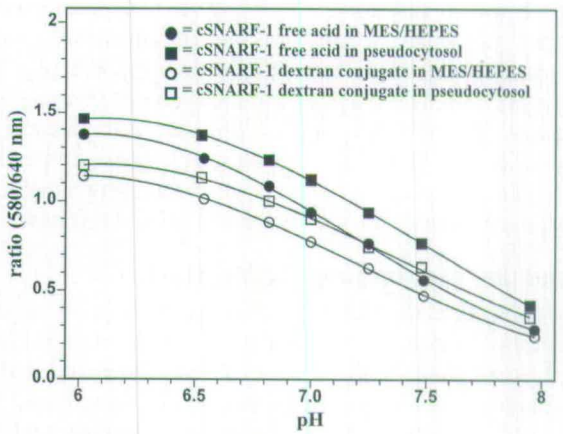

Fig. 7. In vitro calibrations for the pH response of cSNARF-1 imaged by CLSM.

Calibration of the pH response of cSNARF-1

The pH-dependent responses of cSNARF-1 free acid and the 10 kDa dextran conjugate of cSNARF-1 were assessed in vitro for our specific imaging set up using: (1) simple MES/Hepes buffer solution, and (2) 'pseudocytosol' solution designed to mimic the intracellular environment (Fig. 7).

In both calibration solutions, cSNARF-1 fluorescence ratios for the two dyes gave an approximately linear response over the range pH 6.9-7.3. Between pH 6.0 and 8.0 the response was sigmoidal; below pH 5.5 dye precipitation occurred. Although the four calibration curves were broadly similar, two significant differences were noted. First, the ratio values obtained for the dextran-dye were lower than those obtained for the dye free

acid. Calibration of data from dextran injected cells was, therefore, performed with the dextran in vitro. Second, with both the free acid and dextran dyes, 'pseudocytosol' solution caused a shift in ratios to slightly lower values relative to MES/Hepes solution. The effects of the 'pseudocytosol' appeared to be greater at alkaline pH resulting in a slight change in the slope of the calibration curve relative to MES/Hepes. In addition, the absolute fluorescence intensities recorded for the same concentration of dye at each pH were roughly three times higher in the pseudocytosol than in the simple buffer solutions.

In vitro calibrations using MES/Hepes buffers were simple, quick, easy to perform, and very reproducible. These calibrations provided good estimates of ΔpH as well as a means of comparison between different sets of data by taking into account day-to-day and cell-to-cell variations, and differences between dyes. The similarity between the pseudocytosol and simple buffer in vitro calibrations provided further support that a reasonable estimate of ΔpH_{cyt} could be obtained. With this calibration the pH_{cyt} determined was similar to previously reported values of pH (Guern et al., 1991). Small pH_{cyt} changes, which had been imposed on cells by permeant weak acid treatments (ΔpH_{cyt} ~0.2 unit), were also reported convincingly by the in vitro calibration. Despite the corroborative evidence gathered to support the value of our calibrations, there is no guarantee that the estimated pH values quoted provide a truly accurate measure of absolute pH_{cyt}. The values given are, therefore, the best estimate currently available without the use of an independent method of pH determination such as pH-sensitive microelectrodes.

An in situ calibration using ionophores to equilibrate pH_{cyt} and pH_{ext} (Davies et al., 1990) could not be achieved reliably here because of two major limitations. First, it was difficult to stably and reproducibly clamp pH_{cyt} at a particular level. Second, the ionophore treatment disrupted cell structure, caused dye sequestration within organelles and increased dye loss from cells.

Cytoplasmic pH in tip-growing cells

No pH_{cyt} gradient with a ΔpH >0.1 pH unit was detected along a midline through the central region of the apical 50 μm nor between different regions around the periphery of the apical 15 μm (covering the region of tip extension) of any of the three growing cell types examined (Fig. 8). In Fig. 8D apparent acidic regions at the extreme (<1 μm) cell periphery were attributed to dye binding to the cell wall.

Ratio images of *Dryopteris* rhizoids proved difficult to analyse because of the thin layer of peripheral cytoplasm within cells and dye sequestration into acidic vacuoles (Fig. 5). With the ×40 dry objective no significant differences in pH_{cyt} were found between cytoplasm in the extreme apical 3 μm and at the cell periphery up to 50 μm behind the tip (n=7). Imaging with the ×60 oil objective and Kalman filtering were used to provide increased spatial resolution to better distinguish the sparse cytoplasm from contaminating vacuolar signal and gave similar results (n=6). Fig. 8D′, which shows a clear gradient in apparent pH_{cyt}, is included to demonstrate how easily ratio images can be misinterpreted without proper reference to cytological features (Figs 5 and 8D′).

Estimated values of average pH_{cyt} over the first 30 μm of each of the three cell types are given in Table 4. The average

Table 4. Average cytoplasmic pH over the first 30 μm of cells determined bycSNARF-1 ratio imaging

Type of dye used	Cell type	Mean pH_{cyt} (±s.d.)	n	Objective	Type of medium
AM-ester	*Neurospora*	7.23±0.05	31	×40 dry	Liquid medium
AM-ester	*Neurospora*	7.20±0.03	8	×60 oil	Liquid medium
AM-ester	*Neurospora*	7.25±0.07	6	×40 dry	Agarose
Dextran	*Neurospora*	7.57±0.04	6	×40 dry	Agarose
AM-ester	*Agapanthus*	7.20±0.05	56	×40 dry	Agar
Free acid	*Agapanthus*	7.20±0.05	8	×40 dry	Agar
AM-ester	*Dryopteris*	7.15±0.02	7	×60 oil	Liquid medium

pH values for individual images were calculated on the basis of in vitro calibrations using MES/Hepes buffers. Standard deviations were determined from variation in the average pH_{cyt} of n individual cells.

pH_{cyt} values obtained for ester-loaded cells were very similar (pH 7.15-7.25; also see Fig. 8A,C and D). No significant difference in average pH_{cyt} measurement was obtained by ratio imaging ester-loaded *Neurospora* hyphae with either the ×40 dry or ×60 oil immersion objective. However, the pH_{cyt} value obtained for *Neurospora* hyphae loaded with the dextran-dye was significantly higher (pH 7.57; also see Fig. 8B). The lower pH_{cyt} estimated for ester-loaded cells could not be attributed to oxygen deprivation because similar pH_{cyt} values were obtained from *Neurospora* hyphae sandwiched between two coverslips (liquid medium) and from hyphae (on agarose) lacking an overlying coverslip (Table 4). No correlation was found between the growth rates and average pH_{cyt} values of individual *Neurospora* hyphae which varied from pH 7.02 to 7.29 in ester-loaded cells and from pH 7.51 to 7.59 in dextran-dye loaded cells (data not shown).

Effects of manipulating internal pH on apical growth

Ratio imaging revealed that the application of a cell permeant weak acid (50 mM sodium propionate) at pH 7.0 resulted in the cytoplasm of *Neurospora* hyphae being acidified evenly (Fig. 9A-H). Immediately after this treatment, hyphal tips became swollen causing a slight increase in hyphal length (Fig. 9A-E). Five to ten minutes after treatment a new tip was generated, narrower than that of the parent hypha, which gradually increased its growth rate (Fig. 9A and F-H). Eventually this new tip with acidified pH_{cyt} acquired a stable growth rate which was slower (2-3 μm $minute^{-1}$) than its parent hypha (14-15 μm $minute^{-1}$, Fig. 9A, n=5). Similar treatments with propionate at pH 6.0 or 6.5 resulted in even greater acidification of pH_{cyt}, an initial hyphal swelling and complete inhibition of subsequent tip regeneration (n=5). Addition of a cell permeant weak base (50 mM trimethylamine) at pH 8.0 caused increased alkalinisation of hyphal cytoplasm and a similar pattern of hyphal swelling and tip regeneration (n=5) as observed after weak acid treatment at pH 7.0. The shifts in internal pH due to weak acid (pH 7.0) or base (pH 8.0) treatment were only stable for approximately 10-15 minutes. Thereafter, the pH_{cyt} slowly returned towards its original value.

Agapanthus pollen tubes proved much more sensitive than *Neurospora* hyphae to propionate and were very prone to bursting in the presence of 30 mM sodium propionate. Treatment with 15 mM propionate at pH 6.0 or 7.0 evenly acidified the cytoplasm and resulted in tip swelling but a new tip was not regenerated (n=8). Addition of a cell permeant weak base (30 mM ammonium chloride) caused even alkalin-

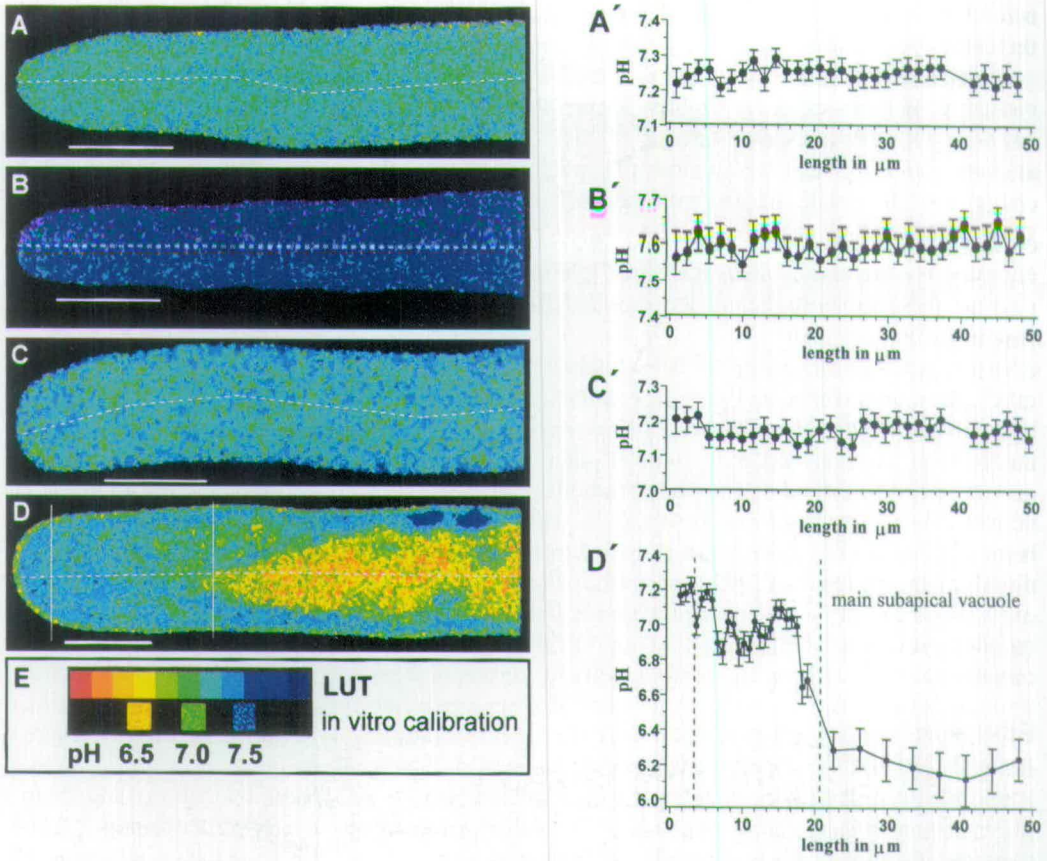

Fig. 8. Cytoplasmic pH in the apical regions of growing cells examined by confocal ratio imaging of cSNARF-1. All cells were ester-loaded with cSNARF-1, except the hypha in Fig. 8B which was pressure-injected with 10 kDa cSNARF-1 dextran. Typical examples are shown and similar results were found for at least five cells in each case. Ratio images correspond to median confocal optical sections through cells. (A,B) Hyphae of *Neurospora*. (C) Pollen tube of *Agapanthus*. (D) Rhizoid of *Dryopteris*. (A′, B′, C′, D′) Graphs of pH_{cyt} along a midline through the cells shown in the corresponding A-D. Error bars represent the 95% Bayesian interval. (E) Pseudocolour scale with corresponding pH values from in vitro calibration (MES/Hepes buffer) and small regions of corresponding ratio images at pH 6.5, 7.0 and 7.5. Bars, 10 μm.

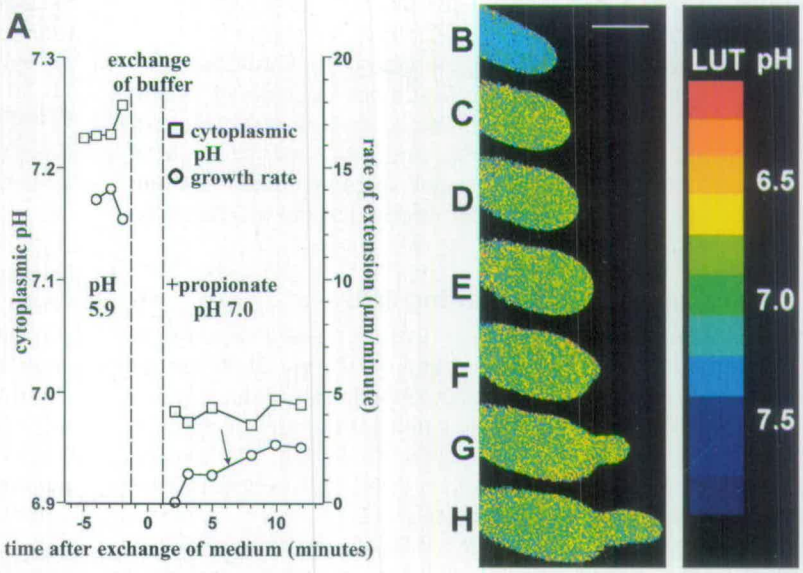

Fig. 9. Effects of acidifying the pH_{cyt} of a *Neurospora* hypha with sodium propionate buffered medium at pH 7.0. The hypha was continuously ester-loaded with cSNARF-1. (A) Plot of pH_{cyt} and growth rate against time before and after exchange from standard (pH 5.9) to sodium propionate buffered medium. A period of physical stress due to medium exchange is indicated between the dashed lines. The arrow shows the point at which a new tip was generated. (B-H) Ratio images of the same hypha analysed in A showing pH_{cyt} and tip morphology two minutes before treatment (B), and two (C), three (D), five (E), eight (F), ten (G) and twelve (H) minutes after treatment. Similar results were obtained with five other hyphae. Bar, 10 μm.

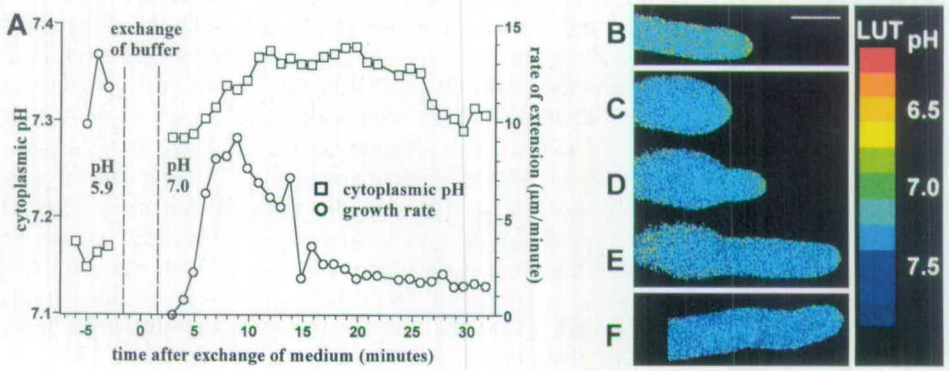

Fig. 10. Effects of pH_{ext} manipulation on tip morphogenesis and growth rate of a *Neurospora* hypha ester-loaded with cSNARF-1. (A) Plot of pH_{cyt} and growth rate against time after changing the pH_{ext} from pH 5.9 to 7.0. (B-F) Ratio images of the same hypha as shown in (A) three minutes before changing the pH_{ext} (B), and five (C), six (D), eight (E) and 20 (F) minutes after changing the pH_{ext}. Note that there is an initial swelling of the hyphal tip (C) followed by the regeneration of a new tip (C-F). Similar results were obtained with 5 other hyphae. Bar, 10 μm.

isation of pollen tube cytoplasm, swelling of the tip but again tip growth did not resume (n=8).

Exposure of *Dryopteris* rhizoids to 30 mM sodium propionate at pH 6.0 altered pH_{cyt} to an even acidic level throughout cells within 3 minutes (n=10). The pH change was associated with a rapid redistribution of apical cytoplasm and cessation of growth. Cells only remained viable if the duration of propionate treatment was <15 minutes. Rhizoid growth was not resumed until 12-18 hours after returning to normal medium (pH 5.6) and generally involved the generation of a new tip at a position slightly subapical to the original. Similar effects on growth were observed after treating rhizoids with 30 mM sodium propionate at pH 7.0 or 30 mM ammonium chloride at pH 7.0 or 8.0. Propionate treatment at pH 7.0 was unstable and gave apparent pH values of <7.0 (n=5). With ammonium chloride at pH 8.0, the pH_{cyt} elevation stabilised after 3 minutes. The pH_{cyt} change after treatment at pH 7.0, however, was unstable and after an initial rapid alkalinisation the pH_{cyt} value gradually increased to a similar level as for the pH 8.0 treatment (n=20). Recovery after exchange to normal medium was similar to that observed after propionate treatment.

Effects of manipulating extracellular pH on apical growth

Extracellular pH treatments were also found to change the pH_{cyt} and growth rate of the three cell types.

In *Neurospora* hyphae ester-loaded with dye, an increase in the pH_{ext} from 5.9 (normal medium) to 7.0 resulted in a gradual, transient elevation in pH_{cyt} by 0.2-0.3 pH units within 10-15 minutes and a reduced growth rate which stabilised after 20-30 minutes (Fig. 10, n=5). Increasing the pH_{ext} to 8.0 immediately led to an increase in pH_{cyt} by 0.5-0.6 pH units which declined towards normal values over ~30 minutes (data not shown). At pH_{ext} 8.0, hyphal growth rate was reduced to <4 μm $minute^{-1}$ (n=5), and tips tended to exhibit an undulating growth pattern and underwent increased apical branching (Fig. 11A).

Agapanthus pollen tubes responded differently to pH_{ext} manipulation. Pollen tubes were normally grown in medium at pH 6.0. Treatment with unbuffered medium at pH 8.0 or 4.5 caused a transient shift in pH_{cyt} of <1.0 pH units (+ or −, respectively) which was associated with a disruption of tip morphology and growth rate (n=20). After changing the medium to pH 4.5, the pH_{cyt} recovered to normal levels within one minute of treatment, growth continued but the tip diameter became transiently narrower, recovering to its full width within two minutes (Fig. 11B). After changing the medium to pH 8.0, tip growth temporarily ceased and then within 1-5 minutes the tip underwent swelling, the pH_{cyt} recovered, and a new tip emerged from the swelling within 3-7 minutes.

Dryopteris rhizoids required strong buffering of pH_{ext} (5-25 mM MES/Hepes) before effects on growth were observed. Changing the normal, unbuffered pH 5.6 medium to buffered medium at pH 6.0 had little effect on growth. However, buffered medium at pH 7.0 or 8.0 caused cytoplasmic rearrangement and withdrawal from the tip, apical swelling and temporary cessation of polarised growth in all cases (Fig. 11D′). Tip growth resumed 6-12 hours later in cell populations (Fig. 11C and D′). Technical difficulties prevented examination of pH_{cyt} continuously over the period from the alteration of pH_{ext} to the time at which cells had undergone changes in apical morphology. At the two time points examined, immediately upon pH modification and at the first signs of changes in apical morphology, no shift in pH_{cyt} could be detected (n=6).

DISCUSSION

pH_{cyt} gradients are not a common feature of tip-growing cells

This study has shown that pronounced longitudinal pH_{cyt} gradients (ΔpH >0.1 pH unit) are not present within the apical 50 μm of actively growing fungal hyphae, higher plant pollen tubes and fern rhizoids indicating that pH_{cyt} gradients of this type are not a general feature of tip-growing cells.

The existence of pronounced pH_{cyt} gradients in tip-growing cells has been a controversial topic. The best published data showing a pH_{cyt} gradient associated with tip growth has come from the analysis of rhizoids in the brown alga *Pelvetia* using confocal ratio imaging and ion-selective microelectrodes (Gibbon and Kropf, 1994). Evidence for pH_{cyt} gradients in other tip-growing cells (e.g. Turian, 1979; Roncal et al., 1993) is poor because the methodologies used in these studies have

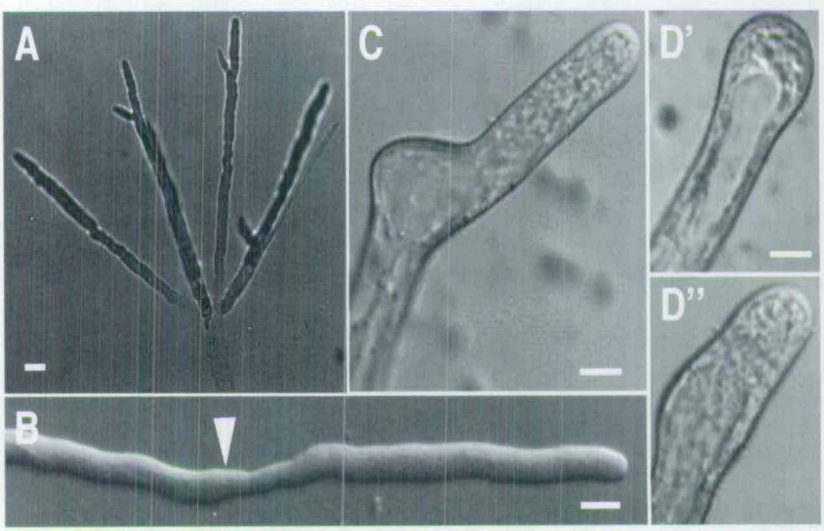

Fig. 11. The effects of pH_{ext} manipulation on tip growth and behaviour. Examples shown are typical for similarly treated populations of cells.
(A) *Neurospora* hyphae at pH 8.0 showing undulating growth pattern and increased branching.
(B) *Agapanthus* pollen tube initially grown at pH 6.0 and then exposed to an adjusted medium at pH 4.5 (from arrow). Note the pollen tube initially narrowed and then recovered to the normal diameter.
(C) *Dryopteris* rhizoid eight hours after exchange of medium from pH 5.6 to 7.0. (D′ and D″) *Dryopteris* rhizoid three hours (D′) and eight hours (D″) after transfer to growth medium at pH 8. Note that the rhizoid has responded by initially swelling before normal tip growth was resumed. Bars, 10 μm.

since been found to be inadequate as a result of the development of improved methods of pH_{cyt} analysis (such as employed in the present study) which provide less equivocal results. In support of our conclusion that pH_{cyt} gradients are not a general feature of tip-growing cells, Herrmann and Felle (1995) failed to detect a gradient (>0.1 pH unit) in growing root hairs by using ion-selective microelectrodes. Although the absence of pronounced pH_{cyt} gradients would appear to be the norm, it cannot be discounted that they may exist in certain cell types such as algal rhizoids.

An alternative biophysical approach, using a combination of in vitro experimentation and theoretical analysis, has been used to investigate the possible existence of pH_{cyt} gradients in cells (Al-Baldawi and Abercrombie, 1992). This work with animal cytoplasm showed that estimates of the rate of proton diffusion, the buffer capacity of the cytoplasm and rates of proton flux across membranes would tend to favour a pronounced ΔpH (>0.1 unit) only over distances >25 μm. However, their study did not preclude the possibility of more localised pH domains, which could arise from localised fixed buffering components (e.g. cytoskeletal proteins). Clearly, polarised plant and fungal cells are capable of generating large proton currents involving spatially separated proton transport activities (Weisenseel et al., 1979; Harold and Caldwell, 1990; Feijo et al., 1995) but in light of the absence of a pH_{cyt} gradient in root hairs (Herrmann and Felle, 1995), and in the tip growing cells studied here, such proton flux must be dealt with by a combination of the metabolic activity (Sanders and Slayman, 1982), proton pumping (Guern et al., 1991) and cytosolic buffering of cells (Al-Baldawi and Abercrombie, 1992) which together make up the cellular buffering capacity.

Confocal ratio imaging of cSNARF-1 is presently the best method for detecting pH_{cyt} gradients

Simultaneous, dual channel confocal ratio imaging is the most suitable method for visualising pronounced pH_{cyt} gradients in tip growing cells. However, this procedure is potentially fraught with artefacts and thus requires rigorous controls. In order to validate our conclusion that pronounced pH_{cyt} gradients were absent in the three types of tip-growing cells studied, we carefully assessed the specific problems of cell perturbation during imaging, dye partitioning within organelles (Seksek et al., 1991; Opitz et al., 1994), $R_{S/N}$ and 'edge' artefacts in ratio images (Bright et al., 1987; Pawley, 1995), and calibration of cSNARF-1 (Fricker et al., 1994). A pronounced longitudinal pH_{cyt} gradient was defined in this study as having a ΔpH of >0.1 pH unit over a distance >2 μm for two reasons: first, these were the limits of the precision of pH measurement and spatial resolution which could be routinely achieved by confocal ratio imaging of cSNARF-1 within healthy cells. Second, ΔpH of >0.1 pH unit are within the range considered to be of physiological significance (Busa and Nuccitelli, 1984; Guern et al., 1991). Our results do not discount the possible presence of highly localised pH gradients which might be associated with the plasma membrane (Roos, 1992).

Previously reported pH_{cyt} values for plant and fungal cells usually lie between pH 6.8 and 7.9 (e.g. see Sanders and Slayman, 1982; Guern et al., 1991). In our study, the estimated values of mean pH_{cyt} with ester-loaded dye were between pH 7.15 and 7.25 for the three cell types. With *Neurospora* hyphae loaded with the dextran dye by pressure injection, however, the estimated mean pH_{cyt} was pH 7.57. It is generally believed that the results obtained with dextran dyes provide a better estimate of pH_{cyt} because of their superior localisation and retention within the cytosol (Haugland, 1992; Miller et al., 1992). It is significant that, although the pH_{cyt} values estimated with ester-loaded free dye and pressure-injected dextran dye in *Neurospora* differed, no significant pH_{cyt} gradient was detected with either.

With each dye type, the estimated pH_{cyt} was very reproducible between individual cells and variation in average pH_{cyt} between individual cells was within the limits of precision of measurement for the imaging technique. This is in agreement with the general finding that pH_{cyt} is tightly regulated within growing cells (Guern et al., 1991).

For the work reported here, cSNARF-1 proved to be the most appropriate dye. Another ratio dye widely used to measure pH_{cyt} is BCECF (Haugland, 1992), but this has a number of disadvantages compared with cSNARF-1. First, in *Neurospora* it exhibits more pronounced sequestration within vacuoles (unpublished results; Slayman et al., 1994). Second, BCECF is a dual excitation dye requiring sequential excitation at two wavelengths. Improved temporal resolution can be achieved with cSNARF-1 which is excited at one wavelength and detected simultaneously at two wavelengths. However, using confocal ratio imaging of BCECF it has recently been demonstrated that pronounced pH_{cyt} gradients are not associated with growing *Lilium* pollen tubes (M. D. Fricker, personal communication) which provides further confirmation of our findings.

Evidence that pH_{cyt} gradients have a fundamental role in regulating tip growth is poor

The lack of pronounced pH_{cyt} gradients in the cell types examined here during active tip growth and additionally, the work of Herrmann and Felle (1995) in root hairs, argues strongly against a fundamental role for gradients of this type regulating the polar organisation and active processes of tip growth. This conclusion is further supported by our finding that *Neurospora* hyphae continued to grow in the presence of relatively high concentrations of cell permeant propionic acid (pKa 4.87) which would be expected to collapse any pH_{cyt} gradient.

If the results obtained by Gibbon and Kropf (1994) are correct then a tip-focused pH_{cyt} gradient may be a feature peculiar to growing rhizoids of fucoid algae such as *Pelvetia*. We attempted to confirm their results by examining the growing rhizoids of the related alga *Fucus serratus*. However, our attempts proved unsuccessful due to problems in attaining a suitably high level of dye loading relative to chloroplast autofluorescence in these cells (R. M. Parton and J. Love, unpublished results).

Gibbon and Kropf (1994) found that 10 mM propionic acid (at pH 7.0) dissipated the pH_{cyt} gradients and drastically reduced growth of *Pelvetia* rhizoids. They suggested that these observations provided evidence for a pH_{cyt} gradient regulating tip growth in these cells. The validity of this interpretation is open to question. Herrmann and Felle (1995) performed similar weak acid treatments on root hairs and recorded similar inhibitory effects on growth. However, in the absence of a detectable pH_{cyt} gradient within growing root hairs, they concluded that the inhibitory effects of the weak acids on growth were due to a disruption of the normally maintained

pH_{cyt}. Treatment of cells with membrane permeant weak acids may have a number of non-specific effects relevant to tip growth, including: (1) both organellar pH and cytosol pH will be affected and changes in organellar pH may be important for certain processes involved in tip growth (e.g. the exocytotic pathway). (2) Acidifying cells can increase the cytosolic calcium concentration (Felle, 1988; Guern et al., 1991). Artificially induced increases in cytosolic free calcium have been shown to inhibit tip growth in pollen tubes (Franklin-Tong et al., 1993; Malhó et al., 1994). (3) The membrane potential will be changed by cytoplasmic acidification which will affect ion transport across membranes. Such non-specific effects may explain the inhibition of tip growth in both *Agapanthus* and *Dryopteris* cells, although the possible existence of highly localised unseen pH_{cyt} gradients cannot be ignored.

pH_{cyt} and pH_{ext} do have a role in regulating tip growth

It is clear from our results that both pH_{cyt} and pH_{ext} have a significant influence on the growth of the three cell types analysed. Tip growth was sensitive to any alteration in the normally maintained pH_{cyt}. Changing pH_{ext} influenced the rate of tip growth, the width of cell tips, and the formation of new tips (branch formation). Altering pH_{ext} was commonly accompanied by a transient change in pH_{cyt}. However, it is unlikely that the effects of altering pH_{ext} were due to this transient influence on pH_{cyt} alone, consider increased branching in *Neurospora* which continues throughout the period of culture at increased pH_{ext}. Changes in membrane potential and transport activities may also be important.

pH_{cyt} regulation is undoubtedly an important aspect of cellular physiology. It has been proposed as a mechanism by which cells co-ordinate the regulation of various processes that lack any other common factors and also may provide a regulatory link between metabolic state and physiological responses, such as those involved in tip growth (Busa and Nuccitelli, 1984; Felle, 1996). However, the pervasive nature of H^+ throughout all cellular processes makes it difficult to determine strict cause and effect relationships and to assign specific second messenger functions.

APPENDIX

Statistical analysis by Bayesian inference was used to obtain 95% error bounds for estimates of the mean ratio value of images obtained by sampling small (14×14 pixel) areas. The Bayesian approach permits probability statements to be made regarding unknown population parameters such as mean ratios, variances and correlations, and provides a popular paradigm for statistical inference (O'Hagan, 1994; Leonard et al., 1989; Leonard and Hsu, 1992).

The statistical analysis here assumed that the distribution of fluorescence pixel intensity values in both the Ch-1 and Ch-2 images could each be approximated by a Normal distribution. Hence our model of the data contained two 'unknown' population means and variances, which needed to be estimated by analysis of the small sample area data. We also permitted the possibility that a correlation exists between the fluorescence intensity values of corresponding pairs of pixels from Ch-1 and Ch-2 images (i.e. an unknown population linear correlation between pairs of observations). The assumptions were completed by assuming that any linear combination of pairs of pixel values in a fluorescence image pair were also normally distributed.

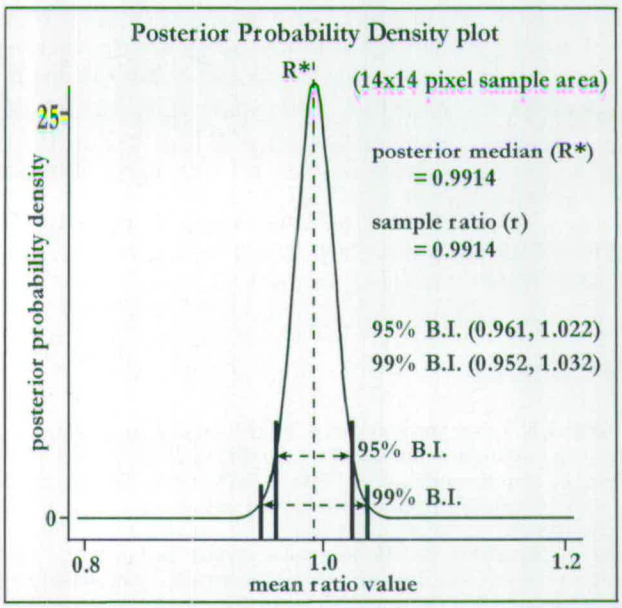

Fig. 12. Example of a posterior probability density plot for the mean ratio value for a corresponding pair of fluorescence images of cSNARF-1 free acid in MES/Hepes buffer at pH 7.0. The posterior probability density function was derived, according to the Bayesian theory of inference as described in the Appendix, on the basis of variation in pixel values from corresponding 14×14 pixel areas sampled from the fluorescence image pair. The 95% and 99% Bayesian intervals (BI) are shown. These correspond to a 95% and 99% posterior probability thatthis range covers the mean ratio (R).

Error bounds were required for our estimates of the ratio R of the mean intensities of the populations of pixels in a fluorescence image pair obtained from sampling small areas of the image pair. These could, in general, be calculated from a sample of n (in this case n=14×14) independent pairs of pixel values. As an extension of Kappenman et al. (1970), we employed a Bayesian approach, under particular uniform prior assumptions carefully selected to guarantee an almost exact frequency coverage for our 95% intervals if $n \geq 100$.

A mathematical solution was derived and incorporated into a computer program which provided plots of the 'posterior probability density function' (posterior p.d.f.) for R which summarise the information about R, a posteriori (i.e. after incorporating the data) when there is uniform information, a priori (i.e. prior to viewing the data). An example is given in Fig. 12 for sampling an in vitro calibration image (pH 7.0) with a 14×14 pixel box size. The area under the curve between R values of 0.961 and 1.022 is the 95% Bayesian interval (i.e. there is a 95% posterior probability that R is in that interval). Convenient error bounds were provided by equal-tailed Bayesian 95% and 99% intervals (Fig. 12). A convenient point estimate of R is the posterior median (R*) = 0.991. Note that this probability distribution is not a Normal distribution and is unusual in that standard deviation and mean values are not appropriate (because they do not exist). In extreme cases such distributions can be quite obviously skewed, bumpy or bimodal.

We thank Emeritus Professor David Finney and Dr Bruce Worton of the University of Edinburgh Statistical Laboratory for practical statistical advice. We are also grateful to Dr Lionel Jaffe (Marine Biological Laboratory, Woods Hole, Mass., USA) for his critical reading of the manuscript, Dr Mark Fricker (Dept of Plant Science, University of Oxford) for helpful discussions, and to Dr Tony Collins (University of Edinburgh) for helpful advice on computing matters. The research was supported by an AFRC Research Studentship (to R.M.P.), a TMR Fellowship (ERBFMBICT 950455) from the EC (to S.F.) and a BBSRC Studentship (to T.C.J.).

REFERENCES

Al-Baldawi, N. F. and Abercrombie, R. F. (1992). Cytoplasmic hydrogen ion diffusion coefficient. *Biophys. J.* **61**, 1470-1479.

Berger, F. and Brownlee, C. (1993). Ratio confocal imaging of free cytoplasmic calcium gradients in polarising and polarised *Fucus* zygotes. *Zygote* **1**, 9-15.

Bright, G. R., Fisher, G. W., Rogowska, J. and Taylor, D. L. (1987). Fluorescence ratio imaging microscopy: temporal and spatial measurements of cytoplasmic pH. *J. Cell Biol.* **104**, 1019-1033.

Busa, W. B. and Nuccitelli, R. (1984). Metabolic regulation via intracellular pH. *Am. J. Physiol.* **246**, R409-R438.

Cogswell, C. J. and Larkin, K. G. (1995). The specimen illumination path and its effect on image quality. In *Handbook of Biological Confocal Microscopy* (ed. J. B. Pawley), pp. 27-137. Plenum Press, New York.

Davies, J. M., Brownlee, C. and Jennings, D. H. (1990). Measurement of intracellular pH in fungal hyphae using BCECF and digital imaging microscopy. Evidence for a primary proton pump in the plasmalemma of a marine fungus. *J. Cell Sci.* **96**, 731-736.

Derksen, J. Rutten, T., Lichtscheidl, I. K., Dewin, A. H. N., Pierson, E. S. and Rongen, G. (1995). Quantitative-analysis of the distribution of organelles in tobacco pollen tubes - implications for exocytosis and endocytosis. *Protoplasma* **188**, 267-276

Dyer, A. F. and Cran, D. G. (1976). The formation and ultrastructure of rhizoids on protonemata of *Dryopteris borreri* Newm. *Ann. Bot.* **40**, 757-765.

Feijo, J. A., Malhó, R. and Obermeyer, G. (1995). Ion dynamics and its possible role during in vitro pollen germination and tube growth. *Protoplasma* **187**, 155-167.

Felle, H. (1988). Cytoplasmic free calcium in *Riccia fluitians* and *Zea mays*: interaction of Ca^{2+} and pH? *Planta* **176**, 248-255.

Felle, H. (1996). Control of cytoplasmic pH under anoxic conditions and its implication for plasma membrane proton transport in *Medicago sativa* root hairs. *J. Exp. Bot.* **47**, 967-973.

Franklin-Tong, V. E., Ride, J. P., Read, N. D., Trewavas, A. J. and Franklin, F. C. H. (1993). The self-incompatibility response in *Papaver rhoeas* is mediated by cytosolic free calcium. *Plant J.* **4**, 163-177.

Fricker, M. D., Tlalka, M., Ermantraut, J., Obermeyer, G., Dewey, M., Gurr, S., Patrick, J. and White, N. S. (1994). Confocal fluorescence ratio imaging of ion activities in plant cells. *Scanning Microsc.* **S8**, 391-405.

Gibbon, B. C. and Kropf, D. L. (1991). pH gradients and cell polarity in *Pelvetia* embryos. *Protoplasma* **163**, 43-50.

Gibbon, B. C. and Kropf, D. L. (1994). Cytosolic pH gradients associated with tip growth. *Science* **263**, 1419-1421.

Grabski, S., Xie, X. G., Holland, J. F. and Schindler, M. (1994). Lipids trigger changes in the elasticity of the cytoskeleton in plant-cells - a cell optical displacement assay for live cell measurements. *J. Cell Biol.* **126**, 713-726.

Guern, J., Felle, H., Mathieu, Y. and Kurkdjian, A. (1991). Regulation of intracellular pH in plant cells. *Int. Rev. Cytol.* **127**, 111-173.

Harold, F. M. and Caldwell, J. H. (1990). Tips and currents: electrobiology of apical growth. In *Tip Growth in Plant and Fungal Cells* (ed. I. B. Heath), pp. 59-89. Academic Press, London.

Haugland, R. P. (1992). *Molecular Probes: Handbook of Fluorescent Probes and Research Chemicals*. Molecular Probes, Inc., Eugene, Oregon.

Heath, I. B., editor (1990). *Tip Growth in Plant and Fungal Cells*. Academic Press, San Diego.

Herrmann, A. and Felle, H. H. (1995). Tip growth in root hair-cells of *Sinapis-alba* 1 - significance of internal and external Ca^{2+} and pH. *New Phytol.* **129**, 523-533.

Jackson, S. L. and Heath, I. B. (1993). Roles of calcium ions in hyphal tip growth. *Microbiol. Rev.* **57**, 367-382.

Kappenman, R. F., Geisser, S. and Antle, C. E. (1970). Bayesian and Fiducial solutions for the Fieller-Creasy problem. *Sankhya, Indian J. Stat.* **32**, 331-340.

Knight, H., Trewavas, A. J. and Read, N. D. (1993). Confocal microscopy of living fungal hyphae microinjected with Ca^{2+}- sensitive fluorescent dyes. *Mycol. Res.* **97**, 1505-1515.

Lemasters, J. J., Chacon, E., Zahrebelski, G., Reece, J. M. and Nieminen, A.-L. (1993). Laser scanning confocal microscopy of living cells. In *Optical Microscopy - Emerging Methods and Applications* (ed. B. Herman and J. J. Lemasters), pp. 339-354. Academic Press, London.

Leonard, T. and Hsu, J. S. J. (1992). Bayesian inference for a covariance matrix. *Annals Statist.* **20**, 1669-1696.

Leonard, T., Hsu, J. S. J. and Tsui, K.-W. (1989). Bayesian marginal inference. *J. Am. Statist. Assoc.* **84**, 1051-1058.

Malhó, R., Read, N. D., Pais, M. S. and Trewavas, A. J. (1994). Role of cytosolic free calcium in the reorientation of pollen tube growth. *Plant J.* **5**, 331-341.

Malhó, R., Read, N. D., Trewavas. A. J. and Pais, M. S. (1995). Calcium channel activity during pollen tube growth and reorientation. *Plant Cell* **7**, 1173-1184.

Miller, D. B., Callaham, D. A., Gross, D. J. and Hepler, P. K. (1992). Free Ca^{2+} gradient in growing pollen tubes of *Lilium*. *J. Cell Sci.* **101**, 7-12.

O'Hagan, A. (1994). *Kendall's Advanced Theory of Statistics. Vol. 2: Bayesian Inference*. Edward Arnold, London.

Oparka, K. J., Murphy, R., Derrick, R., Prior, D. A. M. and Smith, J. A. C. (1991). Modification of the pressure-probe technique permits controlled intracellular microinjection of fluorescent probes. *J. Cell Sci.* **98**, 539-544.

Opitz, N., Merten, E. and Acker, H. (1994). Evidence for redistribution-associated intracellular pKa shifts of the pH-sensitive fluoroprobe carboxy-SNARF-1. *Plugers Arch.* **427**, 332-342.

Parton, R. M. (1996). *Confocal microscopy analysis of the roles of intracellular ph in the regulation of polarised growth of Dryopteris protonemata*. PhD thesis, University of Edinburgh.

Pawley, J. B. (1995). Fundamental limits in confocal microscopy. In *Handbook of Biological Confocal Microscopy, 2nd edn* (ed. J. B. Pawley), pp. 19-37. Plenum Press, New York.

Pierson, E. S., Miller, D. D., Callaham, D. A., Shipley, A. M., Rivers, B. A., Cresti, M. and Hepler, P. K. (1994). Pollen tube growth is coupled to the extracellular calcium ion flux and the intracellular calcium gradient: Effect of BAPTA-type buffers and hypertonic media. *Plant Cell* **6**, 1815-1828.

Read, N. D., Allan, W. T. G., Knight, H., Knight, M. R., Malhó, R., Russell, A., Shacklock, P. S. and Trewavas, A. J. (1992). Imaging and measurement of cytosolic free calcium in plant and fungal cells. *J. Microsc.* **166**, 57-86.

Roncal, T., Ugalde, U. O. and Irastorza, A. (1993). Calcium-induced conidiation in *Penicillium cyclopium*: calcium triggers cytosolic alkalinisation at the hyphal tip. *J. Bacteriol.* **175**, 879-886.

Roos, W. (1992). Confocal pH topography in plant cells - acidic layers in the peripheral cytoplasm and the apoplast. *Botan. Acta* **105**, 253-259.

Sanders, D. and Slayman C. L. (1982). Predominent role of oxidative metabolism, not proton transport, in the eukaryotic microorganism *Neurospora*. *J. Gen. Physiol.* **80**, 377-402.

Seksek, O., Henry-Toulmé, N., Sureau, F. and Bolard, J. (1991). SNARF-1 as an intracellular pH indicator in laser microspectrofluorometry: a critical assessment. *Anal. Biochem.* **193**, 49-54.

Sheppard, C. J. R., Gan, X., Gu, M. and Roy, M. (1995). Signal-to-noise in confocal microscopes. In *Handbook of Biological Confocal Microscopy, 2nd edn* (ed. J. B. Pawley), pp. 19-37. Plenum Press, New York.

Slayman, C. L., Moussatos, V. V. and Webb, W. W. (1994). Endosomal accumulation of pH indicator dyes delivered as acetoxymethyl esters. *J. Exp. Biol.* **196**, 419-438.

Turian, G. (1979). Cytochemical gradients and mitochondrial exclusion in the apices of vegetative hyphae. *Experientia* **35**, 1164-1166.

Vogel, H. J. (1956). A convenient growth medium for *Neurospora* (medium N). *Microbiol. Gen. Bull.* **13**, 42-43.

Weisenseel, M. H., Dorn, A. and Jaffe, L. F. (1979). Natural H^+ currents traverse growing roots and root hairs of barley (*Hordeum vulgare* L.). *Plant Physiol.* **64**, 512-518.

(Received 17 December 1996 - Accepted 14 March 1997)

dye resulted in extreme sequestration of dye within organelles, especially the pleiomorphic vacuolar network of fungal hyphae.[20,21] To overcome these problems of dye sequestration, we recently used pressure injection to introduce the Ca^{2+}-sensitive, 10 kDa dextran conjugate of Oregon Green-1 into growing hyphae (Fischer, S. & Read, N. D., unpubl.). Initial results clearly demonstrate excellent retention of the dye within the cytosol and the loaded dye can be shown to be highly responsive to changes in cytosolic free Ca^{2+} when hyphae are treated with a high concentration of extracellular Ca^{2+}. Tip-focused gradients in cytosolic free Ca^{2+} have not yet been observed but this may simply be due to the fact that a single wavelength dye has been used. Ion gradients are best observed if ratio imaging with dextran-conjugated ratiometric dyes, or ratiometric dye pairs, is performed. The problem with single wavelength dyes is that it is difficult to distinguish between differences in ion concentration and variations in dye brightness caused by factors such as variable dye concentration, dye photobleaching or dye leakage from the cytosol. In principle, ratio measurements are independent of the amount of dye fluorescence measured and proportional to the free ion concentration, allowing for improved calibration of ion concentration.[20,22]

It is now well established that both Ca^{2+} signalling and pH homeostasis are extremely important for tip growth in fungi and both may offer potentially useful targets for novel antifungal compounds.[23]

REFERENCES

1. Dixon, G. K., Copping, L. G. & Hollomon, D. W. (eds), *Antifungal Agents. Discovery and Mode of Action.* βios Scientific Publishers, Oxford, 1985.
2. Heath, I. B., *Tip growth in Plant and Fungal Cells.* Academic Press, San Diego, 1990.
3. Gow, N. A. R., Tip growth and polarity. In *The Growing Fungus*, ed. N. A. R. Gow & G. M. Gadd. Chapman & Hall, London, 1995, pp. 277–99.
4. Read, N. D., Fischer, S., López-Franco, R., Rentel, M. C. & Bracker, C. E., Fluorescent staining of the Spitzenkörper: evidence for endocytosis and membrane recycling during hyphal tip growth. Submitted.
5. Parton, R. M., Fischer, S., Malhó, R., Papasouliotis, O., Jelitto, T. C., Leonard, T. & Read, N. D., Pronounced cytoplasmic pH gradients are not required for tip growth in plant and fungal cells. *J. Cell Sci.*, **110** (1997) 1187–98.
6. López-Franco, R., Bartnicki-García, S. & Bracker, C. E., Pulsed growth in fungal hyphal tips. *Proc. Natl Acad. Sci. USA*, **91** (1994) 12228–32.
7. López-Franco, R., Howard, R. J. & Bracker, C. E., Satellite Spitzenkörper in growing hyphal tips. *Protoplasma*, **188** (1995) 85–103.
8. Bartnicki-García, S., Bartnicki, D. D., Gierz, G., López-Franco, R. & Bracker, C. E., Evidence that Spitzenkörper behaviour determines the shape of a fungal hypha: a test of the hyphoid model. *Exp. Mycol.*, **19** (1995) 153–9.
9. López-Franco, R. & Bracker, C. E., Diversity and dynamics of the Spitzenkörper in growing hyphal tips of higher fungi. *Protoplasma*, **195** (1996) 90–111.
10. Bracker, C. E., Murphy, D. J. & López-Franco, R., Laser microbeam manipulation of cell morphogenesis in growing fungal hyphae. In *Proceedings of Functional Imaging and Optical Manipulation of Living Cells.* Society of Photo-Optical Instrumentation Engineers, Bellingham, Washington, vol. 2983, 1997, pp. 67–80.
11. Reynaga-Peña, C. G., Gierz, G. & Bartnicki-García, S., Analysis of the role of the Spitzenkörper in fungal morphogenesis by computer simulation of apical branching in *Aspergillus niger. Proc. Natl Acad. Sci. USA*, **94** (1997) 9096–101.
12. Betz, W. J., Mao, F. & Smith, C. B., Imaging exocytosis and endocytosis. *Curr. Opinion Neurobiol.*, **6** (1996) 365–71.
13. Vida, T. A. & Emr, S. D., A new vital stain for visualizing vacuolar membrane dynamics and endocytosis in yeast. *J. Cell Biol.*, **128** (1995) 779–92.
14. Reider, S. E., Banta, L. M., Köhrer, K., McCaffery, J. M. & Emr, S. D., Multilamellar endosome-like compartment accumulates in the yeast vps28 vacuolar protein sorting mutant. *Mol Biol. Cell*, **7** (1996) 985–99.
15. Seiler, S., Nargang, F. E., Steinberg, G. & Schliwa, M., Kinesin is essential for cell morphogenesis and polarized secretion in *Neurospora crassa. EMBO J.*, **16** (1997) 3025–34.
16. Turian, G., Cytochemical gradients and mitochondrial exclusion in the apices of vegetative hyphae. *Experientia*, **35** (1979) 1164–6.
17. Roncal, T., Ugalde, U. O. & Irastorza, A., Calcium-induced conidiation in *Penicillium cyclopium*: calcium triggers cytosolic alkalinization at the hyphal tip. *J. Bacteriol.*, **175** (1993) 879–86.
18. Levina, N. N., Lew, R. R., Hyde, G. J. & Heath, I. B., The roles of Ca^{2+} and plasma membrane ion channels in hyphal tip growth of *Neurospora crassa. J. Cell Sci.*, **108** (1995) 3405–17.
19. Robson, G. D., Prebble, E., Rickers, A., Hosking, S., Denning, D. W., Trinci, A. P. J. & Robertson, W., Polarized growth of fungal hyphae is defined by an alkaline pH gradient. *Fungal Genet. Biol.* **20** (1996) 289–98.
20. Read, N. D., Allan, W. T. G., Knight, H., Knight, M. R., Malhó, R., Russell, A., Shacklock, P. S. & Trewavas, A. J., Imaging and measurement of cytosolic free calcium in plant and fungal cells. *J. Microsc.*, **166** (1992) 57–86.
21. Knight, H., Trewavas, A. J. & Read, N. D., Confocal microscopy of living fungal hyphae microinjected with Ca^{2+}-sensitive fluorescent dyes. *Mycol. Res.*, **97** (1993) 1505–15.
22. Parton, R. M. & Read, N. D., Calcium and pH imaging in living cells. In *Light Microscopy in Biology—A Practical Approach*, 2nd edn, ed. A. J. Lacey. IRL Press, Oxford, 1998 (in press).
23. Read, N. D., Collis, A. J., Fischer, S. & Jelitto, T. C., Calcium signalling and pH homeostasis as novel targets for antifungal compounds. In *Antifungal Agents. Discovery and Mode of Action*, ed. G. K. Dixon, L. G. Copping & D. W. Holloman. βios Scientific Publishers, Oxford, 1995, pp. 279–83.